DISSERTATION

submitted to the
Combined Faculties for the Natural Sciences and for Mathematics
of the Ruperto-Carola University of Heidelberg, Germany
for the degree of
Doctor of Natural Science

Presented by
Dipl. biol. **Jessica Fuhrmeister**
Born in Wiesbaden, Germany

Heidelberg, March 2015

The role of hepatic Growth Arrest and DNA Damage-inducible 45 beta (GADD45β) in adaptive metabolic control

Referees: Prof. Dr. Ursula Klingmüller

Prof. Dr. Stephan Herzig

ACKNOWLEDGEMENT

This work would not have been possible without the help and contribution of several people to whom I would like to express my sincere gratitude.

- Thank you Stephan Herzig for giving me the opportunity to work in this wonderful and unique division.
- Thank you Adam Rose for giving me a chance to perform my PhD studies, for your guidance, your advice, and for sharing your immense knowledge and experience with me. Thank you for your support and understanding also in times of personal issues. In short: I wish that every PhD student had such great boss.
- Thank you Annika, Oksana and Katharina S. for teaching me techniques and for your constant help. You were invaluable during animal and virus work. Special thanks go to our Hiwis for making uncountable SDS gels.
- Thank you Tjeerd for your help with the TSE system and the isolation of primary hepatocytes.
- Thank you Mauricio, Anja, Allan, Katharina N., Astrid and Dan for sharing samples.
- Thank you Ashley and Bilgen, the god of Western Blotting, and Adriano for all your ideas and advice, and for sharing your knowledge with me – without you I would have been lost in the insulin signaling pathway! Thank you Ashley and Adriano for proofreading.
- Thank you Claus Kremoser and Ursula Klingmüller for being part of my DKFZ Thesis Advisory Committee, for your guidance and helpful criticism and suggestions.
- Thank you Stephan Frings and Thomas Hofmann for being part of my examining board.
- Thank you Jürgen Okun, Kathrin Schmidt, Emil Karaulanov, and Matthias Blüher for your collaboration and analyses.
- Thank you Jess, Thomas and Jonas for the good atmosphere in our small group, for the sweets and chocolate and not to forget the delicious cupcakes and macarones to chase away the Monday blues! Thank you Nicola for being such an enthusiastic and talented intern/Bachelor student, for all your work and the cool survival kit. Thank you A170s for the awesome time; it's been great working with you.
- Thank you Aish, Asrar, Irem, Ivo, Julia, Nico, Sushma and Martin for all the fun we had together in social activities, PhD parties and board game nights. You brightened up my time as PhD student.
- Thank you Daniel for your indestructible positive attitude and patience, for encouraging me, for listening to me, for enduring my moods, for laughing with me, for holding me when I'm down – in other words: thank you for everything you give me.
- A special gratefulness goes to you, Mom and Dad! Thank you for everything you have done for me in the last 30 years! Without you I would not be typing these words. You were always there for me, never gave up on me and supported me with all that you could give.

ABSTRACT

In mammals, the balance of energy storage and breakdown is essential for the maintenance of whole body energy homeostasis. An imbalance between energy intake and expenditure as well as an impaired adaption of the central metabolic organs to changes in nutrient availability (so-called metabolic inflexibility) is tightly associated with the onset and progression of obesity and type II diabetes (T2D) and represents a hallmark of the metabolic syndrome. The metabolic syndrome is associated with a spectrum of liver abnormalities described as non-alcoholic fatty liver disease (NAFLD). Thereby, intracellular fat accumulation leads to hepatic lipotoxicity, cellular stress and dysfunction. While the liver is recognized as a key organ contributing to systemic metabolic control, the molecular mechanisms of liver metabolism in coordinating metabolic flexibility remain still puzzling.

In order to determine the molecular mechanisms involved in metabolic flexibility and to find genes which display certain 'inflexibility' in conditions of metabolic dysfunction, a liver transcriptome analysis was performed on obese-diabetic *db/db* and wild type mice under fasting and fed conditions. Array results have uncovered one 'inflexibility' gene in the liver: GADD45β, a member of the "growth arrest and DNA damage-inducible 45" (GADD45) gene family. In particular, we have observed a strong upregulation of liver *Gadd45b* expression upon food deprivation in healthy animals, which was markedly less pronounced in *db/db* mice. While GADD45β is reported to be involved in hyperplasia of hepatocytes and in liver regeneration, there are no studies examining the role of GADD45β in metabolic function.

In this work, we have characterised GADD45β as a nutrient starvation-induced gene, which is differentially expressed in disease and ageing. Congruently, liver *Gadd45b* mRNA levels were lower in fasted men with T2D than in healthy individuals. *Gadd45b* induction was liver specific and not compensated by an induction of the other GADD45 family members. Furthermore, we could show that the *Gadd45b* induction is reversible after re-feeding and intrinsic to hepatocytes.

In the present work we describe for the first time a novel role for hepatic GADD45β in adaptive metabolism under the stress of food deprivation and nutrient overload. A whole-body deletion of the gene caused an accumulation of triglycerides and cholesterol in the liver under fasting conditions and in a mouse model for steatosis. Also, GADD45β KO mice were more insulin resistant after 4 months on high fat diet. Inversely, a liver-restricted GADD45β overexpression in systemic GADD45β KO mice could partially reverse their dysregulated fasting lipid metabolism, and GADD45β overexpression in *db/db* mice could partially reverse their diabetic phenotype.

While the exact mechanism(s) by which GADD45β mediates its effects remain unclear we conclude that GADD45β may be a missing link between lipid and glucose homeostasis under conditions of nutrient stress, thereby protecting from metabolic dysfunction.

ZUSAMMENFASSUNG

Für Mensch und Tier ist die Ausgewogenheit zwischen Energiespeicherung und –verwertung essentiell für die Aufrechterhaltung der Körperhomöostase. Ein Ungleichgewicht hierbei sowie eine beeinträchtigte Anpassungsfähigkeit der zentralen Stoffwechselorgane an wechselnde Nährstoffbedingungen (sogenannte metabolische Inflexibilität) sind eng verknüpft mit der Entstehung und dem Verlauf von Fettleibigkeit und Diabetes Mellitus Typ 2 (DM2) und sind ein Kennzeichen für das Metabolische Syndrom. Dieses ist mit einer Reihe von Störungen der Leber assoziiert, bei denen intrazelluläre Fettanreicherung zu Lipotoxizität, zellulärem Stress und zur Dysfunktion führen (Nicht-alkoholische Fettlebererkrankungen). Während es allgemein anerkannt ist, dass die Leber eine Schlüsselfunktion in der systemischen Stoffwechselkontrolle einnimmt, sind die molekularen Mechanismen zur Koordination der metabolischen Flexibilität nicht vollständig aufgeklärt.

Um die molekularen Mechanismen zu entschlüsseln, die der metabolischen Flexibilität zugrunde liegen, und dabei Gene zu bestimmen, die bei Stoffwechselstörungen ‚inflexibel' reguliert sind, haben wir eine Transkriptom-Analyse an Lebern von adipös-diabetischen *db/db* und gesunden Wildtyp-Mäusen unter verschieden Nahrungsbedingungen durchgeführt. Dabei haben wir einen Kandidaten gefunden: GADD45β, ein Mitglied der „growth arrest und DNA damage-inducible 45" (GADD45) Familie. Wir konnten in Wildtyp-Mäusen eine starke Hepatozyten-spezifische Hochregulation von *Gadd45b* bei Nahrungsentzug beobachten, welche in *db/db* Mäusen deutlich weniger ausgeprägt war. Es ist bekannt, dass GADD45β in der Hyperplasie von Hepatozyten und in der Leberregeneration involviert ist, jedoch gibt es noch keine Studie, in welcher die Rolle von GADD45β in der Stoffwechselkontrolle untersucht wurde.

In der vorliegenden Arbeit haben wir GADD45β als ein durch Nährstoffmangel induziertes Gen charakterisiert, dessen Expression in metabolischen Krankheiten und im Alter dysreguliert ist. Übereinstimmend damit waren die Leber-*Gadd45b* mRNA-Spiegel in nüchternen Männern mit DM2 geringer als in gesunden Individuen. Die Induktion von *Gadd45b* war dabei nicht durch die Induktion der anderen GADD45 Familienmitglieder kompensiert. Des Weiteren beschreiben wir zum ersten Mal eine neuartige regulatorische Funktion für GADD45β im adaptiven Metabolismus unter Nahrungsentzug und -überschuss. Ein „knockout" (KO) dieses Gens führte zu einer stärkeren Akkumulation von Triglyzeriden und Cholesterin in der Leber von nüchternen Mäusen sowie bei einem Mausmodel für Steatose. Zudem waren KO-Mäuse nach 4 Monaten auf einer Hochfett-Diät insulinresistenter als Wildtyp-Mäuse. Umgekehrt konnten wir mit einer Leber-spezifischen GADD45β-Überexpression in gefasteten KO-Mäusen deren dysregulierten Fettstoffwechsel sowie in *db/db* Mäusen deren diabetisches Erscheinungsbild teilweise verbessern.

Obwohl noch nicht geklärt ist auf welche Weise GADD45β seine Effekte vermittelt, so können wir trotzdem aus unseren Beobachtungen schließen, dass GADD45β unter Stresssituationen wie Nährstoffmangel und –überschuss eine Verbindung zwischen Fett- und Glukose-Homöostase darstellen könnte, wobei es eine schützende Rolle vor Stoffwechselschäden einnimmt.

INDEX

1. INTRODUCTION

1.1 Metabolic flexibility – a hallmark of human metabolic health

The discontinuity in supply and demand for energy requires the adaptation and coordination of the metabolic organs, a concept referred to as metabolic flexibility [1]. Metabolic flexibility is defined as the ability of a system (i.e. whole organism, organ, tissue, or cell) to adjust fuel oxidation to fuel availability [2] and to switch from lipid oxidation during fasting to carbohydrate oxidation during feeding conditions [3].

The maintenance of body weight relies on the fine balance between energy intake and energy expenditure. Energy can be expended by performing physical activity and producing heat (thermogenesis). Also, energy is used by basic cellular functions which include adenosine triphosphate (ATP) turnover such as Na^+-K^+-pumps and Ca^{2+}-pumps in the endoplasmic and sarcoplasmic reticulum. Indirect calorimetry is used to determine energy expenditure by calculating the heat that living organisms produce by measuring their O_2 consumption and CO_2 production from consuming substrates (such as carbohydrate, lipid and proteins) [4]. Each substrate produces a different amount of energy (kcal) and a different cost in terms of CO_2 to be removed. The ratio of CO_2 produced to O_2 consumed is referred to as the respiratory quotient (RQ).

$$RQ = \frac{VCO2}{VO2}$$

Depending on the nutrient energy source the RQ lies between 0,7 (fat) and 1,0 (carbohydrates) [1,2]. The RQ is about 0,8 at rest with a mixed diet. But also amino acid or protein oxidation is considered to have a RQ value between 0,8 and 0,9. Such measurements are used to calculate the basal metabolic rate which is the rate of energy expenditure at rest. Metabolic flexibility can also be assessed by using the change in RQ which should drop in healthy individuals when switching to lipid oxidation during fasting conditions [5]. At the state of rest the RQ corresponds to the respiratory exchange ratio (RER). The determination of the RQ is limited since it accounts for the heat production at the cellular level. On the contrary, the RER is easily measured at the nose or mouth, but this also means that the RER only serves as an estimate of the RQ.

Short-term variations in energy intake or energy expenditure lead to either slightly positive or negative energy balances which are mostly buffered by an adjustment of oxidation to intake. During long-term energy balance however, energy expenditure eventually has to match energy intake, otherwise macronutrients are either stored or lost [6]. If this is not the case, metabolic homeostasis can no longer be maintained sometimes resulting in metabolic disorders, the bases of which are not fully understood.

1.2 Metabolic inflexibility – when metabolic control goes awry

1.2.1 Obesity

According to the World Health (WHO) organisation, overweight and obesity are defined as abnormal or excessive fat accumulation that presents a risk to health. The Body mass index (BMI) is commonly used to classify overweight and obesity in adults. It is defined as a person's weight in kilograms divided by the square of his height in meters (kg/m^2). Overweight is defined as a BMI greater or equal to 25. People with a BMI greater or equal to 30 are considered obese. The causes for obesity are a combination of genetic predisposition, an increase in physical inactivity, and an increased intake of energy-dense food [7]. Recent research also links changes in the composition of the gut microbiota to obesity [8,9], which is most likely due to altered dietary composition and caloric intake.

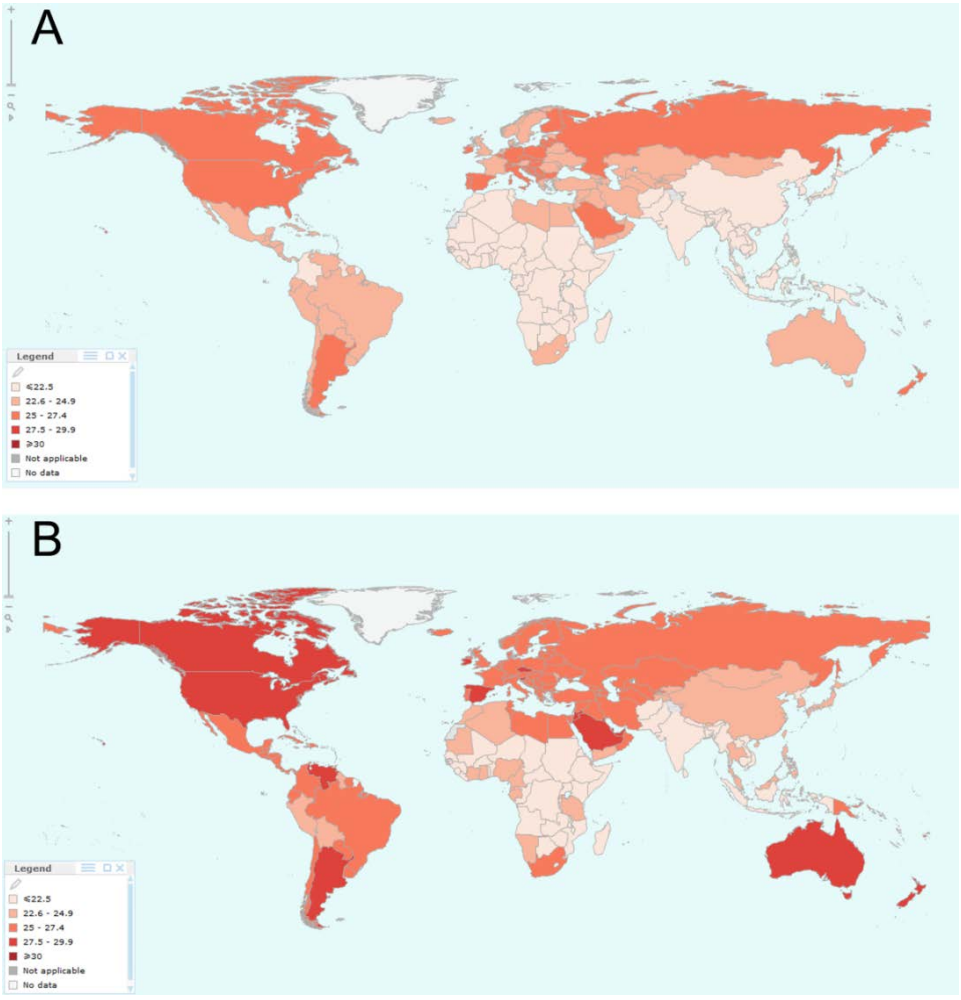

Figure 1: Obesity as a pandemic. Incidence of obesity defined by a body mass index (BMI) ≥ 30 in 1980 (A) and 2008 (B). Legends indicate BMI. From: global database on body mass index WHO, 2011.

Obesity is becoming a major health problem not only in developed countries, but increasingly so also in developing countries. According to recent reports from the WHO (fact sheet number 311, 2014) worldwide obesity has nearly doubled since 1980 (Fig. 1). In 2008, more than 1,4 billion

adults older than 20 were overweight, with the tendency rising, demonstrating that overweight and obesity can be considered a global epidemic. Overweight and obesity are risk factors for a number of chronic diseases, including diabetes, cardiovascular diseases, sleeping-breathing disorders and cancer [10,11], and are nowadays linked to more deaths worldwide in comparison to those caused by malnutrition [7]. Around 3,4 million adults die each year as a result of being overweight or obese. In 2013, more than 42 million children under the age of five were overweight, emphasising the rising need for new approaches for prevention or treatment.

1.2.2 The metabolic syndrome

Increasing evidence points to metabolic inflexibility as a key dysfunction of the cluster of disease states called metabolic syndrome. The metabolic syndrome is a loosely defined condition first described in 1988 by G.M. Reaven who defined it as a constellation of metabolic derangements then known as syndrome X [12]. Several organisations have recommended clinical criteria for the diagnosis of the metabolic syndrome such as high blood pressure (hypertension), high blood sugar (hyperglycaemia), insulin resistance, high triglycerides, low HDL cholesterol, high LDL cholesterol, a low-grade pro-inflammatory state, excess abdominal fat accumulation, and microalbuminuria (high urinary albumin secretion or albumin:creatinine ratio) (Fig. 2) [13-15]. The exact causes and underlying mechanisms are very complex and still under debate. Among the contributing interacting factors are genetics [16], family history of type 2 diabetes (T2D), stress, sleeping disorder [17], advanced age and risk factors for obesity such as sedentary lifestyle [18] and diet (particularly sugar-sweetened beverage consumption). As a consequence, individuals with the metabolic syndrome are at increased risk for developing cardiovascular diseases (CVD) and T2D or further secondary disorders such as non-alcoholic fatty liver disease (NAFLD). However, it is not clear whether obesity or insulin resistance is the cause of the metabolic syndrome or if they are consequences of a more far-reaching metabolic derangement.

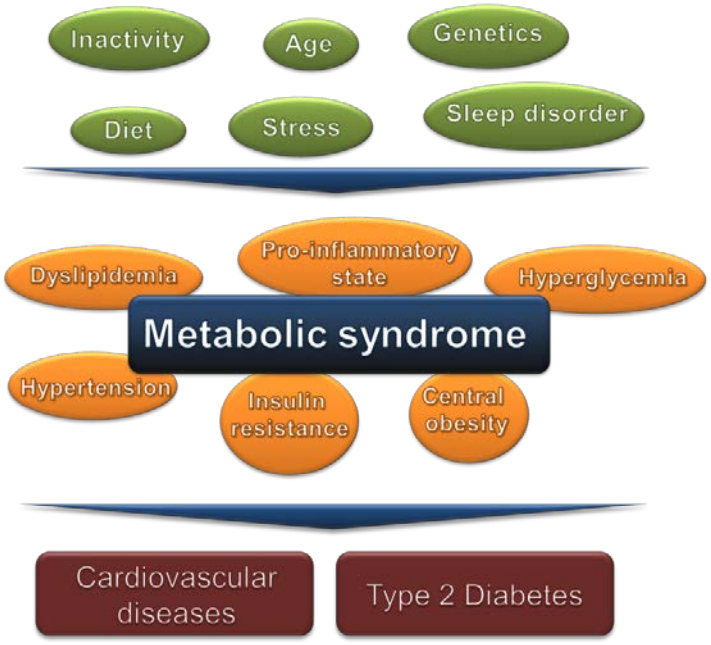

Figure 2: The metabolic syndrome. Causes (green), complications (orange) and consequences (red) of the cluster of disorders called the metabolic syndrome.

Given the increasing prevalence of the metabolic syndrome worldwide, largely as a consequence of the ongoing obesity epidemic, it is of high importance to find new treatment strategies. Lifestyle modification with increased physical activity and weight loss are recommended to be at the core of treating or preventing obesity. In addition, there is a general consensus that the risk for CVD and T2D should be managed by personalised medication aiming at controlling blood sugar, cholesterol, lipids, and high blood pressure [19-21]. But due to the complexity of the metabolic syndrome current therapies have failed to cure the disorder as a whole.

1.2.3 Non-alcoholic fatty liver disease

Obesity is associated with a spectrum of liver abnormalities described as non-alcoholic fatty liver disease (NAFLD) [22]. Within NAFLD cases one can distinguish between a state of accumulated intrahepatic triglycerides without inflammation (steatosis) or with inflammation and fibrosis (non-alcoholic steatohepatitis (NASH)) [23]. Steatosis has been defined as an intrahepatic triglyceride content of >5% of liver volume or liver weight [24], or when 5% or more of hepatocytes contain visible intracellular triglycerides (TG) [25]. Steatosis develops when the rate of fatty acid (FA) input (uptake of plasma free fatty acids (FFA) and *de novo* lipogenesis) is greater than the rate of FA output (fatty acid oxidation and FA export within very low-density lipoproteins (VLDL)).

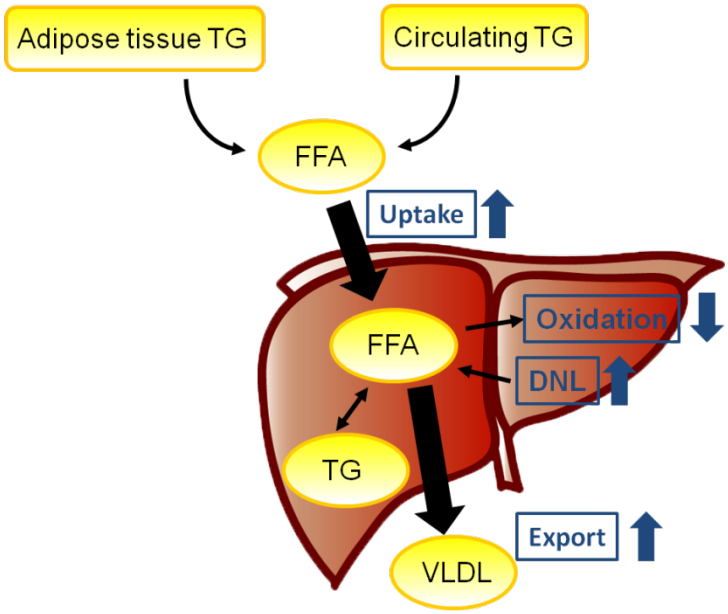

Figure 3: Fatty acid metabolism and the development of non-alcoholic fatty liver disease in obese persons. TG, triglyceride; FFA, free fatty acid; VLDL, within very low-density lipoprotein; DNL, *de novo* lipogenesis. Adapted and modified from [23].

Obesity-associated NAFLD together with hepatic and systemic inflammation are key factors involved in the development of insulin resistance and T2D (Fig. 3) [26]. The rate of release of FFA from adipose tissue and delivery to the liver and skeletal muscle is augmented in obese persons resulting in increased FFA uptake by the muscle and the liver and together with a greater *de novo* lipogenesis ultimately leading to intracellular FA accumulation. On the other hand, the production and secretion of TG in VLDL as a mechanism to remove excess FA is increased. However, since

FA oxidation is inhibited and *de novo* lipogenesis is stimulated by increased plasma glucose and insulin, the rate of TG secretion is not able to compensate for the rate of TG production. As a result, FA taken up by the liver are not oxidized or exported but are converted into TG and stored within lipid droplets. Consequently, these persons demonstrate hypertriglyceridaemia as well as TG accumulation in liver and muscle. In addition, certain FA intermediates can impair insulin signalling and lead to insulin resistance [27]. However the cause-effect relationship is not entirely solved, and it is still under debate whether NAFLD causes the described metabolic alterations or whether these abnormalities cause NAFLD [23].

1.2.4 Insulin resistance and type 2 diabetes

Insulin resistance is a physiological condition whereby the organs of the body fail to respond to the hormone. When organs of the body become resistant to insulin, hyperglycaemia results. Chronic elevations in blood glucose stimulates the pancreas to increases the production of insulin, resulting in hyperinsulinaemia. Insulin resistance can affect the skeletal muscle (impaired insulin-mediated glucose uptake), the liver (impaired insulin-mediated suppression of glucose production), or the adipose tissue (impaired insulin-mediated suppression of lipolysis) [23]. NAFLD is associated with insulin resistance independently of obesity [28,29], and, as stated in 1.2.3, it is still unclear whether NAFLD is the cause or the effect of insulin resistance. The complexity is highlighted by the observation that steatosis is not always associated with insulin resistance [30-32]. It is rather speculated that the esterification of excess FA into TG may protect the hepatocytes by preventing the accumulation of potential toxic intracellular FA [33,34].

Similar to the metabolic syndrome, insulin resistance is a complex metabolic disorder which cannot be explained by a single etiological pathway. There three major mechanisms are proposed to play crucial roles in the pathogenesis of insulin resistance: (1) ectopic lipid accumulation, (2) endoplasmic reticulum stress and activation of the unfolded protein response, (3) systemic inflammation [35]. The development of insulin resistance from ectopic lipid accumulation and the role of the liver will be addressed in 1.3.

The endoplasmic reticulum (ER) is an intracellular organelle responsible for the coordinated synthesis, folding and trafficking of proteins. Unfolded or misfolded proteins are detected and removed from the cell via degradation by the proteasome system. Hypoxia, toxins, viral infections, and alterations in energy and substrates can lead to cell stress and the accumulation of unfolded proteins within the ER initiating an adaptive response known as the unfolded protein response (UPR) in order to regain organelle function [36]. Activation of three ER transmembrane sensors, inositol requiring enzyme-1 (IRE1α), PKR-like ER kinase (PERK) and activating transcription factor 6 (ATF6), aims at reducing unfolded proteins by increasing membrane biogenesis, halting protein translation, increasing ER-associated degradation genes and enhancing expression of ER chaperons. Activation of the UPR is reported to be involved in the pathogenesis of insulin resistance [37-39] but the underlying mechanisms are still under investigation. ER stress response has been shown to be induced by saturated FA in rats by activation of c-Jun N-terminal

kinase (JNK) which in turn can inhibit insulin signalling through serine phosphorylation and/or degradation of the insulin receptor substrate (IRS1) [37].
Several studies show the impact of adipose tissue and intrahepatic inflammation on the development of insulin resistance [40,41]. The adipose tissue macrophage content and secretion of adipose tissue inflammatory proteins (such as interleukin 6 (IL-6), tumour necrosis factor α (TNFα) and chemokine (C-C motif) ligand 2 (CCL2)) are greater in obese than lean subjects [42] and in subjects with NAFLD compared to BMI-matched subjects with normal intrahepatic TG content [43], but the relative contribution in comparison with other potential factors for insulin resistance is not known. Several studies have demonstrated that cytokines increase adipose lipolysis which in turn may contribute to insulin resistance [44-46]. Also, altered adipocyte biology in obesity leads to a shift in other adipocytokines released from these cells: while leptin and resistin are produced to a larger extent, adiponectin release is reduced, all together leading to worsened insulin sensitivity and the development of metabolic syndrome [47]. In addition, the activation of hepatocellular NF-κB is reported to be involved in insulin resistance by upregulating the production of pro-inflammatory cytokines, such as IL-6, that often affect insulin action [48,49].

Insulin resistance is a feature of T2D, wherein patients demonstrate a relative lack of insulin despite primarily functional β-cells of the pancreas and thus have hyperglycaemia and are glucose intolerant. In contrast, patients with type 1 diabetes have an absolute lack of insulin due to the destruction of β-cells in the pancreas. The majority of patients with diabetes suffer from T2D (~90%), and its prevalence is drastically increasing in parallel with its main cause, obesity [50]. In 2010 there were approximately 285 million people diagnosed with the disease compared to around 30 million in 1985 [51]. Long-term complications from high blood glucose can include CVD, stroke, diabetic retinopathy where eyesight is affected, kidney failure, and poor blood flow in the limbs leading to amputations [52]. Since T2D is mainly associated with obesity and the metabolic syndrome, they share the same risks and the same strategies for treatment and prevention.

1.2.5 Mouse models for metabolic disorders

Due to ethical and practical limitations in regards to tissue collection and therapeutic interventions (e.g. testing of drugs) in humans, animal models have become an important tool for gaining insights into the underlying mechanisms of human diseases, their risks and progression profile as well as to study approaches for therapy. About 99% of mouse genes have a homolog in human [53]. Metabolic, physiological and behavioural stresses can be tested in mice and in many cases mouse models mimic the situation in humans [54]. Thus, mouse models are an adequate animal model for studying the biology of metabolic disorders such as obesity, diabetes or altered lipid metabolism, and may help to identify novel genes contributing to the onset or prevention of diseases [55].

In order to translate results found in laboratory model systems to the clinical situation and subsequently to the development of therapeutic or prevention strategies of the disease, it is

important that the animals model used to study metabolic disorders incorporate the pathological patterns and histological alterations found in the course of the disease, such as weight gain, dyslipidaemia or insulin resistance [56].

Several mouse lines have been established that serve as experimental models for metabolic diseases. Among them are the most frequently used monogenic mouse models for obesity and diabetes (leptin receptor deficient *db/db* mice [57,58] and leptin deficient *ob/ob* mice [59]) and a polygenic mouse model for obesity and pre-diabetes (NZO mice [60]). Similar to *db/db* mice, the Zucker rat has a loss of the leptin receptor and shows similar phenotypes [61,62]. In recent years, studies have revealed that melanocortin or the melanocortin receptor (MC4R) critically regulate food intake and body weight [63], and so MC4R deficient mice are more frequently being used to study the development of late-onset obesity [64]. Furthermore, metabolic dysfunction can be induced in healthy wild type mice by environmental interference. In some mouse strains, long-term feeding a diet rich in fat (HFD) results in obesity, impaired glucose tolerance, dyslipidaemia, expression of pro-inflammatory cytokines, oxidative stress, increased sensitivity to endotoxins and an impaired function of the intestinal barrier [65,66] closely resembling the pathological and molecular alterations found in humans with NAFLD. The severity, progression and specific features of the disease depend not only on the amount of dietary fat (30-75% of total calories) but also on the quality of fat and fatty acid composition. In addition, not every mouse strain is similarly responsive to a HFD [67]. C57Bl6/J mice for example develop more severe diet –induced insulin resistance than A/J mice [68]. High fat diets are furthermore used to promote the development of NASH from steatosis in genetic animal models (e.g. *ob/ob* mice). A more severe degree of liver damage can be obtained by feeding a diet deficient in methionine and choline (MCD) [69,70]. Mice fed a MCD diet rapidly (with 2-3 weeks) develop steatosis and subsequently necrosis and liver injury due to enhanced hepatic uptake of fatty acids and impaired secretion of VLDL particles from the liver, processes for which methionine and choline are essential in human and mouse. Despite causing faster and more severe NASH, the MCD diet lacks some characteristics of NAFLD found in humans, such as insulin resistance and obesity. On the contrary, it is reported that mice on MCD diet lose up to 35% of their body weight within 4 weeks [70]. In addition to the diets mentioned, researchers emphasise that a shift in dietary pattern towards a sugar-rich diet may also be a risk factor for the development of NAFLD in humans, and hence, nowadays, also fructose-rich diets or “western style diets” (fast food diets) containing a combination of fat and sugar are used to study NAFLD [71-74]. Moreover, the prevalence of the metabolic syndrome and NASH are increased with aging since the onset of obesity and diabetes increases with age [75-77], and natural physiological changes inherent to the process of aging may trigger or promote the development of the metabolic syndrome later in life. Therefore, aged mice can also be used to study the onset and progression of fatty liver diseases and metabolic disorders.

For this work both genetic and diet-induced models of obesity models were used, namely *db/db*, *ob/ob*, NZO/NZB mice as well as HFD and MCD diet. Also, geriatric mice were used for analysis.

1.3 The liver and its role in health and disease

As described in section 1.1, the balance of energy storage and breakdown is essential for the maintenance of whole body energy homeostasis. The discontinuity in supply and demand for energy therefore requires the adaptation and coordination of the organism at several, from cellular integration of nutrient/hormonal signals to inter-organ communication and assimilation. Each major metabolically active organ, such as liver, adipose tissue, muscle, pancreas, intestines and brain, senses and integrates nutritional, neural and endocrine signals and can thereby participate in carbohydrate, lipid and amino acid metabolism in a tissue-specific manner.

It is commonly accepted that the liver, being the largest internal organ and gland of the human body, is a pivotal contributor to metabolic control. Nutrients, hormones or drugs are delivered to the liver principally by the portal vein which transports its content from the gastrointestinal tract and the spleen directly to the liver. Due to this central position, the liver has a wide range of functions, including uptake and digestion of nutrients, detoxification, protein synthesis and hormone production. The liver consists of different cell types: parenchymal and non-parenchymal cells. The liver parenchymal cells, also called hepatocytes, make up 80% of the liver volume. The remaining non-parenchymal cells are mainly endothelial cells, hepatic stellate cells, immune reactive Kupffer cells, and natural killer cells [78].

1.3.1 Liver carbohydrate and lipid metabolism

One of the liver's primary functions is the regulation of glucose, lipid and protein metabolism which is mainly controlled by insulin and glucagon, two hormones with opposing roles. Whereas glucagon triggers catabolism (break down of molecules into smaller units to release energy), insulin promotes anabolism (build-up of molecules from smaller units to store energy) (Fig. 4).

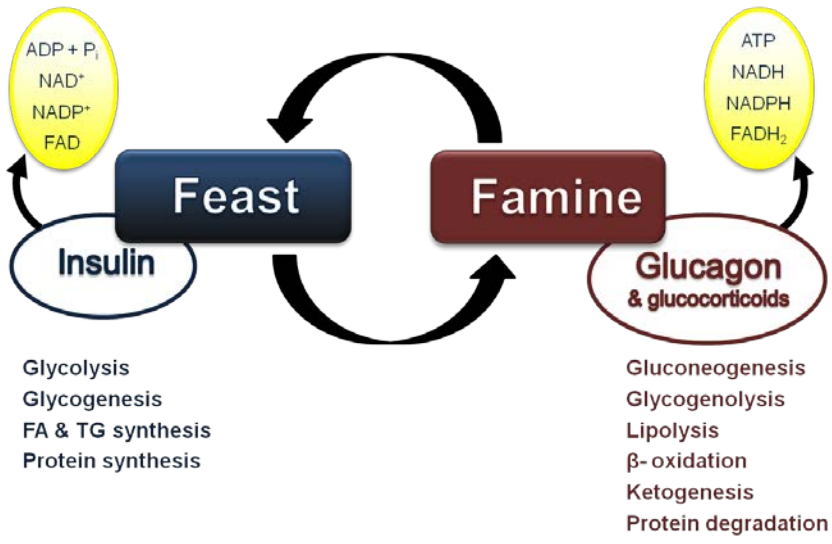

Figure 4: The role of insulin and glucagon in adaptive metabolism. While insulin (left) promotes anabolism to store energy during times of food excess, glucagon and glucocorticoids (right) trigger catabolism to release energy during times of food deprivation. Adapted and modified from Dr. Roldan de Guia, PhD Thesis, Herzig Lab.

After food intake, a first breakdown of macro-nutrients occurs in the gastrointestinal tract, where carbohydrate polysaccharides are converted into simple sugars, protein polypeptides into shorter

peptides and amino acids, and lipids hydrolysed and packed with apolipoproteins. The absorbed nutrients are then transported to the liver via the blood and lymphatic stream and enter hepatocytes via facilitated diffusion (glucose), active co-transport (amino acids) or with the help of transport proteins (FA) and receptor-mediated processes (cholesterol). During fasting, macronutrients are broken down in muscle and adipose tissue and then transported to the liver via the same route.

The fate of the nutrients, either being metabolised for energy storage or energy production, depends on the substrate availability and the metabolic state of the cell and the organism. Glucose is metabolised via the glycolytic pathway into pyruvate (Fig. 5). From there it can be converted into acetyl-CoA and either serves as energy source in mitochondria via the Krebs cycle and electron transport chain, or it is used for fatty acid, triglyceride and cholesterol synthesis (lipogenesis). Alternatively, glucose molecules can be used for the synthesis of glycogen. If this reaction is saturated, conversion of glucose into fats takes place. On the other hand, glucose can be generated either from pyruvate after degradation of proteins into amino acids or of triglycerides into glycerol (gluconeogenesis), or from glucose-6-phosphate after glycogen breakdown (glycogenolysis). Glucose can also enter the pentose-phosphate pathway via glucose-6-phosphate where it can generate metabolites needed for nucleotide synthesis and the reducing equivalent NADPH.

The blood glucose concentration is balanced through mechanisms that either produce or consume glucose. Hepatic glucose production (HGP) is regulated by the hormone insulin which is released from the pancreas when blood glucose or fatty acid levels rise. Insulin can inhibit HGP via the direct and indirect actions [79,80]. The indirect influence of insulin on HGP is mediated by the tissues that respond to insulin levels. As such, glucagon secretion from the pancreas is reduced [81], non-esterified fatty acids (NEFA) release from adipose tissue is diminished [82], the supply of gluconeogenic precursors from fat and muscle are reduced [83], and the brain provides neural input to the liver when insulin levels rise [84,85], all leading to a decrease in HGP. In experiments on conscious overnight-fasted dogs it could be shown that insulin has also a direct effect on the liver to reduce HGP [86,87]. On the other hand, a manipulation of the hepatic insulin receptor in mice did not inhibit insulin's ability to suppress HGP [88], and also a restauration of the insulin receptor in mice lacking this receptor could not restore insulin's function to reduce HGP [89]. Thus, the indirect actions of insulin seem to be dominant. Apart from insulin, also adrenaline, glucagon and somatotropin are involved in the regulation of the blood glucose concentration. Adrenaline and glucagon promote the release of glucose from depots, whereas somatotropin inhibits glucose uptake by cells. Together they are released when blood glucose levels decrease. Glucocorticoids [90] and T_3/T_4 hormones work by reinforcing the effects of adrenaline and glucagon [91].

Hormone	leads to	via	at
Insulin	Decrease	Inhibition of glucose production	Liver
		Stimulation of glucose uptake	Muscle, fat
		Stimulation of glycogensynthesis	Muscle, liver
		Stimulation of glycolysis	Muscle, liver
Glucagon	Increase	Stimulation glycogenolysis	Liver
		Stimulation of gluconeogenesis	Liver
		Inhibition of glycogensynthesis	Liver
Catecholamine	Increase	Stimulation glycogenolysis	Muscle, liver
		Inhibition of glycogensynthesis	Muscle, liver
		Inhibition of insulin release	pancreas
Glucocorticoids	Increase	Inhibition of glucose utilisation	Muscle, fat
		Stimulation of gluconeogenesis	Liver
T_3/T_4	Increase	Stimulation glycogenolysis	Muscle, liver
Somatotropin	Increase	Stimulation of gluconeogenesis	Liver
		Inhibition of glucose utilisation	Muscle, fat

Table 1: Hormonal regulation of the blood glucose concentration. Modified and adapted from Mutschler, Schaible, Vaupel: Anatomie, Physiologie, Pathophysiologie des Menschen, 6. Auflage 2007

Apart from playing a central role in the regulation of glucose homeostasis, the liver is also a key organ in the control of lipid metabolism [92]. The term lipid encompasses molecules such as triglycerides, fatty acids, phospholipids, sterol-containing metabolites such as cholesterol and others. NEFA can be taken up by the cell with the help of transport proteins such as fatty acid transport protein (FATP), fatty acid translocase (CD36), caveolin-1 and fatty acid binding protein (FABP). Once inside the cell, fatty acids can be used to generate energy during a process called β-oxidation. Therein, fatty acids are transported across the mitochondria or peroxisome membrane with the help of carnitine palmitoyltransferase-I (CPT-I) where they are broken down to acetyl-CoA which then enters the Krebs cycle to form NADH and ATP or is used to generate cholesterol or ketone bodies (ketogenesis).. Alternatively, acetyl-CoA can be used for the generation of TG which in turn are either stored in the liver or released into the circulation as very low density lipoprotein (VLDL) particles. Instead of being used as energy source, FA can also be converted into other lipid species such as sphingolipids and glycerophospholipids. Taken together, TG and FA within the liver come from four different sources: (1) from the diet, (2) *de novo* lipogenesis (DNL), (3) from lipolysis in adipocytes, and (4) cytoplasmic TG stores. Cholesterol, which is either taken up by the liver from the diet or synthesized from acetyl-CoA, is used as a component of biomembranes and for the synthesis of bile acids, steroid hormones (e.g. androgens, oestrogens, and glucocorticoids) and vitamin D.

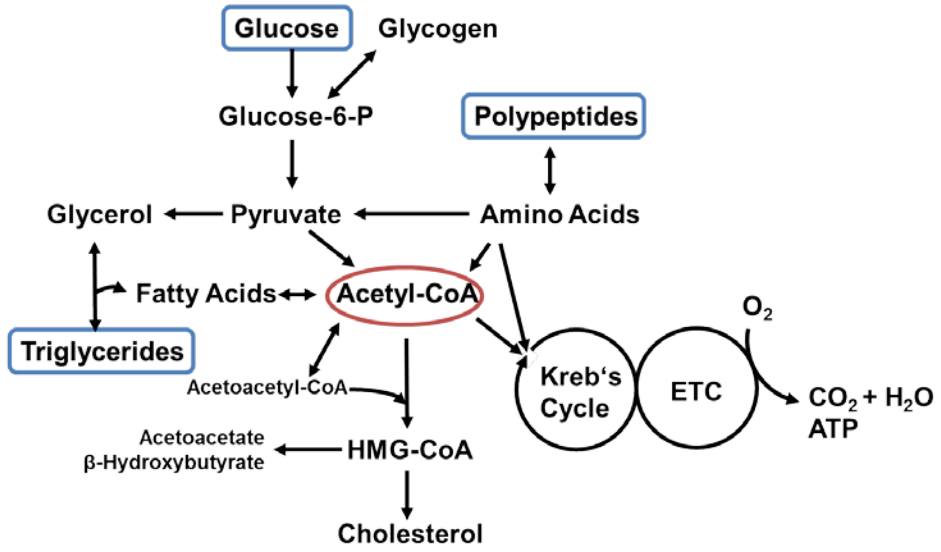

Figure 5: Metabolism of carbohydrates, lipids and proteins in hepatocytes. ETC, Electron transport chain. Adapted and modified from Dr. Roldan de Guia, PhD Thesis, Herzig Lab.

1.3.2 The lipoprotein pathway

Due to their hydrophobic nature, TG and cholesterol have to be transported through the blood circulation in lipoproteins. Lipoproteins are composed of an outer shell containing amphipathic phospholipids, non-esterified cholesterol and apolipoproteins, and an inner core containing the TG and cholesterol esters. They can be classified according to their sizes and densities which are the result of their composition (Table 1). Furthermore, the composition of each lipoprotein particle determines where it will be metabolised.

Lipoprotein	Density [g/dL]	Diameter [nm]	Apolipoproteins	Lipid composition [%]		
				TG	C	P
Chylomicrons	< 0,930	75-1200	B48, E, A1, A2, A4, C2, C3	80-95	2-7	3-9
VLDL	0,930-1,006	30-80	B100, E, C2, C3	55-80	5-15	10-20
IDL	1,006-1,019	25-35	B100, E	20-50	20-40	15-25
LDL	1,019-1063	18-25	B100	5-15	40-50	20-25
HDL	1,063-1,21	5-12	A1, A2, A5	5-10	15-25	20-30

Table 2: Characteristics of lipoprotein particles. VLDL, very low density lipoprotein; IDL, intermediate density lipoprotein; LDL, low density lipoprotein; HDL, high density lipoprotein; % lipid content indicates percentages of triglycerides (TG), cholesterol ester (C) and phospholipids (PL) within the respective lipoprotein class, the remaining part consists of apolipoproteins. The density was determined by ultracentrifugation and the diameter by gel electrophoresis. Adapted from [93].

The formation and degradation of lipoproteins can be summarised in the lipoprotein pathway (Fig. 6). This pathway can be divided in to three arms: (1) the transport of TG and cholesterol from the diet (exogenous pathway), (2) the transport of hepatic lipids (endogenous pathway), and (3) the reverse cholesterol transport (RCT). TG from the diet cannot be absorbed by the duodenum and

are first hydrolysed into monoacylglycerol and free fatty acids and subsequently moved to absorptive enterocytes in the intestines. There TG are rebuilt from their fragments and packaged with apolipoproteins and cholesterol to form chylomicrons which are collected by the lymph system and transported to the large vessels near the heart before entering the blood circulation. The chylomicrons serve first muscle and adipose tissue with energy. TG in lipoproteins cannot be taken up by the cell directly and have to be first converted into NEFA and monoacylglycerol by lipoprotein lipases (LPL) which is on the wall of the capillaries in the peripheral tissues [94]. The TG-depleted chylomicron remnants containing cholesterol esters are then recognized by the liver [95], where the cholesterol esters are taken up by the cell via receptor-mediated processes involving the low-density lipoprotein receptor (LDLR), lipolysis-stimulated lipoprotein receptor (LSR), LDLR-related protein (LRP), and the scavenger receptor 1 (SRB1).

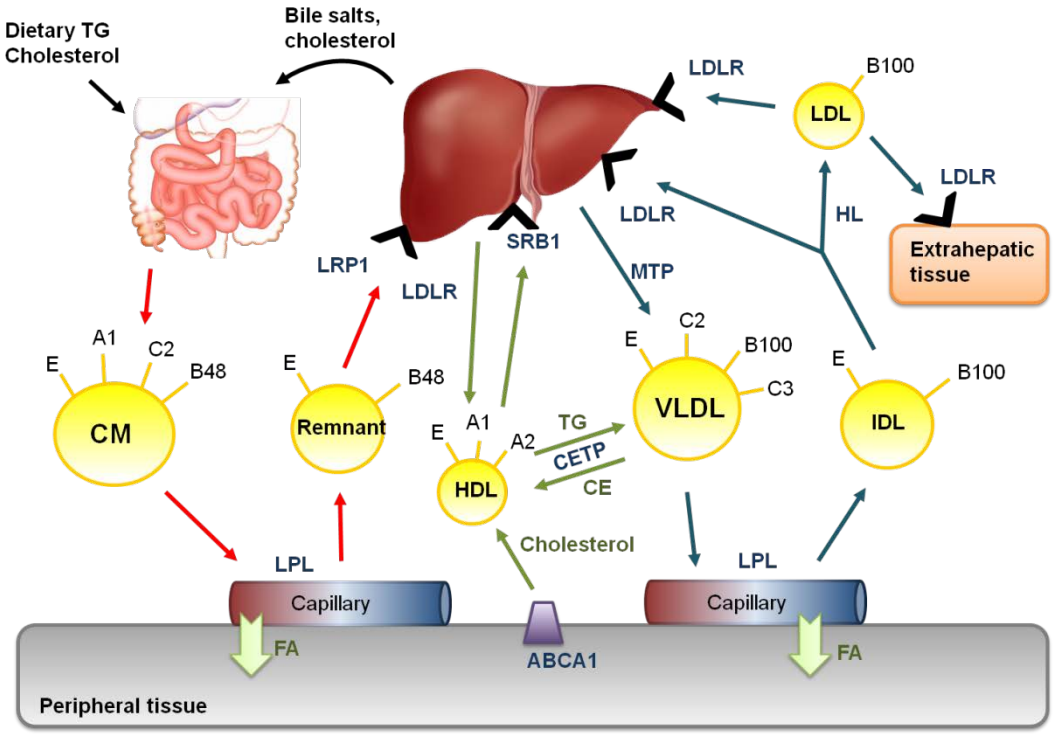

Figure 6: The lipoprotein pathway. Shown are the exogenous (red arrows) and the endogenous lipoprotein pathway (blue arrows), as well as the reverse cholesterol transport (green arrows). For details, see text. TG, triglyceride; CM, chylomicrons; LPL, lipoprotein lipase; FA, fatty acid; HDL, high density lipoprotein; VLDL, very low density lipoprotein; IDL, intermediate density lipoprotein; LDL, low density lipoprotein; ABCA1, ATP-binding cassette protein 1; CETP, cholesteryl ester transfer protein; CE, cholesteryl ester; LRP1, LDLR-related protein 1; LDLR, low-density lipoprotein receptor; SRB1, scavenger receptor 1; HL, hepatic lipase; E, A1, A2, C2, C3, B48 and B100 refer to apolipoproteins. Adapted and modified from [96,97].

VLDL particles, together with IDL and LDL, are the major transport vehicles of the endogenous lipoprotein pathway. VLDL particles are assembled in the endoplasmic reticulum (ER) which is strictly regulated by TG availability and regulatory proteins such as microsomal TG transport protein (MTP). The structure of VLDL particles resembles that of chylomicrons [98]. VLDL particles are hydrolysed in peripheral tissues by LPL, thereby providing adipose tissue and muscle with energy in the form of fatty acids. IDL particles result from VLDL breakdown and can be taken up by the liver via LDL receptors. IDL is further hydrolysed by hepatic lipase to low

density lipoprotein (LDL) with cholesterol-esters as main cargo. LDL can be cleared by the liver but in humans, the major amount of cholesterol is transported in the LDL fraction into the periphery. There they can be oxidized and taken up by macrophages leading to the formation of so called lipid filled foam cells. Foam cells can aggregate within the arterial wall and subsequently form atherosclerotic plaques which are associated with myocardial infarction and stroke [97].

Whereas cholesterol is transported to the periphery via LDL particles, it is carried back to the liver via HDL particles in a mechanism called the reverse cholesterol transport (RCT) [99-101]. It is due to these functions of LDL and HDL that they are called “Bad and good cholesterol” by the general public. Whereas an increase in LDL particles is associated with increased risk for atherosclerosis and heart disease, an increase of HDL is reported to have beneficial effects on health [102]. HDL is synthesized by the liver or intestine together with ATP-binding cassette protein 1 (ABCA1) of the peripheral tissues. The liver can take up these HDL particles via SRB1. Alternatively, some cholesterol-esters are transferred from HDL to VLDL particles in exchange for TG with the help of cholesteryl ester transfer protein (CETP). VLDL particles are then hydrolysed to IDL and LDL and either taken up by the liver or peripheral tissues. Either way, cholesterol transported to the liver can now be excreted in the form of bile salts.

1.3.3 Dyslipidaemia and insulin resistance

As already mentioned in 1.2.3, obese and diabetic individuals suffer from failure to suppress hepatic glucose production and FA efflux from adipose tissue, as well as defective fasting-induced skeletal muscle lipids utilisation. Furthermore, the transition from FA efflux to storage in response to a meal is also compromised in these disease states. The rate of release of FA from adipose tissue and delivery to the liver and muscle is increased in obese persons with NAFLD, which results in an increase in hepatic and muscle FFA uptake. As a consequence intracellular FAs accumulate within hepatocytes without further oxidisation. Instead, they are esterified to TG and stored within lipid droplets. Predominantly due to increased VLDL secretion by the liver as a compensatory reaction to the increased FA esterification, lipoprotein metabolism is disturbed in these individuals, a state called dyslipidaemia [103,104]. Once in the serum, cholesterol-ester transfer protein (CETP) transfers TG and cholesterol between VLDL and HDL or LDL leading to a reduction HDL and an accumulation of LDL particles. In addition, VLDL and LDL clearance are impaired with insulin resistance. Thus, the characteristics of this pathologic state are increased plasma TG and LDL-cholesterol levels, while HDL-cholesterol is decreased [105].

There are different approaches to treat dyslipidaemia. One of them is a change of lifestyle as it has been also proposed for the treatment of the metabolic syndrome (see. 1.2.2). Other strategies aim at personalised medicine in form of pharmaceutical intervention. In that regard it had been suggested to administer drugs such as statins or fibrates which can help to reduce risk for developing atherosclerosis [106,107]. However, statin treatment can have adverse effects such as hepatotoxicity [108] and myopathy [109]. Other pharmacologic agents for the treatment of

dyslipidaemia are the cholesterol-absorption inhibitor ezetimibe, the lipolysis inhibitor niacin, bile acid sequestrants and omega-3 fatty acids [110,111].

Hepatic accumulation and increased hepatic release of TG observed in obese and diabetic patients is associated with insulin resistance [27,112]. Genetic rodent models that have altered expression of lipid transport proteins, such as LPL, LSR or CD36, provide evidence for the role of ectopic lipid accumulation in the pathogenesis of insulin resistance [95,113,114]. Moreover, it has been shown that in humans, the ectopic storage of fat in the liver, more so than skeletal muscle or adipose tissue, is associated with impaired metabolism [115,116]. The mechanisms of action might involve hepatokines, proteins released from the steatotic liver [117,118]. Furthermore, the incomplete oxidation of FA generates ketone bodies and acylcarnitines, which might also have adverse effects on insulin action, potentially linking mitochondrial dysfunction to insulin resistance [119]. However, the interaction between mitochondria and insulin sensitivity is very complex and controversial, and might not only be tissue-specific, but also dependent on the site of the impairment [120,121].

The cellular mechanisms responsible for FA-induced insulin resistance in muscle and liver are not completely clear (Fig. 7). It is suggested that excessive intracellular lipid intermediates generated by FA metabolism, in particular, diacylglycerol (DAG), long-chain fatty acyl-CoA, ceramide, lysophosphatidic acid (LPA), and phosphatidic acid (PA), can have adverse effects on insulin action [35,122-124]. They might interfere with insulin action by activating protein kinase C (PKC), mammalian target of rapamycin (mTOR) and nuclear factor κB (NF-κB), and inhibiting AKT. But in current literature, it is questioned whether a defect in insulin signalling is obligatory for causing insulin resistance [125]. Some investigators have proposed that insulin's ability to suppress hepatic glucose output does not require the canonical insulin signalling pathway [88,89,126] nor AKT as an obligate intermediate for proper insulin signalling [127]. It is speculated that within the liver not only a linear (canonical) insulin signalling pathway exists (via insulin receptor→insulin receptor substrate (IRS)→ phosphatidylinositol-3-kinase (PI3K)→ 3-phosphoinositide dependent protein kinase-1 (PDPK1)→AKT) to activate or suppress forkhead box protein O1 (FOXO1), but also a non-canonical pathway independent of AKT which has yet to be identified. The divergent point of the non-canonical pathway from the canonical pathway could reside between IRS and AKT, specifically downstream of PDPK1 which affects not only AKT but also an atypical protein kinase C (aPKCλ), thereby controlling gluconeogenesis [128]. Alternatively, it is postulated that a non-autonomous pathway exists which includes adipose signalling to hepatocytes via free fatty acids. In this model the insulin resistance of adipose tissue, particularly visceral adipose, to suppress NEFA production leads to hepatic NEFA oversupply and thus impaired insulin suppression of HGP through an as yet undefined mechanism [129-131]. The discrepancy about the major underlying mechanism responsible for insulin resistance and the metabolic syndrome shows how much more investigation is needed in order to define the responsible players and thus, for the development of treatment strategies.

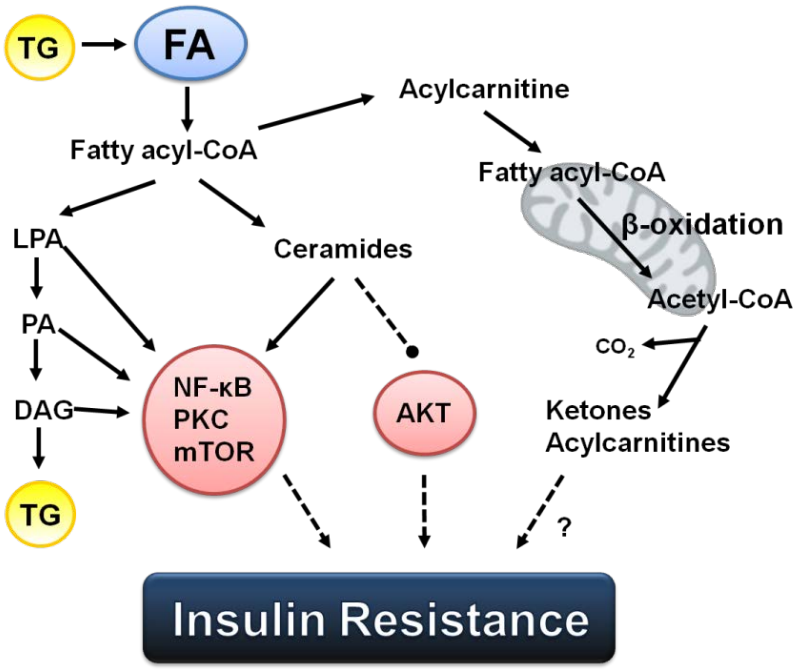

Figure 7: Fatty acid metabolism and insulin resistance. Potential cellular mechanism that might link the accumulation of fatty acids (FA) and their lipid intermediates to the development of insulin resistance. TG, triglyceride; FA, fatty acid; LPA, lysophosphatidic acid; PA, phosphatidic acid; DAG, diacylglycerol; NF-κB, nuclear factor κB; PKC, protein kinase C; mTOR, mammalian target of rapamycin; AKT, protein kinase B. Adapted and modified from [23].

1.4 Growth arrest and DNA damage-inducible 45 (GADD45) gene family

Starvation as well as an oversupply of nutrients, both severe stresses for the organism, requires adaptation to these situations on many levels, from the single cell to the communication between organs, in order to maintain homeostasis. As for every environmental or physiological stress, the cellular response is very complex, involving countless interconnected and associated pathways, with an abundance of regulators and effectors.

The metabolic challenges described so far lead to adaptive changes in cell signalling, ultimately leading to ER stress, mitochondrial dysfunction or inflammation. As soon as the cells cannot cope anymore with the stress situation they are confronted with, they go into programmed cell death (apoptosis). Indeed, it is described that apoptosis is associated with insulin resistance and different degrees of NAFLD [132-135], and is often linked to an excess of unoxidised long-chain fatty acids (lipoapoptosis) [136].

Apoptosis is often also triggered by other environmental agents, such as ionizing radiation (X-rays) or nonionizing radiation (UV light), physiological processes which produce activated oxygen species and other reactive molecules, or alkylating agents, such as methyl methanesulfonate (MMS). They all have in common that they induce DNA damage. Genotoxic stress which leads to DNA damage is unavoidable, and cells have developed mechanisms to deal with its consequences and to maintain their integrity. DNA damage can be repaired during cell cycle arrest by various base-excision repair mechanisms [137]. However it will induce apoptosis if

damage is extensive and repair efforts fail. Whether a cell is getting repaired from DNA damage or undergoes apoptosis depends on the severity of the damage and the cell-type, but how the underlying pathways, such as the ATM/p53 tumour suppressor pathway [138,139] or the p38/JNK kinase pathway [140-142], interact to decide whether it comes to cell cycle arrest or cell death is not fully understood. Key players in the perception and coordination of cellular stress are the members of the Growth arrest and DNA damage-inducible (GADD) 45 family.

GADD45 genes were first cloned in the late 1980s and early 1990s [143-146]. There are three family members: GADD45α (former GADD45), GADD45β (former MyD118), and GADD45γ (former CR6) which are located on three different chromosomes (chromosome 1, 19, and 9 for GADD45α, GADD45β and GADD45γ, respectively). The best described member of the GADD45 family is GADD45α. Distinct isoforms for GADD45α and GADD45γ are produced through alternative splicing [147], but it has not been established yet whether there is a functional difference between these isoforms. They are evolutionary conserved and share 55-57% overall identity at the amino acid level. They are small (18kDa), highly acidic (pI=4,0-4,2) and are localised primarily within the cell nucleus [148,149]. GADD45 proteins are able to form homo- and hetero-dimers [150-152], and are differentially expressed in several tissues including heart, brain, spleen lungs, liver, skeletal muscles, kidneys, and testes [144]. GADD45 proteins are non-enzymatic. Their actions are executed through interactions with protein partners or the modulation of DNA/RNA accessibility to other proteins. The interaction of GADD45 proteins with their partner protein is regulated at the level of expression, cellular localisation and posttranslational modification of both interaction partners. Indeed, GADD45 proteins were observed to harbour several threonine and tyrosine phosphorylation as well as acetylation sites [153].

1.4.1 GADD45 proteins in stress responses: the dual role in apoptosis and survival

It has been shown that GADD45 proteins function as stress sensors and are implicated in the control of cell cycle arrest [154], DNA repair, cell survival [155,156], tumour development, senescence and apoptosis where they act in a synergistic manner [157-159]. Therefore they physically interact with other cellular proteins that are involved in cell cycle regulation and stress response, such as proliferating cell nuclear antigen PCNA [148,160-162], p21 (p21/WAF1/CIP1 also known as cyclin-dependent kinase inhibitor 1) [148,149,162], Cdc2/cyclinBI [159,163,164], or MEKK4 (also MAP3K or MTK1) [165] (Fig. 9). Furthermore, GADD45α was the first stress-induced protein discovered that was transcriptionally regulated by p53 [166,167] with the p53 binding site being in the third intron of GADD45 [168]. Whether GADD45 proteins exert a pro- or anti-apoptotic function depends on the severity of DNA damage. For example, in the case of irreparable damage, increased expression of GADD45β triggers apoptosis via TGFβ→MEKK4→p38/JNK and blockage of GADD45β suppresses apoptosis induced by TGFβ [169,170]. In the case of moderate DNA damage, GADD45β acts as anti-apoptotic agents via inhibition of the MKK7→JNK pro-apoptotic pathway [152,171,172] (Fig. 8).

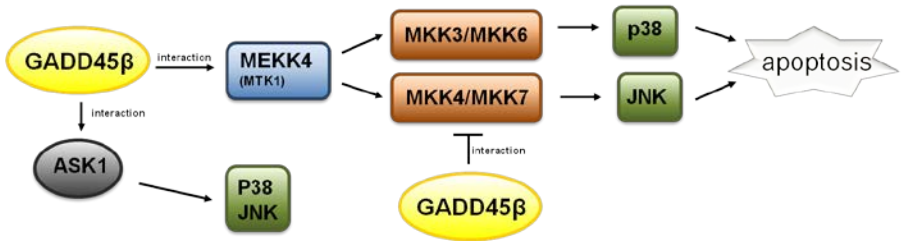

Figure 8: The dual role of GADD45β in apoptosis and survival. GADD45β induction can either lead to apoptosis via MEKK4→p38/JNK, or prevent apoptosis by inhibition of the MKK7→JNK pro-apoptotic pathway, depending on the severity of the DNA-damage. GADD45, growth arrest and DNA damage-inducible 45; MEKK4, MAP kinase kinase kinase 4; p38, p38 mitogen-activated protein kinases; JNK, c-Jun N-terminal kinase; ASK1, Apoptosis signal-regulating kinase 1; MKK3/6/4/7, MAP kinase kinase 3/6/4/7.

The implication of GADD45 proteins in DNA repair links them to their role in epigenetics. They are able to facilitate the physical approach of several proteins to DNA through active DNA demethylation [173-176], chromatin remodelling [177] and post-transcriptional RNA regulation [178].

GADD45 proteins have similar, but not identical functions along different stress response pathways. Each protein has a different pattern of cell-specific [144,179] and stimulus-induced expression, regulation and interaction partners, presumably reflecting different signaling pathways. For example, whereas *Gadd45a* expression is simulated by physical or chemical stress (UV radiation, X-rays, γ-radiation, low-frequency electromagnetic fields, hypoxia, hyperosmosis, low pH, arsenic, cisplatinum, methyl methanesulfonate, ethanol, cigarette smoke condensate and others), different inducers of oxidative stress including sodium arsenite as well as inflammatory (IL-6, IL-12 and IL-18) and pro-apoptotic cytokines (TGFβ and TNFα) stimulate the expression of *Gadd45b* and *Gadd45g* (see suppl. table 1 for references).

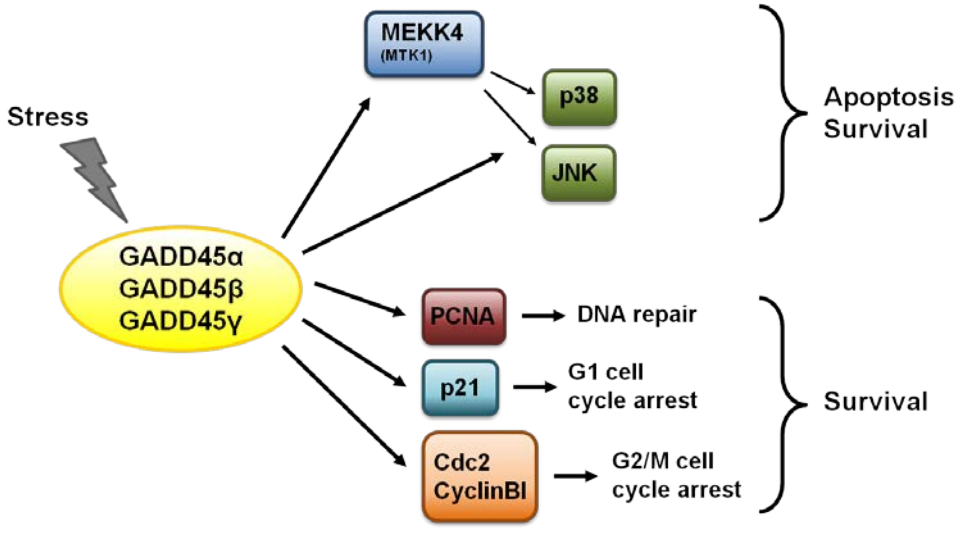

Figure 9: GADD45 proteins in stress response. GADD45 proteins physically interact with other proteins during stress response. GADD45, growth arrest and DNA damage-inducible 45; MEKK4, MAP kinase kinase kinase 4; JNK, c-Jun N-terminal kinase; PCNA, proliferating cell nuclear antigen; cdc2, cell division cycle 2. Adapted and modified from [180].

1.4.2 GADD45 proteins in cell differentiation, the immune response and neuronal function

Apart from playing a role in the cell's fate by controlling the balance between DNA repair, apoptosis or senescence, GADD45 proteins are also implicated in other cellular processes. It was shown that GADD45 family members play an important role in cell differentiation, both during embryogenesis and throughout adulthood. For example, GADD45γ is involved in neuronal differentiation [181,182] and development of male gonads [183], and GADD45β is required for somite segmentation [184], differentiation of chondrocytes [185] and neural development [186]. Furthermore, all three GADD45 proteins are important players in myeloid differentiation and thus haematopoiesis [143,187]. Apart from influencing differentiation, GADD45 proteins are crucial for maintaining a stem cell pool [188]. Moreover, GADD45 proteins contribute to survival not only at the cellular level but also by modulating the immune response on the organismal level. Especially GADD45β and GADD45γ stimulate proliferation of T helper 1 (Th1) cells and activation of the immune system [189,190], thereby contributing to enhanced immune surveillance [191] and elimination of cells that might display autoimmune behaviour [192]. Through the involvement of GADD45 family members in neuronal differentiation [193] and demethylation, they are also implicated in other neuronal functions [194]. As such, it has been shown that GADD45β is crucial for axonal plasticity [195], brain recovery and long-term memory [196].

1.4.3 GADD45 proteins in stress signalling

The common basis of all actions of all three GADD45 family members lies in the connection of upstream sensors and downstream effectors. Thus, their effect is stimulus- and cell type-dependent, as well as variable due to different (downstream) interaction partners. In most cases, in response to stress, the GADD45 proteins stimulate the p38/JNK MAPK signalling pathway, thus increasing the sensitivity of cells to growth arrest, apoptosis or survival [165,169,190,197,198] (Fig. 11). For example, GADD45 proteins bind to an N-terminal domain of MEKK4 (MTK1) (amino acids 147 – 250) thereby inducing a conformational change of MEKK4 which leads to a dimerization, auto-phosphorylation and activation of MEKK4 [165], which results in JNK and p38 activation. GADD45β is also an interaction partner of MKK4 [155] and MKK7 [199] (Fig. 10), thereby functioning as an inhibitor of both proteins and preventing hereby the activation of JNK, as well as of apoptosis signal-regulating kinase 1 (ASK1) [199] which also activates JNK and p38 [200] (Fig. 8).

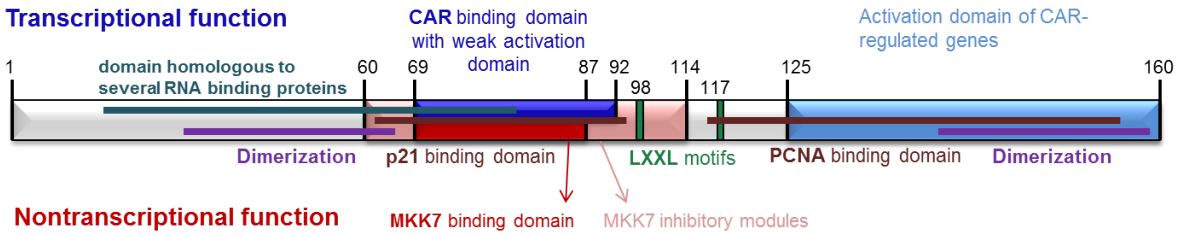

Figure 10: The GADD45β peptide and its functional domains. GADD45β, as all GADD45 family members, is described to bind several upstream sensors, such as the constitutive androstane receptor (CAR), as well as downstream effectors, such as MAP kinase kinase 7 (MKK7), cyclin-dependent kinase inhibitor 1 (p21) and proliferating cell nuclear antigen (PCNA). Furthermore, it is reported that GADD45 proteins can form dimers and have hence a dimerization domain. Moreover, the GADD45β peptide shows a LXXL motif (a sequence of 5 amino acids where L = leucine and X = any amino acid) and a RNA binding domain.

Importantly, GADD45 proteins and stress kinases seem to form a feedback loop with GADD45 proteins not only modulating the activity of stress kinases, but also being under the control of p38 and JNK kinases [201]. In addition to their described role in MAPK stress signalling, GADD45 family members are also important regulators in several other pathways. For example, GADD45β mediates TGF-β-induced cell death [169,170], but CAR-induced cell survival [202-204] (Fig. 11). It is noteworthy, that GADD45β confers a transcriptional function upon CAR-stimulation and –binding, hence also having a role as transcriptional coactivator beside its impact on protein activity (Fig. 10). In accordance to this finding, GADD45 also possesses a domain homologues to several other RNA binding proteins and a so-called LXXL motif (a contiguous sequence of 5 amino acids where L = leucine and X = any amino acid) characteristic for transcriptional co-regulators [205].

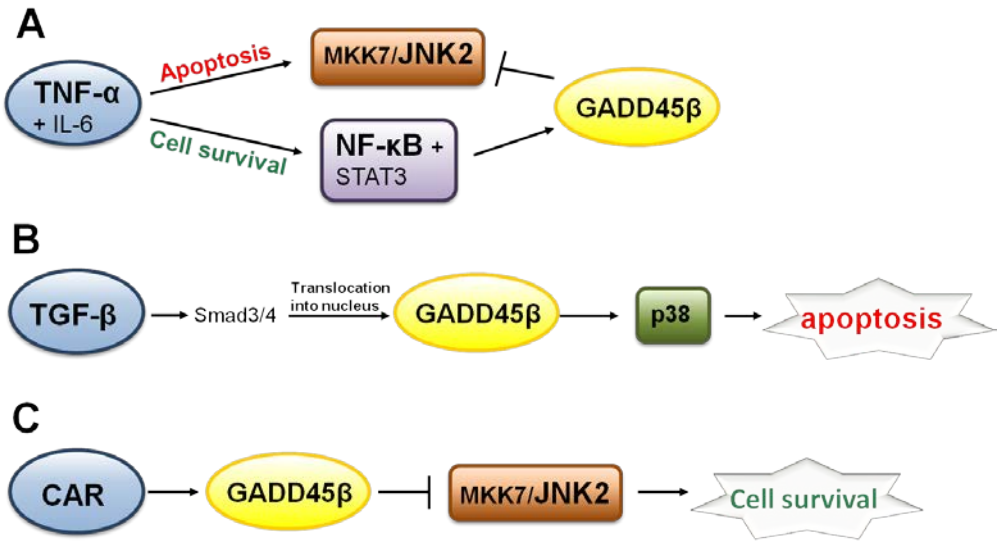

Figure 11: GADD45β in stress signalling. GADD45β has pro- and anti-apoptotic functions, dependent on the stimulus and interaction partners. It can prevent tumour necrosis factor α (TNF-α)-induced apoptosis by inhibiting MKK7→JNK (A). Alternatively, it mediates transforming growth factor β (TGF-β)-induced apoptosis (B), or constitutive androstane receptor (CAR)-stimulated cell survival (C). GADD45β, growth arrest and DNA damage-inducible 45 β; p38, p38 mitogen-activated protein kinases; JNK2, c-Jun N-terminal kinase 2; MKK7, MAP kinase kinase 7; NF-κB, nuclear factor κB; STAT3, signal transducer and activator of transcription 3; Smad3/4, Mothers against decapentaplegic homolog 3/4.

1.4.4 GADD45 proteins in aging and age-related diseases

The basic processes described so far, where GADD45 proteins are implicated in (DNA repair, cellular survival, senescence and apoptosis), are linked to aging and age-related diseases. In general, the ability to cope with stress situation is important for animal survival and longevity [206], and the overexpression of stress-related proteins (such as sirtuins, heat shock proteins, superoxide dismutase, or catalase) in certain tissues leads to longer life span of model organisms [207]. As such, the stress-associated GADD45 proteins are also involved in aging, longevity and age-related diseases [208]. An orthologue of GADD45α in Drosophila, D-GADD45, has been described to be a longevity regulator [209] by conferring stress-resistance [210] and delaying neurodegeneration [211] without compromising life quality factors such as physical activity and female fertility.

Aging is a major risk factor for cancer. The anti-tumour activity of GADD45 proteins was shown both *in vitro* and *in vivo* studies. Whereas ectopic expression of GADD45 members induced apoptosis in several tumour cell lines [148,157,198,212-215], deletion of GADD45 members resulted in genomic instability [216], increased sensitivity to carcinogenesis [217], and lower immune response against implanted tumour cells [191,218]. Furthermore, GADD45 genes are deleted or silenced in several tumour identities by hypermethylation [215,219]. Such epigenetic changes typically occur with advanced age [220]. In contrast to this anti-cancer role (e.g. in Ras-driven breast cancer) are reports that GADD45 proteins promote cancer growth (e.g. Myc-driven breast cancer). This opposing function may depend on the type of oncogenic stimuli [221].

GADD45 proteins are also involved in other age-related diseases. For example, GADD45α is highly expressed in neurons of Alzheimer's disease patients where it is thought to protect the neurons from apoptosis induced by extracellular accumulation of β-amyloid [222,223]. GADD45α is also upregulated in an *in vitro* model for dopamine-induced neurotoxicity which is related to the pathogenesis of Parkinson's disease [224]. Thus, increased expression of GADD45α in age-related neurodegeneration might be a protective mechanism against neuro-toxic stress. The same could also be the case for atherosclerosis [225].

1.4.5 GADD45 proteins in metabolism

Taken together, GADD45 proteins are characterised by a plenitude of actions. A decreased induction of GADD45 members may have large-scale consequences, such as accumulation of DNA damage, genomic instability, and disrupted cellular homeostasis, which are hallmarks of aging and aging-related disorders such as tumorigenesis, reduced responsiveness to stress, and immunological and metabolic disorders [208]. In contrast, even though they are interesting candidate genes, there are only few studies describing a role for GADD45 members in metabolic function. Specifically, GADD45β has been described to be involved in hyperplasia of hepatocytes [203,204] and to promote survival in liver regeneration [226] which is known to have a metabolic requirement [227]. Moreover, GADD45β plays a role in the phosphorylation of the autophagy

regulator autophagy protein 5 (ATG5) through MEKK→p38α and thereby inhibiting starvation-induced autophagosome-lysosome fusion and, thus, autophagy [228,229]. Also, GADD45γ has been reported to have regulatory functions in metabolism, being induced by cold and playing a role in adaptive thermogenesis by activating uncoupling protein a (UCP1) via p38→oestrogen-related receptors γ (ERRγ) [230]. Furthermore, GADD45α was implicated in promoting muscle atrophy upon fasting, muscle immobilization, and muscle denervation by causing reprogramming of muscle gene expression. It was shown to be a downstream effector of activating transcription factor 4 (ATF4) during fasting-induced muscle atrophy [231], but is induced by histone deacetylase 4 (HDAC4) in denervated muscle where ATF4 is not involved [232].

It is also suggested that GADD45 proteins have anti-diabetic potential. GADD45α is potently induced by the peroxisome proliferator-activated receptor γ (PPARγ) agonist and anti-diabetic drug Troglitazone [233,234], and GADD45β expression is increased by insulin by activating the mammalian target of rapamycin (mTOR) pathway [235]. It is speculated that the underlying mechanism might involve the GADD45β-mediated inhibition of the TNFα-induced JNK pathway which is implicated in the development of insulin resistance [236,237].

2. Aim of the study

The aim of my PhD studies was to identify novel regulatory functions of GADD45 proteins for systemic metabolism, with special emphasis on GADD45β. Therefore, hepatic GADD45β was characterised in various mouse models of metabolic diseases as well as under the stress of nutrient depletion. GADD45β knock down and overexpression tools were generated in order to investigate its potential relevance in *in vivo* loss- and gain-of-function experiments. My final goal was to define a novel control level of hepatic energy homeostasis and to describe a novel role for GADD45β in the transition of pre-diabetic obesity to malign obesity and type 2 diabetes.

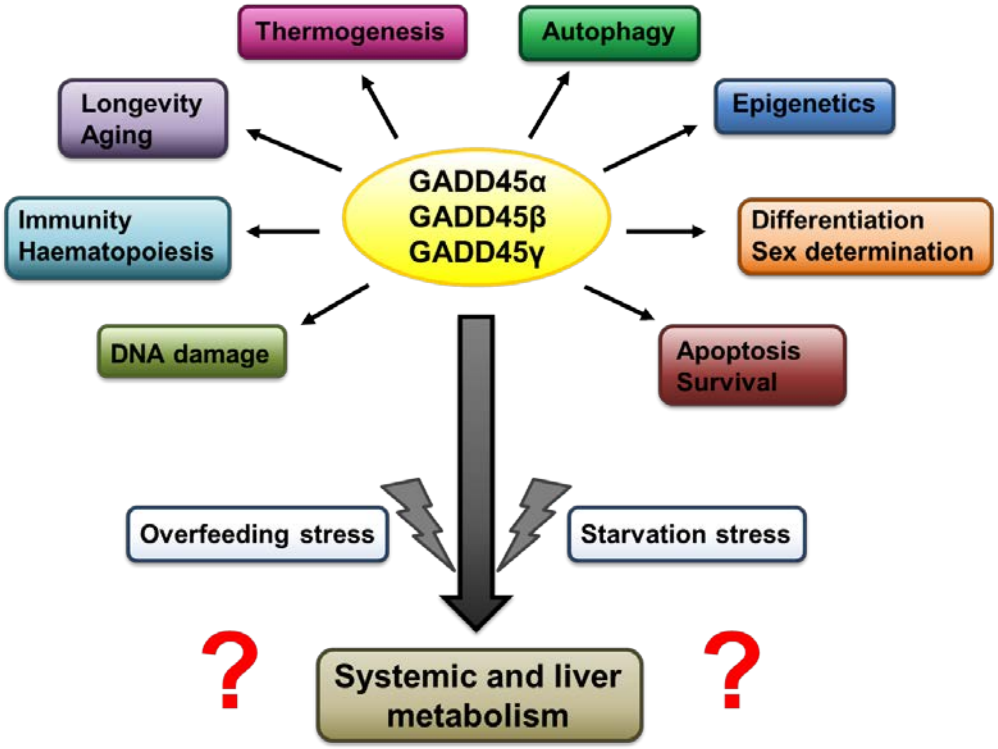

Figure 12: Aim of the study. GADD45 proteins are known to be involved in many biological contexts, for example DNA damage repair, haematopoiesis and immunity, aging and longevity, thermogenesis, autophagy, epigenetics, differentiation and sex determination, as well as in cell survival and cell death. But which role they play in systemic and hepatic metabolism upon nutrient deprivation or overload is not known.

3. RESULTS

3.1 *Gadd45g* is a candidate inflexible gene in metabolic disorder

3.1.1 Discovery of *Gadd45g* by transcriptome analysis in *db/db* mice

It is commonly accepted that the liver is a pivotal organ contributing to metabolic control. It is the primary site of glucose production and can provide alternate substrates such as ketone bodies under fasting conditions. Previous studies in our laboratory (Herzig Lab) have demonstrated that hepatic gluconeogenic, fatty acid and bile acid metabolism are controlled on a hormonal and nutritional level via transcriptional complexes [238-242]. To extend our knowledge of such processes we need to further characterise novel pathways involved in the control of liver metabolic function and dysfunction. One strategy to uncover novel molecular mechanisms contributing to metabolic flexibility in the fasted to fed transition could be to dissect the liver transcriptome to uncover select genes which display certain 'inflexibility' in conditions of metabolic dysfunction. Therefore, diabetic *db/db* mice and corresponding wild type healthy mice were either fasted for 48 hours or fasted for 48 hours and refed for 24 hours. RNA was extracted and pooled and analysed by gene chip and principle component analyses to determine differentially regulated mRNA transcripts between the conditions. The Principle Component Analysis (PCA) a statistical procedure where a set of observations of possibly correlated variables are converted into a set of values of linearly uncorrelated variables called principal components. PCA is used to structure, facilitate and illustrate extensive data sets. In this coordinate system the greatest variance comes to lie on the first coordinate (called the first principal component), the second greatest variance on the second coordinate, and so on. In our case the "WT refed" and "WT fasted" conditions are separated along the X axis, whereas "*db/db* refed" and "WT refed" conditions are separated along the Y axis. This means more genes were differentially regulated due to the nutritional state relative to the genotype condition as compared to "WT refed". The "*db/db* fasted" condition was separated along both components. This work was done by a former PhD student of the lab, Prachiti Narvekar, and remains unpublished. Further details can be found in her PhD thesis which is available in our institute. Several candidates were found (Fig. 13A) one of which was a member of the GADD45 gene family, *Gadd45g* (Fig.13B). In particular, there was a strong upregulation of liver *Gadd45g* expression upon starvation which was absent in livers of *db/db* mice.

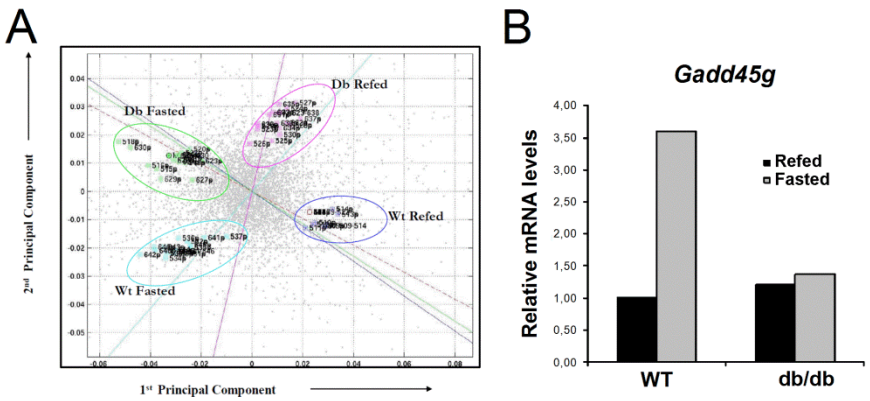

Figure 13: Transcriptome profiling of 48h fasted and 24h refed wild-type and *db/db* mice. (A) PCA with four clusters representing the four conditions ("WT refed", "WT fasted", "db refed" and "db fasted"). "WT refed" and "WT fasted" conditions are separated along the X axis, whereas "*db/db* refed" and "WT refed" conditions are separated along the Y axis. (B) Bar graph of relative mRNA levels of one of the differentially expressed genes, *Gadd45g*. Black bars represent the refed and grey bars represent the fasted animals used as in (A). n=4-6 per group. Adapted from Dr. Prachiti Narvekar, PhD Thesis, Herzig Lab.

These data were further validated by real-time quantitative PCR (Fig. 14).

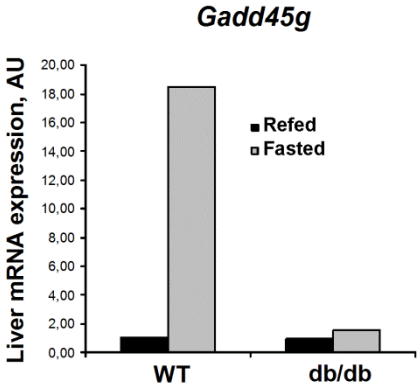

Figure 14: Validation of the microarray result from figure 13. *Gadd45g* expression in *db/db* and healthy control (WT) mice which were sacrificed after being fasted for 48h hours (fasted) or refed for 24h (refed) before sacrifice. Liver mRNA was analysed by RT-qPCR. Values are fold induction relative to "WT refed". n=4-6 per group. Adapted from Dr. Prachiti Narvekar, PhD Thesis, Herzig Lab.

3.2 GADD45β is induced upon nutrient depletion and dysregulated in disease and ageing

GADD45 family members are known to be rapidly induced by a wide variety of genotoxic stress stimuli such as methyl methanesulfonate (MMS), sorbitol and ultra violet (UV) light [159,243]. Each protein has a different pattern of cell-specific and stimulus-induced expression, presumably reflecting different signaling pathways. In most publications this induction is described in the context of DNA repair, cell cycle regulation and apoptosis [159,244] and little is known about their role in metabolic stress situations. Consequently, it was of interest to follow up on the results from the transcriptome analysis (see figure 13) and to examine all three members of the GADD45 family in the livers of mice with metabolic disorders.

3.2.1 Hepatic *Gadd45b* expression pattern is constant between various mouse models of obesity and diabetes

Gadd45a, Gadd45b and *Gadd45g* expression levels were measured in livers of *db/db*, *ob/ob* and NZO mice to compare with levels observed in wild type counterparts. In all three studies, healthy and diabetic mice were sacrificed either in the 24 hour fasted or *ad libitum* (fed) state (Figure 15). We could confirm the upregulation of liver *Gadd45g* expression upon starvation, an effect absent in livers of *db/db* mice (Fig. 15A, panel 3). However this induction pattern could not be observed in the other two mouse models (Fig.15B and C, panel 3). *Gadd45a* expression was only mildly affected by fasting in all three models (Fig. 15A, B and C, panel 1). In contrast, the third member of the GADD45 family, *Gadd45b,* was potently affected in wild type mice upon nutrient depletion (Fig. 15A, panel 2). There was a strong induction of liver *Gadd45b* after food withdrawal which was markedly less pronounced in *db/db* mice. Importantly, this induction pattern was consistent between the models and could also be seen in *ob/ob* versus wild type and NZO versus NZB mice (Fig. 15 and C, panel 2).

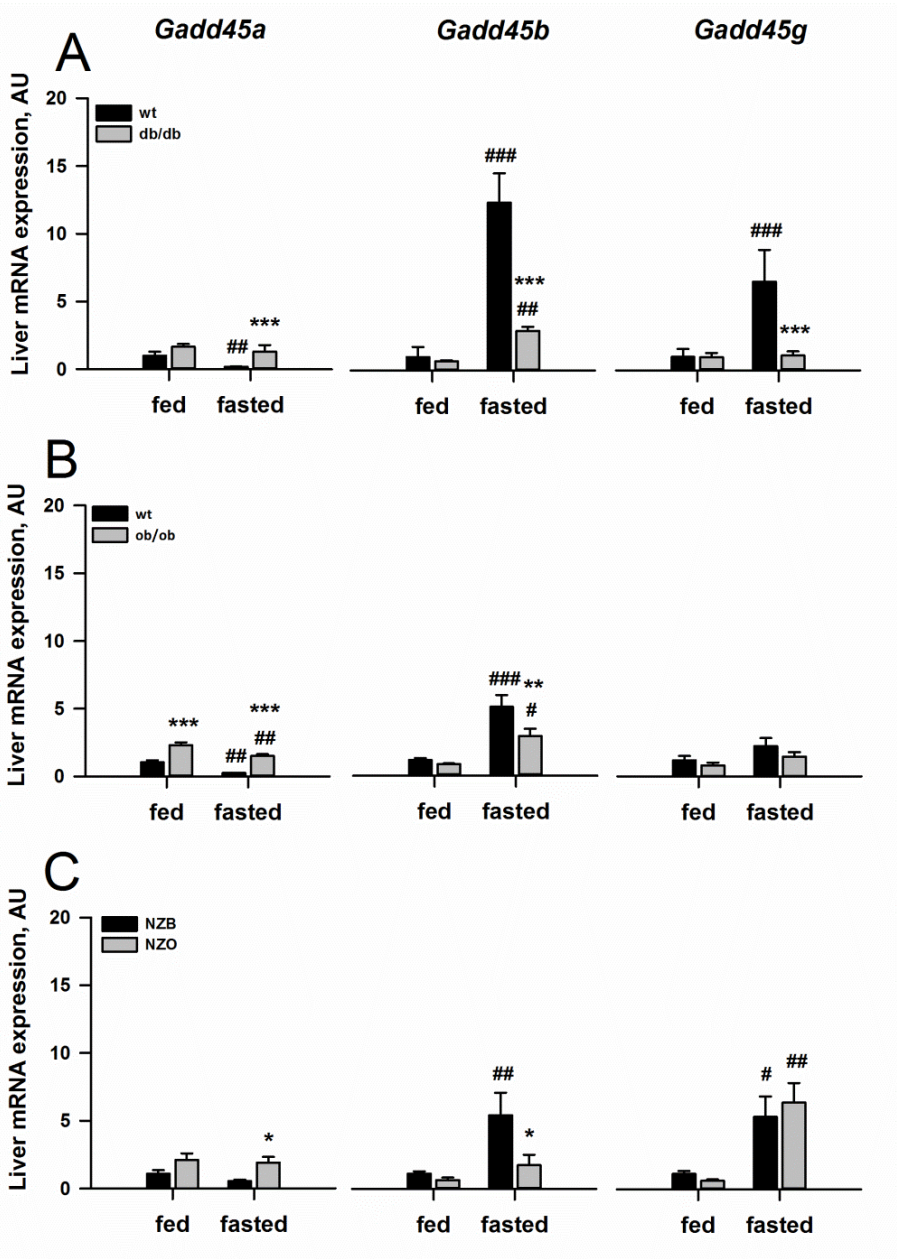

Figure 15: Liver *Gadd45a, Gadd45b* and *Gadd45g* mRNA expression in different mouse models of obesity. Male wild-type (WT) and *db/db* (A) or *ob/ob* (B), as well as New Zealand Black (NZB) and New Zealand Obese (NZO) (C) mice were fed *ad libitum* (fed) or fasted for 24h (fasted) where indicated and mRNA levels were analysed by RT-qPCR. Values are fold induction relative to "WT/NZB fed". Mean ± SEM; n=4 per group; * genotype effect, # effect of fast time; (*) p ≤ 0.05, (**) p ≤ 0.01, (***) p ≤ 0.001.

3.2.2 The induction of GADD45β also occurs at the protein level

To investigate whether the fasting-induced upregulation of *Gadd45b* is restricted to mRNA levels, proteins from liver samples of *db/db* and wild type mice were extracted and analysed by immunoblotting. As seen in figure 16, GADD45β protein levels are potently increased upon food deprivation in wild type but not in diabetic animals.

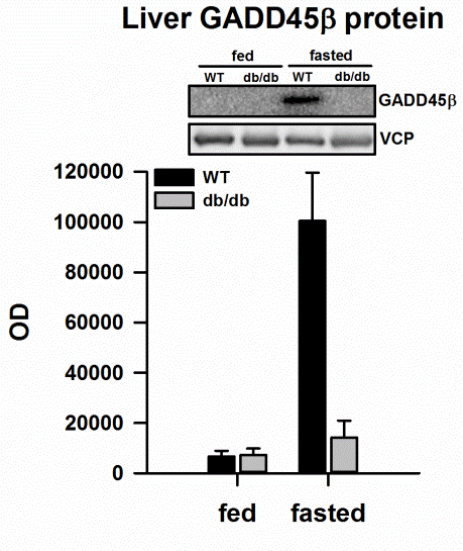

Figure 16: Protein expression of liver GADD45β. Protein lysates were obtained from male obese/type 2 diabetic (*db/db*) and corresponding wild type (WT) healthy mice being either fasted for 24h (fasted) or fed *ad libitum* (fed). Antibodies against GADD45β and the loading control (VCP) were used. Mean ± SEM; n=4 per group.

3.2.3 The fasting-induced upregulation of *Gadd45b* is reversible after re-feeding

It is reported that *Gadd45* expression is increased within minutes upon certain stimuli [245] and that *Gadd45b* induction is regulated by distinct mechanisms in a stress-specific manner (either at the level of mRNA transcription or mRNA stability) [243]. We were now interested to determine how long *Gadd45b* expression is augmented and whether it is reversible after refeeding. Therefore C57Bl6/J mice were fasted for different durations or refed for fixed amounts of time before sacrifice. We could show that the hepatic *Gadd45b* expression followed a time course, having the highest peak after 48 hour starvation, diminishing after the return of food and reducing beyond basal levels after 24 hours of refeeding (Fig. 17).

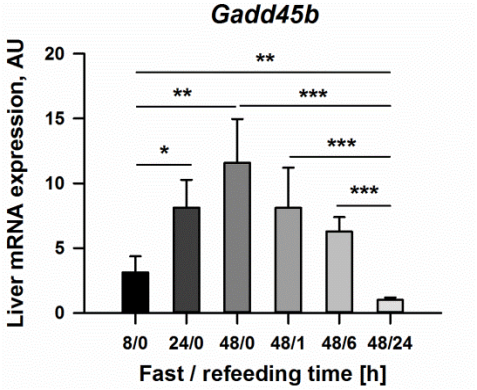

Figure 17: Liver *Gadd45b* mRNA expression during different times of fasting and refeeding. Male C57Bl6/J mice were fasted for various durations with subsequent various durations of refeeding as indicated. mRNA levels were analysed by RT-qPCR. Values are fold induction relative to the 24h refed group. Mean ± SEM; n=4 per group; (*) p ≤ 0.05, (**) p ≤ 0.01, (***) p ≤ 0.001.

3.2.4 The fasting-induced upregulation of *Gadd45b* is liver-specific

Since the fasting-induced upregulation of *Gadd45b* was first discovered in the liver of healthy wild type animals compared to diabetic mice, we next examined the expression levels in other tissues of this study. A comparison of the *Gadd45b* expression levels in other metabolic organs such as brown adipose tissue (BAT), abdominal white adipose tissue (aWAT), the gastrocnemius muscle (GC) and the liver showed that the effect of nutrient starvation on *Gadd45b* expression was most pronounced in the liver, wherein the largest difference between wt and *db/db* mice in the fasted state was observed (Fig. 18).

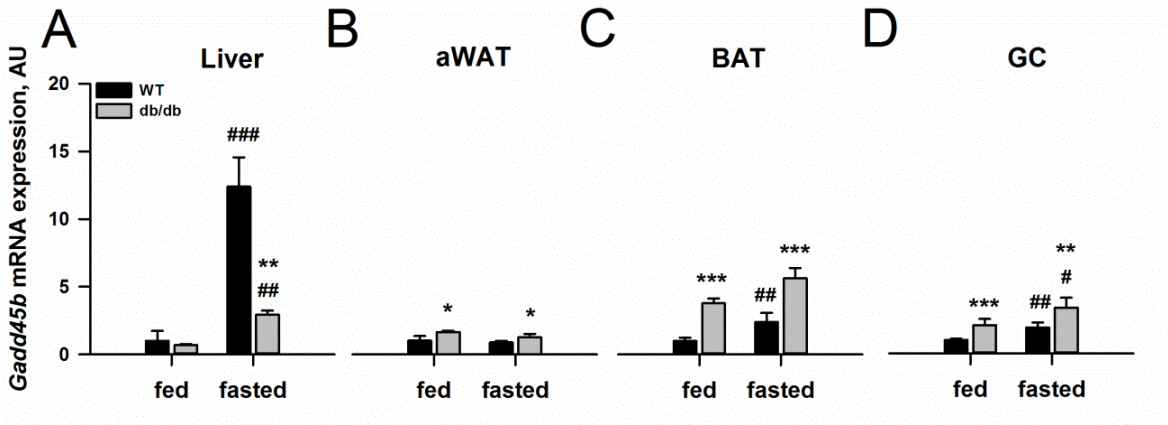

Figure 18: *Gadd45b* expression in different mouse organs. Male wild-type (WT) and *db/db* mice were fed *ad libitum* (fed) or fasted for 24h (fasted) where indicated and *Gadd45b* mRNA levels were subsequently analysed by RT-qPCR in liver (A), abdominal white tissue (aWAT; B), brown adipose tissue (BAT; C) and gastrocnemius muscle (GC, D). Values are fold induction relative to "WT fed". Mean ± SEM; n=4 per group; * genotype effect, # effect of fast time; (*) $p \leq 0.05$, (**) $p \leq 0.01$, (***) $p \leq 0.001$.

3.2.5 Analysis of other GADD45 family members in different tissues of *db/db* mice

Since also *Gadd45g* showed a mild induction upon fasting in liver of healthy mice which was absent in livers of *db/db* mice (Fig. 15A, panel 3), we next compared the expression levels of both *Gadd45a* and *Gadd45g* in aWAT, BAT and GCM in the same study (Fig. 19). Similar to *Gadd45b*, neither *Gadd45a* nor *Gadd45g* showed an augmentation in their mRNA levels in aWAT or BAT. The expression levels in general were very low for both genes in all tissues. Only *Gadd45a* was differently expressed in GCM of *db/db* mice in the fasted state compared to wild type mice (Fig. 19C, panel 1). This is in accordance to recent reports showing that *Gadd45a* is induced upon fasting in skeletal muscle and required for muscle atrophy [231], a condition also found in *db/db* mice [246].

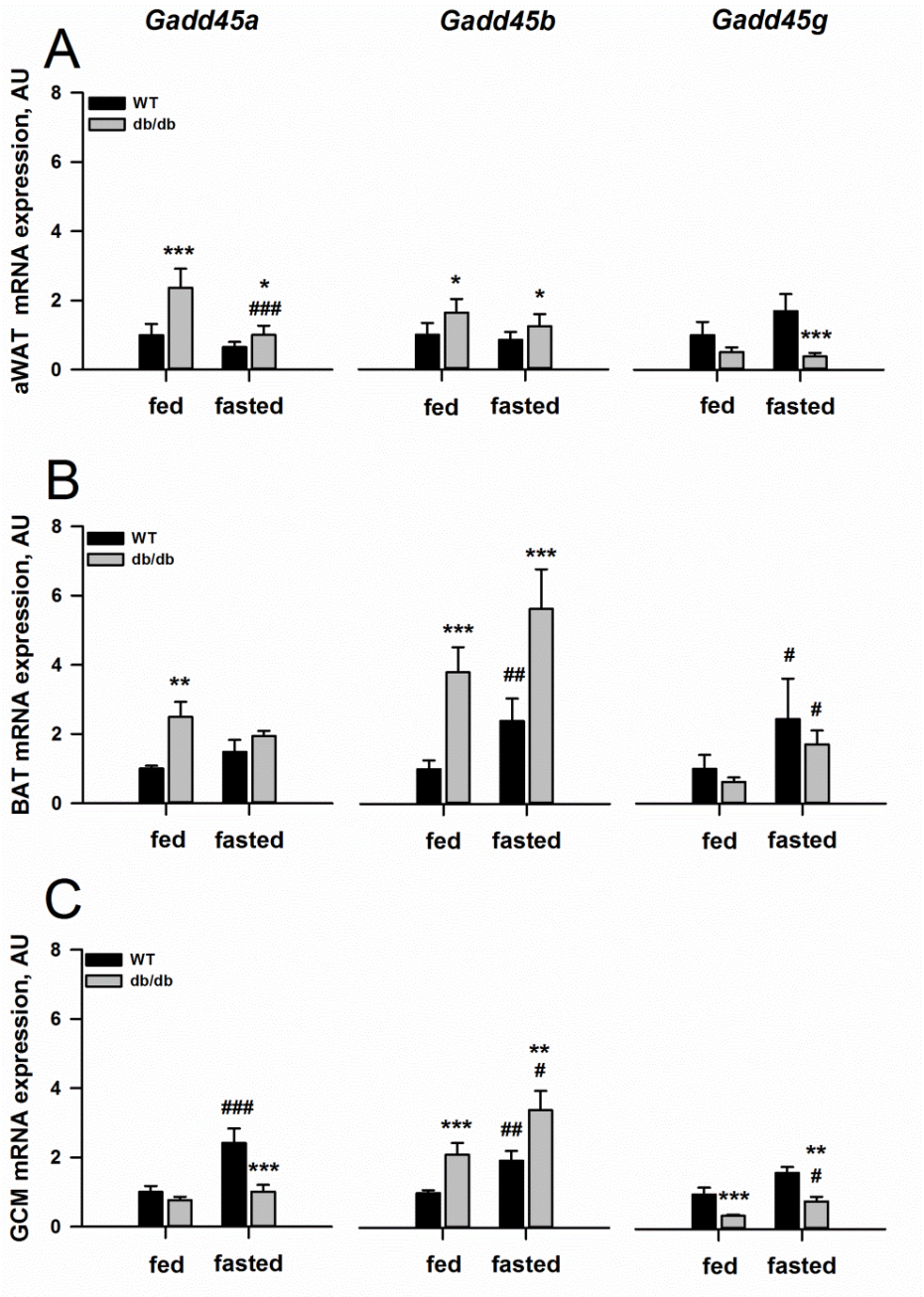

Figure 19: *Gadd45a, Gadd45b* and *Gadd45g* mRNA expression in different mouse organs. Male wild-type (WT) and *db/db* mice were fed *ad libitum* (fed) or fasted for 24h (fasted) where indicated and mRNA levels were analysed by RT-qPCR in abdominal white tissue (aWAT; A), brown adipose tissue (BAT; B) and gastrocnemius muscle (GC, C). Values are fold induction relative to "WT fed". Mean ± SEM; n=4 per group; * genotype effect, # effect of fast time; (*) $p \leq 0.05$, (**) $p \leq 0.01$, (***) $p \leq 0.001$.

3.2.6 The fasting-induced upregulation of hepatic *Gadd45b* occurs in hepatocytes

Since the fasting-induced increase of *Gadd45b* in the liver was very potent (~ 12x), we hypothesised that this induction is intrinsic to hepatocytes since they represent the majority of cells in the liver [78] and are known to be affected by nutritional status [247]. To test whether the induction of *Gadd45b* is hepatocyte-specific, C57Bl6/J mice were sacrificed *ad libitum* or after being fasted for 24 hours. The liver was collagenase-perfused and liver cell populations were

isolated by differential centrifugation into hepatocyte and non-parenchymal fractions (NP). The mRNA expression of *Gadd45b*, as well as cell-type specific markers including *Hnf4a* (hepatocytes), *Cd31* (endothelial cells), *Des* (Stellate cells) and *Emr1* (Kupffer cells) from the fractions were subsequently quantified. As shown in figure 20, the expression level of *Cd31* (Fig. 20A), *Des* (Fig. 20B), and *Emr1* (Fig. 20C) were exclusively present in the NP fraction, which shows that there are no NP cells in the hepatocyte fraction and the separation was successful. The expression level of *Hnf4a* (Fig. 20D, was significantly lower in the NP fraction, even though not to the same extent as for *Cd31, Desmin* and *Emr1*. This indicates that the separation of hepatocytes from the NP fraction was incomplete. Nevertheless, there was a significant fasting-induced increase of *Gadd45b* expression in the hepatocyte fraction (Fig. 20E). The large variability might be due to a suboptimal experimental setup and isolation protocol.

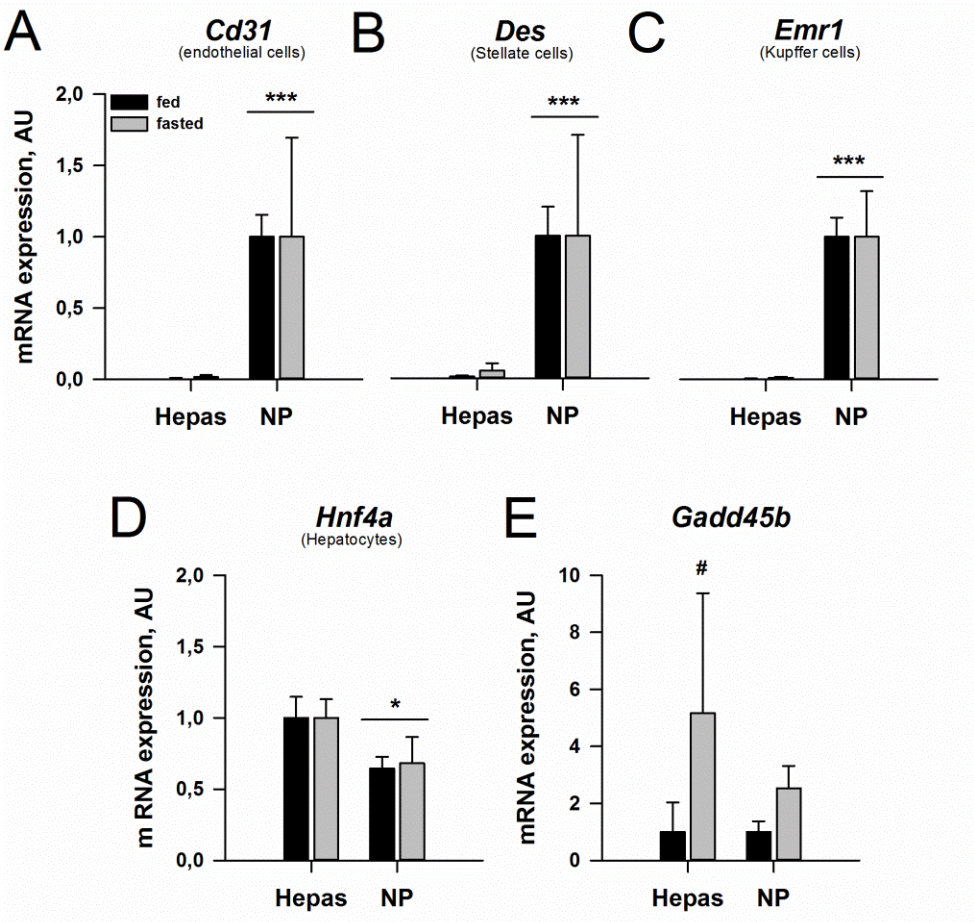

Figure 20: Gene expression analysis in hepatocytes and non-parenchymal cells. Male C57Bl6/J mice were fed *ad libitum* (fed) or fasted for 24h (fasted) after which the liver was collagenase-perfused and liver cell populations were isolated by differential centrifugation into hepatocyte (Hepas) and non-parenchymal (NP) fractions. The mRNA levels of cell-type specific markers including *Cd31* (endothelial cells; A), *Des* (Stellate cells; B), *Emr1* (Kupffer cells; C), and *Hnf4a* (hepatocytes; D), as well as from *Gadd45b* (E) from the fractions, were subsequently analysed by RT-qPCR. Values are fold induction relative to "NP fed" (A-C) or "Hepas fed" (D-E). Mean ± SEM; n=3 per group; * cell type effect, # effect of fasting; (*) $p \leq 0.05$, (**) $p \leq 0.01$, (***) $p \leq 0.001$.

3.2.7 *Gadd45b* is also induced upon nutrient depletion *in vitro*

To investigate which nutrient, when deprived, is responsible for the elevation of *Gadd45b*, a differentiated, nontransformed hepatocyte cell line (AML12) was used [248]. For this purpose, cells were incubated with a series of specified cell culture media where certain nutrients were missing. In a first experiment the self-made medium (called “PBS full”) was compared to the regular growth-medium DMEM/F-12 to exclude the possibility of an induction of *Gadd45b* (Fig. 21A left and right panel). Afterwards the self-made medium was composed of two media, the “base medium” and the “supplement medium” which were mixed to different degrees in order to reduce the nutrients. The “base medium” contained all the components crucial for cell survival and was always used at a fixed concentration. The “supplement medium” contained all the nutrients in question and its concentration varied between conditions (Fig. 21B). In a third experimental setup, specific nutrients were removed from the “supplement medium” while all the other components were kept at standard concentrations. This specific nutrient was added back to the medium as 1% of its usual concentration (Fig. 21C). In a last experiment, nutrients were removed in groups of two from the “supplement medium” and added subsequently to the cells (Fig. 21D). The compositions of all media are listed in the methods section 5.2.9.

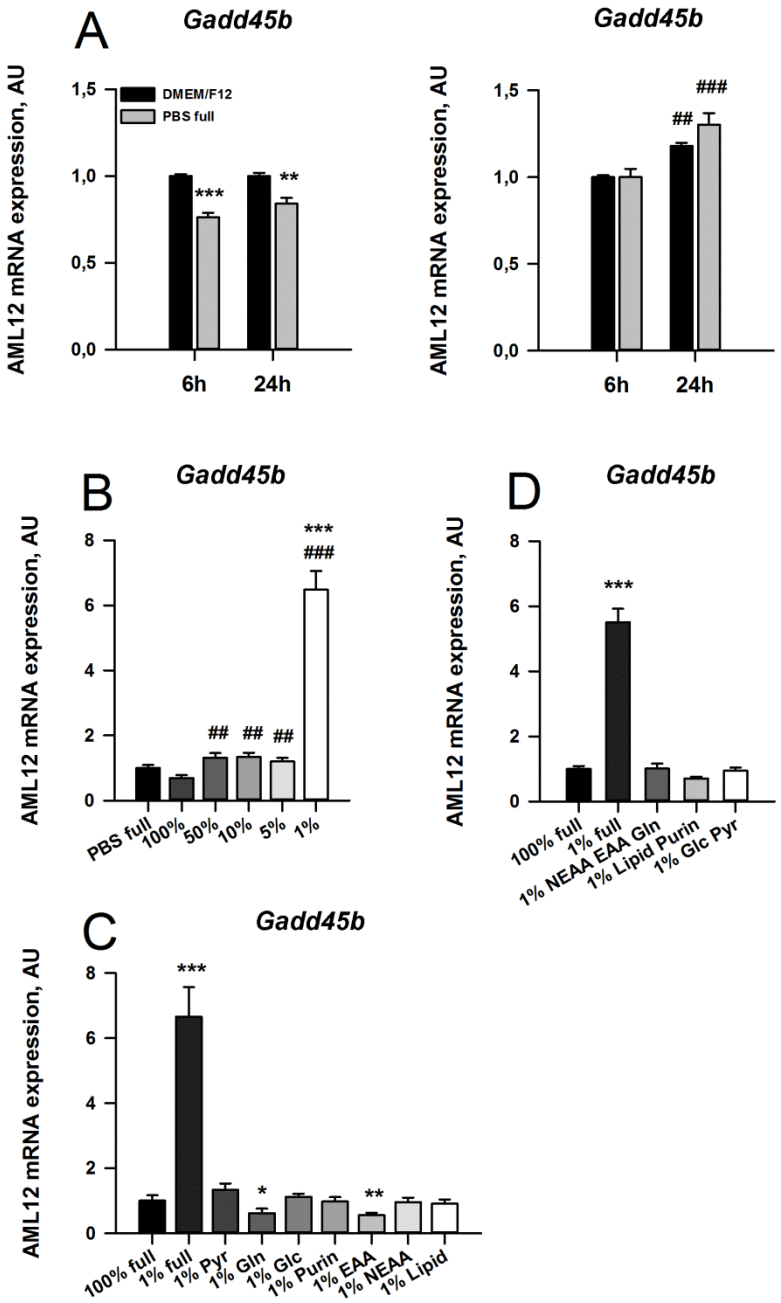

Figure 21: *Gadd45b* expression in AML12 cells under different nutritional conditions. (A) AML12 cells were cultivated in standard DMEM/F-12 or self-made "PBS full" for either 6h or 24h before harvest. The left panel shows values as fold induction relative to DMEM/F-12, the right panel shows values as fold induction relative to 6h treatment. * effect of medium, # effect of time. (B) AML12 cells were cultivated for 24h either in "PBS full" or a medium consisting of "supplement medium" at 100%, 50%, 10%, 5% or 1% of "base medium". Values are fold induction relative to "PBS full". * relative to "PBS full", # relative to "100%". (C) AML12 cells were cultivated for 24h either in a medium consisting of "supplement medium" and "base medium" in a 1:1 ration ("100% full"), in a medium consisting of "supplement medium" and "base medium" in a 1:0,01 ration ("1% full"), or in full medium with either 1% pyruvate (Pyr), glutamine (Gln), glucose (Glc), purine/pyrimidine (Purine), essential amino acids (EAA), non-essential amino acids (NEAA), or lipids. Values are fold induction relative to "100% full". * relative to "100% full". (D) Same as in (C) but two components reduced to 1%. AML12 mRNA was always analysed by RT-qPCR. Mean ± SEM; n= 3 per group; (*) $p \leq 0.05$, (**) $p \leq 0.01$, (***) $p \leq 0.001$.

As shown in Fig. 21A, there was no induction of *Gadd45b* in the self-made medium "PBS full". The mRNA levels were rather reduced after 6 hours and after 24 hours of incubation (left panel).

Gadd45b levels were slightly but significantly increased after 24 hours incubation in both media compared to 6 hours incubation (right panel). Therefore, cells were harvested after 24 hours incubation in the following experiments. The mixture of “base medium” with “supplement medium” led to a slight induction of *Gadd45b* when mixed 1:2, 1:10 or 1:20 (Fig. 21B). However, a reduction of all variable nutrients to 1% of the original concentration led to a strong increase of *Gadd45b* levels. Reducing one (Fig. 21C) or pairwise combinations of nutrients (Fig 21D) did not lead to an increase in *Gadd45b* levels. Only the restriction of all components caused the induction as seen before These results lead us to believe that the combined restriction of all nutrients during starvation is responsible for and induction of *Gadd45b* and not a single candidate or a specific type of nutrient.

3.2.8 *Gadd45b* is mildly upregulated by AMPK pathway in primary hepatocytes

Next, we were interested to test if a non-nutrient component is responsible for the induction of hepatic *Gadd45b*. It is known that *Gadd45b* expression is induced by certain cytokines such as TNF-α [156]. It is also postulated that *Gadd45b* expression might be induced by insulin [235]. Therefore we isolated primary hepatocytes from C57Bl6/J and treated them with different compounds such as TNF-α or insulin for 8 or 24 hours at different concentrations (Fig. 22). Furthermore, we included AICAR (an analogue of AMP that is capable of stimulating AMP-dependent protein kinase (AMPK) activity), forskolin (activates the enzyme adenylyl cyclase and increases intracellular levels of cAMP resulting in activation of cAMP-sensitive pathways such as protein kinase A (PKA)), IFNγ and a medium without FCS. As shown in figure 22 only the incubation with 200 µM of AICAR led to a mild increase in *Gadd45b* expression levels, whereas 10 µM of Forskolin and 25 ng/ml IFNγ led to a decrease in mRNA expression levels. This is in accordance with AMPK being activated during nutrient deprivation leading to induction of energy-producing, catabolic pathways [249].

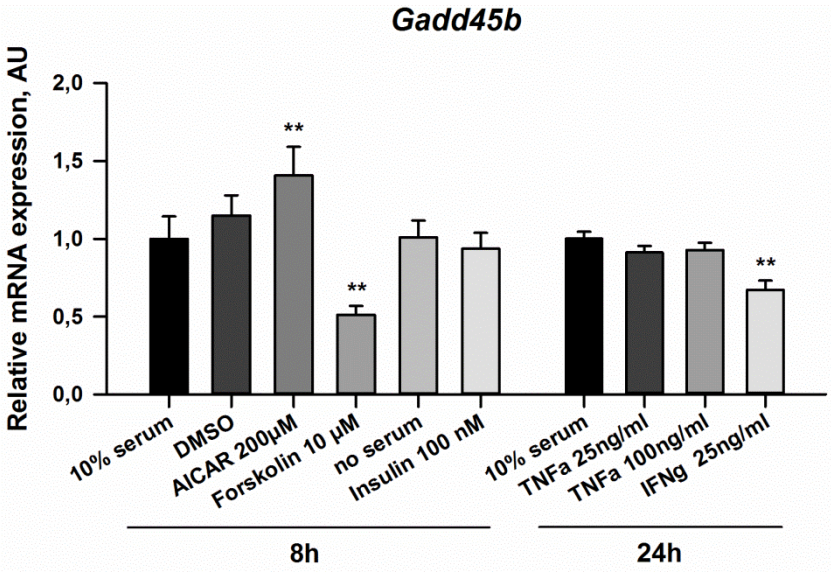

Figure 22: *Gadd45b* expression in primary hepatocytes treated with different cell stimuli. Male C57Bl6/J mice were sacrificed *ad libitum*. The liver was collagenase-perfused and primary hepatocytes were isolated before being treated for 8h or 24h with different cell stimuli as indicated. mRNA levels were analysed by RT-qPCR. Values are fold induction relative to “10% serum”. Mean ± SEM; n=4 per group; * relative to “10% serum” at respective time point; (*) $p \leq 0.05$, (**) $p \leq 0.01$

3.2.9 *Gadd45b* is not affected in a mouse model of type 1 diabetes

To investigate if the observed absence of fasting-induced elevation in hepatic *Gadd45b* levels in *db/db* mice is a secondary effect of a disturbed β-cell function, we measured liver mRNA levels in healthy C57Bl6/J mice and in mice rendered insulin deficient and diabetic by treatment with the β-cell toxin streptozotocin [250,251]. As shown in figure 23 *Gadd45b* was not induced in livers of mice suffering from experimental insulin-deficient diabetes.

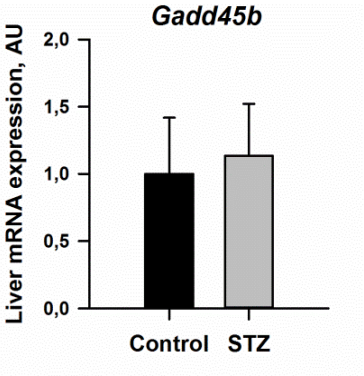

Figure 23: Liver *Gadd45b* expression of mice with type 1 diabetes or healthy mice. Male C57Bl6/J mice were injected with either 60 mg/kg STZ intraperitoneally on 6 subsequent days (STZ) or with vehicle (sodium citrate, control). Mice were sacrificed 6 months after treatment was started. Liver *Gadd45b* mRNA levels were subsequently analysed by RT-qPCR. Values are fold induction relative to "control". Mean ± SEM; n=10-13 per group.

3.2.10 The fasting-induced upregulation of *Gadd45b* is blunted in aged mice

Aging is characterized by an overall impairment of cellular function. Aged mice have altered glucose and fatty acid metabolism and whole body homeostasis compared to young mice resulting in common metabolic, inflammatory, cardiovascular and neurodegenerative diseases [252]. In the course of her own PhD studies, Dr. Katharina Niopek (Herzig Lab) performed a transcriptome analysis with liver samples from 22 month old and 12 week old mice, both groups either fasted for 16 hours or refed for 6 hours before sacrifice. One differentially expressed gene in those four groups was *Gadd45b*. Subsequently, we performed RT-qPCR analysis on those liver samples. We could confirm that *Gadd45b* expression was potently induced upon fasting young mice (Fig 24B). This induction was absent in fasted aged animals, resembling the mRNA expression pattern in *db/db* versus wild type mice (Fig. 15). *Gadd45g* showed a similar mRNA expression profile (Fig 24C).

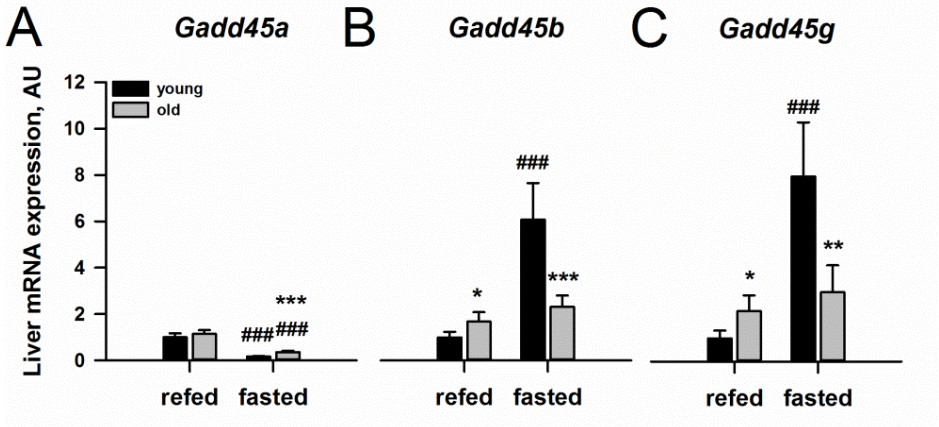

Figure 24: Liver *Gadd45a*, *b* and *g* expression in old and young mice. Male C57Bl6/J mice at the age of 22 months (old) or 12 weeks (young) were sacrificed after being fasted for 16h hours (fasted) or refed for 6h (refed) before sacrifice. Liver mRNA levels were analysed by RT-qPCR. Values are fold induction relative to "young refed". Mean ± SEM; n=5 per group; * age effect, # effect of fast time; (*) $p \leq 0.05$, (**) $p \leq 0.01$, (***) $p \leq 0.001$.

3.2.11 Liver *GADD45B* is also dysregulated in men with type 2 diabetes

Even though animal models are broadly used for the study of human biology and diseases, one might still question whether this is an accurate approach considering some stark differences between the two species resulting from adaptation to their respective environments during evolution [253]. Hence, for true translational validity, observations made in animals have to be confirmed in humans. We examined the liver *GADD45B* mRNA levels of lean and obese patients with or without type 2 diabetes. As shown in figure 25 liver *GADD45B* expression (as ratio *GADD45B/HPRT1*) was lower in fasted diabetic men (T2D) than in men with normal glucose tolerance (NGT) independent of the degree of obesity (lean, subcutaneous fat (SC), visceral fat (VIS)). Due to the scatter in the NGT groups, only the difference between the SC groups was significant, but there was also a significant main effect of T2D between the three NGT and the three T2D groups (not shown).

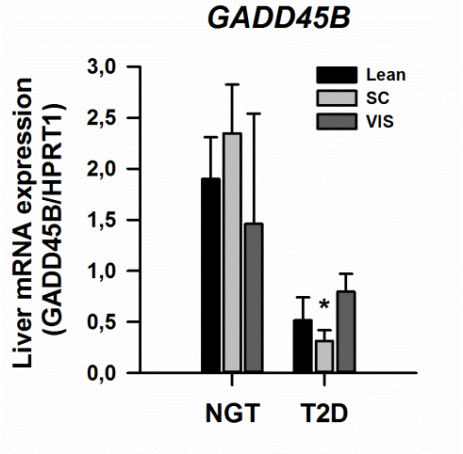

Figure 25: Liver *GADD45B* expression of lean and obese patients with type 2 diabetes or healthy men. Liver tissue samples were obtained by open liver biopsy from men with type 2 diabetes (T2D) or normal glucose tolerance (NGT). The patients were divided according to their body composition into lean men or men with subcutaneous (SC) or visceral (VIS) fat. Liver *GADD45B* mRNA levels were subsequently analysed by RT-qPCR and normalized to Hypoxanthine-Phosphoribosyl-Transferase 1 (HPRT1). Mean ± SEM; n=14-23 per group; * diabetes effect; (***) $p \leq 0.001$.

3.3 GADD45β plays a role in adaptive metabolism during the stress of nutrient deprivation

To gain insights into the potential importance of GADD45β for healthy and pathophysiologic liver function, we examined mice with whole body deletion of GADD45β. In particular, because we observed stark regulation of GADD45β by fasting, we wanted to examine a possible functional role for GADD45β in adaptive metabolism of nutrient depletion.

Under fasting conditions, there is a complex interplay between the tissues in order to supply the energy needs of the body. Falling blood sugar levels lead to an inhibition of insulin secretion by the β-cells of the pancreas and an increased production of glucagon by the α-cells of the pancreas. Together with glucocorticoids from the adrenal cortex of the adrenal gland, glucagon stimulates several processes that collectively serve to increase and maintain normal concentrations of glucose in the blood. They signal to a variety of tissues. In the liver they lead to glycogen breakdown (glycogenolysis) and glucose production (gluconeogenesis) followed by glucose release from the liver. Furthermore they inhibit glucose uptake by muscle and adipose tissue, mobilize amino acids from extrahepatic tissues as substrates for gluconeogenesis, and

stimulate fat breakdown (lipolysis) in adipose tissue. FA are released from adipose tissue and taken up by the liver to be oxidized via β-oxidation to provide energy. In prolonged fasting, free fatty acids are broken down for the generation of ketone bodies. After feeding, the rise in blood glucose level is reduced by insulin which promotes glucose uptake by various tissues. Moreover, insulin stimulates the liver for glycogenesis to restore glycogen depots as well as *de novo* lipogenesis. Overnutrition results in perturbation of these reciprocal control mechanisms with failure to suppress hepatic glucose production as well as impaired transition from FA efflux to storage in response to a meal.

3.3.1 Whole body GADD45β KO affects systemic and liver lipid metabolism upon fasting

For a first assessment of a possible functional role of GADD45β in adaptive metabolism, GADD45β KO and WT littermates were starved for 24 hours before sacrifice. A blood sample was taken before food withdrawal. As expected, food withdrawal led to a significant (14%) reduction in body weight after 24 hours with no difference between genotypes (Fig. 26A). At the time of sacrifice, the weights of liver, aWAT and GCM were noted and normalized to the body weight. There was no difference between GADD45β KO and WT with regards to any of the tissue masses (Fig. 26B).

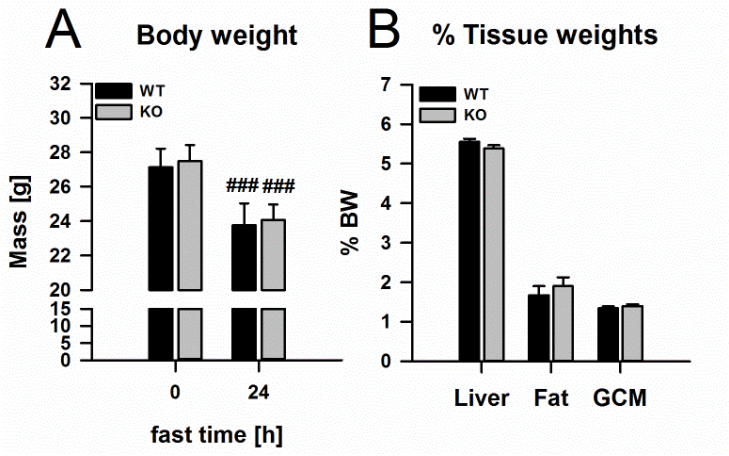

Figure 26: Body and tissue weights in GADD45β KO and WT mice. (A) Body weight of male GADD45β KO and WT littermates was measured before (0h) or after (24h) food withdrawal. (B) Tissue weights were measured after 24h fasting during preparation of the same mice as in (A) and normalized to body weight. Mean ± SEM; n=5-8 per group; * genotype effect, # effect of fast time; (*) $p \leq 0.05$, (**) $p \leq 0.01$, (***) $p \leq 0.001$.

After processing the blood, the serum was analysed for its concentrations in NEFA, TG, glycerol, cholesterol, ketone bodies, alanine and branched-chain amino acids (BCAA). Surprisingly, we could observe a difference in the serum NEFA concentration between GADD45β KO and WT mice. As expected, in both groups fasting led to an increase in serum NEFA, but the increase in GADD45β KO mice was significantly lower (15%) compared with GADD45β WT animals (Fig. 27A). Also serum TG, glycerol and ketone body concentrations were elevated by fasting but with no difference between genotypes (Fig.27B, C and E). Due to the limited amount of serum from fed animals, cholesterol, alanine and BCAA levels could only be measured in the serum of fasted mice (Fig. 27D). There was no difference between GADD45β KO and WT mice in their cholesterol concentration. Interestingly, GADD45β KO mice had a 50% reduction in both amino acids. As

expected, blood glucose concentrations were reduced upon fasting, with no difference between genotypes (Fig. 27F).

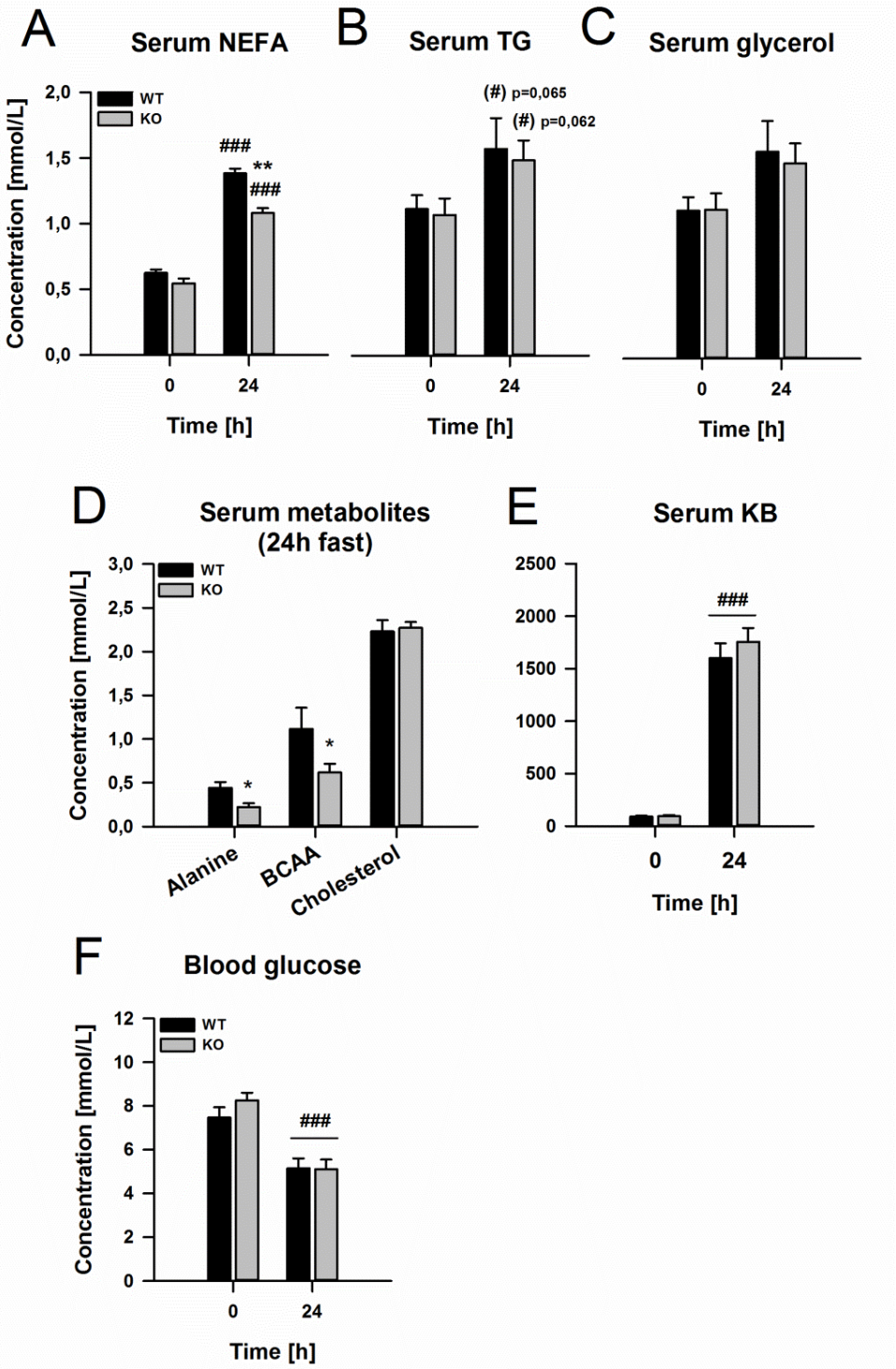

Figure 27: Serum metabolites in GADD45β KO and WT mice. Serum non-esterified fatty acids (NEFA, A), triglycerides (TG, B), glycerol (C), ketone bodies (KB, E) and blood glucose (F) of male GADD45β KO and WT littermates was measured before (0h) or after (24h) food withdrawal. Serum alanine, branched-chain amino acids (BCAA) and cholesterol from the same animals were measured only after 24h fasting (D). Mean ± SEM; n=5-8 per group; * genotype effect, # effect of fast time; (*) $p \leq 0.05$, (**) $p \leq 0.01$, (***) $p \leq 0.001$.

With the hint that systemic metabolism might be affected by a deletion of GADD45β we next examined the livers of the GADD45β KO and WT mice. Even though there was no difference in

liver weight upon fasting (Fig. 26B), we could see a difference in the TG content of the liver (Fig. 28A) with GADD45β KO mice having a 250% higher concentration than WT mice. Liver concentration of NEFA, cholesterol and glycogen were not significantly different. Interestingly, the reduced concentration of serum alanine and BCAA in GADD45β KO mice (Fig. 27D) was accompanied by a significant increase in liver protein concentration compared to WT mice (Fig. 28B). Therefore, GADD45β seems to play a role in adaptive metabolism during the stress of nutrient deprivation, especially affecting lipid and amino acid homeostasis.

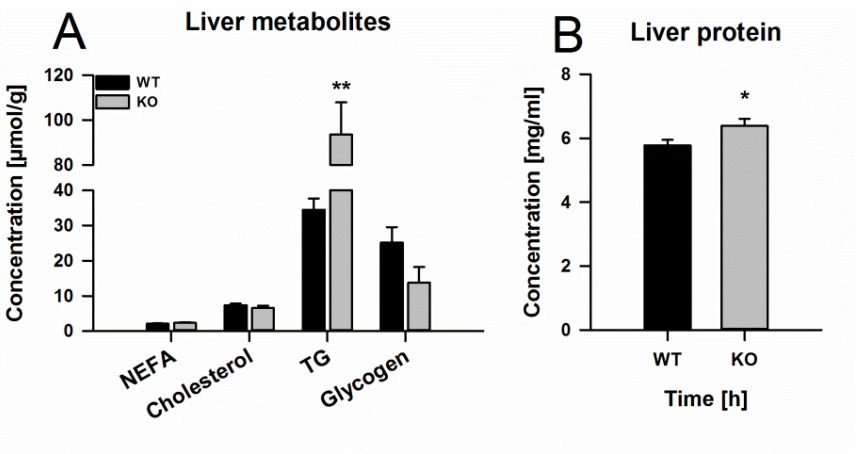

Figure 28: Liver metabolites in GADD45β KO and WT mice. Liver non-esterified fatty acids (NEFA), cholesterol, triglycerides (TG) and glycogen (A) as well as liver protein concentration (B) of male GADD45β KO and WT littermates was measured after 24h fasting. Mean ± SEM; n=5-8 per group; * genotype effect; (*) $p \leq 0.05$, (**) $p \leq 0.01$, (***) $p \leq 0.001$.

3.3.2 Whole body GADD45β KO affects fasting hepatic amino acid and acyl carnitine metabolism only mildly

During fasting, all cells in the body begin to break down protein resulting in a release of amino acids into the bloodstream, which can subsequently be converted into glucose by the liver and serve for energy production. The main amino acid substrate for gluconeogenesis in the liver is alanine [254] and glutamine for the gastrointestinal tract and the kidneys. The branched-chain amino acid carbon skeleton is oxidised in the muscle to generate energy [255] while the nitrogen moiety is transaminated to pyruvate, forming alanine, which is released into the blood. Since most of our muscle mass is protein, this phenomenon is responsible for the wasting away of muscle mass during starvation.

We have observed a difference in the serum concentrations of NEFA, alanine and BCAA between GADD45β KO and WT mice with GADD45β KO mice having less NEFA and less of both amino acids. Also, GADD45β KO mice accumulate proteins together with TG in the liver upon starvation. We were hence interested if a deletion of GADD45β also affects the metabolism of other amino acids or acyl carnitines. Carnitines and their acyl esters (acylcarnitines) are essential compounds for the metabolism of fatty acids by assisting in the transport and metabolism of fatty acids into mitochondria. In addition, carnitine is required to remove any surplus of acyl groups from mitochondria and to export acetyl and other short chain acyl groups from peroxisomes. These activities influence in turn many aspects of carbohydrate and lipid metabolism, including the regulation of insulin secretion by pancreatic β-cells [256]. Amino acid and acylcartinine profiling was performed on liver samples from GADD45β KO and WT mice via electrospray-ionisation

mass spectrometry and the results normalised to the total amino acids or acylcarnitine concentration, respectively. As shown in figure 29, there was no difference between GADD45β KO and WT in any amino acid, expect for ornithine. Also, liver alanine and BCAA did not seem to be affected by whole body depletion of GADD45β.

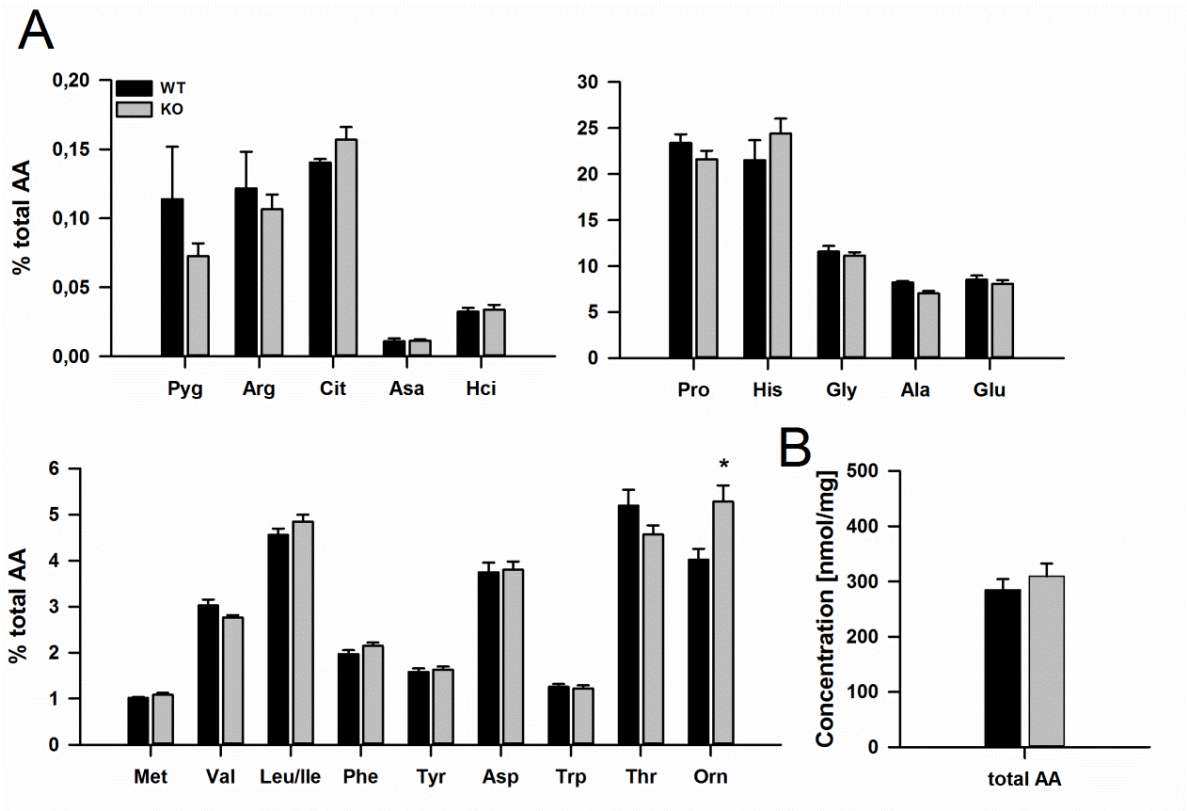

Figure 29: Liver amino acids in GADD45β KO and WT mice. Liver amino acids of male GADD45β KO and WT littermates were measured after 24h fasting and normalized to the total amino acid concentration (B). A list with full names can be found in suppl. table 6. Mean ± SEM; n=5-8 per group; * genotype effect; (*) $p \leq 0.05$, (**) $p \leq 0.01$, (***) $p \leq 0.001$.

Also for acylcarnitines, there was no striking effect of GADD45β KO (Fig. 30). Only the medium chain acylcarnitines C6 (hexanoylcarnitine) and C10 (decanoylcarnitine) as well as glutarylcarnitine (Glut) were reduced in livers of GADD45β KO mice. Total acylcarnitines, carnitine (C0) as well as acetyl carnitine (C2) were not changed either (Fig. 30B).

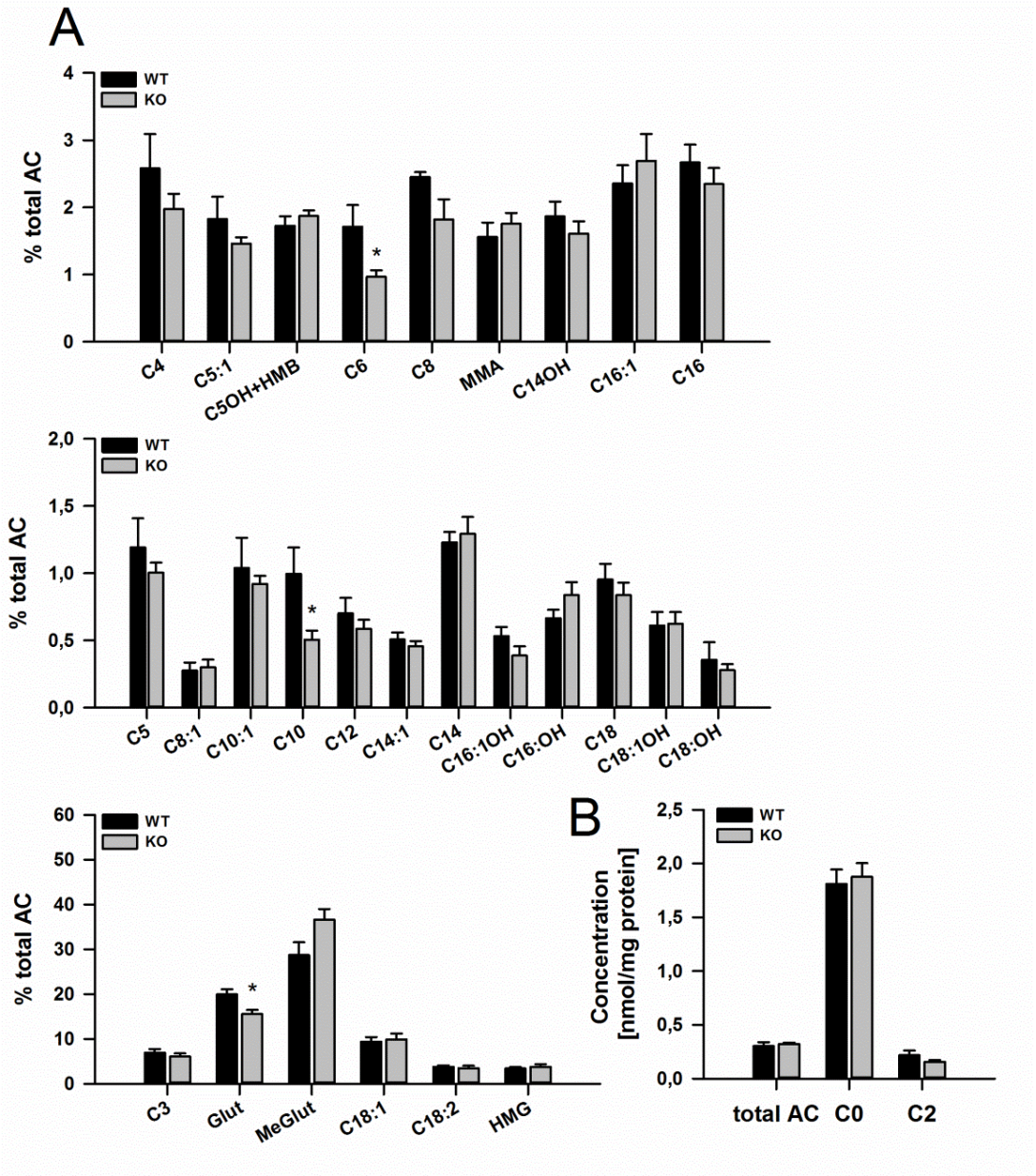

Figure 30: Liver acylcarnitines in GADD45β KO and WT mice. Liver acylcarnitines of male GADD45β KO and WT littermates were measured after 24h fasting and normalized to the total acylcarnitine concentration. Also free carnitine (C0) and acetylcarnitine (C2) were measured (B). A list with full names can be found in suppl. table 5. Mean ± SEM; n=5-8 per group; * genotype effect; (*) $p \leq 0.05$, (**) $p \leq 0.01$, (***) $p \leq 0.001$.

3.3.3 The loss of GADD45β is not compensated by an induction of the other GADD45 family members

Since also *Gadd45g* showed a mild induction upon fasting in livers of healthy but not of *db/db* mice (Fig. 15A, panel 3), we were interested if the effect we saw upon adaptive metabolism in GADD45β KO mice was accompanied by an increase of the other GADD45 family members. Therefore we measured the mRNA levels of *Gadd45a* and *Gadd45g* in the livers of fasted GADD45β KO and WT mice. There was no compensatory increase in expression of any of the two GADD45 family members (Fig 31). We could also confirm that all GADD45β KO animals used for the study had indeed a homozygous loss of the gene.

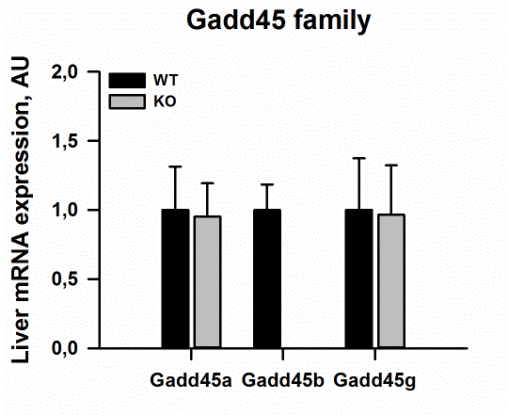

Figure 31. Liver *Gadd45a*, *Gadd45b* and *Gadd45g* expression in GADD45β KO and WT mice. Male GADD45β KO and WT littermates were sacrificed after being fasted for 24h hours. Liver mRNA levels were subsequently analysed by RT-qPCR. Values are fold induction relative to "WT". Mean ± SEM; n=5-8 per group.

3.3.4 Whole body GADD45β KO mice do not have altered systemic oxidative metabolism

To measure indirect calorimetry, GADD45β KO and WT littermates were housed in an indirect open circuit calorimeter that provides measures of oxygen consumption (VO_2) and carbon dioxide production (VCO_2). We used the PhenoMaster system from TSE for that purpose. Apart from measuring energy intake and energy expenditure, as well as metabolic substrate selection, this system also concurrently monitors food and water consumption, and locomotor activity. The mice were acclimated to that system for 4 days before food withdrawal. 24 hours later food was given back and the mice were monitored for another period of 3 days before sacrifice. For the analysis, the mean values from the last 6 hours of the light phase or the dark phase were used, starting with the light phase in the pre-fast period and ending with the dark phase in the refed period.

An overall analysis of the parameters from figure 32A (light phase) and 32B (dark phase) showed that, before food withdrawal, the WT mice were more active and consumed more food and water during the dark phase. Furthermore, pre-fasting RER levels were lower during the light phase (~0,9) relative to the dark phase (~1,0), showing that they switched from oxidation of more fat during their inactive time to the oxidation of more carbohydrates during their active time. Following food removal, parameters drastically changed. Water consumption and activity were reduced, although still comparatively higher in the dark phase. After an initial increase of body weight during the light phase, accounting for the first period after food withdrawal, the body weight dropped as expected. Also, since external food supply is gone, the mice have to rely on their internal energy storages and mobilise first their glycogen and then their fat reserves. This is also visible in figure 32. During the initial light phase after food withdrawal, the RER dropped to ~0,8 (Fig. 32A), followed by a decrease further to 0,7 as fasting proceeds (Fig. 32B). This means that the mice switched from carbohydrate to completely fat oxidation and can consequently be considered metabolically flexible. After refeeding, the mice ate and drank more and were also more active relative to before food withdrawal. Also the RER increased drastically, overshooting its value in the light phase before reaching its steady state level during the dark phase. Most importantly, when comparing GADD45β KO and WT littermates, one did not observe any

difference in any of the parameters measured. GADD45β KO and WT littermates displayed similar metabolic flexibilities, and did not differ in their systemic oxidative metabolism.

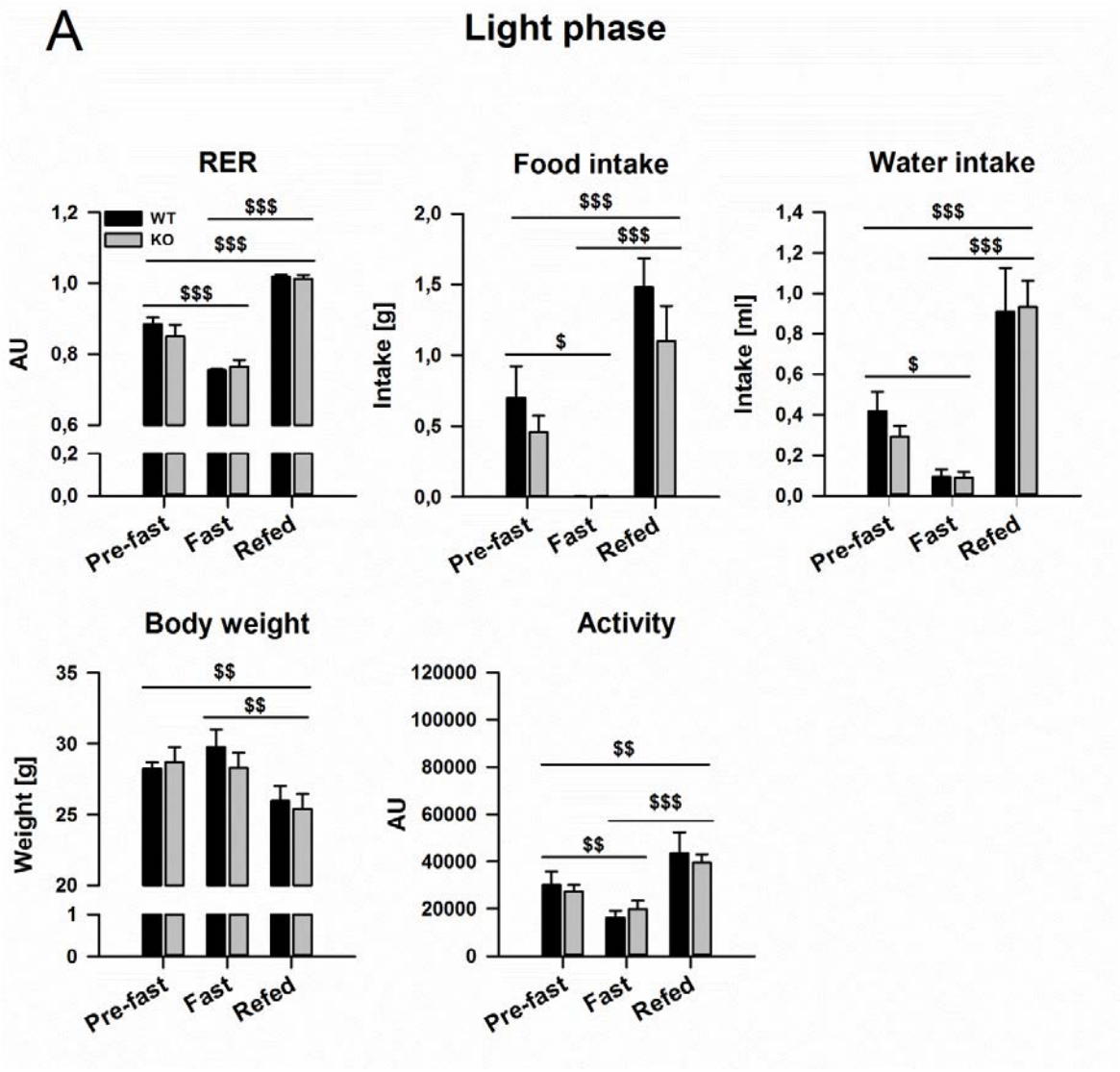

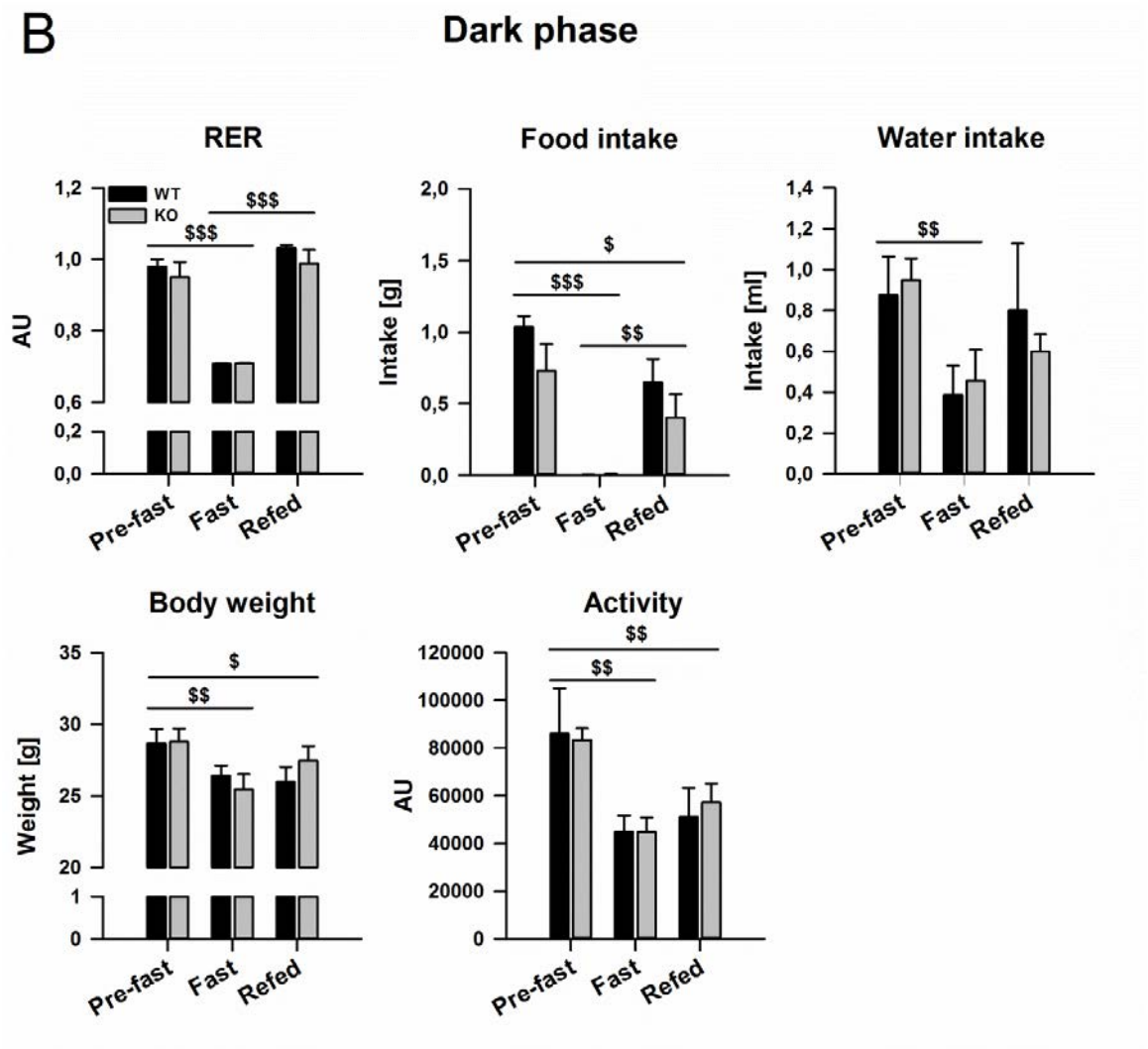

Figure 32: Assessment of systemic oxidative metabolism by indirect calorimetry in GADD45β KO and WT mice. Male GADD45β KO and WT littermates were housed in the PhenoMaster system (TSE). After an acclimation period (pre-fast) , they were fasted for 24h before food was given back (refed). During this time, the respiratory exchange rate (RER), food and water intake, body weight and activity was monitored. The mean values from the last 6 hours of the light phase (A) or the dark phase (B) were calculated, starting with the light phase during the pre-fast period and ending with the dark phase during the refed period. Mean ± SEM; n=4-6 per group; $ effect of time; (*) $p \leq 0.05$, (**) $p \leq 0.01$, (***) $p \leq 0.001$.

3.3.5 GADD45γ plays no comparable role to GADD45β in adaptive metabolism during nutrient depletion

The next question to be addressed was whether a deletion of GADD45γ would confer similar effects on lipid metabolism as did a knockout of GADD45β. Therefore we starved female GADD45γ WT and KO littermates for 24 hours before sacrifice. Male GADD45γ KO mice cannot develop gonads during embryogenesis and display a male-to-female sex switch, and thus, cannot be used for analysis [183,257]. Using RT-qPCR on liver samples we could confirm the total absence of *Gadd45g* (Fig. 33) in GADD45γ KO mice. Furthermore, we could not observe a compensatory induction of *Gadd45b* in GADD45γ KO and WT mice (Fig. 33).

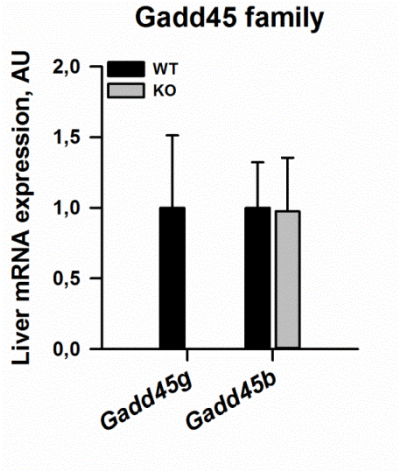

Figure 33: Liver *Gadd45b* and *Gadd45g* expression in GADD45γ KO and WT mice. Female GADD45γ KO and WT littermates were fasted for 24h before sacrifice. Liver mRNA levels were subsequently analysed by RT-qPCR. Values are fold induction relative to "WT". Mean ± SEM; n=5 per group.

As expected, fasting of the mice for 24 hours resulted in a significant decrease in body weight with no difference between genotypes (Fig. 34A). Also the tissue weights of liver, aWAT, BAT and GCM did not show any distinction between the two groups (Fig. 34B).

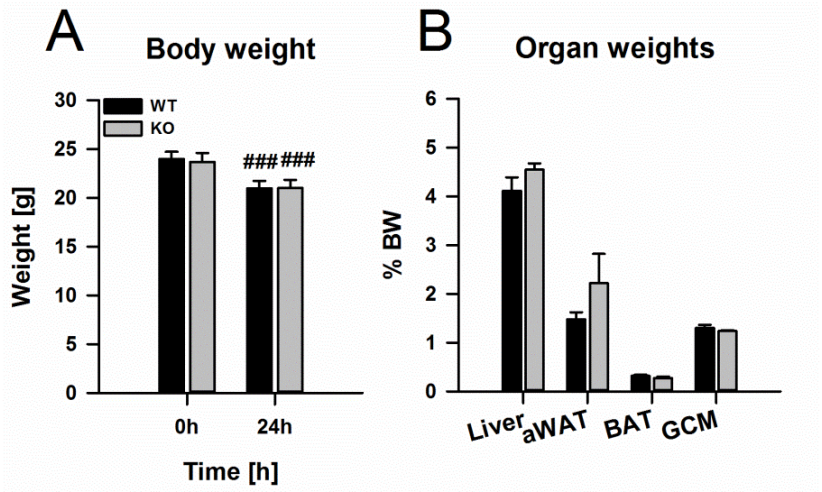

Figure 34: Body and tissue weights in GADD45γ KO and WT mice. (A) Body weight of female GADD45γ KO and WT littermates was measured before (0h) or after (24h) food withdrawal. (B) Tissue weights were measured after 24h fasting during preparation of the same mice as in (A) and normalized to body weight. Mean ± SEM; n=5 per group; * genotype effect, # effect of fast time; (*) $p \leq 0.05$, (**) $p \leq 0.01$, (***) $p \leq 0.001$.

Analysis of the serum metabolites did also not reveal any difference between GADD45γ KO and WT littermates (Fig. 35). Fasting blood glucose did not differ (Fig. 35A), neither did any of the metabolites (NEFA, TG, glycerol and cholesterol).

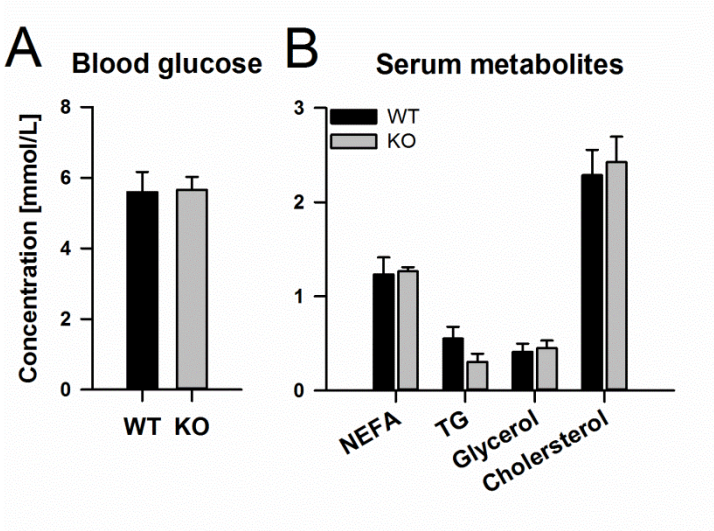

Figure 35: Serum metabolites in GADD45γ KO and WT mice. Blood glucose (A) and serum metabolites (non-esterified fatty acids (NEFA), triglycerides (TG), glycerol, and cholesterol; B) of female GADD45γ KO and WT littermates were measured 24h after food withdrawal. Mean ± SEM; n=5 per group.

As for the GADD45β WT and KO mice, the lipid profile of the liver was assessed (Fig. 36). Again, there was no difference in hepatic NEFA, TG or cholesterol content between the two groups.

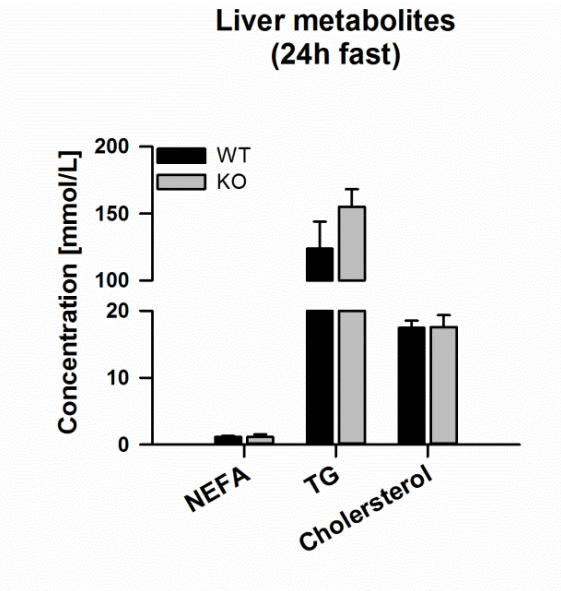

Figure 36: Liver metabolites in GADD45γ KO and WT mice. Liver metabolites (non-esterified fatty acids (NEFA), triglycerides (TG) and cholesterol) of female GADD45γ KO and WT littermates were measured 24h after food withdrawal. Mean ± SEM; n=5 per group.

3.3.6 Whole body GADD45β KO impairs liver lipid metabolism on a methionine and choline deficient diet

Given the observation that TG accumulated in the liver of fasted mice with loss of GADD45β it was our aim to better understand this phenotype by challenging mice with a methionine and choline deficient (MCD) diet or a matching control (Con) diet for 3 weeks. Through a series of mechanisms, the MCD diet causes an accumulation of triglyceride and fatty acids in the liver as the liver cannot form new lipoprotein particles for secretion, ultimately resulting in liver injury [70].

The MCD diet can also be considered nutrient deprivation since this diet lacks methionine and choline. We first measured the mRNA expression of *Gadd45b* in the liver of GADD45β KO and

WT littermates fed either the MCD or control diet. At the same time, we tested for the homozygous depletion of GADD45β and checked for a compensatory increase of its two family members. *Gadd45b* was induced upon MCD diet feeding with no concomitant increase in *Gadd45a* or *Gadd45g* expression (Fig. 37). Furthermore, we could not detect any *Gadd45b* mRNA in the GADD45β KO mice.

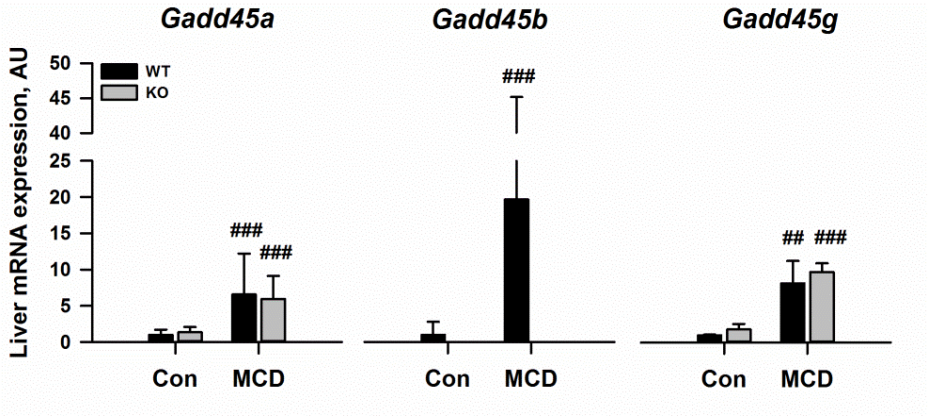

Figure 37: Liver *Gadd45a*, *Gadd45b* and *Gadd45g* expression in GADD45β KO and WT mice on MCD or control diet. Male GADD45β KO and WT littermates were either fed a diet deficient in methionine and choline (MCD) or a matching control diet (Con) for three weeks before sacrifice. Liver mRNA levels were subsequently analysed by RT-qPCR. Values are fold induction relative to "WT Con". Mean ± SEM; n=2-6 per group; * genotype effect, # diet effect; (*) $p \leq 0.05$, (**) $p \leq 0.01$, (***) $p \leq 0.001$.

Feeding GADD45β KO and WT littermates the MCD or control diet revealed no difference in genotype for most of the measured phenotypic parameters. All mice had a significantly lower blood glucose level at the day of sacrifice (30%, Fig. 38D), with no difference seen between genotype. All animals on the MCD diet lost weight during the three weeks of treatment (Fig. 38A), with a higher weight difference induced by MCD in WT mice relative to that observed in KO mice. The decrease in blood glucose and body weight is in accordance with current literature [69]. The tissue weights, normalised to body weight, did not change by feeding a MCD diet, nor was there a difference between GADD45β KO and WT mice (Fig. 38B, C, E and F). This is surprising given that the MCD diet is used to induce steatosis with severe accumulation of lipids in the liver. Liver weights were not significantly changed between the groups.

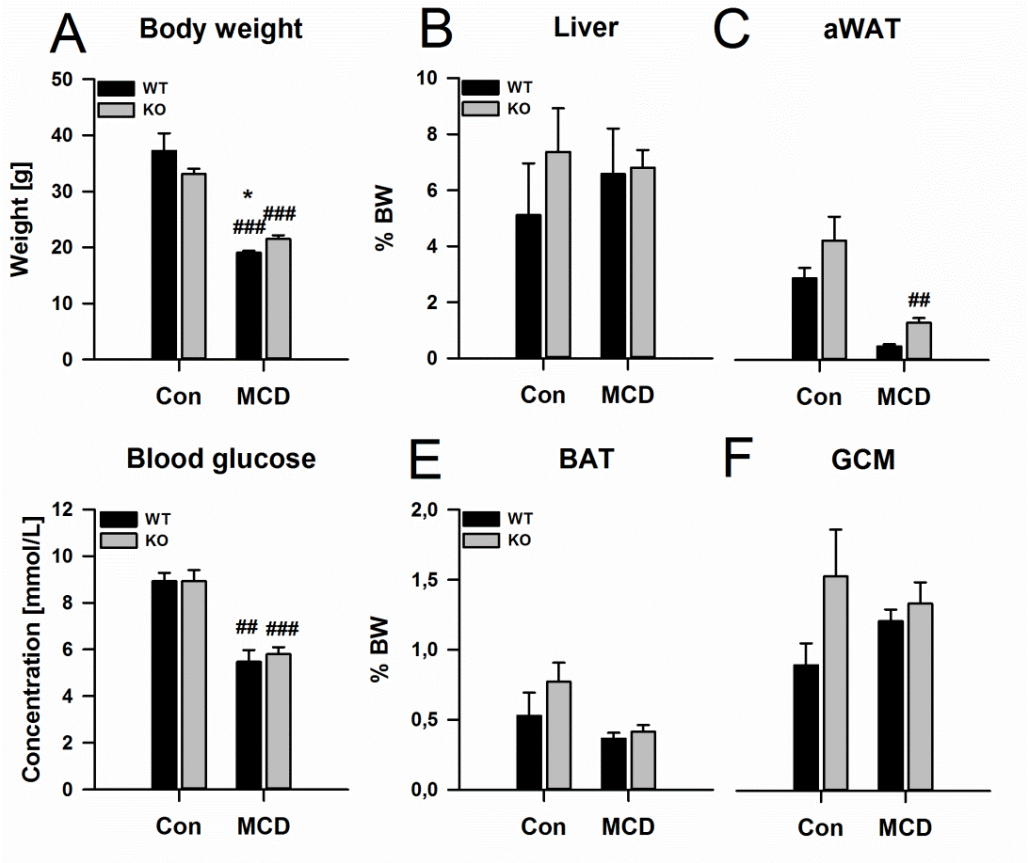

Figure 38: Body and tissue weights as well as blood glucose in GADD45β KO and WT mice on MCD or control diet. Male GADD45β KO and WT littermates were either fed a diet deficient in methionine and choline (MCD) or a matching control diet (Con) for three weeks before sacrifice. Body weight (A), liver weight (B), abdominal weight adipose tissue weight (aWAT, C), blood glucose (D), brown adipose tissue weight (BAT, E) and gastrocnemius muscle weight (GCM, F) was measured during preparation of the mice. Tissue weights (B, C, E, F) were normalized to body weight. Mean ± SEM; n=2-6 per group; * genotype effect, # diet effect; (*) $p \leq 0.05$, (**) $p \leq 0.01$, (***) $p \leq 0.001$.

The loss in body weight was also visible by analysing the body composition by magnetic resonance imaging (MRI). Body composition was measured before the start and at the end of the treatment. As shown in figure 39, mice on control diet gained weight during the three weeks mainly through an increase in fat mass (Fig. 39B) rather than lean mass (Fig 39A). Interestingly, GADD45β KO mice gained less fat mass on control diet. In contrast, mice on MCD diet lost weight through a loss in both lean and fat mass. There was no effect of genotype on the change in lean mass (Fig. 39A), but GADD45β WT mice lost less fat mass than their KO littermates. Paradoxically, GADD45β KO mice on MCD diet appeared to have more aWAT than WT mice at the end of the study (Fig.38C), hence the aggravated loss in fat mass observed by MRI in GADD45β KO mice might be due to a loss of other fat pads such as inguinal fat.

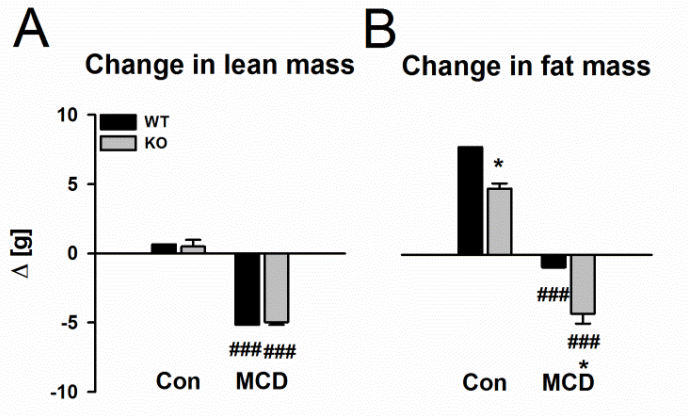

Figure 39: Body composition in GADD45β KO and WT mice on MCD or control diet. Male GADD45β KO and WT littermates were either fed a diet deficient in methionine and choline (MCD) or a matching control diet (Con) for three weeks before sacrifice. Body composition was measured at the beginning and at the end of the study and analysed as the change in lean mass (A) and fat mass (B) between the two time points. Mean ± SEM; n=2-6 per group; * genotype effect, # diet effect; (*) $p \leq 0.05$, (**) $p \leq 0.01$, (***) $p \leq 0.001$.

The loss of body weight when fed a MCD diet (Fig. 38A) could be due to decreased feed efficiency, as assessed by the amount of weight gain per food energy intake, or less energy intake. Indeed, feed efficiency was reduced in GADD45β KO and WT mice with no difference between genotypes (Fig. 40B). In contrast, total energy intake was not different between the four groups (Fig. 40D). Interestingly, GADD45β KO mice on MCD diet tended to drink more water than mice of any other group (Fig. 40C).

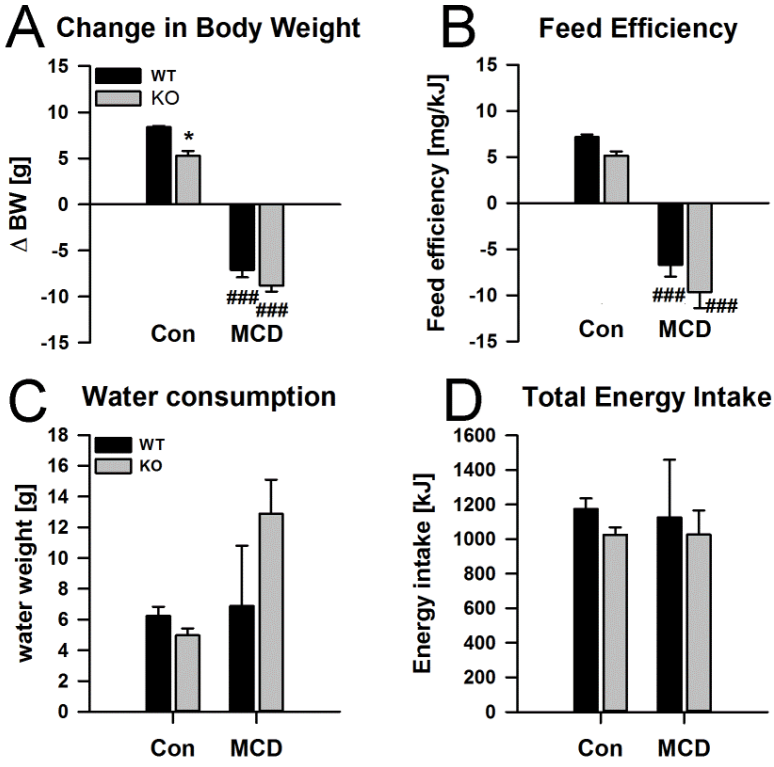

Figure 40: Energy usability in GADD45β KO and WT mice on MCD or control diet. Male GADD45β KO and WT littermates were either fed a diet deficient in methionine and choline (MCD) or a matching control diet (Con) for three weeks before sacrifice. Body mass (A) was measured at the beginning and at the end of the study and analysed as the change between the two time points. Feed efficiency (B) and total caloric intake (D) were determined by measuring the food consumption within one day. Water consumption (C) was also measured within 24h. Mean ± SEM; n=2-6 per group; * genotype effect, # diet effect; (*) $p \leq 0.05$, (**) $p \leq 0.01$, (***) $p \leq 0.001$.

At the termination of the experiment, mice were sacrificed in the *ad libitum* fed state and comprehensive analyses of blood serum and liver metabolite levels were carried out. Analysis of

the serum metabolites revealed a significant decrease of TG (Fig. 41B) and cholesterol (Fig. 41C) with no change in other lipid metabolites (Fig. 41A and D).). Accumulation of lipids in the liver following MCD feeding results from impaired formation of TG-containing VLDL particles and increased uptake of FA. Therefore, it is not surprising that serum TG levels were reduced on a MCD diet. Also, this lipid accumulation is accompanied with increased liver injury. We could measure an elevation of alanine aminotransferase (ALT) levels in mice fed the MCD diet (Fig. 41E), a cytosolic enzyme of the hepatocyte commonly measured clinically as a part of a diagnostic evaluation of hepatocellular health. Healthy individuals show an activity of less than 50 U/L. This was the case for mice fed the control diet. It is noteworthy that GADD45β depletion exacerbated liver injury.

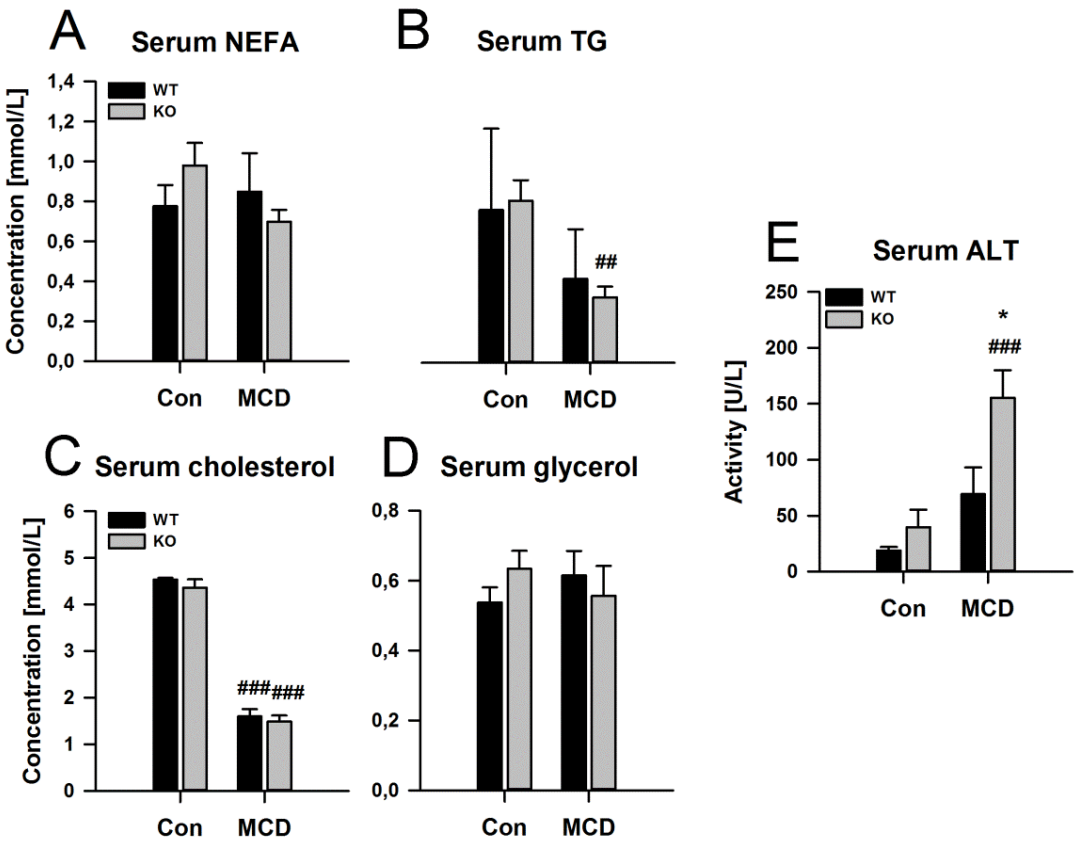

Figure 41: Serum metabolites in GADD45β KO and WT mice on MCD or control diet. Male GADD45β KO and WT littermates were either fed a diet deficient in methionine and choline (MCD) or a matching control diet (Con) for three weeks before sacrifice. Serum non-esterified fatty acids (NEFA, A), triglycerides (TG, B), cholesterol (C), glycerol (D) and alanine aminotransferase (ALT, E) were measured after processing the blood. Mean ± SEM; n=2-6 per group; * genotype effect, # diet effect; (*) $p \leq 0.05$, (**) $p \leq 0.01$, (***) $p \leq 0.001$.

As seen in figure 42, GADD45β KO mice showed an accumulation of liver triglycerides (Fig. 42B), glycerol (Fig. 42C) and cholesterol (Fig. 42D). This is in agreement with the reduced serum TG and cholesterol seen in GADD45β KO mice on MCD diet (Fig. 41B and C). Also, there was a slight increase in liver NEFA content in GADD45β KO mice on MCD diet (Fig. 42A). Surprisingly, GADD45β WT mice did not show the expected accumulation of lipids in the liver when maintained

on the MCD diet. Interestingly, GADD45β KO mice showed a decrease in the glycogen content of the liver when fed a MCD diet (Fig. 42E).

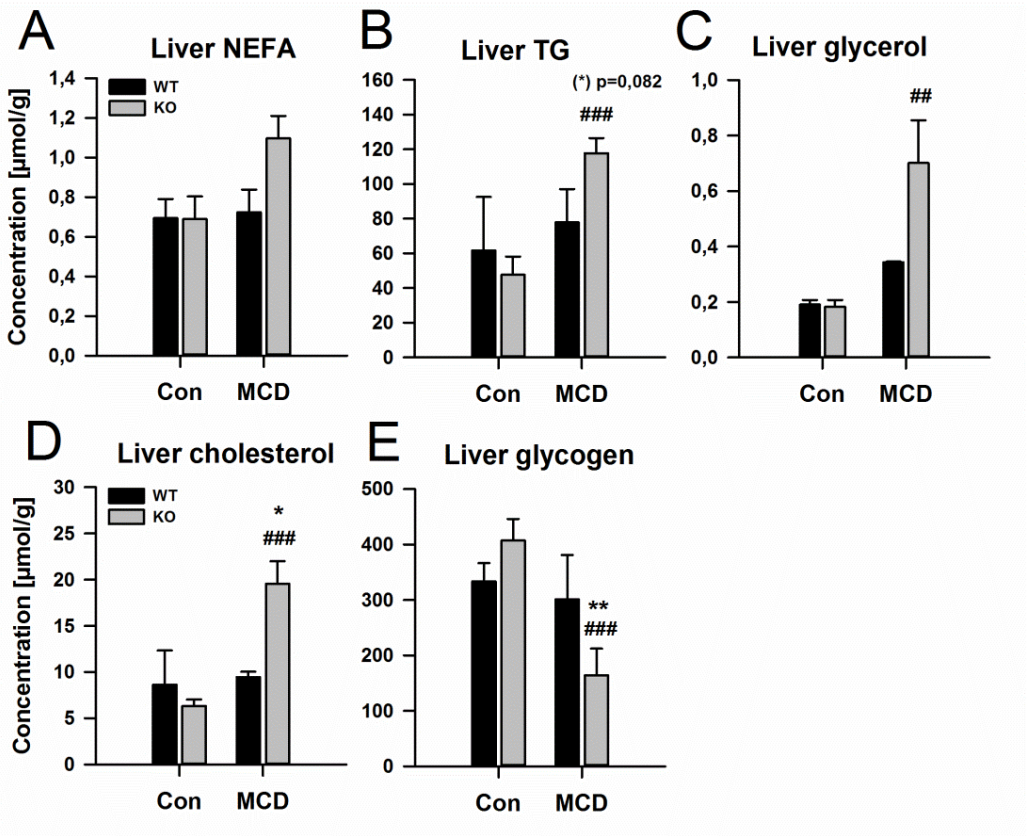

Figure 42: Liver metabolites in GADD45β KO and WT mice on MCD or control diet. Male GADD45β KO and WT littermates were either fed a diet deficient in methionine and choline (MCD) or a matching control diet (Con) for three weeks before sacrifice after which liver non-esterified fatty acids (NEFA, A), triglycerides (TG, B), glycerol (C), cholesterol (D) and glycogen (E) were measured. Mean ± SEM; n=2-6 per group; * genotype effect, # diet effect; (*) $p \leq 0.05$, (**) $p \leq 0.01$, (***) $p \leq 0.001$.

3.3.7 The impact of GADD45β KO on systemic amino acid and acyl carnitine metabolism during methionine and choline deficient diet is only mild

Since mice fed a MCD diet do not take up dietary methionine, they have to find other internal sources for this amino acid. As an essential amino acid, methionine is not synthesized *de novo* in humans and other animals. Although mammals cannot synthesize methionine, they can still regenerate it from homocysteine via methionine synthase in a reaction that requires vitamin B_{12} as a cofactor. Alternatively they have to break down proteins to increase their pool of methionine. Hence we were interested whether mice fed a MCD diet showed differences in serum amino acids and whether there was an influence of the GADD45β allele. Also, since MCD diet has a strong effect on lipid handling and influences serum TG levels, we also performed a profiling of serum acylcarnitines. As shown in figure 43, feeding the mice a MCD diet did not have a striking effect on serum amino acids. Only a few amino acids were reduced in their content relative to total amino acids which were increased overall on MCD diet (Fig. 43B). Those amino acids were methionine, as expected, valine, tyrosine and arginine (Fig. 43A).

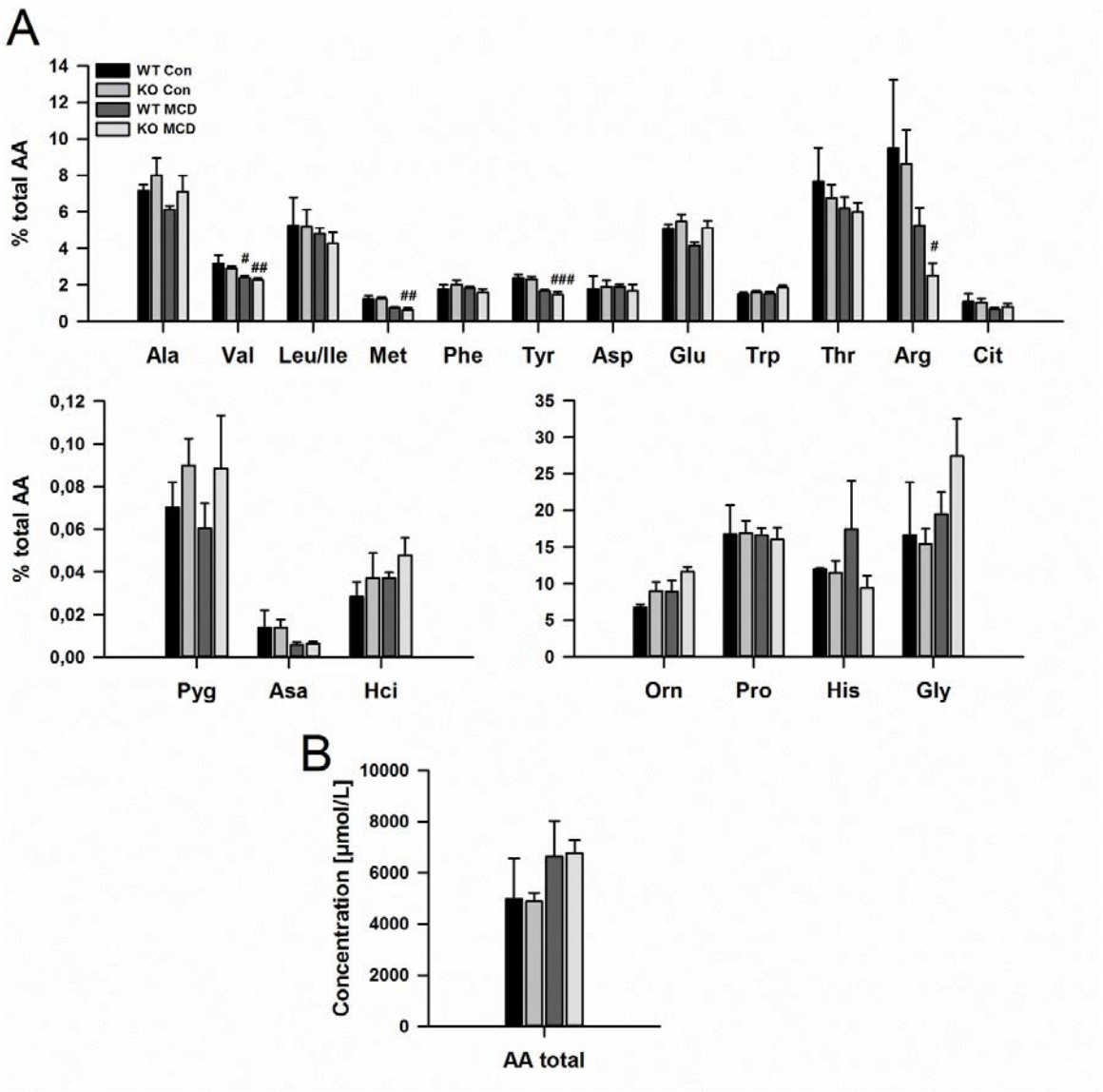

Figure 43: Serum amino acids in GADD45β KO and WT mice on MCD or control diet. Serum amino acids of male GADD45β KO and WT littermates were measured after being fed either a diet deficient in methionine and choline (MCD) or a matching control diet (Con) for three weeks before sacrifice (A). Concentrations are normalised to the total amino acid concentration (B). A list with full names can be found in suppl. table 6. Mean ± SEM; n=2-6 per group; * genotype effect, # diet effect; (*) $p \leq 0.05$, (**) $p \leq 0.01$, (***) $p \leq 0.001$.

In a similar manner, the concentrations individual acylcarnitine species were generally not altered upon MCD diet consumption (Fig.44). Only acylcarnitines C10:1 (decenoylcarnitine), C18:2 (linoleylcarnitine) and MeGlut (α-methylglutarylcarnitine) were increased on MCD diet (Fig. 44A). Total acylcarnitines, carnitine (C0) as well as acetyl carnitine (C2) were not changed either (Fig. 44B). None of the measured acylcarnitines differed between genotypes.

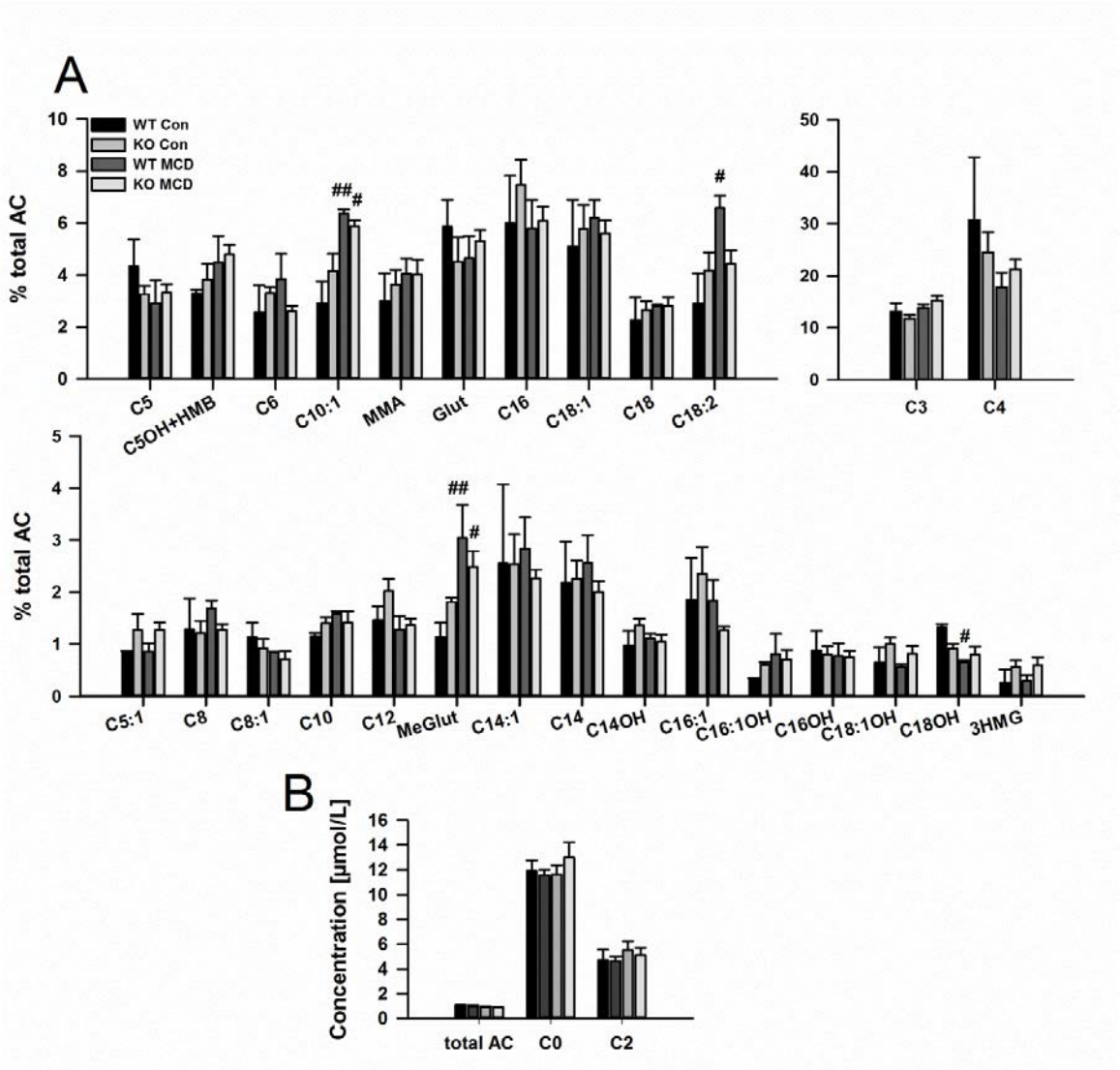

Figure 44: Serum acylcarnitines in GADD45β KO and WT mice on MCD or control diet. Serum acylcarnitines of male GADD45β KO and WT littermates were measured after being fed either a diet deficient in methionine and choline (MCD) or a matching control diet (Con) for three weeks before sacrifice (A). Concentrations are normalised to the total acylcarnitine concentration (B). Also free carnitine (C0) and acetylcarnitine (C2) were measured (B). A list with full names can be found in suppl. table 5. Mean ± SEM; n=2-6 per group; * genotype effect, # diet effect; (*) $p \leq 0.05$, (**) $p \leq 0.01$, (***) $p \leq 0.001$.

3.3.8 *db/db* mice show similar fasting effects on some serum parameters as seen in GADD45β KO mice

Since hepatic *Gadd45b* and *Gadd45g* were first discovered to be upregulated under the metabolic stress of fasting in healthy but not in diabetic *db/db* animals, we now characterised *db/db* mice further in terms of their metabolic reaction towards fasting. In the course of his PhD studies, Dr. Roldan de Guia (Herzig Lab) could already confirm that *db/db* mice are obese and diabetic having significant higher body weight, body fat and blood glucose levels, less lean mass, but almost twice as big livers at WT mice (see Fig. 3.2 of his PhD thesis). Most importantly, many abnormalities in serum parameters in *db/db* mice resembled what we have observed in GADD45β KO mice. Specifically, in *db/db* mice the increase of serum NEFA levels upon fasting was not as

striking as in WT mice, showing that they are metabolic inflexible in times of food deprivation. Also, whereas *db/db* mice had higher serum TG levels in the fed state, they did not respond with an increase of serum TG levels upon fasting as do the WT mice. We next quantified the hepatic NEFA and TG from these *db/db* and WT mice (Fig. 45). Liver NEFA levels did not change upon fasting in either group (Fig. 45A). We could confirm that *db/db* mice had dyslipidaemia through the massive accumulation of liver TGs in the fed state. Interestingly, only WT mice showed an increase in liver TG content upon fasting, reaching the same level as *db/db* mice (Fig. 45B).

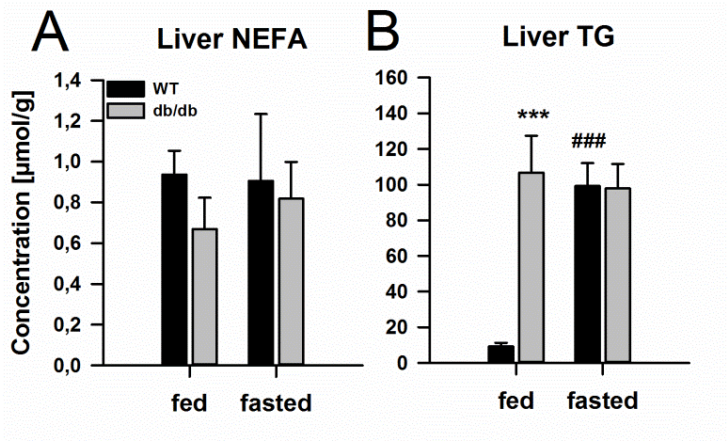

Figure 45: Liver metabolites in *db/db* and WT mice. Male wild-type (WT) and *db/db* mice were fed *ad libitum* (fed) or fasted for 24h (fasted) where indicated and liver non-esterified fatty acids (NEFA, A) and triglycerides (TG, B) were measured. Mean ± SEM; n=4 per group; * genotype effect, # effect of fasting; (*) $p \leq 0.05$, (**) $p \leq 0.01$, (***) $p \leq 0.001$.

3.3.9 Systemic lipid metabolism is also disturbed in aged mice

Based on the observation that the induction of liver *Gadd45b* upon fasting is blunted in aged mice, as it is in diabetic mice, we were interested if we would also see age-dependent differences in lipid handling. While the transcriptome analysis with liver samples from 22 months old and 12 weeks young mice was performed by Dr. Katharina Niopek (Herzig Lab), the analysis of serum and the liver was done by her intern Astrid Wendler. Serum and liver parameters in aged mice resembled those seen in GADD45β KO and *db/db* mice. Specifically, there was a blunted fasting-induced increase in serum NEFA concentrations in aged mice compared to young mice. Also, while both groups had the same blood glucose levels in the fed state, upon fasting old mice did not reduce their blood glucose levels to the same extent as young mice. Additionally, only young mice showed an increase in liver TG content upon fasting, while old mice did not show any difference between the fed and fasted state, showing that old mice are in a state of metabolic inflexibility.

3.3.10 The reduction in liver *GADD45B* also correlates with altered systemic lipid metabolism in humans

To test whether changes in GADD45β plays a role in the adaptive metabolism during the stress of nutrient deprivation in humans, we performed correlation analysis of serum parameters from lean and obese patients with and without T2D. Since *GADD45B* expression levels did not depend on the obese status but showed a significant reduction in all diabetic men (see Fig. 25), we grouped lean and obese patients for correlation analysis. In the Appendix, one can find a table with the

results of the dissected analysis (Suppl. table 4). As shown in figure 46, the concentrations of serum TG (Fig. 46A), fasting plasma glucose (Fig.46B), homeostatic model assessment for insulin resistance (Fig.46C) (HOMA-IR, a medical formula for quantifying insulin resistance [258]) and serum NEFA (Fig. 46D) correlated negatively with liver *GADD45B* levels (but HOMA-IR and NEFA showed a tendency towards significance). This means that men with lower liver *GADD45B* expression levels had increased serum NEFA and TG concentrations, a higher blood glucose level and were more insulin resistant.

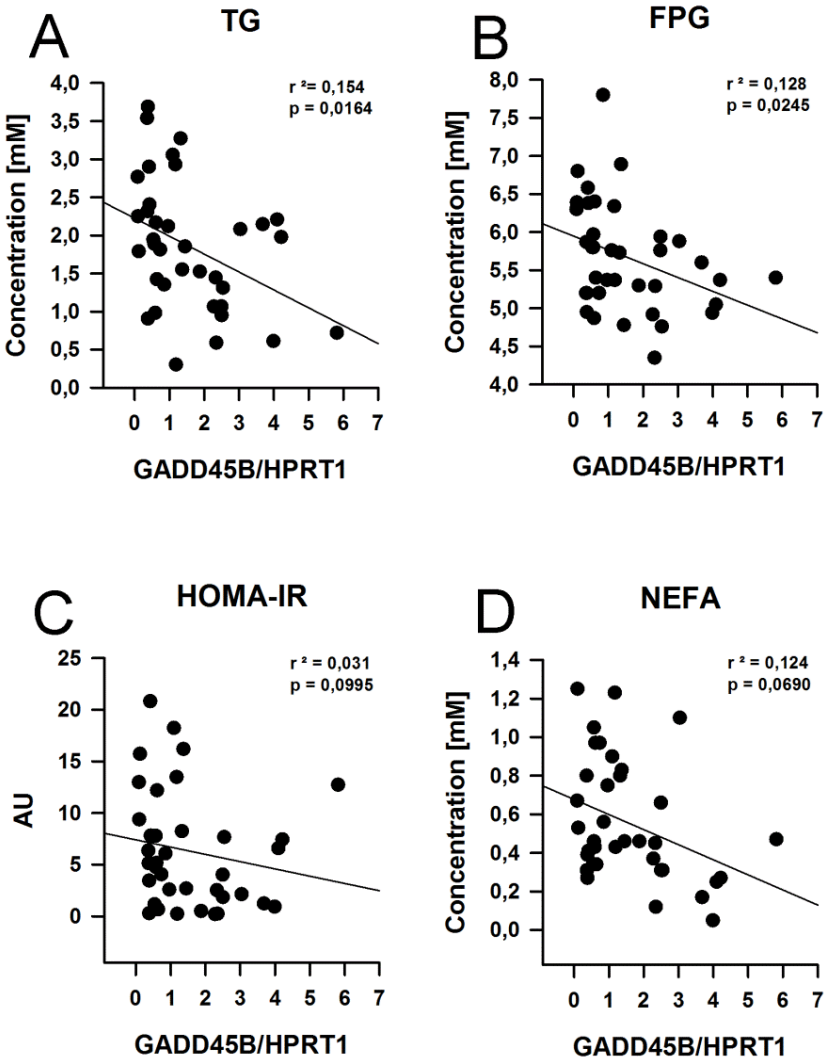

Figure 46: Serum metabolites, fasting plasma glucose and HOMA-IR in correlation to liver *GADD45B* expression levels in human. 37 Caucasian lean and obese men were fasted overnight and underwent abdominal surgery between 8 and 10 am during which liver biopsies were taken. Liver *GADD45B* mRNA levels were subsequently analysed by RT-qPCR and normalized to Hypoxanthine-Phosphoribosyl-Transferase 1 (HPRT1). Serum triglycerides (TG, A), fasting plasma glucose levels (FPG, B) and non-esterified fatty acids (NEFA, D) were measured and homeostatic model assessment for insulin resistance (HOMA-IR, C) was calculated. Correlation was determined using Shearman's correlation coefficient. Mean ± SEM; n=37.

3.4 GADD45β plays a role in regulating insulin sensitivity in chronic stress of nutrient overload

Since it is postulated that increased flux of hepatic lipids may be linked to insulin resistance [124,259], the next step was to induce fatty liver and insulin resistance in GADD45β WT and KO mice and determine if GADD45β plays also a role in the chronic supply of nutrients and adaptation of the organism to changes in metabolism.

3.4.1 GADD45β KO mice are more insulin resistant after 4 months on a high fat diet

Feeding mice diet rich in fat (HFD, 60% of total energy) is a more physiological alternative to induce obesity, diabetes and fat accumulation in the liver, than the MCD diet. Over the course of several weeks, feeding a HFD results in weight gain, development of hyperglycaemia, hyperinsulinaemia, hypertension and an increased TG content in adipose tissue, serum and liver [66]. For our purpose, GADD45β KO and WT mice were kept on a HFD or a matching control diet (NFD, 10% of total energy) for four months. The first analysis to be done was to confirm the complete depletion of GADD45β in GADD45β KO mice and to see if there was a compensatory induction of other GADD45 family members. As shown in Fig. 47, the genotype could be confirmed and there was no increase in *Gadd45a* or *Gadd45g* expression level when GADD45β was absent.

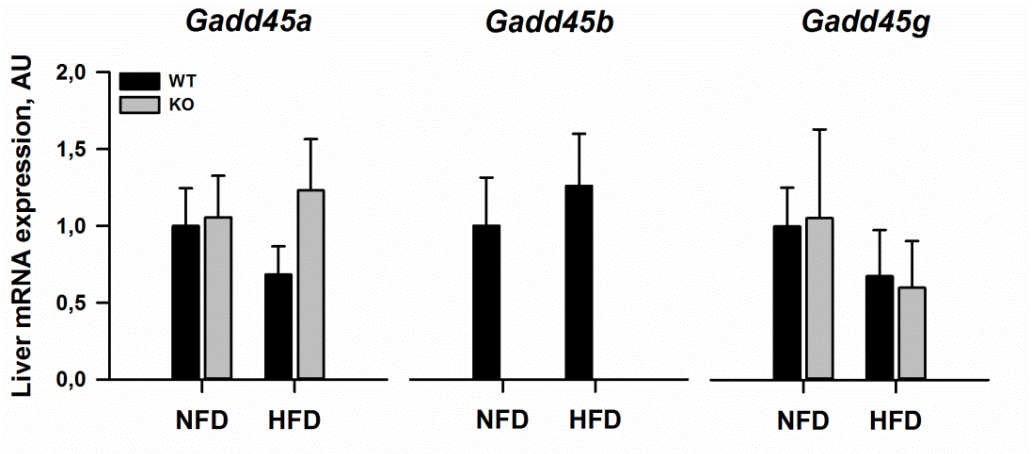

Figure 47: Liver *Gadd45a*, *Gadd45b* and *Gadd45g* expression in GADD45β KO and WT mice on HFD or control diet. Male GADD45β KO and WT littermates were either fed a diet high in fat (HFD) or a matching control diet (NFD) for 16 weeks before sacrifice. Liver mRNA levels were subsequently analysed by RT-qPCR. Values are fold induction relative to "WT NFD". Mean ± SEM; n=6-9 per group.

Next, we investigated if the presence or absence of GADD45β would make a difference in in body composition when fed a HFD. As expected, at the end of 4 months mice on HFD gained over 100 % of the weight of mice on NFD (Fig. 48A). Interestingly, GADD45β KO mice on NFD gained more weight than WT animals, but there was no effect of genotype when fed a HFD. The fat and lean mass before, during and at the end of the study was assessed by magnetic resonance imaging (MRI) (Fig. 48B and C). GADD45β KO and WT mice showed similar changes in fat and lean mass, both parameters increased on HFD. It seems as if the difference in body weight on

NFD between GADD45β KO and WT mice was a result of gaining more fat mass while having the same amount of lean mass.

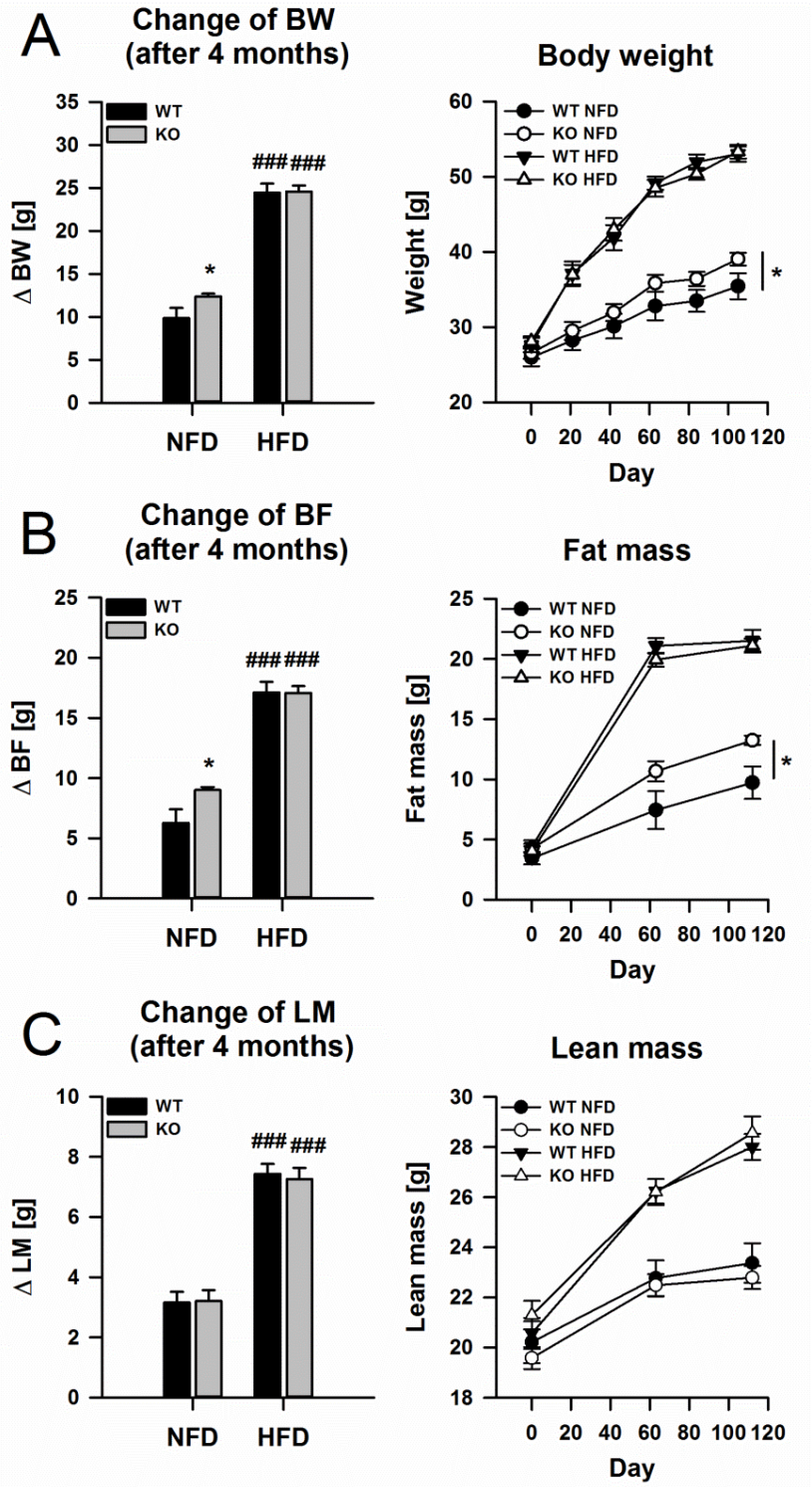

Figure 48: Body composition in GADD45β KO and WT mice on HFD or control diet. Male GADD45β KO and WT littermates were either fed a diet high in fat (HFD) or a matching control diet (NFD) for 16 weeks before sacrifice. Body weight was measured every three weeks (A, right) and the difference between the beginning and the end of the study was calculated (A, left). Body composition was measured at the beginning, in the middle and at the end of the study and analysed as the change in body fat (BF, B) and lean mass (LM, C) between day 0 and day 112 Mean ± SEM; n=6-9 per group; * genotype effect, # diet effect; (*) $p \leq 0.05$, (**) $p \leq 0.01$, (***) $p \leq 0.001$.

The body composition was further analysed during the preparation of the mice. The change in body weight was also reflected in total body weight gain (Fig. 49B). Animals on HFD had significantly higher body weight, but there was no difference between genotypes. Also, GADD45β KO mice on NFD were heavier than their WT littermates. This difference was due to a higher percentage of abdominal fat in GADD45β KO mice (Fig. 49D). On HFD, however, there was no difference between GADD45β KO and WT mice. Liver weights were the same between the groups on NFD and HFD, but GADD45β WT mice on HFD had slightly heavier livers than their KO littermates (Fig. 49C). Together with the body and tissue weights, we also measured blood glucose levels (Fig. 49A). As expected, mice on HFD were hyperglycaemic, with GADD45β KO mice having even slightly higher glucose levels.

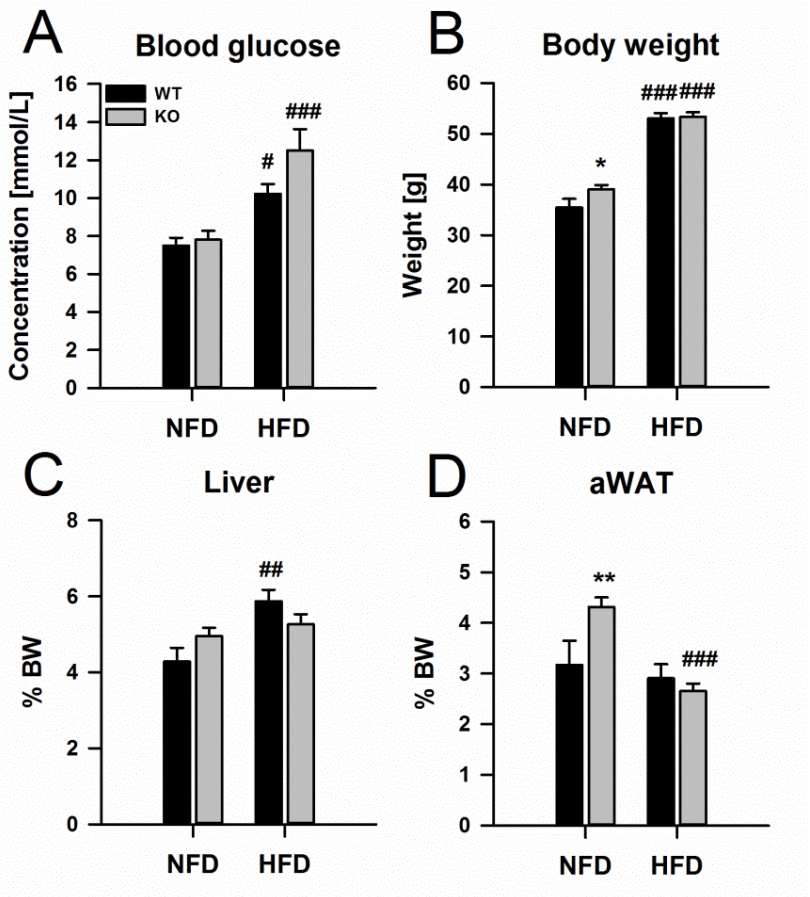

Figure 49: Body and tissue weights as well as blood glucose in GADD45β KO and WT mice on HFD or control diet. Male GADD45β KO and WT littermates were either fed a diet high in fat (HFD) or a matching control diet (NFD) for 16 weeks before sacrifice. Blood glucose (A), body weight (B), liver weight (C) and abdominal weight adipose tissue weight (aWAT, D) were measured during preparation of the mice. Tissue weights (C and D) were normalized to body weight. Mean ± SEM; n=6-9 per group; * genotype effect, # diet effect; (*) $p \leq 0.05$, (**) $p \leq 0.01$, (***) $p \leq 0.001$.

Next we were interested if a knockout of GADD45β would influence the systemic and hepatic metabolism during an oversupply of fat and nutrients. In general there was no or if at all only a mild effect of genotype on serum metabolites. Circulating NEFAs were reduced on HFD in both groups (Fig. 50A), whereas there was no effect on serum TG (Fig. 50B). Serum glycerol and cholesterol were higher in GADD45β KO mice on NFD compared to their WT littermates (Fig. 50C

and D). On HFD however, there was no effect of genotype. Serum cholesterol levels were increased on HFD in both groups.

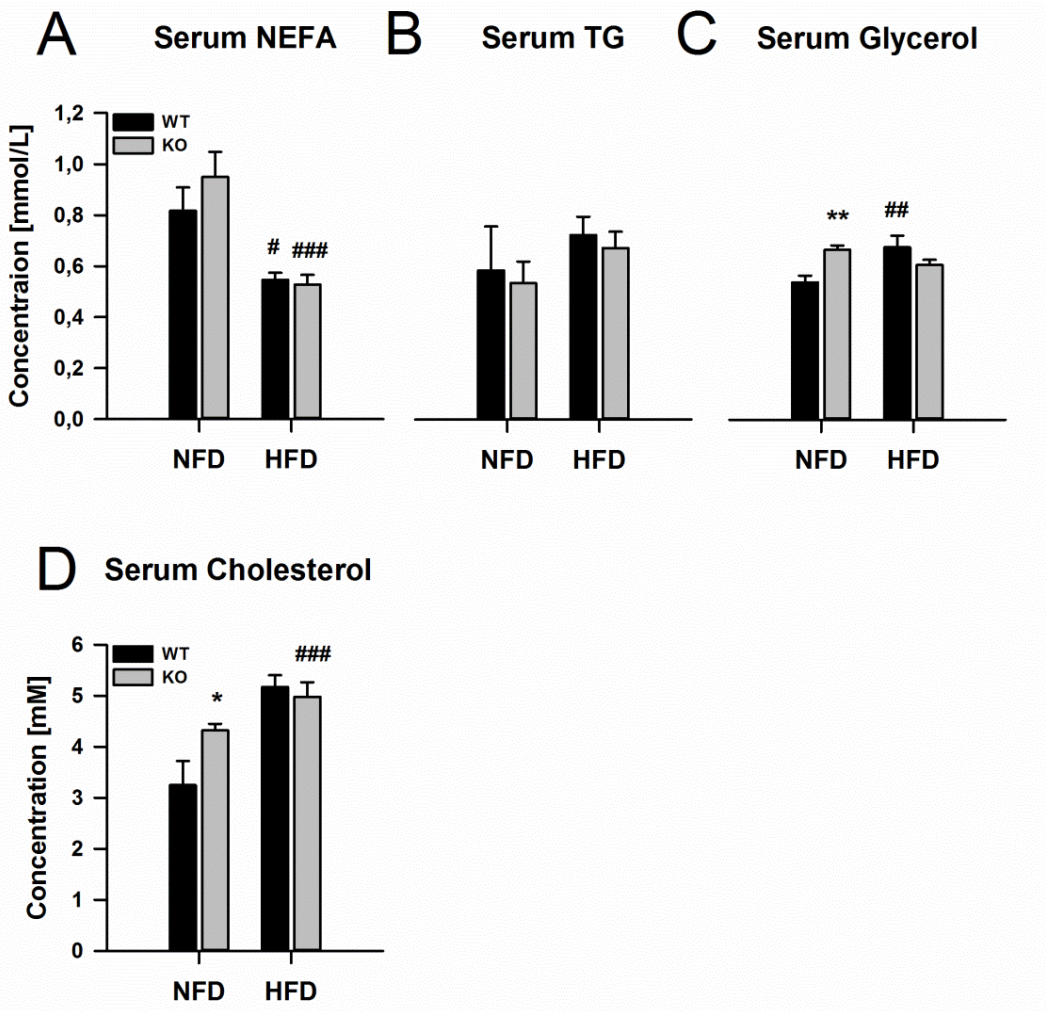

Figure 50: Serum metabolites in GADD45β KO and WT mice on HFD or control diet. Male GADD45β KO and WT littermates were either fed a diet high in fat (HFD) or a matching control diet (NFD) for 16 weeks before sacrifice. Serum non-esterified fatty acids (NEFA, A), triglycerides (TG, B), glycerol (C) and cholesterol (D) were measured after processing the blood. Mean ± SEM; n=6-9 per group; * genotype effect, # diet effect; (*) $p \leq 0.05$, (**) $p \leq 0.01$, (***) $p \leq 0.001$.

Analysis of liver metabolites revealed no difference between GADD45β KO and WT, neither on NFD nor on HFD. We could confirm that feeding a HDF increased the levels of TG in the liver over 100% (Fig. 51B), and also liver cholesterol was 100% increased (Fig. 51C), but no metabolite showed an effect of genotype. The same holds true for liver NEFA levels (Fig. 51A).

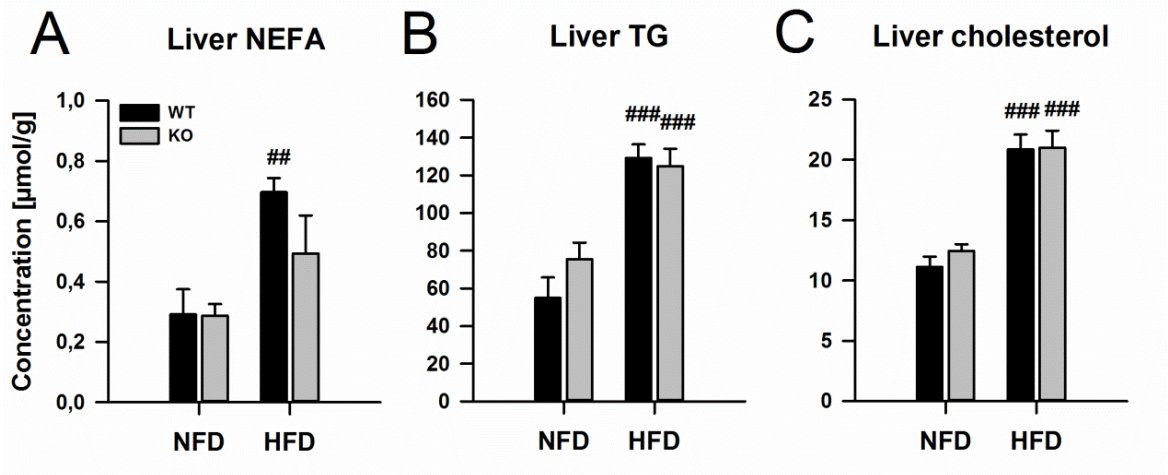

Figure 51: Liver metabolites in GADD45β KO and WT mice on HFD or control diet. Male GADD45β KO and WT littermates were either fed a diet high in fat (HFD) or a matching control diet (NFD) for 16 weeks before sacrifice. Liver non-esterified fatty acids (NEFA, A), triglycerides (TG, B), and cholesterol (C) were measured after processing the blood. Mean ± SEM; n=6-9 per group; * genotype effect, # diet effect; (*) $p \leq 0.05$, (**) $p \leq 0.01$, (***) $p \leq 0.001$.

After completing the metabolic profiling of GADD45β KO and WT fed a HFD or control diet, which did not reveal a striking phenotype effect, we went back to the original question if GADD45β might be involved in the response of the organism to overnutrition on the level of glucose/insulin homeostasis.

The first measurements were performed after 4 weeks on HFD or NFD, when for a glucose tolerance test (GTT) 5 µl/g body weight of a 20% glucose solution was injected into the peritoneum of fasted mice and blood samples were taken to determine how quickly the sugar could be cleared from the blood (Fig. 52). Already after one month on HFD, mice had higher fasting glucose levels than mice fed a NFD (Fig. 52A). After glucose administration glucose levels were increased in all mice. Although the total blood concentration was higher in mice on HFD (Fig. 52A), their rise in glucose levels relative to their basal level was not higher than in mice on NFD (Fig. 52B). Taking the total glucose levels into account (Fig. 52A), the area under the curve was higher for mice on HFD, with no difference between GADD45β KO and WT mice (Fig. 52C).

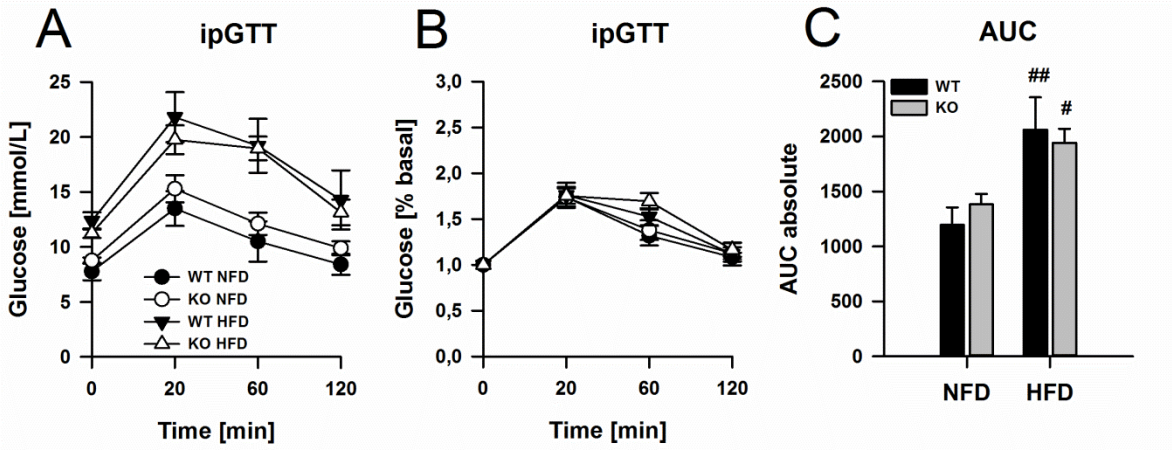

Figure 52: GTT in GADD45β KO and WT mice on HFD or control diet. Male GADD45β KO and WT littermates were either fed a diet high in fat (HFD) or a matching control diet (NFD) for 4 weeks when an intraperitoneal glucose tolerance test (ipGTT) was performed as described in the methods section. Blood glucose levels were measured after 20, 60 and 120 minutes and shown as total concentrations (A) and as percentage from basal levels (B). From (A) the area under the curve mas calculated (AUC, C). Mean ± SEM; n=6-9 per group; * genotype effect, # diet effect; (*) $p \leq 0.05$, (**) $p \leq 0.01$, (***) $p \leq 0.001$.

After 4 months on HFD or NFD an insulin tolerance test (ITT) was performed. As such, 1 U insulin/kg body weight was injected intraperitoneally into the mice and blood glucose levels were monitored for 120 minutes. As shown in figure 53, all mice on HFD had higher blood glucose concentrations (Fig. 53A) and were not responsive to exogenously administered insulin during the ITT despite being administered double the absolute dose owing to their higher body mass. In contrast, mice fed a NFD showed a drop in their blood glucose concentration (Fig. 53B). Since the basal level of blood glucose was higher when fed a HFD, and also the drop in glucose concentration was lower than in NFD fed animals (Fig. 53D), the resulting area under the curve (AUC) was bigger on HFD compared to NFD fed animals (Fig. 53C). Most interestingly, GADD45β KO mice fed a HFD had an even higher AUC than their WT littermates on the same diet.

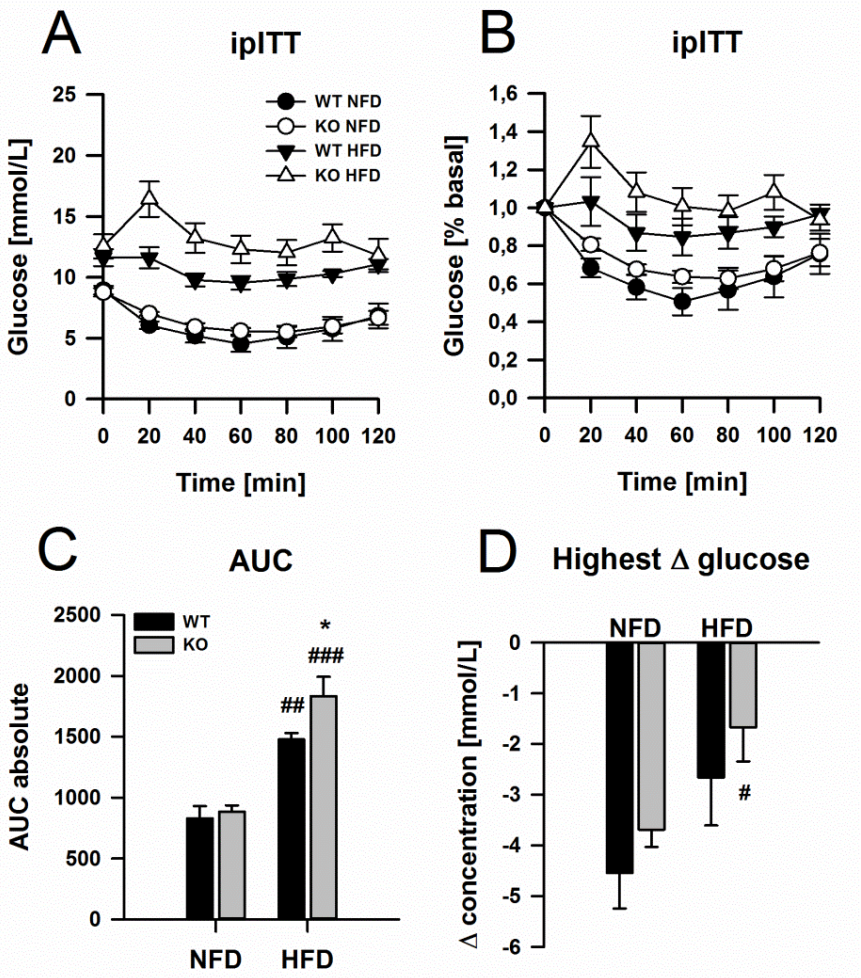

Figure 53: ITT in GADD45β KO and WT mice on HFD or control diet. Male GADD45β KO and WT littermates were either fed a diet high in fat (HFD) or a matching control diet (NFD) for 16 weeks before sacrifice. One week before, an intraperitoneal insulin tolerance test (ipITT) was performed as described in the methods section. Blood glucose levels were measured every 20 minutes and shown as total concentrations (A) and as percentage from basal levels (B). From (A) the area under the curve mas calculated (AUC, C) and the highest drop in glucose concentration relative to time point 0 was determined (D). Mean ± SEM; n=6-9 per group; * genotype effect, # diet effect; (*) $p \leq 0.05$, (**) $p \leq 0.01$, (***) $p \leq 0.001$.

From blood taken during fasting sampling in the GTT and ITT glucose and insulin concentrations were measured to calculate the HOMA-IR (Fig. 54). Blood glucose levels were always lower in mice on NFD than in mice on HFD, both after 4 and 16 weeks on the diet (Fig. 54A). Blood glucose concentrations did not change over time and did not show an effect of genotype at either time point. Unlike blood glucose levels, serum insulin levels changed over time (Fig. 54B). Already after 1 month on HFD, mice had augmented serum insulin levels which increased strikingly within the following three months. Whereas there was no difference between GADD45β KO and WT mice on HFD after 1 month, GADD45β KO had a significantly higher insulin concentration when fed a HFD for 4 months. Insulin resistance can be assessed by the use of the HOMA-IR, which takes the fasting glucose and insulin concentrations into account. As shown in figure 54C, all mice on HFD had a higher HOMA-IR than mice fed a NFD, but GADD45β KO mice on HFD for 4 months had a significant higher HOMA-IR value than their WT littermates on the

same diet. Taken together, these data show that GADD45β KO mice were more insulin resistant after 4 months on HFD.

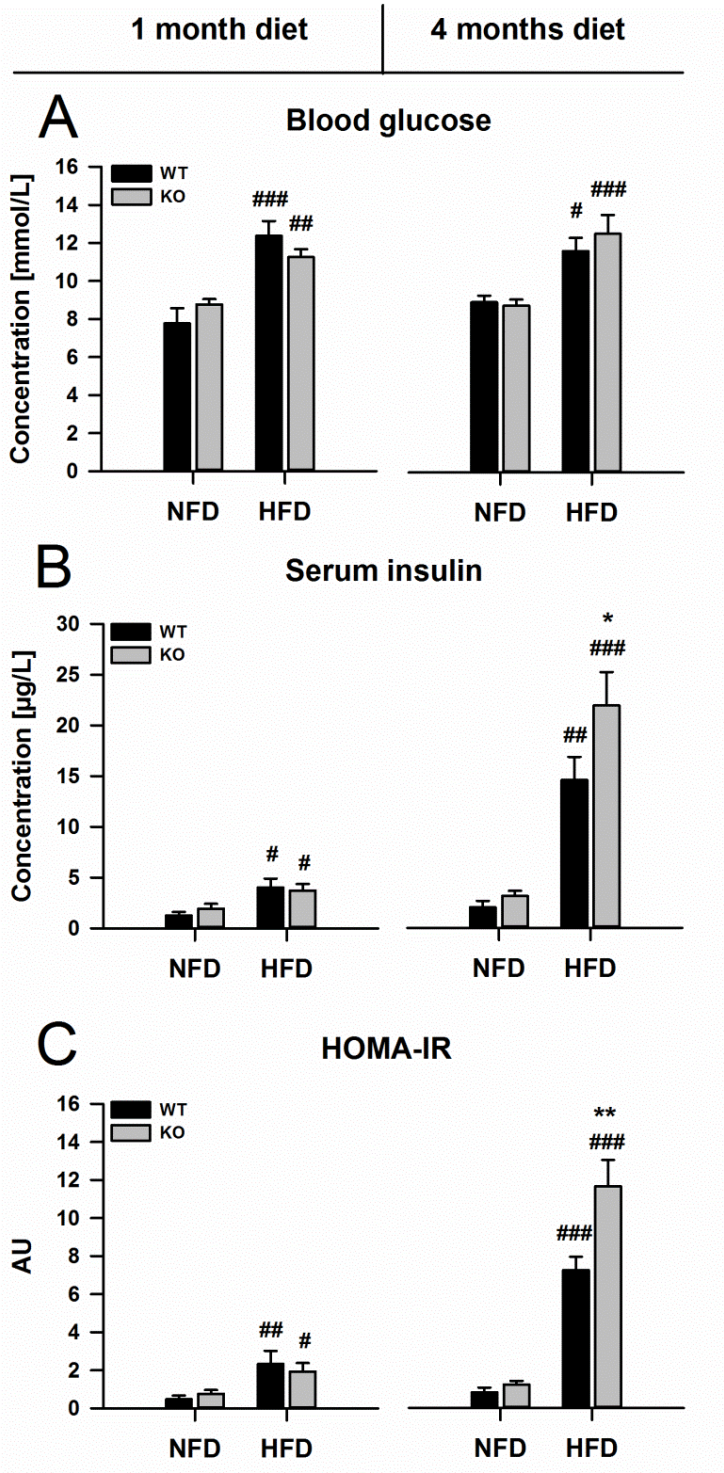

Figure 54: Fasting blood glucose, serum insulin and HOMA-IR of GADD45β KO and WT mice on HFD or control diet. Male GADD45β KO and WT littermates were either fed a diet high in fat (HFD) or a matching control diet (NFD) for 16 weeks before sacrifice. After 1 and 4 months fasting blood glucose (A) and serum insulin (B) were measured and the homeostatic model assessment for insulin resistance (HOMA-IR, C) was calculated. Mean ± SEM; n=6-9 per group; * genotype effect, # diet effect; (*) $p \leq 0.05$, (**) $p \leq 0.01$, (***) $p \leq 0.001$.

3.4.2 The impact of GADD45β KO on systemic amino acid and acyl carnitine metabolism during high fat diet is only mild

Even though we did not observe a difference between GADD45β KO and WT in their lipid profiling under HFD conditions, we could see a difference in regard to their insulin sensitivity with GADD45β KO mice being more insulin resistant than their WT littermates. This result prompted us us to examine the serum amino acid and acylcarnitine concentrations. It is reported, that circulating BCAA in the background of a HFD are involved in the induction of obesity-associated insulin resistance [260-262], and also certain acylcarnitine species are increased in T2D [263-266] due to an increased BCAA catabolic flux, dysregulated mitochondrial function or incomplete long-chain fatty acid oxidation [267].

As shown in figure 55, there was a tendency for total amino acid levels to be increased on HFD, but when normalizing to the total amino acid concentration, there was no difference in BCAA or any other amino acids between GADD45β KO and WT mice.

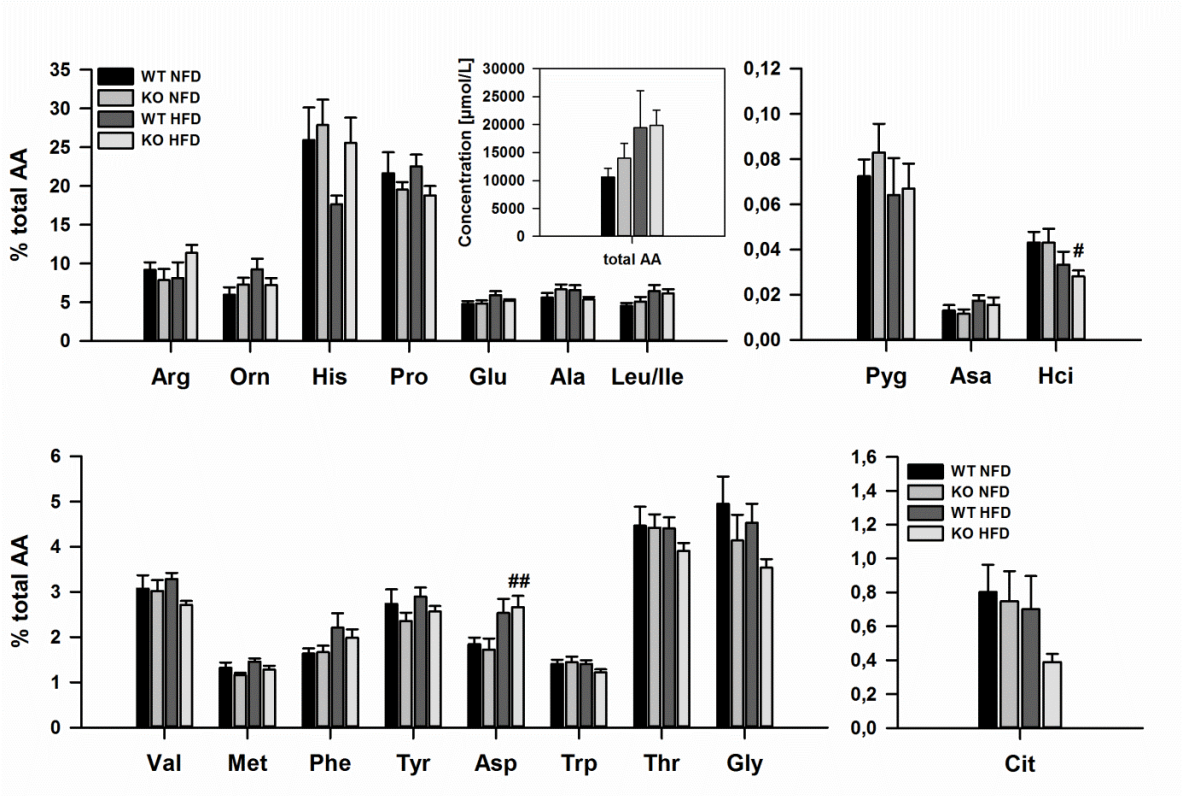

Figure 55: Serum amino acids in GADD45β KO and WT mice on HFD or control diet. Serum amino acids of male GADD45β KO and WT littermates were measured after being fed either a diet high in fat (HFD) or a matching control diet (NFD) for 4 months before sacrifice. Concentrations are normalised to the total amino acid concentration (small insert). A list with full names can be found in suppl. table 6. Mean ± SEM; n=6-9 per group; * genotype effect, # diet effect; (*) p ≤ 0.05, (**) p ≤ 0.01, (***) p ≤ 0.001.

Also the effect of GADD45β deletion on acylcarnitine concentrations was only mild (Fig. 56A). There were only a few acylcarnitines whose concentration increased upon HFD feeding, which are all long-chained, namely C18 (stearoylcarnitine), C18:1OH (3-OH-octadecenoylcarnitine), C16OH (3-OH-palmitoylcarnitine) and Glut (glutarylcarnitine). This is in accordance with recent

literature, where in particular long chain acylcarnitines are reported to be involved in obesity-related insulin resistance [263,264,266]. None of these showed a difference between the genotypes, however, C16:1OH (3-OH-hexadecenoylcarnitine) concentrations were increased in GADD45β KO mice compared to all other groups. Also, total acylcarnitines, free carnitine (C0) as well as acetyl carnitine (C2) were not changed either (Fig. 56B).

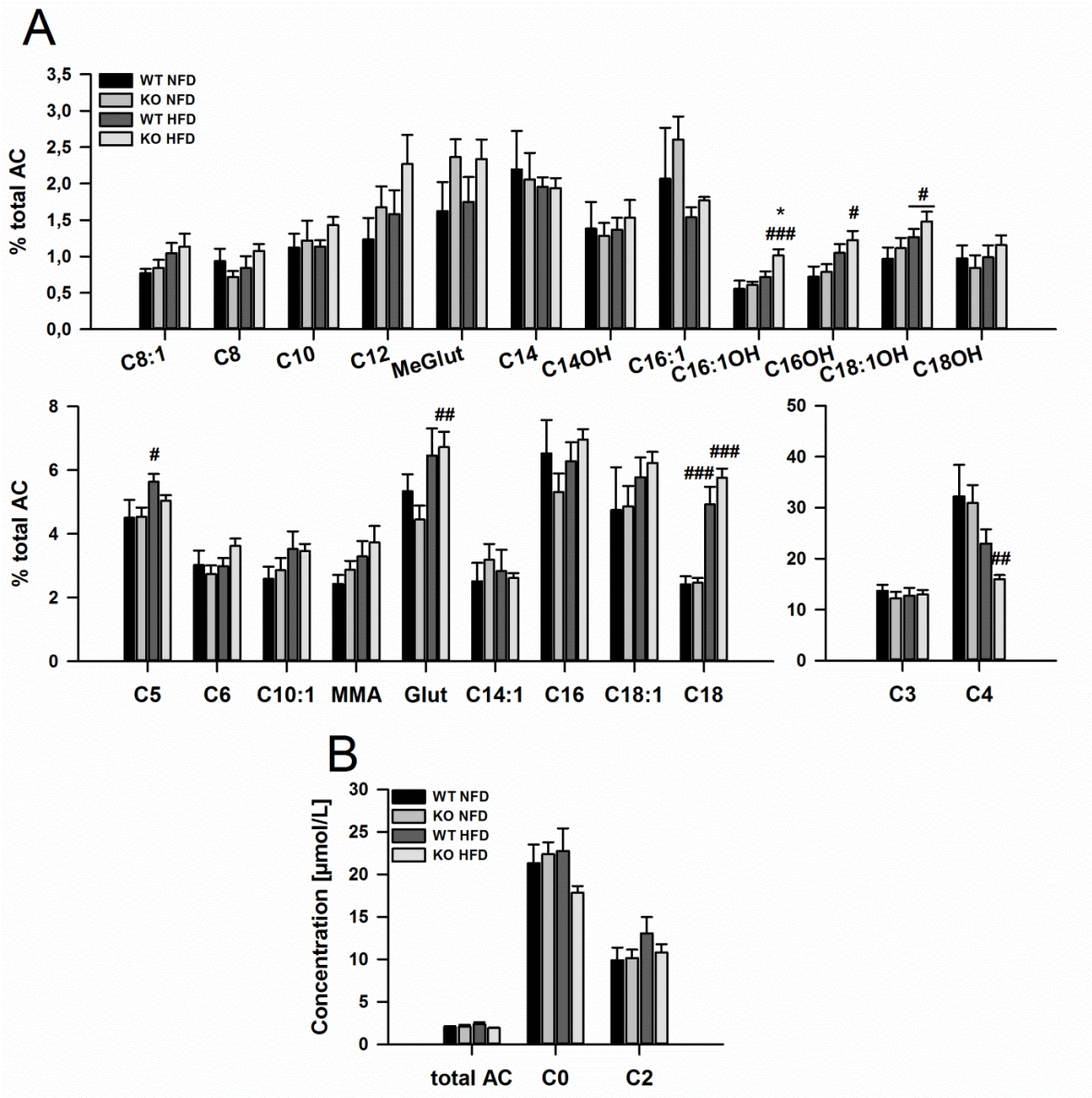

Figure 56: Serum acylcarnitines in GADD45β KO and WT mice on HFD or control diet. Serum acylcarnitines of male GADD45β KO and WT littermates were measured after being fed either a diet high in fat (HFD) or a matching control diet (NFD) for 4 months before sacrifice (A). Concentrations are normalised to the total acylcarnitine concentration (B). Also free carnitine (C0) and acetyl carnitine (C2) were measured (B). A list with full names can be found in suppl. table 5. Mean ± SEM; n=6-9 per group; * genotype effect, # diet effect; (*) $p \leq 0.05$, (**) $p \leq 0.01$, (***) $p \leq 0.001$.

3.5 Effect of hepatic GADD45β overexpression on the observed phenotypes

To investigate if hepatic GADD5β plays a crucial role in mediating the observed effects on lipid handling and insulin resistance, gain-of-function experiments were performed. Adenoviruses (AD) are commonly used as vector systems to transport exogenous DNA to cells or organs, so recombinant adenoviruses were generated, which contained either a liver-specific vector for the expression of a flag-tagged *Gadd45b* cDNA or an empty vector as control. 1 x10^9 infectious units per recombinant virus were injected into mice via their tail vein. The viruses were thereafter transported through the vascular system and trapped liver while other tissues are barely affected. Since adenoviruses can be cleared from the system of the host after approximately 14 days, experiments were terminated at the ideal time point for phenotypic analysis which has been shown to be one week after virus application [241].

3.5.1 The designed GADD45β overexpression construct is functional *in vitro*

Before adenovirus production could be started, it had to be verified that the generated GADD45β overexpression construct is able to generate an overexpression of GADD45β *in vitro*. Therefore, we transfected HEK293 cells with pENTR-Flag vectors either harboring the GADD45β sequence or a non-specific sequence as control together with a vehicle control, using PEI as a transfection reagent. Cells were harvested 48 hours later, and the protein levels of GADD45β were assessed by immunoblotting. As shown in figure 57, GADD45β could be detected only in cells transfected with the GADD45β-flag vector. Consequently, the vectors could be used to produce adenovirus particles (see methods section 5.3.1).

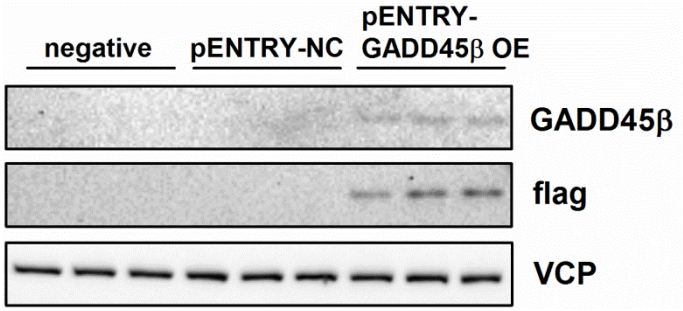

Figure 57: Cloning of expression constructs for GADD45β overexpression. HEK293 cells were transfected with pENTRY vectors containing the GADD45β sequence (pENTRY-GADD45β OE) or a non-specific sequence (pENTRY-NC) or vehicle (negative). 48 hours later the cells were harvested and the protein levels of GADD45β were assessed by immunoblotting using GADD45β- or flag-antibody, and VCP-antibody as loading control. Results from 3 independent experiments are shown.

3.5.2 Adenoviruses for the overexpression of GADD45β are functional *in vitro*

Prior to *in vivo* use, the generated adenovirus for the overexpression of GADD45β was tested in HEK293 cells. For this purpose, cells were infected with different doses (MOI = cells in well/virus ifu per µl) of adenoviruses either carrying a vector for the expression of a flag-tagged *Gadd45b*

cDNA (AD-GADD45β OE) or an empty vector as control (AD-NC). The cells were incubated for 24 hours and the protein levels of GADD45β were assessed by immunoblotting with an antibody against the flag tag. As shown in figure 58, only cells that received the AD-GADD45β OE showed a dose-dependent expression of GADD45β. Thus the generated viruses were functional and could be used for *in vivo* applications.

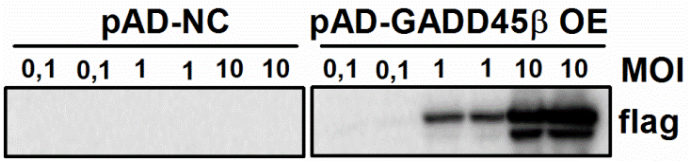

Figure 58: Infection of HEK293 cells with adenovirus. HEK293 cells were infected with increasing doses (MOI = cells in well/virus ifu per µl) of adenoviruses containing a vector for the expression of a flag-tagged *Gadd45b* cDNA (AD-GADD45β OE) or an empty vector as control (AD-NC). Cells were harvested 24 hours later and the protein levels of GADD45β were assessed by immunoblotting using flag-antibody.

3.5.3 Two pilot studies confirm the liver-specific overexpression of GADD45β via adenovirus administration *in vivo*

To test if the generated adenoviruses confer a liver-specific overexpression of GADD45β, two pilot studies were conducted. For the first study, only GADD45β WT mice received the AD-GADD45β OE, and one week later, half of these mice were fasted for 24 hours before sacrifice. For the second pilot study, AD-NC or AD-GADD45β OE viral particles were administered to GADD45β KO mice, which were sacrificed in the random fed state. For both studies genomic DNA and RNA was extracted to measure the hepatic viral load and *Gadd45b* mRNA levels, respectively. Here, liver samples from animals which did not receive adenoviruses were also included as controls.

As shown in figure 59A, application of the adenoviruses via the tail vein resulted in successful sequestration of the virus in the liver, in agreement with the literature [268,269]. One animal from the fasted and one animal from the fed group showed less viral load, which correlated with levels of the *Gadd45b* mRNA (Fig. 59B) and GADD45β protein levels (Fig. 59C). Interestingly, virus-mediated GADD45β overexpression seemed to overcome the fasting-mediated induction of *Gadd45b* (Fig. 59B); the fed group showed in average similar mRNA expression levels compared to the fasted group.

In the second pilot study, adenovirus administration was not as successful as it was in the first pilot study. Viral load in livers from mice receiving the AD-GADD45β OE was bigger than in mice receiving the AD-NC (Fig. 59D). This may be due to inconsistent application of the virus via tail vein injection and hence the virus particles might not have reached the liver. Since the mice were sacrificed *ad libitum*, *Gadd45b* levels should be low. AD-GADD45β OE administration led to a strong induction of *Gadd45b*, whereas AD-NC injection resulted in similar expression levels as compared to the control animals (Fig. 59E). Even though the mRNA expression was strong, it

was hard to detect GADD45β at the protein level (Fig. 59F). But nevertheless a faint band could be detected in the animals with AD-GADD45β OE.

Taken together, the generated adenoviruses harbouring a vector for the liver-specific overexpression of GADD45β were shown to be functional and were therefore used in subsequent gain-of-function experiments.

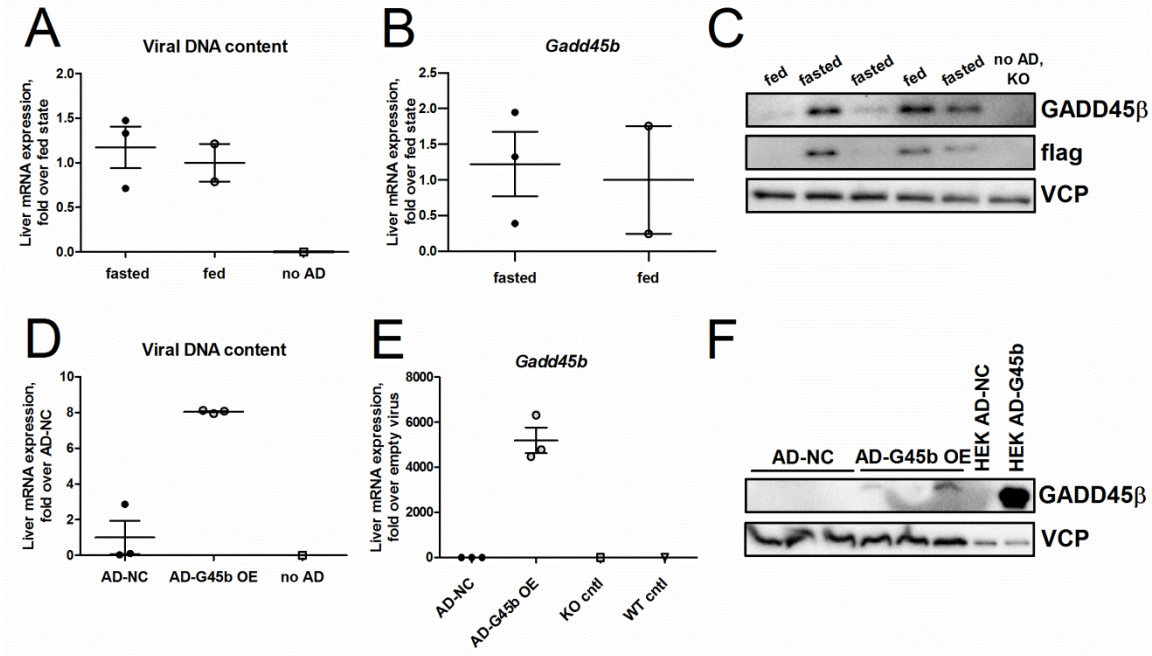

Figure 59: Liver *Gadd45b* mRNA and GADD45β protein levels in GADD45β KO and WT mice after adenovirus administration. Five male GADD45β WT mice received the AD-GADD45β OE, and after one week three of them were fasted for 24 hours before sacrifice (fasted) whereas the other two mice were sacrificed *ad libitum* (fed) (A-C). Other six GADD45β KO mice received AD-NC or AD-GADD45β OE particles and were sacrificed *ad libitum* one week later (D-F). Viral DNA content (A, D) and *Gadd45b* mRNA levels (B, E) were analysed by RT-qPCR, GADD45β levels by immunoblotting (C, F) using antibodies against GADD45β, the flag tag or the loading control (VCP).

3.5.4 GADD45β overexpression in GADD45β KO mice can partially reverse their dysregulated fasting lipid metabolism

In a first attempt to rescue the phenotype observed with GADD45β KO mice under the stress of nutrient deprivation by liver-specific GADD45β overexpression, GADD45β KO and WT mice received 1 x10^9 infectious units per recombinant virus (AD-NC or AD-GADD45β OE), and one week later were fasted for 24 hours before sacrifice. As shown in figure 60, the injection of AD-GADD45β OE into the tail vein led to a strong increase of *Gadd45b* levels in the liver in GADD45β KO and WT animals compared to those animals which received the AD-NC (Fig. 60A). Interestingly, GADD45β KO animals with AD-GADD45β OE had almost the same expression levels as their WT littermates, although variation was bigger in this group (Fig. 60B).

A

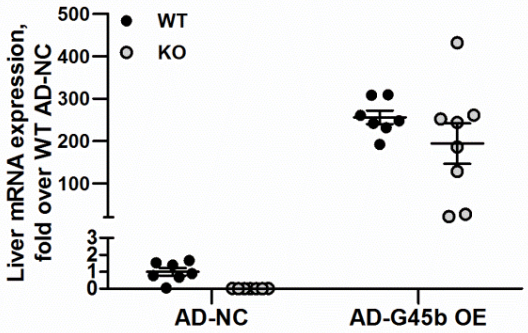

B

Genotype	Virus	Fold over WT AD-NC
WT	NC	0,89952829
WT	NC	0,676867817
WT	NC	0,048389426
WT	NC	0,771435338
WT	NC	1,669118361
WT	NC	1,398730114
WT	NC	1,535930654
KO	NC	0,015336988
KO	NC	0,021890336
KO	NC	0,008973482
KO	OE	0,012080455
KO	NC	0,000393564
KO	NC	0,000379089
KO	NC	0,00028147
WT	OE	260,6838671
WT	OE	309,5872956
WT	OE	308,6399971
WT	OE	231,825823
WT	OE	247,5821108
WT	OE	191,9737903
WT	NC	242,1173158
KO	OE	185,9846473
KO	OE	27,18516599
KO	OE	21,67266008
KO	OE	261,5104228
KO	NC	432,1954298
KO	NC	128,5788813
KO	NC	251,9583323
KO	NC	244,0235956

Figure 60: Liver *Gadd45b* mRNA expression in GADD45β KO and WT mice after adenovirus administration and 24 hours fasting. Male GADD45β KO and WT mice received the AD-GADD45β OE or AD-NC, and after one week they were fasted for 24 hours before sacrifice. Liver *Gadd45b* mRNA levels were analysed by RT-qPCR and are shown as a fold induction relative to WT mice with AD-NC (A). The exact expression values are shown in (B).

After having confirmed that AD-GADD45β OE administration led to an overexpression of GADD45β, the next step was to examine if the blood glucose levels as well as the body and tissue weights were altered upon virus treatment. The body weight one week after virus application did not differ from the body weight before injection, and fasting reduced, this variable to the same extent in both genotypes (Fig. 61A-C). Glucose levels were significantly lower in WT mice with GADD45β overexpression, whereas KO littermates did not show a change in blood glucose values upon AD-GADD45β OE administration (Fig. 61D). This difference was abolished after 24 hour fasting (Fig. 61E). Blood glucose levels dropped with fasting in all groups. As a consequence, only GADD45β WT mice showed a change in blood glucose levels between the fed and fasted state (Fig. 61F). Interestingly, GADD45β overexpression resulted in a heavier liver in GADD45β WT but not in KO mice (Fig. 61G). The weight of abdominal fat was not significantly affected upon GADD45β overexpression (Fig. 61H).

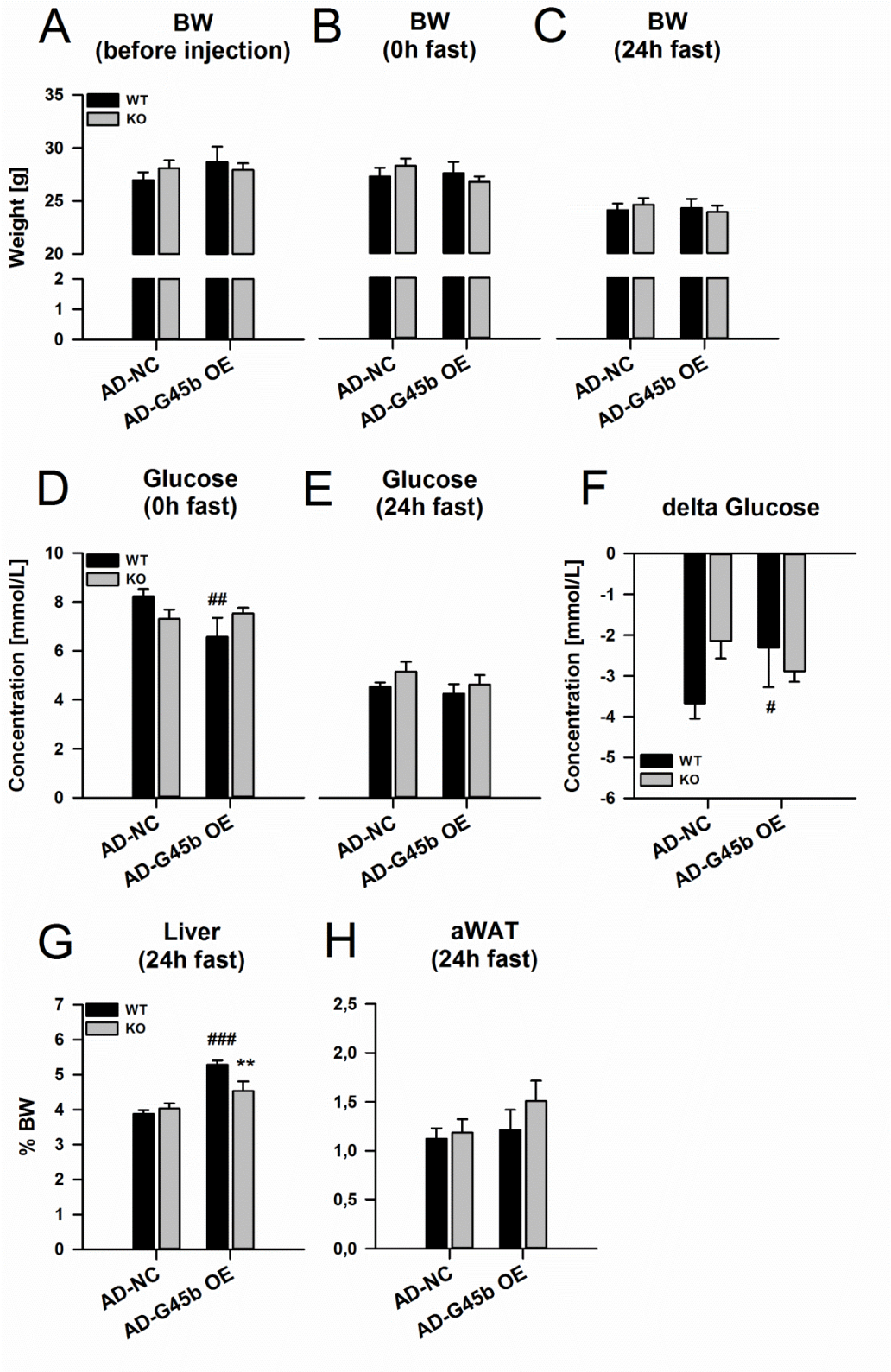

Figure 61: Body and tissue weights as well as blood glucose in GADD45β KO and WT mice after adenovirus administration. Male GADD45β KO and WT mice received the AD-GADD45β OE or AD-NC, and after one week they were fasted for 24 hours before sacrifice. Body weight was measured before virus injection (A), one week after virus injection but before fasting (B) and after 24 hours fasting (C). Blood glucose was measured one week after virus injection but before fasting (D) and after being fasted for 24 hours (E). The change in blood glucose levels between those two time points was determined (F). Liver (G) and adipose tissue weight (aWAT, H) were measured during preparation of the mice and normalized to body weight. Mean ± SEM; n=7-8 per group; * genotype effect, # effect of GADD45β overexpression; (*) $p \leq 0.05$, (**) $p \leq 0.01$, (***) $p \leq 0.001$.

Except for the liver weights, there was no observed differences caused by the genotypes or the administered viruses, and the results seem to mimic what has been shown in the starvation experiment with GADD45β KO and WT mice (see chapter 3.3.1).Next we examined the serum and liver metabolites to see if liver-specific rescue of GADD45β would influence the previously observed disturbances in systemic and liver lipid handling in GADD45β KO mice

Before fasting, serum NEFA levels were the same in all groups (Fig. 62A). Likewise, fasting led to a 160% increase in serum NEFA concentrations in all groups. Remarkably, the blunted increase in serum NEFA which we could observe after 24 hour starvation in GADD45β KO mice was gone after GADD45β overexpression. There was rather a tendency of higher serum NEFA levels in GADD45β KO mice compared to their WT littermates with GADD45β overexpression. Unexpectedly, we could not observe the blunted effect of serum NEFA in the AD-NC control group. There was only a mild blunted effect. Serum TG concentrations were the same in all groups before fasting and did not increase upon fasting (Fig. 62B). Only in GADD45β KO mice with GADD45β overexpression serum TG levels were almost 100% augmented compared to all other groups. Serum glycerol levels were increased upon GADD45β overexpression before food withdrawal but this difference relative to the AD-NC group was abolished after 24 hours of fasting (Fig 62C). Serum glycerol levels increased in the AD-NC group, with no difference between genotypes, whereas serum glycerol concentrations did not change in the AD- GADD45β OE group.

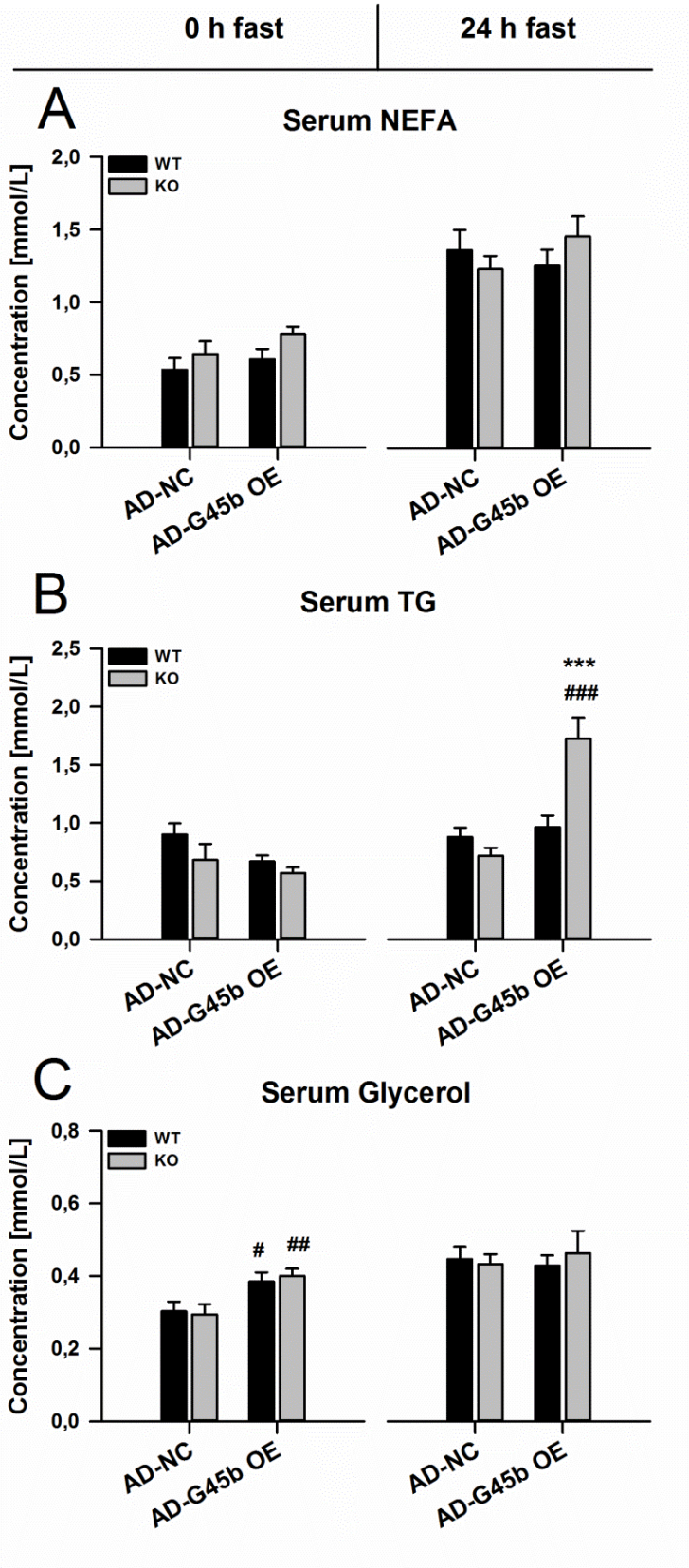

Figure 62: Serum metabolites in GADD45β KO and WT mice after adenovirus administration. Male GADD45β KO and WT mice received the AD-GADD45β OE or AD-NC, and after one week they were fasted for 24 hours before sacrifice. Serum non-esterified fatty acids (NEFA, A), triglycerides (TG, B) and glycerol (C), were measured before (0h) and after (24h) food withdrawal. Mean ± SEM; n=7-8 per group; * genotype effect, # effect of GADD45β overexpression; (*) $p \leq 0.05$, (**) $p \leq 0.01$, (***) $p \leq 0.001$.

GADD45β overexpression had a striking effect on liver metabolites (Fig. 63). Administration of AD-GADD45β OE resulted in a reduction of liver NEFA levels in both GADD45β WT and KO mice (Fig. 63A). The formerly described increase of liver TG in GADD45β KO mice was still measurable after AD-NC application but abolished upon GADD45β overexpression (Fig. 63B). GADD45β overexpression had no effect on liver cholesterol concentrations; they were the same in all four groups (Fig. 63C).

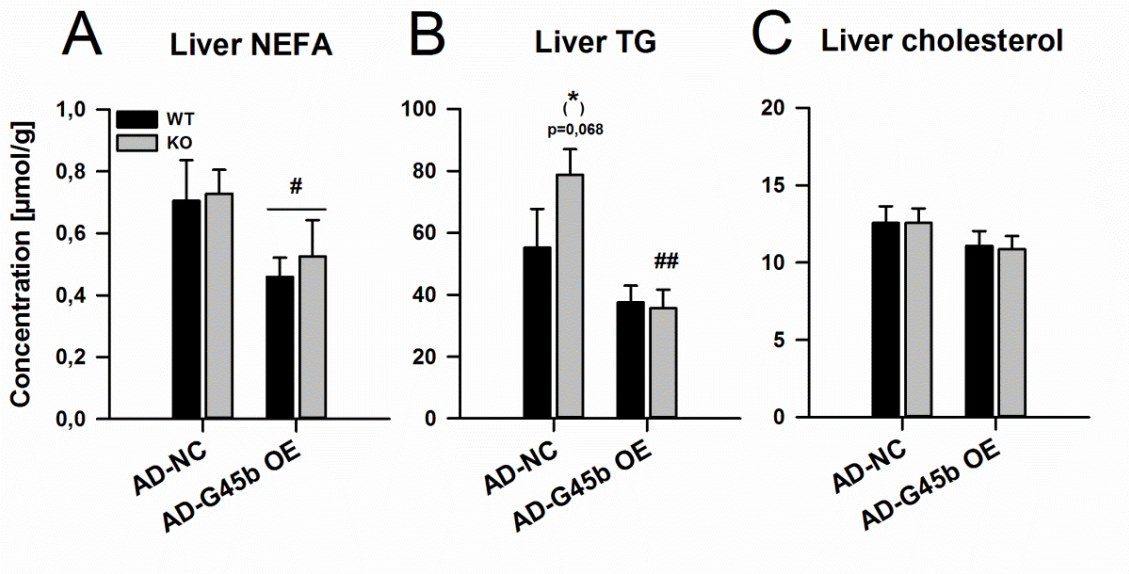

Figure 63: Liver metabolites in GADD45β KO and WT mice after adenovirus administration. Male GADD45β KO and WT mice received the AD-GADD45β OE or AD-NC, and after one week they were fasted for 24 hours before sacrifice. Liver non-esterified fatty acids (NEFA, A), triglycerides (TG, B) and cholesterol (C) were measured after food withdrawal. Mean ± SEM; n=7-8 per group; * genotype effect, # effect of GADD45β overexpression; (*) $p \leq 0.05$, (**) $p \leq 0.01$, (***) $p \leq 0.001$.

Taken together we could partially rescue the observed fasting-induced metabolic derangement in GADD45β KO mice and alleviate lipid accumulation in the liver by overexpressing GADD45β.

3.5.5 GADD45β overexpression in *db/db* mice can partially reverse their diabetic phenotype

In order to verify that the observed fasting-induced effects on serum and liver parameters as well as on insulin sensitivity in *db/db* mice compared to healthy mice are due a reduced expression of GADD45β in the liver, we injected the AD-GADD45β OE or AD-NC into *db/db* and healthy control animals and sacrificed them one week later in the fasted state. As for the rescue experiment with GADD45β KO and WT mice, we first assessed the status of overexpression in the different groups. Two animals had anatomical abnormalities and were excluded from any analysis (animal 2.3 and 3.5). Analysis of mRNA expression levels revealed almost 100fold higher *Gadd45b* expression levels in *db/db* and WT mice with GADD45β overexpression (Fig. 64C). The scatter in WT mice receiving the AD-GADD45β OE was higher than in other groups, and two animals had to be excluded from subsequent analysis due to absent overexpression (Fig. 64B, red). Surprisingly, *Gadd45b* expression levels were the same between WT and *db/db* mice after AD-NC administration. This should not be the case considering that *db/db* mice were not able to induce

GADD45β upon fasting (see initial screen 3.2.1). Surprisingly it was not possible to detect GADD45β at the protein level (Fig. 64A), although positive control lysates indicated that the antibody was clearly functional. Only in liver samples with the highest mRNA expression values (e.g. 2.5, 4.3 and 4.6) was a band for GADD45β visible. Remarkably, almost all of the WT animals did not show a signal on protein level, despite the fact that an induction of GADD45β should have been observed due to fasting. This is in accordance with endogenous GADD45β being generally hard to detect. Nothing is known about the stability and half-life of GADD45β but at least for GADD45γ it is assumed that its stability is very weak and half-life very short (personal communication with Dr. Anastasia Kralli [230]).

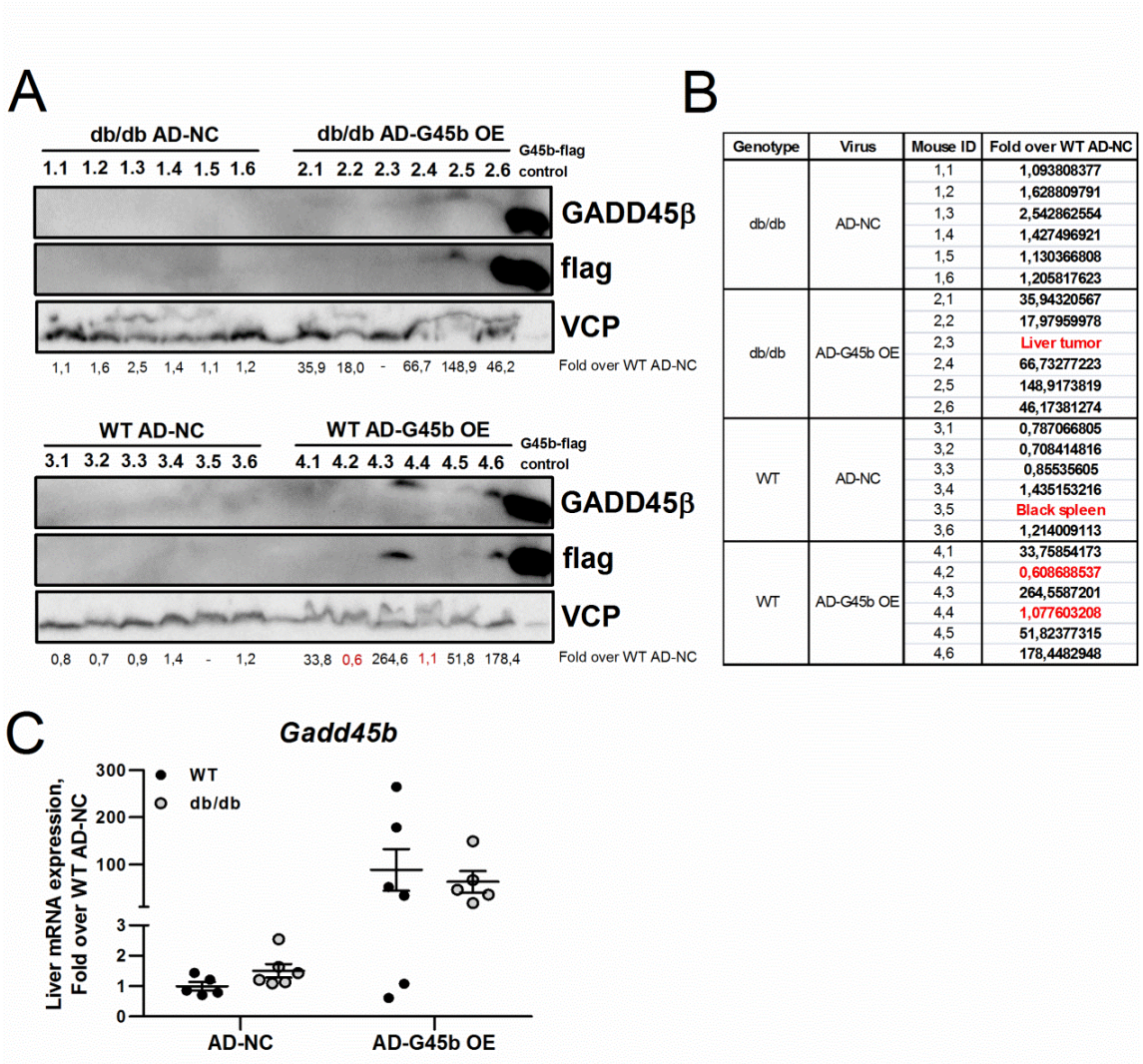

Genotype	Virus	Mouse ID	Fold over WT AD-NC
db/db	AD-NC	1,1	1,093808377
		1,2	1,628809791
		1,3	2,542862554
		1,4	1,427496921
		1,5	1,130366808
		1,6	1,205817623
db/db	AD-G45b OE	2,1	35,94320567
		2,2	17,97959978
		2,3	Liver tumor
		2,4	66,73277223
		2,5	148,9173819
		2,6	46,17381274
WT	AD-NC	3,1	0,787066805
		3,2	0,708414816
		3,3	0,85535605
		3,4	1,435153216
		3,5	Black spleen
		3,6	1,214009113
WT	AD-G45b OE	4,1	33,75854173
		4,2	0,608688537
		4,3	264,5587201
		4,4	1,077603208
		4,5	51,82377315
		4,6	178,4482948

Figure 64: Liver *Gadd45b* mRNA and GADD45β protein levels in *db/db* and control mice after adenovirus administration. Male *db/db* or healthy control mice (WT) received the AD-GADD45β OE or AD-NC, and after one week they were fasted for 24 hours before sacrifice. GADD45β levels were determined by immunoblotting (A) using antibodies against GADD45β, the flag tag or the loading control (VCP). *Gadd45b* mRNA levels were analysed by RT-qPCR and shown as a fold induction relative to WT mice with AD-NC (C). The exact expression values are shown in (B). Animals that were excluded in further analysis are marked in red.

After having confirmed the overexpression of GADD45β in *db/db* and WT mice, we next examined the mRNA expression levels of the other two GADD45 family members GADD45α and GADD45γ (Fig. 65). *Gadd45a* expression was 4-6 times higher in *db/db* mice than in WT mice independently

of GADD45β overexpression. *Gadd45g* expression was higher in *db/db* mice with AD-NC injection and was reduced upon GADD45β overexpression. Overall, both gene expression patterns differed from what we could observe in the initial screen (see. Fig. 15) where fasting resulted in 2-fold higher *Gadd45a* expression in *db/db* mice, and *Gadd45g* expression was 5 times higher in WT mice than in *db/db*. It is also surprising, as mentioned before, that *Gadd45b* expression in WT with AD-NC is not induced but on the same level as in *db/db* mice.

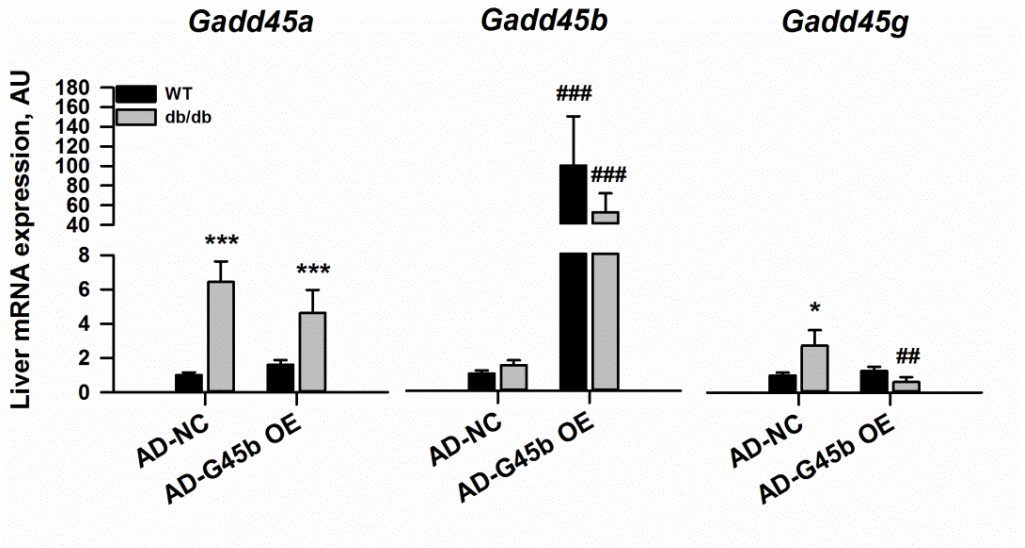

Figure 65: Liver *Gadd45a, Gadd45b and Gadd45g* expression in *db/db* and control mice after adenovirus administration. Male *db/db* or healthy control mice (WT) received the AD-GADD45β OE or AD-NC, and after one week they were fasted for 24 hours before sacrifice. mRNA levels were analysed by RT-qPCR and shown as a fold induction relative to WT mice with AD-NC. Mean ± SEM; n=4-6 per group; * genotype effect, # effect of GADD45β overexpression; (*) $p \leq 0.05$, (**) $p \leq 0.01$, (***) $p \leq 0.001$.

Next, we examined body and tissue weights of the four groups (Fig 66). As expected *db/db* mice were much heavier than control animals both in the fasted and in the fed state and with both recombinant viruses (Fig. 66A). Interestingly, GADD45β overexpression resulted in a slight but significant decrease in body weight in both before and after fasting. Independently of virus, *db/db* mice had much heavier livers and much more aWAT than healthy WT mice (Fig. 66B). WT mice seemed to have a slightly bigger liver and a bit less aWAT with GADD45β overexpression than with AD-NC. Even though the liver weight was higher in *db/db* mice, the percentage relative to body mass was only 2% more than in WT mice (Fig. 66C). This difference was gone after GADD45β overexpression; WT mice with GADD45β overexpression had a higher percentage of liver to total body weight which is comparable to that of *db/db* mice. The opposite was true for aWAT; hepatic GADD45β overexpression resulted in less relative aWAT in WT mice, but not in *db/db* mice.

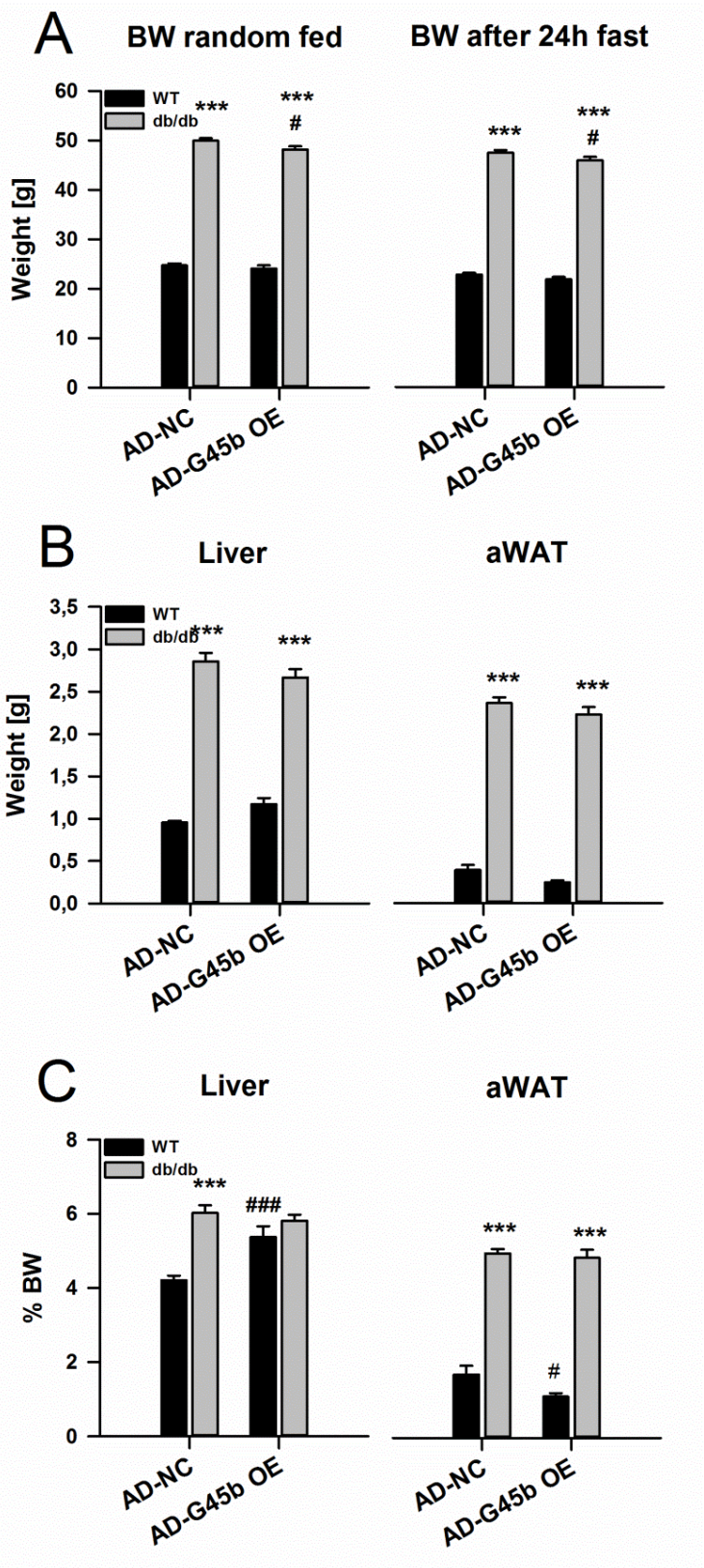

Figure 66: Body and tissue weights in *db/db* and WT mice after adenovirus administration. Male *db/db* and healthy control mice (WT) received the AD-GADD45β OE or AD-NC, and after one week they were fasted for 24 hours before sacrifice. Body weight was measured before and after fasting (A). Liver and adipose tissue weight (aWAT) were measured during preparation of the mice and shown as total weight (B) and normalized to body weight (C). Mean ± SEM; n=4-6 per group; * genotype effect, # effect of GADD45β overexpression; (*) $p \leq 0.05$, (**) $p \leq 0.01$, (***) $p \leq 0.001$.

Apart from having an increase in body, liver and fat weight we could confirm that *db/db* are in a state of hyperglycaemia (Fig. 67). Their blood glucose levels were always higher than that of healthy WT mice, independent of virus application (Fig. 67A) or fasting (Fig. 67B). But most importantly, we could observe a 40% reduction in blood glucose levels in *db/db* with GADD45β overexpression after 6 hour fasting (Fig. 67A) and after 24 hour fasting (Fig. 67B). Also in the random fed state, blood glucose levels were 30% lower in *db/db* mice with GADD45β overexpression (Fig. 67B).

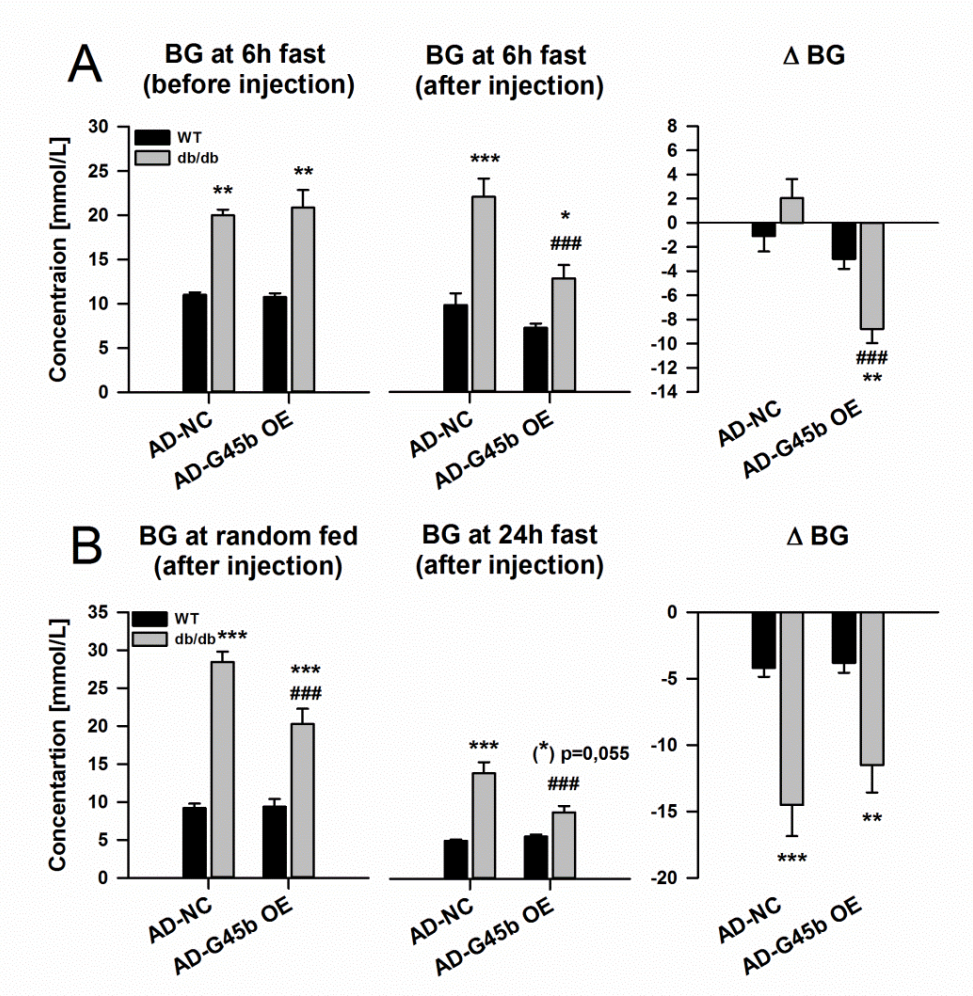

Figure 67: Blood glucose levels in *db/db* and WT mice after adenovirus administration. Male *db/db* and healthy control mice (WT) received the AD-GADD45β OE or AD-NC, and after one week they were fasted for 24 hours before sacrifice. Blood glucose (BG) concentrations were measured before and one week after virus injection after 6 hours of fasting (A), and in the *ad libitum* state and after 24 hours of fasting both one week after virus injection (B). Also the change in blood glucose is shown for both cases. Mean ± SEM; n=4-6 per group; * genotype effect, # effect of GADD45β overexpression; (*) $p \leq 0.05$, (**) $p \leq 0.01$, (***) $p \leq 0.001$.

With the hint that glucose homeostasis might be affected by GADD45β overexpression, we also measured the fasting serum insulin levels before and one week after virus administration, and calculated the HOMA-IR to determine insulin resistance. Similar to their blood glucose levels, fasting insulin concentrations of *db/db* mice were always higher than that of healthy WT mice, independent of virus application (Fig. 68A). But also here we could measure a 45% reduction in

serum insulin levels with GADD45β overexpression. Since serum insulin and glucose are parameters for the calculation of HOMA-IR, it is plausible that the HOMA-IR value was reduced with diminished insulin and glucose levels. This means that *db/db* mice were less insulin resistant with GADD45β overexpression (Fig. 68B).

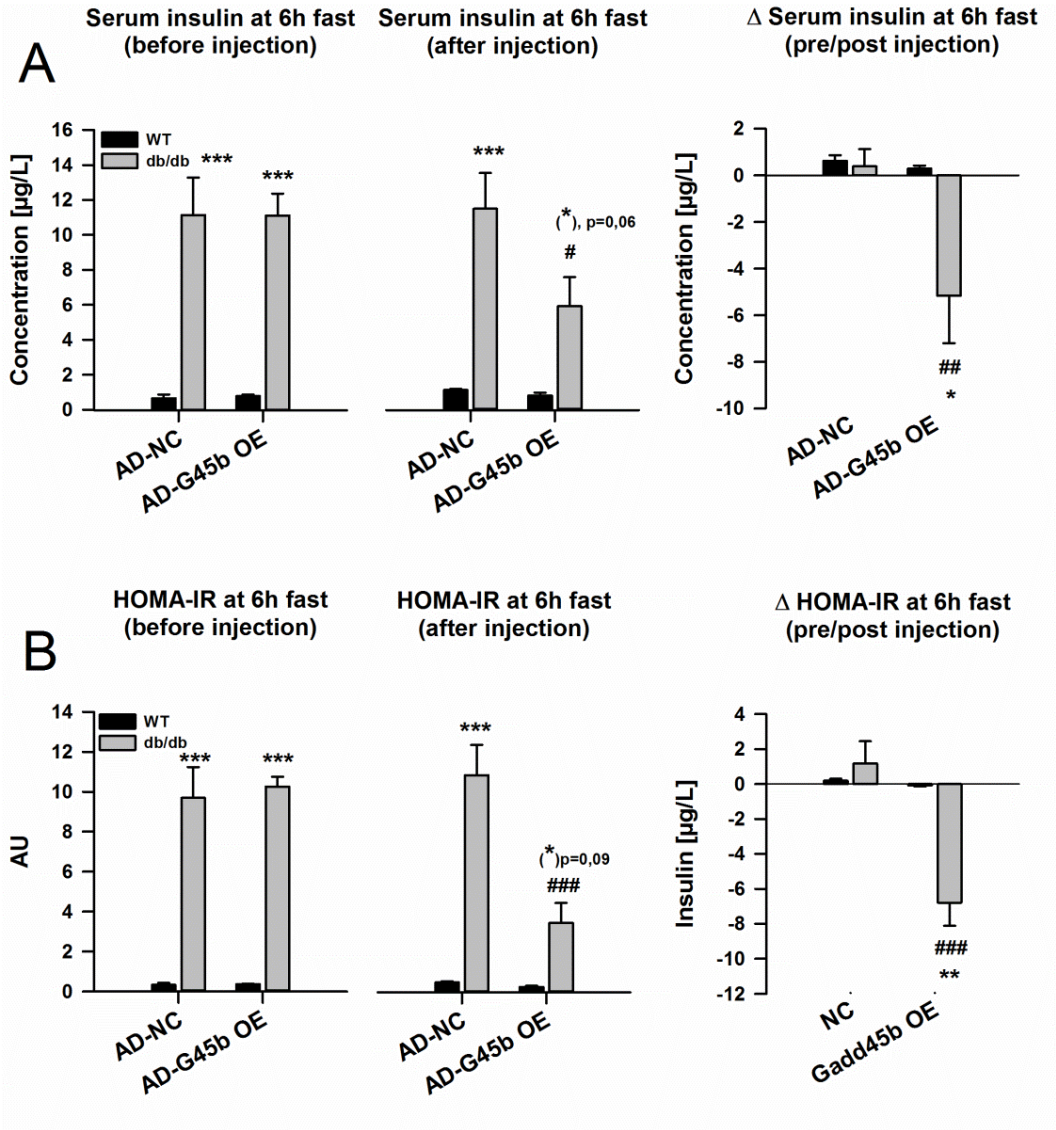

Figure 68: Serum insulin levels and HOMA-IR in *db/db* and WT mice after adenovirus administration. Male *db/db* and healthy control mice (WT) received the AD-GADD45β OE or AD-NC, and after one week they were fasted for 24 hours before sacrifice. Serum insulin concentrations were measured before and one week after virus injection after 6 hours of fasting (A), and homeostatic model assessment for insulin resistance (HOMA-IR) was calculated (B). Also the change in serum insulin levels and HOMA-IR is shown for both cases. Mean ± SEM; n=4-6 per group; * genotype effect, # effect of GADD45β overexpression; (*) p ≤ 0.05, (**) p ≤ 0.01, (***) p ≤ 0.001.

Since overexpression of GADD45β on one hand led to a reduction in blood glucose, insulin and HOMA-IR in *db/db* mice, and on the other hand resulted in a partial rescue of the dysregulated fasting lipid metabolism in GADD5β KO mice (see section 3.5.2), we next were interested if GADD45β overexpression could also reverse the effects seen in *db/db* mice on their serum and liver lipid handling (see section 3.3.8).

As shown in figure 69A, *db/db* mice with AD-NC had higher circulating NEFA levels in the fed state compared to WT control mice. This difference was abolished upon GADD45β overexpression. Fasting increased serum NEFA concentrations in all groups with no difference in genotype or virus. Importantly, the blunted increase in serum NEFA that we could observe before was abolished after GADD45β overexpression. Unexpectedly, serum TG levels were always lower in *db/db* mice in the fed and fasted state (Fig.69B). Upon fasting, TG levels increased independently of GADD45β overexpression in all four groups, with a bigger change in WT mice than *db/db* mice. Most importantly, during fasting serum TG concentrations in *db/db* mice increased more with GADD45β overexpression than with AD-NC. Thus, GADD45β overexpression did not only have an impact on insulin sensitivity of *db/db* mice, it could also reverse the dysregulated systemic lipid metabolism in *db/db* mice and confer higher metabolic flexibility upon nutrient deprivation.

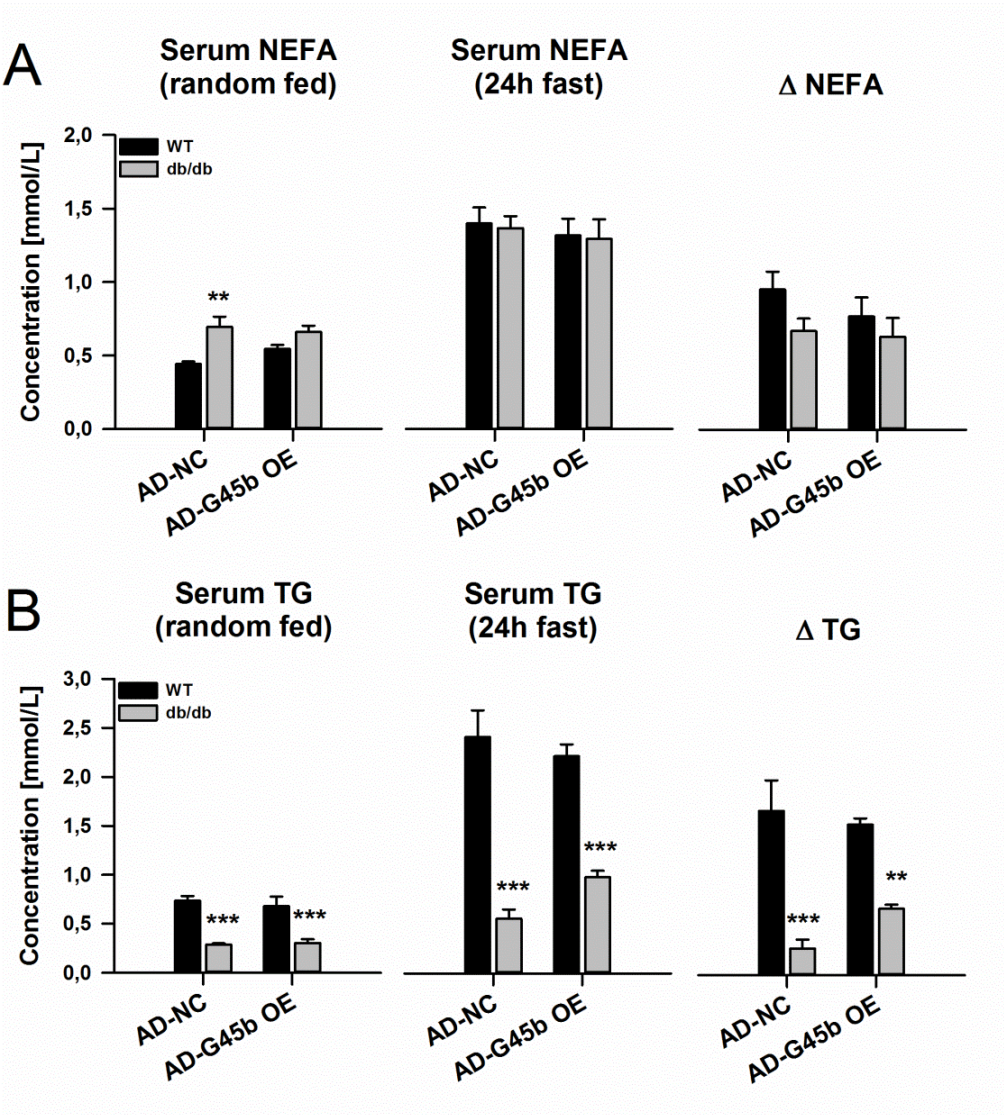

Figure 69: Serum metabolites in *db/db* and WT mice after adenovirus administration. Male *db/db* and healthy control mice (WT) received the AD-GADD45β OE or AD-NC, and after one week they were fasted for 24 hours before sacrifice. Serum non-esterified fatty acids (NEFA, A), and triglycerides (TG, B) were measured before (random fed) and after food withdrawal (24h fast). Also the change in NEFA and TG levels is shown for both cases. Mean ± SEM; n=4-6 per group; * genotype effect, # effect of GADD45β overexpression; (*) $p \leq 0.05$, (**) $p \leq 0.01$, (***) $p \leq 0.001$.

Last, we wanted to investigate if GADD45β overexpression can also lead to a reduction of fasting liver lipids as we have observed in GADD45β KO and WT mice (see in section 3.5.2). As shown in figure 70A, GADD45β overexpression resulted in only a mild reduction of liver NEFA concentrations in WT but not in *db/db* mice. Similarly, GADD45β overexpression only reduced liver TG levels in WT animals, with no effect in TG-laden livers from *db/db* mice (Fig. 70B).

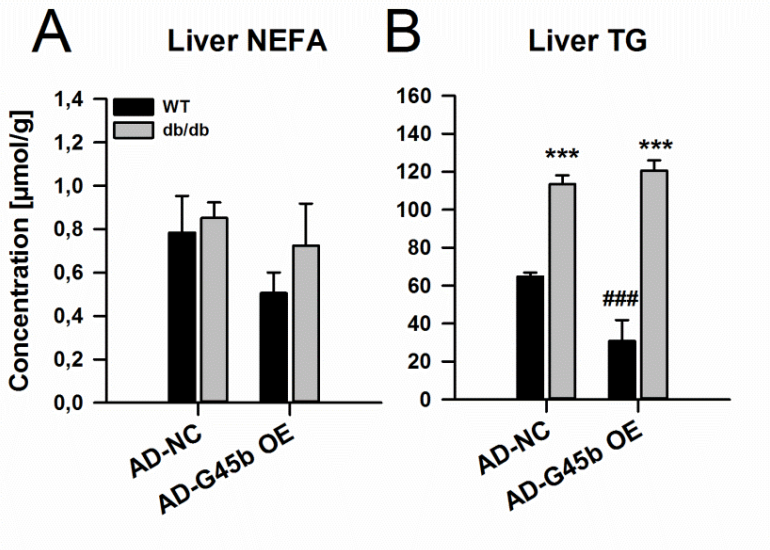

Figure 70: Liver metabolites in *db/db* and WT mice after adenovirus administration. Male *db/db* and healthy control mice (WT) received the AD-GADD45β OE or AD-NC. After one week they were fasted for 24 hours before sacrifice and liver non-esterified fatty acids (NEFA, A), and triglycerides (TG, B) were measured. Mean ± SEM; n=4-6 per group; * genotype effect, # effect of GADD45β overexpression; (*) $p \leq 0.05$, (**) $p \leq 0.01$, (***) $p \leq 0.001$.

Thus, despite only having a mild effect on systemic and hepatic lipid handling, GADD45β overexpression could increase the insulin sensitivity in obese mice by lowering fasting blood glucose and serum insulin levels and hence can partially reverse their obese and diabetic phenotype.

3.6 Analysis of the underlying mechanisms of GADD45β action

In the course of these studies it became more and more evident that GADD45β might have a role in two stress scenarios: 1) nutrient depletion where it might play a role in lipid homeostasis, and 2) nutrient overload where it may confer an effect on insulin sensitivity. The final questions that have arisen concern the mechanism. How can GADD45β play a role in both situations? Where is the missing link? There a several approaches to answer these questions. We addressed the two most obvious ones. (1) Does GADD45β have an influence on the transcription of certain genes? (2) Does GADD45β have an impact on signalling pathways within the cell by modulating protein activity?

3.6.1 The effect of GADD45β may not be mediated via transcriptional regulation

In a first attempt to unravel the mechanisms of GADD45β action, we examined the expression levels of crucial genes involved in detoxification, drug transport and fatty acid metabolism. We could show that some of those genes were indeed slightly altered in GADD45β KO animals (Fig. 71). Specifically GADD45β KO livers had a reduced expression of *CD36* (fatty acid translocase), *Acly* (ATP citrate lyase) and *Cyp2b10* (a CAR target) and an increased expression of *Slco1a1* (an

organic anion transporting polypeptide). In contrast, genes involved in glucose metabolism such as *Pck1* (involved in glycolysis) and *Pdk4* (involved in gluconeogenesis) were unaffected. It is noteworthy that not all examined genes involved in fatty acid metabolism were dysregulated upon GADD45β depletion. Even though the expression of *Acly,* which is involved in FA synthesis, seems to be reduced, there was no effect on other lipogenic markers such as *Cyp4a14* (fatty acid hydroxylase), *Fasn* (fatty acid synthase), or *Acc1* (acetyl-Coa carboxylase). An exemplary gene involved in the breakdown of FA, *Mcad* (medium-chain acetyl-CoA dehydrogenase), was not affected by the absence of GADD45β. Interestingly, the expression of *Slco1a1*, which is involved in bile acid and drug transport, was increased in GADD45β KO, whereas the expression of *Cyp2b10*, which is involved in detoxification, was decreased. Overall, only modest and inconsistent effects were observed of GADD45β KO on the expression of genes involved in FA metabolism, drug transport and detoxification.

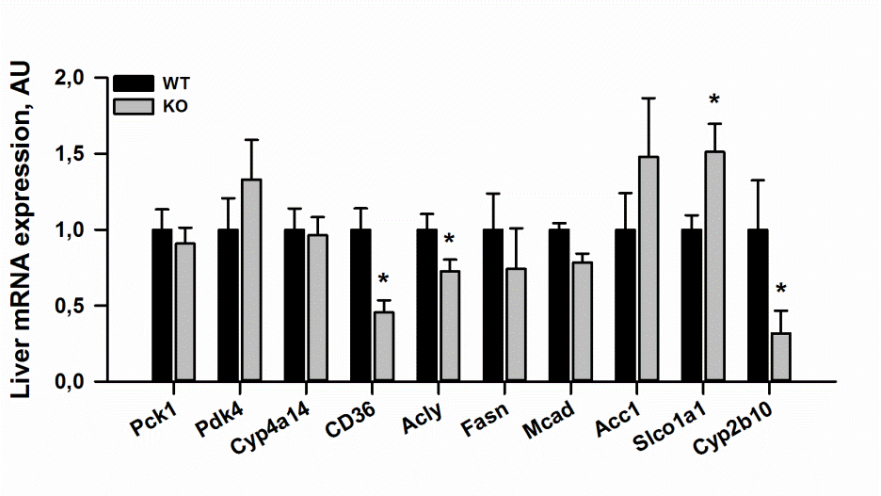

Figure 71: Liver gene expression analysis in GADD45β KO and WT mice. Male GADD45β KO and WT littermates were sacrificed after being fasted for 24h hours. Liver mRNA levels were subsequently analysed by RT-qPCR. Values are fold induction relative to "WT". Mean ± SEM; n=5-8 per group. * genotype effect; (*) $p \leq 0.05$, (**) $p \leq 0.01$, (***) $p \leq 0.001$.

If the effect of GADD45β depletion on the observed gene expression profile was causal, overexpression of GADD45β in turn should change the expression of the affected genes. Hence, we examined the mRNA levels of some of the genes in livers of GADD45β KO and WT mice which received the AD-GADD45β OE or AD-NC. Unexpectedly, gene expression patterns observed in our initial experiment were not faithfully reproduced in our control virus-treated cohort. For example, *CD36* (Fig. 72A), *Acly* (Fig. 72B), *Slco1a1* (Fig. 72C), and *Cyp2b10* (Fig. 72D) expressions were not altered in GADD45β KO mice with AD-NC. But whereas there was no effect of genotype in any of the genes, there was indeed a general effect of GADD45β overexpression. *CD36, Acly* and *Cyp2b10* mRNA levels, which were reduced with GADD45β KO, were increased with GADD45β overexpression, and *Slco1a1* mRNA levels, which were increased with GADD45β KO, were reduced. But since there was no effect of genotype in this experimental mouse cohort, overexpression of GADD45β did in fact not rescue the effects on gene expression observed previously.

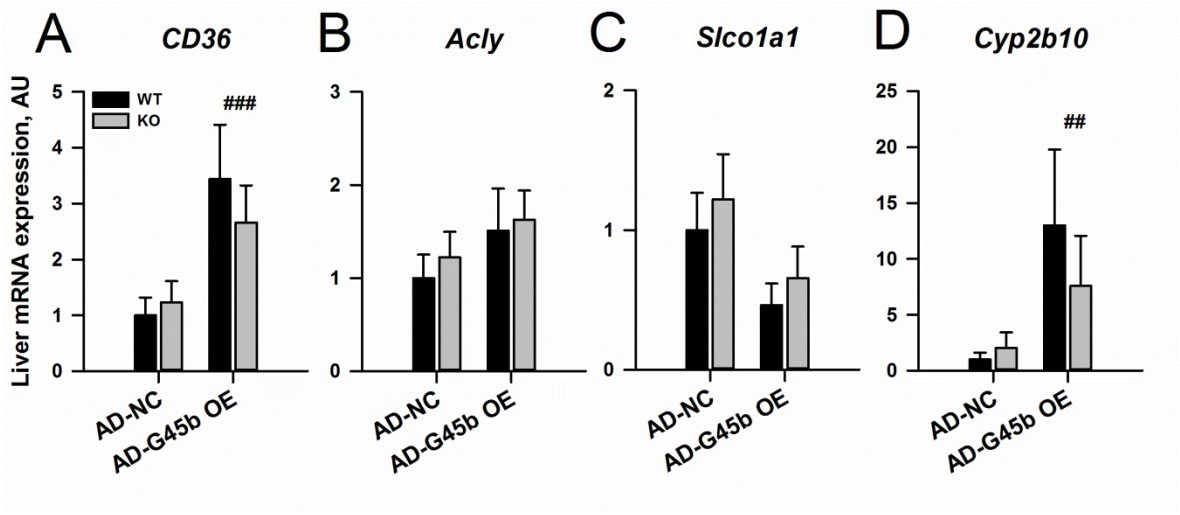

Figure 72: Liver gene expression analysis in GADD45β KO and WT mice after adenovirus administration. Male GADD45β KO and WT mice received the AD-GADD45β OE or AD-NC, and after one week they were fasted for 24 hours before sacrifice. Liver mRNA levels of *CD36* (A), *Acly* (B), *Slco1a1* (C) and *Cyp2b10* (D) were subsequently analysed by RT-qPCR. Values are fold induction relative to "WT AD-NC". Mean ± SEM; n=7-8 per group. * genotype effect, # effect of GADD45β overexpression; (*) $p \leq 0.05$, (**) $p \leq 0.01$, (***) $p \leq 0.001$.

To get a broader idea on the influence of GADD45β on gene expression, we submitted liver RNA samples from starved GADD45β KO and WT littermates to the Genomics and Proteomics Core Facility of the DKFZ where they performed a single read, 50 bp multiplexed run on 3 HiSeq lanes without reading direction with subsequent poly-A purification. The subsequent analysis on differential expression, visualisation and pathway/network of differentially expressed transcripts was performed by Dr. Emil Karaulanov from the Institute of Molecular Biology, Mainz (see Methods section for further details). He filtered robust (consensus) hits by performing several parallel workflows using TopHat and Genomatix GMS for read mapping and CuffDiff (v1.0.3, Galaxy) and DESeq (v1.10.1, Genomatix) for differential expression analysis. In general, there were a few hundred apparently KO-dysregulated transcripts, most of them moderately affected (~2x). Some genes showed differential expression of some transcript isoforms only. Also some genes showed low levels of expression. Generally, there were more down-regulated than up-regulated transcripts. Transcripts belonging to the following genes showed robust up-regulation (>2x): *Ces4a, Cgref1, Cidec, Cntnap1, Derl3, Lad1, Nudt7, Onecut1, Peg10, Pfkfb3, Pitx3, Serpina12, Serpina4-ps1, Slc35f1*. Transcripts belonging to the following genes show robust down-regulation (>2x): *Atp6v0d2, Bmpr2, Cbl, Cdk6, Gprin3, Klf12, Klhl11, Lcn2, Lcor, Lmbrd2, Lnpep, Mib1, N4bp2, Ptar1, Ptpn4, Rel, Sesn3, Themis, Uhmk1, Xpo4, Xrn1, Zbed6, Zfp369, Zfp433.* A complete table with robust hits can be found in the Appendix section. Some differentially expressed genes showed strong 5' -> 3' gradient of differential read enrichment, which was either a peculiar biological phenomenon or a technical artefact from the sample isolation or library preparation (e.g. RNA degradation, batch effects etc.). Functional annotation analysis (DAVID) for down regulated genes was mostly weak which could be due to the low number of affected genes. Supplementary figure 1 shows that most genes affected were clustered as phosphoproteins or were involved in phosphate metabolic processes,

phosphorylation and cell cycle. Latter grouping is not surprising since GADD45β is reported to play a role in senescence and cell cycle control. No significant enrichments could be seen for upregulated genes which could also be due to the low number of genes.

Some of the results of the RNAseq screen with moderate or high gene expression levels were subsequently validated by RT-qPCR. Some hits could be nicely validated (*Lnpep, Onecut1, Nudt7, Lcn2, Tsc22d1, Atp6v0d2, Ces4a*), others did not change (*Vps13b, N4bp2, Zfp, Lcor, Abca1, Serpina4-p1*), and some changed in the expected direction, but with low statistical significance due to high intra-group variability (*Derl3, Saa2, Cidec, Cyp2b9*).

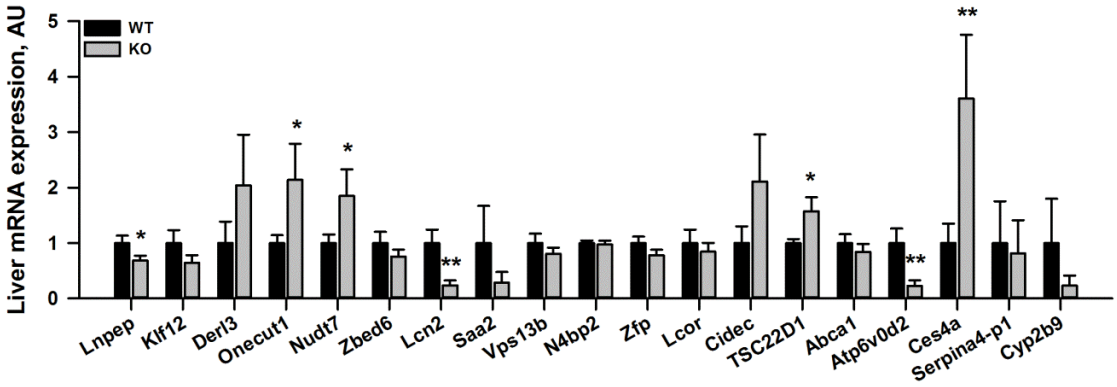

Figure 73: RNAseq validation in GADD45β KO and WT mice. Male GADD45β KO and WT littermates were sacrificed after being fasted for 24h hours. Differentially expressed genes from the RNAseq analysis were subsequently validated by RT-qPCR. Values are fold induction relative to "WT". Mean ± SEM; n=5-8 per group. * genotype effect; (*) $p \leq 0.05$, (**) $p \leq 0.01$, (***) $p \leq 0.001$.

It is surprising that some of the apparently differentially expressed genes could not be validated even though they seem to be clearly affected. Some possible explanations could be: (a) selective mRNA degradation before or during HiSeq library preparation or (b) unspecific (cross-reacting) RT-qPCR primers that report also other paralogs or transcript variants.

The next step was to determine if the rescue of GADD45β could also change the expression of the affected genes. As before, we examined the mRNA levels of some of the RNAseq hits in livers of GADD45β KO and WT mice which received the AD- GADD45β OE or AD-NC. The expression pattern of GADD45β KO and WT should be similar to what has been observed after RNAseq analysis. This was only partially the case (Fig. 74). For *Onecut1* (Fig. 74A) and *Tsc22d1* (Fig. 74C) we could see increased mRNA expression levels in GADD45β KO mice compared to WT littermates, as we also could see it after RNAseq analysis and subsequent validation (Fig. 73). In contrast, there was no effect of genotype for *Nudt7* (Fig. 74B), *Atp6v0d2* (Fig. 74D) or *Ces4a* (Fig. 74E), even though RNAseq analysis revealed *Ces4a* to be the gene with the highest fold change between GADD45β KO and WT. However, we could not observe a compensatory change in gene expression with GADD45β overexpression in any of the genes.

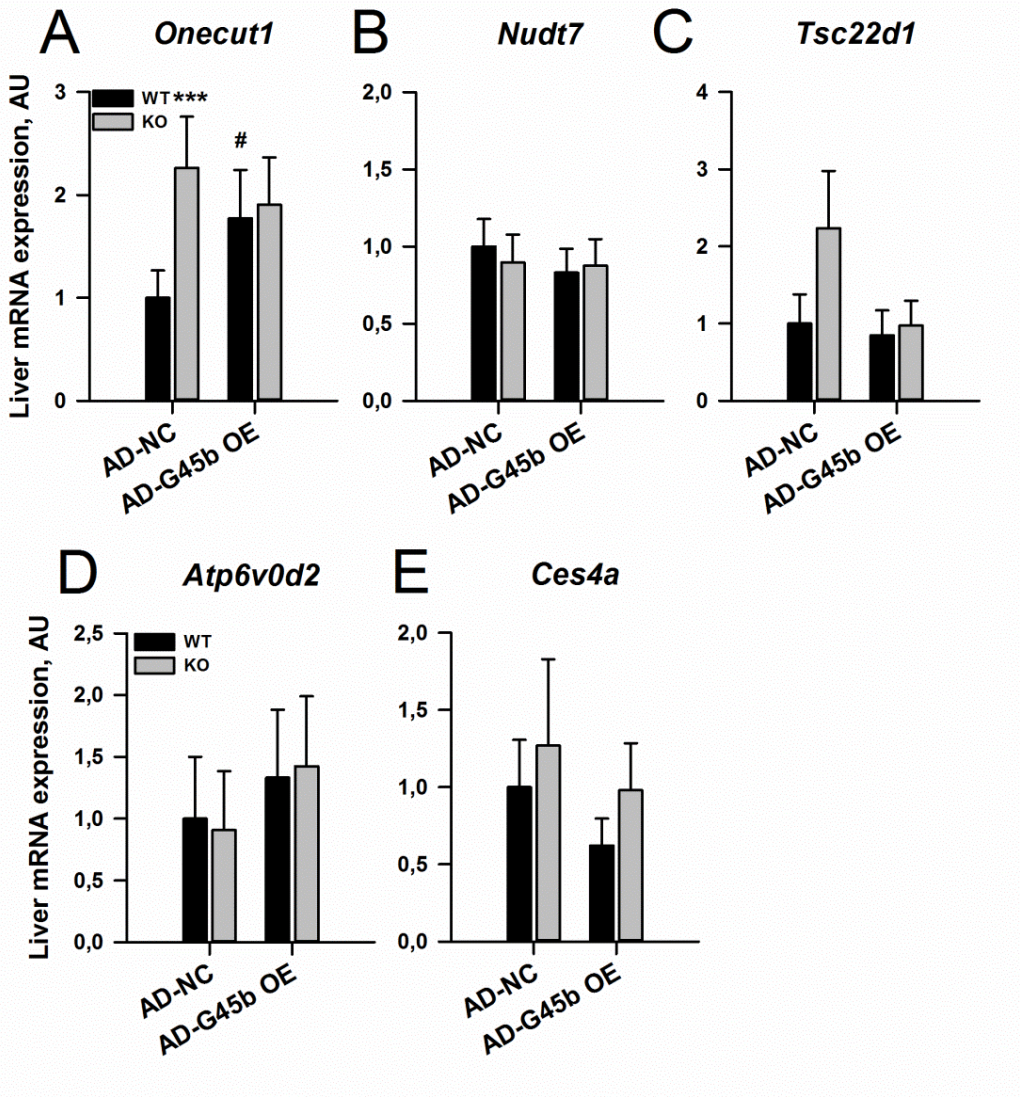

Figure 74: RNAseq validation in GADD45β KO and WT mice after adenovirus administration. Male GADD45β KO and WT mice received the AD-GADD45β OE or AD-NC, and after one week they were fasted for 24 hours before sacrifice. Liver mRNA levels of *Onecut1* (A), *Nudt7* (B), *TSC22D1* (C), Atp6v0d2 (D) and *Ces4a* (E) were subsequently analysed by RT-qPCR. Values are fold induction relative to "WT AD-NC". Mean ± SEM; n=7-8 per group. * genotype effect, # effect of GADD45β overexpression; (*) $p \leq 0.05$, (**) $p \leq 0.01$, (***) $p \leq 0.001$.

Since the influence of GADD45β KO on differentially expressed genes was only mild and we could not confirm every hit by RT-qPCR, together with the fact that the affected genes involved in fatty acid metabolism and detoxification could not be rescued with GADD45β overexpression, we believe that the effect of GADD45β is not via transcriptional regulation even though GADD45β is reported to be a potential transcriptional co-regulator of nuclear receptor transcription factors [203, 205].

3.6.2 The GADD45β-mediated effects on lipid and glucose metabolism are independent of the JNK and p38 pathways

Further investigations to unravel the underlying mechanism of GADD45β action were focused on its potential impact on protein activity and cell signalling pathways. Therefore, protein levels in

GADD45β KO and WT mice fed a HFD or NFD as well as in *db/db* and WT mice with GADD45β overexpression were assessed by immunoblotting. First, we examined if GADD45β mediates its effect on lipid metabolism and insulin sensitivity by its known downstream effectors JNK and p38. JNK has been reported to be activated in diabetic conditions and is implicated in the development of insulin resistance for over one decade [237,270]. There are also studies describing a role for p38 MAPK in the pathogenesis of T2D, although the underlying mechanisms are still under debate [271].

Since we could show that GADD45β KO mice were more insulin resistant after 4 months on a high fat diet, we investigated if this effect was due to altered activities of JNK or p38 activity. Hence, liver proteins from whole tissue extracts were separated by SDS-PAGE and total and phosphorylated p38 and JNK levels were measured by immunoblotting with antibodies against the T180/182 phosphorylation site of p38 and the S265 phosphorylation site of JNK. As shown in figure 75A, the phosphorylation status and thus the activity of p38 was not altered between the groups. Therefore we did not examine the total protein levels. The signal for phospho-JNK was very weak, but it seems as if GADD45β KO mice had a slightly stronger signal when fed a HFD. Therefore we also assessed the levels of total proteins. After normalizing the phospho-JNK levels to the levels of total JNK, we could not see a significant difference between the groups (Fig.75B). Most importantly, the KO of GADD45β did not lead to an increase or decrease of phospho-JNK, neither on NFD nor on HFD.

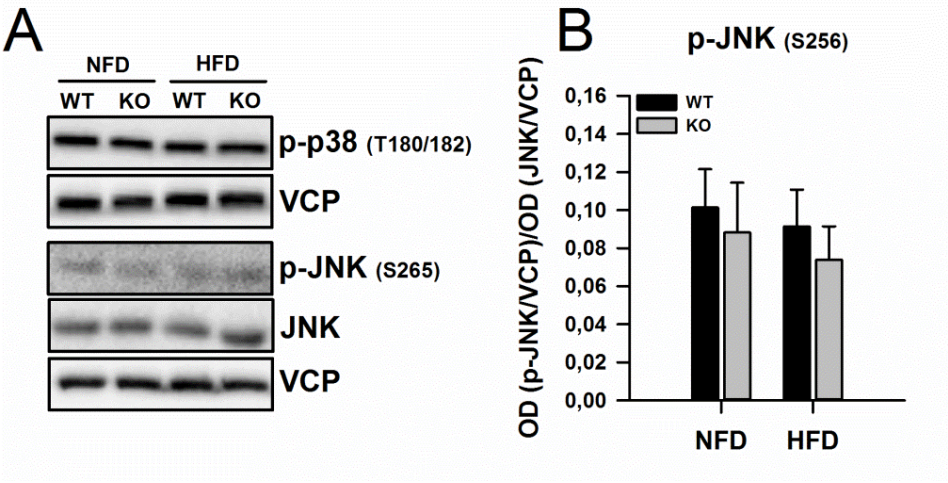

Figure 75: Protein expression of p38 and JNK and their phospho-proteins in GADD45β KO and WT mice on HFD or control diet. Male GADD45β KO and WT littermates were either fed a diet high in fat (HFD) or a matching control diet (NFD) for 16 weeks before sacrifice. Phospho-p38, phospho-JNK and JNK levels were determined by immunoblotting using antibodies against the respective protein or the loading control (VCP). Shown are representative blots (A). The signal intensity was assessed by normalising the optical density (OD) first to VCP and then to total normalised protein (B). Mean ± SEM; n=6 per group.

Next we performed the same analysis with *db/db* and WT mice with AD-GADD45β OE or AD-NC administration where the overexpression of GADD45β in *db/db* mice ameliorated their diabetic phenotype. As shown in figure 76, phospho-JNK levels were always higher in *db/db* than in WT mice. This was expected after AD-NC injection where GADD45β levels should be lower in *db/db* mice (according to the first screen, see section 3.2.2) and consequently should have higher

phospho-JNK levels assuming that GADD45β inhibits MKK4/7 and therefore also JNK activity. In addition, obesity and insulin resistance are characterised by increased JNK activity [272]. With the overexpression of GADD45β one might have expected a reduction of JNK activity in *db/db* and WT animals, although this was not the case.

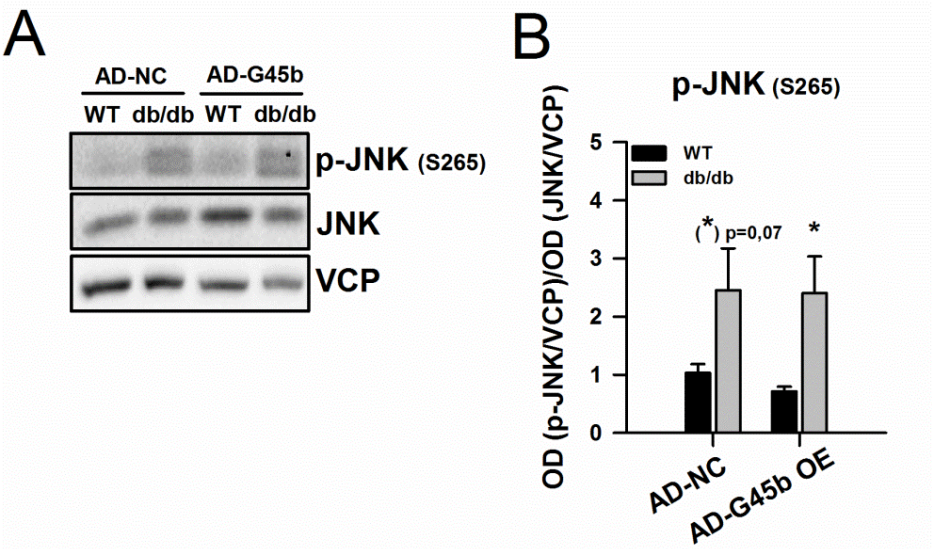

Figure 76: Protein expression of JNK and its phospho-proteins in *db/db* and WT mice after adenovirus administration. Male *db/db* and healthy control mice (WT) received the AD-GADD45β OE or AD-NC, and after one week they were fasted for 24 hours before sacrifice. Phospho-JNK and JNK levels were determined by immunoblotting using antibodies against the respective protein or the loading control (VCP). Shown are representative blots (A). The signal intensity was assessed by normalising the optical density (OD) first to VCP and then to total normalised protein (B). Mean ± SEM; n=3 per group; * genotype effect, # effect of GADD45β overexpression; (*) $p \leq 0.05$, (**) $p \leq 0.01$, (***) $p \leq 0.001$.

Taken together, we conclude that the impact of GADD45β on the insulin sensitivity might be independent of the JNK and p38 pathway.

3.6.3 The impact of GADD45β on the hepatic insulin signalling pathway remains elusive

The further investigation was focused on the insulin signalling pathway. Since GADD45β did not seem to mediate its effect via the JNK or p38 pathway, we were interested if GADD45β would have an influence on the activity of any downstream effector of the insulin receptor and thereby modulate the organism's reaction to nutrient overload. The insulin signalling pathway is a complex network of many proteins and several feedback loops. Thus we focused on the "main track" which is the IRS → PI3K → AKT axis. AKT itself has numerous targets, of which we examined those involved in gluconeogenesis (FOXO1), glycogenesis (GSK3β) and protein synthesis (S6K1).

Since we saw a major effect of GADD45β overexpression on the glucose levels of *db/db* mice, we examined the phosphorylation status of those insulin targets which are involved in gluconeogenesis and glycogenesis, namely FOXO1 and GSK3β. As shown in figure 77A, *db/db* mice had an increased phosphorylation of AKT and its downstream target GSK3β compared to WT mice. Upon GADD45β overexpression phospho-AKT levels were even higher in both *db/db* and WT animals. The same tendency is true for phospho-GSK3β. Phosphorylation of GSK3β

resulted in its inactivation and consequently to a reduction in its inhibitory effect on glycogen synthase and hence in the end promoting glycogen synthesis. This is in accordance with our observation of a reduction in blood glucose in *db/db* mice with GADD45β overexpression.

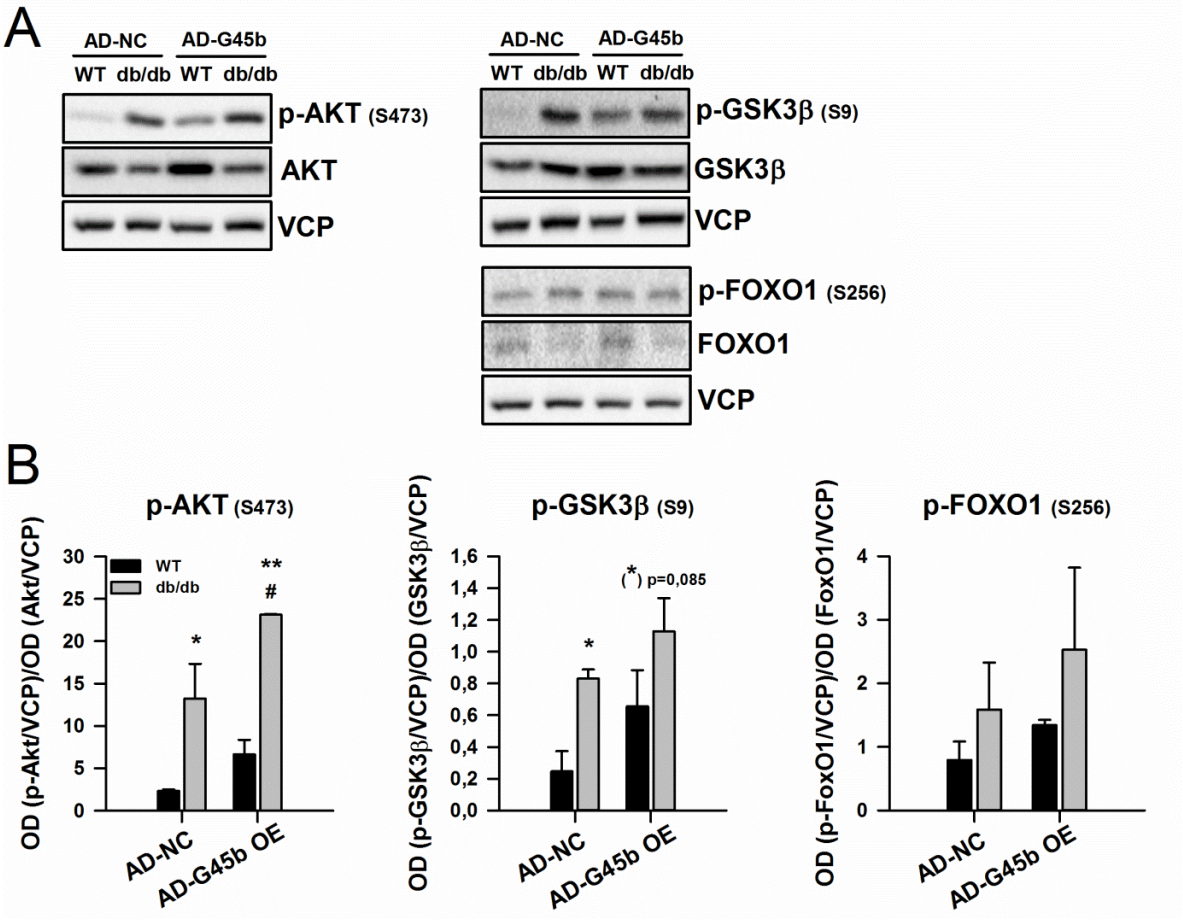

Figure 77: Protein expression of AKT, GSK3β and FOXO1 and their phospho-proteins in *db/db* and WT mice after adenovirus administration. Male *db/db* and healthy control mice (WT) received the AD-GADD45β OE or AD-NC, and after one week they were fasted for 24 hours before sacrifice. Levels of AKT, GSK3β and FOXO1 and their phospho-proteins were determined by immunoblotting using antibodies against the respective protein or the loading control (VCP). Shown are representative blots (A). The signal intensity was assessed by normalising the optical density (OD) first to VCP and then to total normalised protein (B). Mean ± SEM; n=3 per group; * genotype effect, # effect of GADD45β overexpression; (*) $p \leq 0.05$, (**) $p \leq 0.01$, (***) $p \leq 0.001$.

Another downstream target of AKT, FOXO1, was not altered in its phosphorylation status, but in the levels of total protein (Fig. 77A). When examining the ratio of phosphorylated FOXO1 to total FOXO1, it seems that *db/db* mice had a higher FOXO1 phosphorylation status (Fig. 77B). Phosphorylation of FOXO1 decreases hepatic glucose production through a decrease in transcription of glucose 6-phosphatase. Indeed we could measure a decrease in glucose 6-phosphatase mRNA expression in *db/db* mice with GADD45β overexpression (Fig 78).

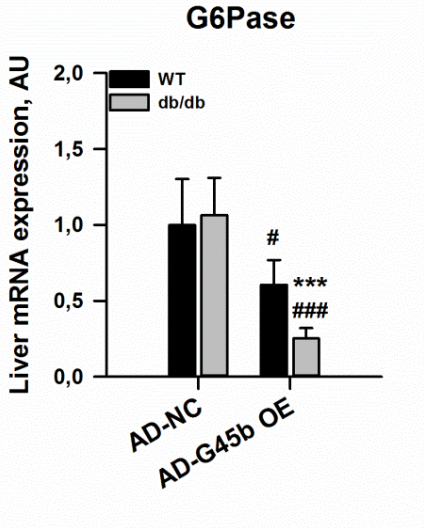

Figure 78: Liver glucose 6-phosphatase expression in *db/db* and control mice after adenovirus administration. Male *db/db* or healthy control mice (WT) received the AD-GADD45β OE or AD-NC, and after one week they were fasted for 24 hours before sacrifice. Glucose 6-phosphatase (G6Pase) mRNA levels were analysed by RT-qPCR and shown as a fold induction relative to WT mice with AD-NC. Mean ± SEM; n=4-6 per group; * genotype effect, # effect of GADD45β overexpression; (*) $p \leq 0.05$, (**) $p \leq 0.01$, (***) $p \leq 0.001$.

With the hint that GADD45β might have an effect on insulin signalling via AKT, the same targets were investigated in the HFD study with GADD45β WT and KO mice. Here we could not see an effect on the phosphorylation status of GSK3β or FOXO1 (Fig. 79C and F). The reason for the discrepancy might be that the *db/db* mice were sacrificed in the fasted state, whereas signalling in the GADD45β KO mice was examined in the fed state. The results are also difficult to compare since both studies were conducted with animal models possessing different etiological causes for their for obesity and insulin resistance.

Furthermore, we could see a decrease in the protein levels of total IRS-1 in mice fed a HFD with no effect of genotype and no change in the phosphorylation status of the protein at Ser1101 (Fig. 79A, H and I). Unfortunately it was not possible to get a signal for other phosphorylation sites such as S307 or T895. Additionally, p85 (the regulatory subunit of PI3K), a downstream target of IRS-1, was reduced in mice on HFD with no effect of genotype (Fig. 79A and J). In contrast to these findings, there was a slight increase in phospho-AKT at both phosphorylation sites (T308 and S473) in mice on HFD (Fig. 79B, D and E) and no effect on GSK3β-phosphorylation (Fig. 79C and F). However, a striking (4x) increase in S6K1-phosphorylation could be observed in GADD45β KO mice fed a HFD compared to all other groups (Fig. 79C and G). This is in accordance with other reports, wherein S6K1 activity was elevated in *ob/ob* and *db/db* mice and negatively regulated insulin signalling under conditions of nutrient satiation [273-275].

Taken together, the impact of GADD45β on insulin signalling when fed a HFD remains controversial. Total IRS-1 seems to be reduced when fed a HFD which was reflected by its downstream target PI3K. This could be an effect of increased insulin resistance. In GADD45β KO mice the levels of both proteins seemed to be even more reduced than in WT mice, although not significantly, which would fit to the observation that GADD45β KO animals were more insulin resistant than their WT littermates. Why AKT phosphorylation would be increased in livers of these mice remains speculative. It might be activated by another (unknown) kinase and not signal via GSK3β but via mTORC1 and S6K1.

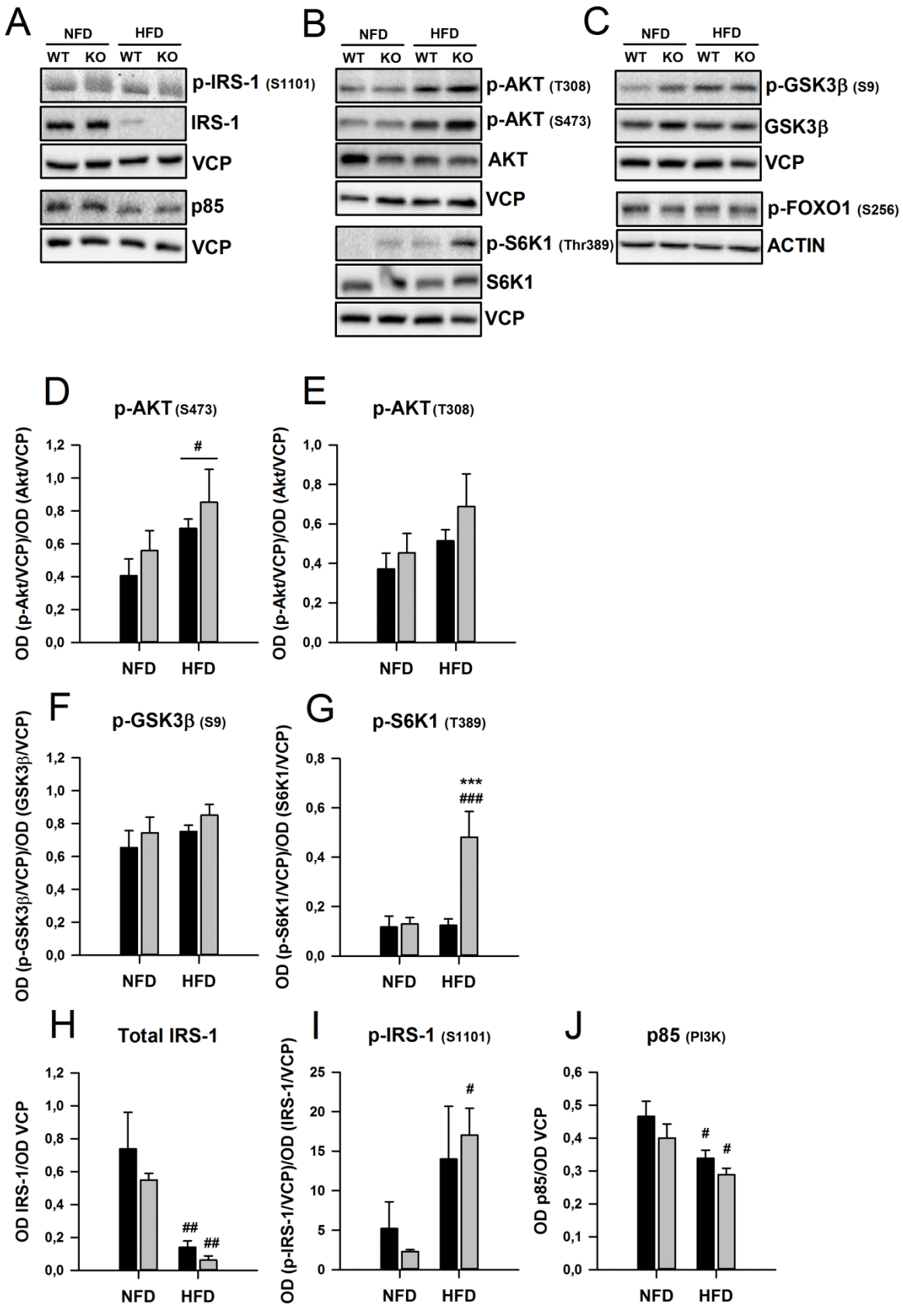
A
NFD
HFD
WT KO WT KO
p-IRS-1 (S1101)
IRS-1
VCP
p85
VCP
B
NFD
HFD
WT KO WT KO
p-AKT (T308)
p-AKT (S473)
AKT
VCP
p-S6K1 (Thr389)
S6K1
VCP
C
NFD
HFD
WT KO WT KO
p-GSK3β (S9)
GSK3β
VCP
p-FOXO1 (S256)
ACTIN
D
p-AKT (S473)
OD (p-Akt/VCP)/OD (Akt/VCP)
NFD
HFD
E
p-AKT (T308)
OD (p-Akt/VCP)/OD (Akt/VCP)
NFD
HFD
F
p-GSK3β (S9)
OD (p-GSK3β/VCP)/OD (GSK3β/VCP)
NFD
HFD
G
p-S6K1 (T389)
OD (p-S6K1/VCP)/OD (S6K1/VCP)
NFD
HFD
H
Total IRS-1
OD IRS-1/OD VCP
NFD
HFD
I
p-IRS-1 (S1101)
OD (p-IRS-1/VCP)/OD (IRS-1/VCP)
NFD
HFD
J
p85 (PI3K)
OD p85/OD VCP
NFD
HFD

Figure 79: Protein expression of IRS-1, p85, AKT, GSK3β, S6K1 and FOXO1 and their phospho-proteins in GADD45β KO and WT mice on HFD or control diet. Male GADD45β KO and WT littermates were either fed a diet high in fat (HFD) or a matching control diet (NFD) for 16 weeks before sacrifice. Levels of IRS-1, p85, AKT, GSK3β, S6K1 and FOXO1 and their phospho-proteins were determined by immunoblotting using antibodies against the respective protein or the loading control (VCP). Shown are representative blots (A-C). The signal intensity was assessed by normalising the optical density (OD) first to VCP and then to total normalised protein (D-J). Mean ± SEM; n=6 per group; * genotype effect, # diet effect; (*) $p \leq 0.05$, (**) $p \leq 0.01$, (***) $p \leq 0.001$.

3.7 Does a hepatocyte-specific loss of GADD45β mimic the effects seen on lipid handling and insulin sensitivity?

In the future our aim is to test whether a hepatocyte-specific deficiency in GADD45β function mimics the phenotype observed in whole-body GADD45β KO mice. Therefore we want to administer recombinant adeno-associated viruses (AAV) into C57Bl6/J mice and keep them on a HFD or NFD to induce insulin resistance. Unlike adenoviruses, these virus particles are not cleared by the host's immune system and, unlike adenovirus, can therefore be used for long term studies [276]. The AAV serotype that was used (AAV2/8) was designed to preferentially infect hepatocytes. The viruses express a specific GADD45β miRNA or non-specific miRNA under the control of a hepatocyte-specific LP1 promoter which is not active in other liver cells such as Kupffer cells [240]. Planned are analyses of fasting blood glucose and serum insulin as performed before, but this time we want to sacrifice the animals in the fasted state to compare the results better with *db/db* mice and to see if they have a dysregulated systemic and liver lipid metabolism.

3.7.1 The designed miRNA against GADD45β is functional *in vitro*

The functionality of the designed miRNA had to be tested *in vitro* before AAV production and administration into animals. Therefore, the plasmids containing the GADD45β miRNA sequence (pcDNA6.2GW/EmGFP-miR mGadd45b) or the empty vector (pcDNA6.2/GWEmGFPmiR-NC) were separately transfected into Hepa1c1 cells together with a vehicle control, using Lipofectamine 2000 transfection reagent. 12 hours later the medium was changed either to normal culture medium (DMEM with additives) or to starvation medium (Hank's buffered saline solution (HBSS) with additives) to induce GADD45β expression. Cells were harvested 8 hours later and the protein levels of GADD45β were assessed by immunoblotting. As shown in figure 80, the addition of starvation medium resulted in a potent increase in GADD45β protein levels in cells transfected with the scrambled control vector and vehicle. Importantly, transfection of the cells with the plasmid containing the GADD45β miRNA sequence resulted in an efficient suppression of GADD45β induction. Since the miRNA sequence was functional, it was subsequently sub-cloned into the pdsAAV-LP1-EGFPmut AAV. The plasmids encoding the miRNA constructs were cotransfected into HEK293T cells with the pDGΔVP helper plasmid [277] and a mutated p5E18-VD2/8 expression vector encoding AAV2 rep and a mutated AAV8 cap protein [278]. The generated virus particles were purified via iodixanol gradient and titred for *in vivo* application.

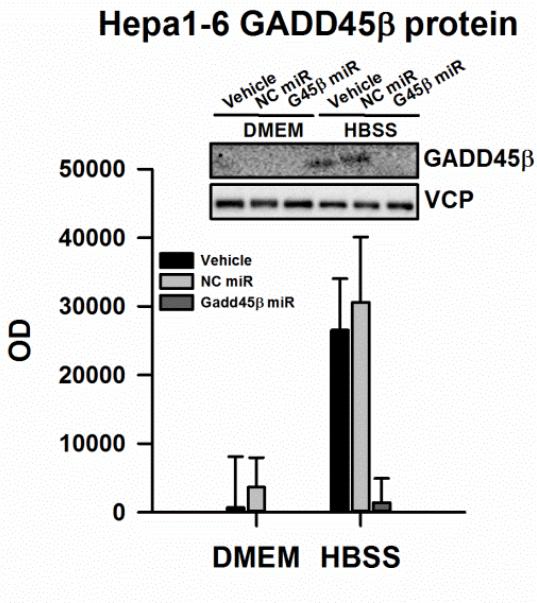

Figure 80: Cloning of AAV miRNA expression construct for long term GADD45β knockdown. Hepa1c1 cells were transfected with plasmids containing a GADD45β miRNA sequence or a scrambled miRNA sequence (NC) or vehicle. 12 hours later the medium was changed either to normal culture medium (DMEM with additives) or to starvation medium (Hank's buffered saline solution (HBSS) with additives) to induce GADD45β expression. Cells were harvested 8 hours later and the protein levels of GADD45β were assessed by immunoblotting using GADD45β -antibody and VCP-antibody as loading control. Results from 3 independent experiments are shown.

3.7.2 A pilot study confirms that administration of AAV harbouring a GADD45β specific miRNA leads to efficient knockdown *in vivo*

Before the planned study can be conducted the functionality of the produced AAV had to be verified in a pilot study. To test for the miRNA-mediated hepatocyte-specific knockdown of GADD45β, 2 x10^{11} virus particles per recombinant AAV were administered via tail vein injection into male C57Bl6/J mice. After three weeks on control diet, fasting was conducted for 24 hours before sacrifice. As shown in figure 81, efficient GADD45β knockdown in the liver could be achieved in three out of five animals. Since the hepatocyte-specificity of this virus system was described previously [242,279], no other tissues were analysed for GADD45β expression.

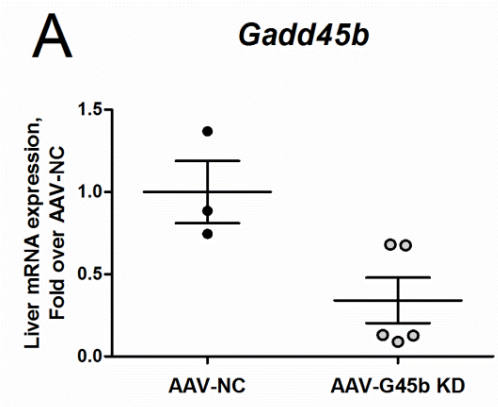

B

Virus	Fold over AAV-NC
AAV-NC	0,745
AAV-NC	0,885
AAV-NC	1,369
AAV-G45b KD	0,089
AAV-G45b KD	0,131
AAV-G45b KD	0,127
AAV-G45b KD	0,676
AAV-G45b KD	0,681

Figure 81: AAV mediated GADD45β knockdown. AAV harbouring a plasmid containing the GADD45β miRNA sequence (GADD45β KD) or a scrambled control sequence (NC) were administered via tail vein injection into male C57Bl6/J mice. After three weeks mice were fasted for 24 hours before sacrifice. GADD45β mRNA levels were analysed subsequently by RT-qPCR and shown as a fold induction relative to "AAV NC" (A). The exact expression values are shown in (B).

Since these results validated sufficient hepatic GADD45B knockdown, we initiated the loss-of-function experiment inmale C57Bl6/J mice. One week later half of the animals switched to HFD. This study was ongoing at the time of preparation of this work.

4. DISCUSSION

Given the increasing prevalence of obesity, insulin resistance and the metabolic syndrome worldwide, accompanied with a lack of successful treatment of these disorders beyond life style and diet interventions, the elucidation and understanding of the underlying and dysregulated mechanisms has become more and more crucial in order to identify novel targets and to allow for more promising interventions. This intention is particularly challenging since the above mentioned metabolic disorders are not characterised by one single pathway gone awry, but by several intertwined and misoperating systems on the intracellular, intercellular or inter-organ level. In the present work we describe for the first time a role for hepatic GADD45β in adaptive metabolism under the stress of food deprivation and nutrient overload. We uncovered GADD45β as a fasting-induced gene, which is inflexibly regulated in different mouse models of obesity, diabetes and aging, as well as in diabetic patients. We propose that this induction is not under hormonal control, but due to sensing lack of nutrients. GADD45β is crucial for systemic and lipid metabolism, and its depletion is accompanied by decreased serum FA but increased liver TG upon starvation. On the other hand, we have evidence that GADD45β is also important for glucose homeostasis. In particular, GADD45β KO mice on HFD are more insulin resistant, and exogenous overexpression can improve the diabetic phenotype in mice. We conclude that GADD45β might be a new link between lipotoxicity and development of insulin resistance through exerting a protective role during increased fatty acid supply either in fasting states or during obesity. However, the mechanism(s) through which GADD45β mediates its effects remains unclear.

4.1 Fasting-induced hepatic GADD45β induction might be due to lack of nutrients

GADD45 proteins are induced by several environmental and physiological stresses such as methyl methanesulfonate (MMS), γ-radiation, ultra violet light, and inflammatory cytokines (see suppl. table 1 for further information). Thus far only mouse GADD45α has been reported to be induced upon the stress of fasting leading to muscle atrophy [231]. In Drosophila, D-GADD45, an orthologue for mouse GADD45α, is slightly induced upon starvation, and overexpression in the nervous system led to an increased resistance to starvation [210]. In the present study we show a potent (> 10-fold) induction of liver GADD45β upon food withdrawal in C57Bl6/J mice (Fig.15). This increase in expression confirms other reports in which, using RNAseq and gene chip arrays, GADD45β was revealed to be one of the most heavily induced genes during starvation [280-282]. In the work at hand we showed this induction was blunted in diabetic and obese mice (Fig. 15). We could also demonstrate that the induction upon fasting followed a time course and was reversible after refeeding (Fig. 17). Furthermore, of the metabolic tissues examined, the induction was limited to the liver (Fig. 18) specifically to hepatocytes (Fig. 20), and was not accompanied by a compensatory increase of other GADD45 family members (Fig. 31). In order to examine which stimulus (e.g. hormone, cytokine, nutrient availability) was responsible for the increase in

GADD45β, several *ex vivo* and *in vitro* experiments were performed. Primary hepatocytes showed a slight (not even 1,5-fold, but significant) induction of *Gadd45b* only after treating them with AICAR, an analogue of AMP that is capable of stimulating AMP-dependent protein kinase (AMPK) activity (Fig. 22). AMPK is known to be activated during nutrient deprivation leading to induction of energy-producing, catabolic pathways [249]. Interestingly, *Gadd45b* expression was not stimulated upon insulin or TNFα treatment, which is in contrast to other reports [156,235]. However, in the study where insulin treatment caused an increase in *Gadd45b* mRNA levels, Rat H4-IIE hepatoma cells were used, and the induction of *Gadd45b* was relatively mild (2-3-fold). The observation that *Gadd45b* mRNA levels are stimulated upon nutrient deprivation could further be confirmed in a differentiated, non-transformed hepatocyte cell line (AML12; Fig. 21). Interestingly, *Gadd45b* was only induced when all nutrients were reduced to 1 % of their original concentration. Omission of a single nutrient, such as glucose or lipids, or two nutrients of a specific class, such as glucose and pyruvate, did not change the expression level. This is in contrast to another publication where microarray expression profiling of amino acid deprived HepG2 human hepatoma cells displayed GADD45β among the upregulated genes [283]. However, this effect could also be attributed to the tumorigenic properties of this cell line. On the other hand, this report is confirming our hypothesis that GADD45β levels are driven by an upstream sensor of nutrient deprivation than a hormonal stimulus or cytokine.

The experiments performed with AML12 cells bear several points for criticism. First of all, more experiments could have been done to confirm that it is the lack of a combination of nutrients, which is responsible for *Gadd45b* induction. For example, one could have used a medium with all nutrients being reduced to 1 % of their original concentration, and then each nutrient could have been added back individually. Also, different combinations of nutrients could have been left out of the medium, not only ones of a specific class.

Furthermore, one has to question how meaningful and physiologically relevant the experiments with AML12 cells are. Even though the cells are not transformed and non-tumourigenic, they are derived from livers of transgenic mice overexpressing transforming growth factor α (TGFα) [248] which overcomes growth and replicating restrictions, so they do not stop replicating in contrast to primary hepatocytes. Thus, they are a more artificial system than primary hepatocytes, liver slices or the mouse per se. Hence, similar experiments should be repeated in those systems. In addition, the blood from fasted animals does not reflect the DMEM/F-12 with deprived nutrients we used in our experiment. Fasting blood has a different composition than fed blood, and also than AML12 medium. In our *in vitro* model we assumed that all nutrients are low or that only special compounds were missing which is not the case in fasting blood. In the end, to find the stimulus responsible for *Gadd45b* induction one should compare serum from fasted and fed mice and treat primary hepatocytes with those.

Taken together, the conducted experiments gave a first indication that GADD45β induction upon fasting might not be mediated by a hormone or cytokine (at least not by those we tested) but rather by the lack of nutrients. However, it is noteworthy, that we did not address the involvement

of transcription factors as a potential mediator of GADD45β induction. It is reported that several transcription factors and coactivators are involved in the starvation response and energy metabolism, such as PPARα [284], FXR [285], CAR [286], PGC-1α [287] and Nrf2 [288] and potentially could be involved in the induction of GADD45β expression. On the other side, owing to their LXXL-motif, GADD45 proteins are described to interact with several nuclear hormone receptors including RXRα, ERα, PPARα/β/γ and act as nuclear receptor coactivators *in vitro* [202,205]. Thus, it would be interesting to test whether GADD45β activity can be modulated by binding to nuclear receptors and whether these interactions are increased during starvation (see outlook section for possible experiments to assess protein-protein interactions).

4.2 GADD45β is required to maintain systemic and hepatic lipid metabolism

One central player in metabolic diseases is nutritional fat, and many proposed causes for obesity and insulin resistance (e.g. chronic inflammation [289], endoplasmic reticulum stress [37], mitochondrial dysfunction [290,291], oxidative stress [292], dysregulated signalling pathways [35,124]) are themselves the cause or consequence of ectopic lipid accumulation [27]. Lipid accumulation leads to stress, wherein the cell or organ has to activate defence mechanisms in order to maintain its functionality. Starvation is the opposite extreme of obesity, but also here the liver and other metabolically active organs have to adapt to the situation by altering their anabolic and catabolic pathways. Similarly to the obese state, during fasting fatty acids are released from the adipose tissue and are taken up by the liver where they are used to generate energy. As a consequence serum NEFA and ketone bodies levels rise. On the other hand, prolonged fasting is accompanied with accumulation of TG in the liver.

We could confirm these fasting phenotypes in C57Bl6/J mice. The mice lost weight (Fig. 26A), had reduced blood glucose levels, and showed an increase in serum ketone bodies and NEFA concentrations (Fig. 27). Also, serum TG and glycerol levels rose as expected due to lipid mobilisation from adipose tissues (Fig. 27). Most interestingly, whole-body GADD45β KO disturbed this adaption to starvation. GADD45β KO mice showed a blunted increase in serum NEFA levels (Fig. 27A), and, most strikingly, accumulated more TG in their livers than WT littermates (Fig. 28A) while their fat and liver weights did not show an effect of genotype (Fig. 26B). In stressing this phenotype further by feeding mice a MCD diet, which leads to steatosis and liver damage, we could recapitulate the observed effect. GADD45β KO mice accumulated more fat (NEFA, TG, glycerol and cholesterol) in their livers (Fig. 42) and showed a higher degree of liver damage compared to WT mice (Fig. 41E), while serum parameters did not differ between genotypes (Fig. 41). In fasted diabetic humans and *db/db* mice a reduction in liver GADD45β expression was associated with an augmentation of serum TG levels in human (Fig. 46A) and a blunted increase of serum NEFA in *db/db* mice (like in GADD45β KO mice) (see Dr. Roldan de Guia's PhD thesis for further detail). Furthermore, we could observe similar effects on some serum and liver parameters in aged mice as seen in GADD45β KO and *db/db* mice (see Astrid

Wendler's Master's report for further detail). On the other hand, we could show that an exogenous overexpression of hepatic GADD45β in whole-body GADD45β KO mice could partially reverse their dysregulated fasting phenotype; liver NEFA and TG concentrations could be reduced (Fig. 63).

The open question that needs to be answered is how GADD45β mediates its effect on lipid homeostasis. One possibility might be by influencing the transcription of downstream target genes, since GADD45β has been described to be a transcriptional coactivator [205]. To address this possibility we submitted liver RNA samples of fasted GADD45β KO and WT mice to the Genomics Core facility at the DKFZ for RNAseq analysis, and also measured the mRNA levels of different genes involved in detoxification (*Cyp2b10)*, drug transport (*Slco1a1)*, FA uptake (*CD36*) and FA metabolism (*Acly, Cyp4a14, Fasn, Acc1)*. In both analyses the effect of GADD45β deletion on differentially expressed genes was inconsistent and only mild (Fig. 71 and 73), and could not be rescued by liver-specific overexpression of GADD45β (Fig. 72 and 74). As a consequence, we conclude that GADD45β might not mediate its influence on lipid metabolism by transcriptional regulation. As the tested genes involved in FA transport and synthesis were not commonly dysregulated upon GADD45β depletion, it seems that, at least on mRNA level, GADD45β has no impact on these aspects of lipid homeostasis. The RNAseq results also do not point to this direction; the DAVID enrichment analysis did not reveal an effect on FA metabolism pathways (Suppl. Figure 1).

Lipid accumulation, as we observed it in GADD45β KO mice, occurs when the rate of FA uptake and *de novo* lipogenesis is greater than the rate of FA oxidation or FA export in form of TG in lipoproteins. This is happing not only in the obese state under nutrient over load, but also during prolonged fasting. Thus, GADD45β could in principle act on any of those aspects. In the fasted state, *de novo* lipogenesis of FA is suppressed, and indeed we could not see an effect of GADD45β KO on genes involved in FA synthesis (*Acly, Cyp4a14, Fasn, Acc1)* (Fig. 71). Additionally, as mentioned above, we doubt that FA uptake is affected by GADD45β deletion (at least on CD36 mRNA level which was initially reduced in GADD45β KO mice, but could not be recapitulated with GADD45β overexpression. Anyway, a reduction in hepatic CD36 would not have resulted in increased liver accumulation [293,294]). We could also show that FA oxidation is not altered in GADD45β KO mice as neither the RER (Fig. 32) nor the formation of ketone bodies (Fig. 27E) or acylcarnitines (Fig. 30) were different between the genotypes. Some possible explanations why GADD45β KO mice showed a blunted increase in serum NEFA levels (Fig. 27A) and an accumulation of TG in the liver (Fig. 28A) could be that either the esterification of NEFA into TG (biosynthesis of TG) was affected, or that the export of FA in form of VLDL-particles was impaired. The latter is true when mice are fed the MCD diet. Feeding GADD45β KO and WT mice a MCD diet for three weeks led to an expected accumulation of liver lipids (Fig. 42) and liver damage (Fig. 41E) together with a decrease in serum TG and cholesterol levels, with GADD45β KO mice showing a more severe phenotype (Fig. 41). However, this study does not exclude the possibly of a concurrent impact of GADD45β on the esterification of FA. Also, fasted

GADD45β KO and WT mice showed a slight increase in serum TG concentrations upon fasting (Fig. 27B) which is not in favour with the possibility of an impaired TG release. Thus, our experiments do not solve the question whether GADD45β KO influences FA conversion into TG or whether it affects FA export. One possibility to address this issue is to track FA in GADD45β KO and WT mice to determine their fate. More specifically, one could perfuse livers of fed and fasted GADD45β KO and WT littermates with radioactive labelled oleate (monounsaturated FA) or palmitate (saturated FA) and examine whether their carbons accumulate in the liver as intermediates of the esterification pathway (e.g. 1-acylglycerol phosphate, phosphatidate, 1,2-diacylglycerol) or as triglycerides. Furthermore, one could inhibit β-oxidation in the fed and fasted state by (+)-decanoylcarnitine, an inhibitor of long chain acylcarnitine transferase [295], or by PPARα antogonists [296] such as GW6471 [297] or MK886 [298], and examine whether GADD45β WT mice have an advantage compared to their KO littermates in handling the increased flux through esterification. The same experiment could also be done combined with feeding a MCD diet. Furthermore, we were critical about an impact of GADD45β on FA uptake since we could not see an effect of GADD45β KO on CD36 mRNA level. However, it might also be that GADD45β interacts with CD36 on protein level to modulate its activity. Furthermore, CD36 is not the only protein responsible for FA uptake. We did not assess whether fatty acid binding protein 4 (FABP4) or FA transport protein (FATP) are affected [299]. Also, acyl-CoA synthetase (ACS) enhances the uptake of FA by catalysing their activation to acyl-CoA esters. All proteins have been shown to positively relate to liver fat content [300,301]. Hence, an increase in the flux of peripherally derived FA to the liver might still occur and has to be considered as an underlying mechanism for GADD45β KO-mediated TG accumulation. Measuring the potential of FA uptake in isolated primary hepatocytes from GADD45β KO and WT animals, as well as ACS activity assays [301], might give insight of the impact of GADD45β on FA uptake. Moreover, an oral lipid tolerance test is a possibility to determine whether GADD45β KO and WT show difference in handling and clearance of excess lipids in the circulation through the liver, which is described to be the major site of TG removal under normal conditions [302,303]. Indeed, fasted GADD45β KO mice showed an enhanced clearance of either TG or NEFA after injecting a lipid mixture compared to WT littermates, which is reflected by lower serum TG levels throughout the test (data not shown).

Triglycerides are stored in lipid droplets within hepatocytes. These lipid droplets are structurally similar to circulating lipoproteins. Lipid droplet-associated proteins are involved in the formation, maturation, secretion, and trafficking of lipid droplets and participate in both lipolysis and lipogenesis [304]. Growing evidence has shown that lipid droplet proteins play a role in the pathophysiology in the fatty liver disease [305,306]. As such, lipid storage droplet protein 5 (LSDP5) has been shown to enhance lipid accumulation in AML12 cells and primary hepatocytes [307], and perilipin (PLIN) gene expression was positively correlated with liver fat content [300]. Hence, it would be interesting to examine whether GADD45β plays a role in assembling lipid droplet formation, thereby exerting its effect on lipid accumulation. For this purpose, lipid droplet-associated proteins can be detected via Western Blotting or immunohistochemistry.

The endoplasmic reticulum (ER) plays not only an import role for the coordinated synthesis, folding and trafficking of proteins, but also for the biosynthesis of TG and cholesterol and the assembly of VLDL particles. It has been shown that ER stress leads to an increase of CCAAT-enhancer-binding protein (C/EBP) [308] and sterol regulatory element-binding protein (SREBP-1) [309], which in turn is responsible for cholesterol and TG uptake and biosynthesis, and hence for lipid accumulation in the liver. It is reported, that this increase in lipid biosynthesis in hyperhomocysteinaemia-induced ER stress is not accompanied by a defect of VLDL release, but that TG and cholesterol export are rather increased [310]. This study suggests that hepatic steatosis is not due to impaired lipid export, but instead results from increased lipid biosynthesis and uptake. On the other hand, mice with hepatocyte-specific deletion of inositol-requiring enzyme 1 α (IRE1α), which has an important role in preventing ER stress, have enhanced hepatic steatosis and reduced plasma lipids due to suppressed apoB-containing lipoprotein secretion [311]. We could show a slight increase of serum TG upon fasting with no difference in genotype (Fig. 27B) suggesting that lipid export was not affected. To confirm that TG originates from the liver one can perform a TG secretion rate assay. Thereby, fasted mice are injected with Triton WR1339. Since Triton WR1339 blocks conversion of VLDL to LDL, the resulting increase in plasma triglyceride and cholesterol concentrations reflect hepatic secretion of VLDL in the absence of LDL uptake [312,313]. Importantly, it has been shown that GADD45β is induced upon ER stress [314], thereby providing a link to enhanced lipid accumulation in GADD45β KO mice. Thus, one might assess if ER stress is involved in the observed effect of our work. Therefore one might overexpress the ER chaperone GRP78/BiP and examine whether ER stress and GADD45β KO-mediated lipid accumulation is reduced. Overexpression of GRP78/BiP has been reported to protect cells from ER stress [315]. Also, ER ultrastructure in GADD45β KO and WT mice could be assessed by electron microscopy.

Recently it has been described that GADD45β can inhibit autophagy [228,229]. Autophagy in turn can regulate lipid stores and metabolism in the liver by a mechanism called lipophagy [316]. Hereby TG and cholesterol are taken up by autophagosomes and delivered to lysosomes for degradation resulting in FA generation which can be used for energy production via β-oxidation [317]. Thus, lipophagy is crucial for maintaining lipid and energy homeostasis, and a decrease in lipophagy is involved in the development of steatosis. Furthermore, a function for autophagy in mediating hepatocyte resistance to death from oxidative stress [318] and in pro-survival pathways has been described [319,320]. Obesity is characterised by a decrease in hepatic autophagy. The underlying mechanism are not completely solved but might include a reduction of autophagy factors (ATF) or impaired fusion of autophagosomes and lysosomes, both leading to decreased autophagy. Furthermore, the accumulation of hepatic fat is accompanied by increased levels of saturated long-chain fatty acids, which can cause lipotoxicty [321] with the result that lipophagy and subsequent β-oxidation are reduced, levels of saturated long-chain fatty acids are increased and apoptosis is eventually triggered. GADD45β might be involved in those chains of events. Since GADD45β is a stress-induced gene and reported to be induced upon palmitic acid treatment in human hepatoma cells (HepG2) [322], it might be induced upon lipotoxicity.

GADD45β inhibits autophagy by preventing the fusion of autophagosomes with lysosomes [229]. Thus, the induction of GADD45β through obesity-mediated lipotoxicity might reduce lipophagy and in the end trigger apoptosis. In this regard apoptosis might be a protective mechanism against an excess of saturated long-chain fatty acids. On the other hand this hypothesis stands in contrast to the involvement of apoptosis in the development of insulin resistance [132-135] and our observation that liver-specific overexpression of GADD45β ameliorates the diabetic phenotype of *db/db* mice. It also does not explain why GADD45β KO mice accumulate more fat in the liver as autophagy should be increased with GADD45β KO, and why we can reduce liver NEFA and TG contents upon liver-specific GADD45β overexpression. Furthermore, detecting delipidated ATG5 [229] by immunoblotting in the fasted state did not reveal any change between the genotypes (data not shown), indicating unaltered regulation of autophagy during fasting in GADD45β KO mice. Taken together, the question is still open whether GADD45β-mediated inhibition of autophagy is involved in the observed effects of GADD45β on lipid metabolism. Staining for autophagosomes and assays to assess apoptosis (e.g. tunel staining [323], caspase activity assays) could help to clarify this issue.

GADD45β might be involved in the adaptive handling of FA supply through another mechanism. GADD45 proteins are involved in p53-mediated apoptosis by being p53-regulated [166,167] and also by contributing to p53 activation via p38 [169]. P53 is activated under stress situations by p38 and other mitogen-activated protein kinases (MAPK) (e.g. JNK, ERK) through phosphorylation of p53 at its N-terminus, which decreases the binding of p53 to mouse double minute 2 homolog (MDM2), resulting in protein stabilisation and accumulation [324-326]. Evidence has accumulated that p53 is not only involved in apoptosis, cell cycle arrest and DNA repair, but also has essential functions of metabolic control by various metabolic pathways [327,328]. These functions are important in the context of preventing development of cancer, but also in responding to metabolic stresses, thereby having profound roles in the development of metabolic diseases. One of these functions is the adaptation to food deprivation. Recently, it has been shown that the MDM2-p53 pathway controls fatty acid oxidation during starvation. In this study, fasting-induced p53 activation led to increased malonyl CoA decarboxylase (MCD) expression, which stimulates malonyl-CoA breakdown and facilitates the transport of FA into the mitochondrial matrix for β-oxidation through enhanced carnitine palmitoyl transferase (CPT1α) activity [329]. These events would be attenuated in our GADD45β KO model due to a decreased activation of p53, consequently leading to reduced FA oxidation but biosynthesis of TG, thereby giving an explanation for the accumulation of TG in the livers of GADD45β KO mice under fasting conditions (Fig. 28A). Although we did not observe a difference in FA oxidation between GADD45β KO and WT mice, it might be worthy to test if the described events play a role in the context of GADD45β deletion. For this purpose, one might determine the activity (phosphorylation) status of p53 by immunoblotting, determine the location of p53 in the cell (it is described to be transported from the nucleus to the cytosol when inactive where it gets degraded [330]) and measure the activity of CPT1α as previously described elsewhere [331]. Furthermore,

one might assess the contribution of FA oxidation and TG synthesis in GADD45β KO and WT mice by determining the ratio of acetyl-CoA and malonyl CoA via enzymatic-colorimetric assays [332,333]. Of note, the mentioned study was performed after food withdrawal. However, it is not clear if the same chain of events play a role in FA oversupply during obesity, and the role of p53 in the adaptive response to FA overload is controversial [331].

One alternative reason why serum NEFA are reduced in GADD45β KO mice upon fasting might be a decrease in lipolysis in adipose tissue and hence a reduced transport of FA to the liver. But since we did not observe a change in fat pat weight [334] (Fig. 26B), we are critical about this possibility. We emphasise that the action of GADD45β is intrinsic to hepatocytes since we could partially rescue the dysregulated lipid phenotype by overexpressing GADD45β in the liver (Fig. 63). Also, we did not observe a drop in in oxygen consumption (Fig. 32), muscle mass (Fig. 26B) and ketone body production (Fig. 27E), or increase in RER (Fig. 32) which might indicate that the fasted mouse had to use other nutrient such as proteins for energy production [335]. To further confirm that TG lipolysis is not altered in GADD45β KO mice one could isolate fat pads from GADD45β KO and WT mice and measure the lipolysis rate (concentrations of NEFA and glycerol) in the presence or absence of the lipolysis stimulant forskolin or a synthetic catecholamine (e.g. isoproterenol). Since adipose triglyceride lipase (ATGL) and hormone-sensitive lipase (HSL) are the major enzymes in adipose tissue TG catabolism [336], measurement of their TG hydrolase activity with radioactive labelled substrates could additionally be performed.

Taken together, we believe that GADD45β may not mediate its effect by transcriptional regulation. From our experiments we conclude, that GADD45β plays a crucial role in hepatic adaptation to changes in FA supply. This function is probably carried out on the site of FA conversion into TG rather than on FA synthesis, oxidation or export. Its involvement in FA uptake is still unclear. Further experiments should be performed to confirm these suggestions and to assess the role of the ER and/or apoptosis as link between GADD45β and lipid homeostasis.

4.3 GADD45β is required to maintain glucose homeostasis

The liver is a crucial organ for whole body energy homeostasis, not only in regulating the use and fate of lipid species, but also by regulating glucose turnover. In times of energy demand, the liver converts fat and polycarbohydrates into glucose, whereas in times of energy oversupply, it converts glucose into polycarbohydrates and fat. This reciprocal mechanism is disturbed in obesity and insulin resistance, which is characterised by a failure to suppress hepatic glucose production and FA efflux from adipose tissue, with the consequence that plasma FA and glucose levels are constantly high and lipids accumulate in the liver.

We could confirm most of these obesity-induced phenotypes by feeding C57Bl6/J mice a diet rich in fat (HFD) for four months. Those mice were hyperglycaemic (Fig. 49A) and had a fatty liver (higher NEFA, TG and cholesterol) (Fig. 51). However, serum NEFA levels were reduced and TG levels did not change on HFD; only serum cholesterol was elevated as expected in a

dyslipidaemic state [103] (Fig. 50). Furthermore we could show that those mice were insulin resistant (Fig. 53). Most importantly, GADD45β KO mice were more insulin resistant after 4 months on HFD than their WT littermates as reflected by a bigger area under the curve during an insulin tolerance test (Fig. 53C) and a higher HOMA-IR (Fig. 54C). Moreover, a reduction in liver *GADD45B* was negatively correlated with fasting plasma glucose levels in men (as well with a tendency for higher HOMA-IR, p=0,099) (Fig. 46). We could also confirm the diabetic phenotype of *db/db* mice. In the fed state they had a 2,5x higher blood glucose level than WT mice. During fasting their blood glucose levels fell, as they did in healthy control animals, but they stayed significant higher (~1,5x) (see Dr. Roldan de Guia's PhD thesis for further detail). Furthermore, those diabetic animals have immense lipid accumulation in their livers (Fig. 45), and upon fasting there were similar effects on serum NEFA levels as seen in GADD45β KO mice (blunted increase) (see Dr. Roldan de Guia's PhD thesis for further detail). Most importantly, we were able to reduce the diabetic phenotype of *db/db* mice by liver-specific overexpression of GADD45β (Fig. 67 and 68). Thereby we could also partially restore the dysregulated systemic lipid metabolism in *db/db* mice and confer higher metabolic flexibility upon nutrient deprivation (Fig. 69).

Of importance, we could not see a difference in glucose homeostasis between GADD45β KO and WT mice after being starved, a situation when the liver is also encountered with an increased flux of FA. Here, GADD45β KO mice accumulated more TG in the liver than WT mice (Fig. 28A), but they had equal fasting blood glucose values and were not hyperglycaemic (Fig. 27F). We could only observe an effect on glucose metabolism under the condition of long-lasting nutrient oversupply, and then only in the context of a loss of function (on HFD) or in the context of a gain of function of GADD45β (in *db/db* mice). GADD45β might not have a direct effect on glucose metabolism, but only confers its influence on lipid homeostasis on insulin resistance during times of nutrient spillover, thereby exerting an indirect influence on glucose homeostasis.

The major metabolic tissues (brain, liver, muscle, fat, pancreas, intestine, kidneys) work together to maintain glucose homeostasis during the fasting-feeding cycle of healthy organisms [337]. Thereby, systemic glucose concentrations are a result of glucose uptake by the liver and other peripheral tissues and by glucose production by the liver and other gluconeogenic organs such as the kidney [338] and intestine [339]. In times of nutrient oversupply, when high glucose levels result in high insulin concentrations, glucose uptake by the muscle and liver is promoted leading to the biosynthesis of glycogen and fat. In the insulin resistant state, however, insulin-mediated skeletal muscle glucose uptake is impaired, which leads to a redirecting of glucose to the liver and a production of more liver fat [35]. These hepatic liver lipids also impair the ability of insulin to suppress glucose production, leading to a hyperglycaemic state. Similar to the regulation of hepatic lipid content, GADD45β can exert its effect on glucose homeostasis either on glucose production or/and on glucose clearance from the system. We propose that GADD45β mediates its advantageous effect through the liver, either by a direct intrinsic effect in the liver, or by indirect effects from the liver to other organs (for example via hepatokines [117,118]), since we could rescue the diabetic phenotype by liver-specific overexpression of GADD45β (Fig. 67 and 68).

However, we cannot confirm with certainty that either the improved glucose clearance or the reduced glucose production is the underlying mechanism. If clearance of blood glucose by the liver was augmented by GADD45β overexpression, then this would lead to a higher conversion rate into TG (after glycogen stores are full), but we did not see an accumulation of liver TG accompanied with reduction of blood glucose levels (Fig. 70). Conversely, in *db/db* mice GADD45β overexpression might improve insulin's ability to suppress glucose production, thereby leading to lower blood glucose levels and as a consequence also lower insulin levels, which is all together reflected by a reduction in insulin resistance. In GADD45β KO animals, insulin's ability to supress glucose is impaired resulting in more severe insulin resistance under HFD conditions. Thus, we think that an effect on glucose production is more likely to be the site of action by which GADD45β exerts its influence. However, more studies have to be conducted in order to confirm this presumption. One might perform glucose uptake assays on isolated muscle or liver tissues to assess the contribution of glucose uptake on our phenotype. In muscle, 2-deoxyglucose can be used for this purpose. Glucose hexokinase phosphorylates 2-deoxyglucose, thereby trapping the product, 2-deoxyglucose-6-phosphate, intracellular since it cannot be further used for glycolysis nor converted back to 2-deoxyglucose. In the liver however, this latter case can happen, since the liver expresses glucose-6-phosphatase (G6Pase), and glucose can be released from the cell again. Hence for the liver, one needs to perform more sophisticated tracer studies [340] in order to determine the affected sites of altered glucose metabolism. Furthermore, in the context of investigating the liver glucose production rate, it would be interesting to determine whether GADD45β KO mice show a different reaction following a pyruvate challenge in the course of a pyruvate tolerance test. Moreover, in a glucose output assay one might measure the ability of primary hepatocytes from fasted GADD45β KO and WT mice to convert lactate or pyruvate into glucose with or without insulin treatment.

We could show that GADD45β overexpression in *db/db* mice lead to an increase in AKT phosphorylation and its downstream target GSK3β (Fig. 77), indicating a promotion of glycogen synthesis and increase in liver glucose uptake rate. Consistent with this result, also FOXO1 phosphorylation status was increased (Fig. 77) leading to an inhibition of its downstream target G6Pase (Fig. 78), which is a key enzyme for gluconeogenesis. Unfortunately we could not see a similar suppression of another key gluconeogenic gene, phosphoenolpyruvate carboxykinase 1 (PCK1, data not shown); its expression was lower in *db/db* mice independent of GADD45β overexpression. Hence, more experiments and analyses should be performed in order to confirm an impact of GADD45β on AKT downstream targets for glucose production and glycogen synthesis. First, glycogen contents in *db/db* and WT mice upon GADD45β overexpression should be assessed. Also, while we showed increased phosphorylation of GSK3β, we did not measure the phosphorylation status of its downstream target glycogen synthase, which should be increased. Also, one might test whether the activity of another AKT downstream target and important transcriptional coactivator involved in gluconeogenesis is inhibited, that of peroxisome proliferator-activated receptor-γ coactivator 1 (PGC-1) [287,341]. PGC-1 needs FOXO1 for its

gluconeogenic function [342], but FOXO1-phosphorylation status was increased and hence the protein degraded.

Considering only the study where GADD45β overexpression in *db/db* mice led to an improvement of their diabetic phenotype, one might conclude that GADD45β has an impact on the insulin signalling pathway, thereby improving insulin‘s ability to supress glucose production. Unfortunately, we could not recapitulate this effect on the insulin signalling pathway with GADD45β KO mice on HFD. Here we could not see an effect on the phosphorylation status of GSK3β or FOXO1 (Fig. 79). On the contrary, AKT phosphorylation seems to be increased on HFD with no effect of genotype (Fig. 79), while its upstream effectors show reduced phosphorylation with no difference between GADD45β KO and WT mice (Fig. 79). This observation raises doubt about an impact of GADD45β on the insulin pathway to mediate its effect on glucose output. It rather goes in line with other theories that insulin's ability to suppress hepatic glucose output does not require the canonical insulin signalling pathway [88,89] or AKT as an obligate intermediate for proper insulin signalling [262]. It is noteworthy, that those non-canonical pathways might be only obvious in the hyperinsulinaemic or fed state, which was the case in our HFD study. The *db/db* experiment in contrast was analysed under fasted conditions.

Surprisingly, we did not find the stress-activated c-Jun amino-terminal kinase (JNK) to be involved in GADD45β's effect on glucose homeostasis (Fig. 75 and 76). However, JNK proteins play an important role in metabolism and are involved in the development of obesity, insulin resistance and T2D by having a direct effect on glucose metabolism and insulin sensitivity [237,272,343]. JNK is activated in signal transduction under conditions of obesity and insulin resistance by several effectors, among them TNFα inducing upstream MAP3K [344,345], reactive oxygen species (ROS) [346], IRE1 during UPR in the ER [37,347], and free FA [345], all leading to dual phosphorylation of JNK by MKK4 and MKK7, which results in phosphorylation of downstream transcription factors of JNK such as c-Jun or effector proteins such as insulin receptor substrate (IRS) [344]. Thus, many paths lead to one outcome: JNK activation and blockage of insulin signalling in a tissue specific-manner. As a consequence, we would have expected JNK levels in animals on HFD or *db/db* mice to be higher than in animals on control diet or WT mice. This was indeed the case for *db/db* mice (Fig. 76), but mice on HFD showed no significant difference compared to mice on NFD, if anything then the tendency was to have a lower phospho-JNK status (Fig. 75). But then we did not see an effect of genotype on HFD and no effect of GADD45β overexpression in *db/db* and WT mice. It has to be emphasised that GADD45β exerts its impact on JNK activity on two different routes: activation via MEKK4 [165] and inhibition via MKK4/7 [152,199,348]. We cannot distinguish between the two pathways in our experiments. One might say HFD and obesity are severe conditions and therefore GADD45β would act via MEKK4→JNK [169]. GADD45β KO would then lead to a reduction in JNK activity and overexpression to an increase in phospho-JNK. We could not see either of both outcomes. On the other hand one might argue that HFD and obesity are characterised by high TNFα levels (which we did not measure to confirm!) and hence JNK levels are high, which we could confirm in *db/db* mice but

not in mice on HFD. GADD45β can be induced by TNFα and acts in a feedback loop to inhibit JNK [171,172]. Thus, GADD45β KO should lead to higher and overexpression to lower JNK activity which we could not observe in either of or two studies. Thus, the inconsistency of our results with the literature and the unknown underlying pathways in our models to induce or inhibit JNK led us to the conclusion that the JNK pathway is not involved in the GADD45β-mediated effect on glucose homeostasis.

One striking effect of GADD45β KO mice fed a HFD was the 4-fold increase in ribosomal protein S6 kinase 1 (S6K1) activity compared to all other groups, even to WT mice fed a HFD (Fig. 79G). S6K1 is an effector of mTOR and sensitive to both insulin and nutrients, including amino acids, and the activity of this protein leads to an increase in protein synthesis and cell proliferation. It is induced by insulin via a canonical pathway including class I PI3K→AKT→mTOR, as well as by amino acids via a non-canonical pathway including class III PI3K→mTOR which might explain why it is induced even though total IRS-1 protein is reduced in GADD45β KO mice fed a HFD (Fig. 79H). It is reported that S6K1 activity negatively regulates insulin signalling under conditions of nutrient oversupply [273-275] through negatively regulating IRS1 function via phosphorylation at different residues such as Ser207, Ser1101 and Ser307 [349,350], whereas the physiological relevance of latter phosphorylation site is under debate [351,352]. So it is surprising that we could not see an increase of phospho(T389)-S6K1 in WT animals fed a HFD, but the deletion of GADD45β triggered some unknown event resulting in a strong upregulation of phospho(T389)-S6K1. As mentioned it is induced upon amino acid overload, which naturally comes along with nutrient excess. There is increasing evidence that elevated dietary protein consumption also contributes to metabolic abnormalities [353-356], which may act through the mTORC1-S6K1 pathway. However, our HFD does not differ in protein content to the control diet and we could not see an effect on the serum amino acid profile (Fig. 55). Moreover, IRS-1 phosphorylation on Ser1101 was not increased in GADD45β KO mice on HFD (Fig. 79I). Hence, more research has to be done to define the cause-effect relationship between GADD45β and S6K1 and which downstream effects are involved with this potent GADD45β KO-mediated upregulation. For that, other possible phosphorylation sites of IRS-1 other than Ser1101 have to be examined. In this context, it has been described that S6K1 mediates IRS1 serine phosphorylation, disrupting its interaction with the insulin receptor and leading to its degradation [357,358]. This would support our observations of a reduction of total IRS-1 in GADD45β KO mice fed a HFD and their increased state of insulin resistance. However, other researchers doubt the involvement of Ser307-phosphorylation in insulin resistance [351,352]. Along that line it would be interesting to know whether there is a connection to the involvement of GADD45β in lipid homeostasis. It has been reported that a liver-specific depletion of S6K1 can ameliorate insulin resistance and steatosis by having an influence on genes involved in lipogenesis [275]. Even though we think that *de novo* lipogenesis of FA might not be the underlying site for GADD45β's action, GADD45β might as well influence S6K1 in modulating the expression of genes involved in FA uptake or esterification. This question might be addressed by liver specific knockdown of S6K1, for example with AAV bearing a miRNA against S6K1, in GADD45β KO and WT animals under food

deprivation and oversupply. However, it is noteworthy that we could not see a comparable increase of S6K1 in *db/db* mice with concomitant decrease upon GADD45β overexpression (not shown), which might be due to the nutrient status during sacrifice or the difference in mouse models.

In general it is difficult to investigate the insulin signalling pathway or any other pathway *in vivo* due to the high variability of animals. It would be advisable to investigate the impact of GADD45β on the lipid or glucose homeostasis in the context of insulin signalling in an *in vitro* model. Here, variations between replicates are lower, the experiments are easily reproducible and results faster to obtain. For example, one might mimic insulin resistance in AML12 cells by oversupply of oleate or palmitate [306,359-361] and treat them with insulin or vehicle in the background of either GADD45β overexpression or knockdown. However, as mentioned in the beginning, *in vitro* experiments should only aim at confirming of *in vivo* results or giving the basis for subsequent *in vivo* studies.

4.4 GADD45β – a link between lipotoxicity and insulin resistance?

Even though the fasting-mediated induction of GADD45β in liver is striking, as is its blunted increase in diabetic mice and men, the observed differences in phenotype in different mouse studies are mild between KO and WT mice. Effects on serum and liver lipids, especially TG, are consistently observed though, which might indicate that GADD45β is indeed involved in the regulation of hepatic lipid metabolism. On the other hand it seems as if GADD45β plays not only a role in acute stress of nutrients depletion, but has also a crucial function in regulating insulin sensitivity in chronic stress of nutrient overload (obesity). With gain of function experiments we could attenuate both the defects in lipid handling and insulin signalling, but currently we are not able to say how GADD45β mediates its effect. Thus, questions that rise when analysing and discussing the results of this work are whether and how the observed effects on lipid and glucose homeostasis can be linked. The role of the insulin signalling pathway is hereby still enigmatic and not taken for granted. As mentioned there are postulations about non-canonical, insulin-independent effects on glucose production. These are partially based on the fact that insulin does not only mediate its regulatory function in a direct way on the liver, but also by indirect means on other organs. As such, it is postulated that a non-autonomous pathway exists which includes adipose signalling to hepatocytes via free fatty acids. The inability of adipose tissue, particularly visceral adipose, in the insulin resistant state to suppress NEFA production leads to hepatic NEFA oversupply and thus impaired insulin suppression of hepatic glucose production through an as yet undefined mechanism [129-131].

ER stress links obesity and insulin resistance [362]. Obesity is associated with the activation of cellular stress signalling and inflammatory pathways, and one key player in the cellular stress response is the ER [363,364]. Cells adapt to ER stress through activation of the unfolded protein response (UPR) as a protective mechanism. Obesity and its associated increase in FA flux to the liver lead to ER stress. ER stress in turn has been shown to promote lipid accumulation. This

situation results in a vicious cycle and promotes the development of insulin resistance. Mice deficient in X-box–binding protein–1 (XBP1), a transcription factor that modulates the ER stress response, develop insulin resistance [37]. GADD45β has a XBP1 binding domain [314], thus giving an alternative explanation for increased insulin resistance in GADD45β KO mice which also show TG accumulation upon fasting (Fig. 28A). Hence, GADD45β might link lipid excess to insulin resistance via ER stress and UPR. However, which exact function it confers in this context is not clear. GADD45β is a stress-induced gene with a protective role under mild or acute xenotoxic stress. Under chronic or more severe stress however, it might promote cell death. It has been shown in drosophila that mild irradiation induces D-GADD45 which promoted stress resistance [210]. Furthermore, GADD45β confers protection against liver toxicity, as fasted GADD45β KO mice had exaggerated liver damage in response to sub-lethal acetaminophen administration (data not shown), indicative of a role for GADD45β in stress-resistance also in mammals. Similar effects can be observed in the mouse and human and are described with the phenomena of hormesis, wherein low dose toxins or mild stress induce an adaptive (hormetic) response, which in turn helps to cope with more severe or harmful factors. This concept can also be applied to metabolic disorders [365]. It is proposed that efficient adaptation to life-style-induced cellular stress, such as inflammation, mitochondrial dysfunction or ER stress, mediates the resistance to obesity and NAFLD. As such, cells adapt to ER stress through UPR which in turn might protect the organism of insulin resistance and glucose intolerance [37,366-368]. However, if the UPR fails to alleviate ER stress, the cell will undergo apoptosis. GADD45β expression might be stimulated upon lipid-induced ER stress to exert a protective, so far unknown role. In GADD45β KO mice this missing hormetic response leads to more lipid accumulation and ER stress and as consequence to more insulin resistance. When the cell cannot handle the stress anymore, it will eventually die, a consequence also inherent to GADD45β.

One might criticize that the described conclusions are based on fasting and feeding studies which are two types of metabolic challenges. However, one has to keep in mind that the mouse is not only undergoing fasting and feeding cycles throughout the day, but also while being fed a high fat-diet. On the surface it might look as if this constant overeating is overcoming this cycle, but in fact also while being on high-fat diet the mouse has times of more and times of less nutrients available for their organs, even though these fluctuations might be lessened. Consequently, the organism has not only an affected lipid handling under fasting conditions when GADD45β is absent, but also under high-fat diet feeding, which might converge with aggravated insulin signalling and impaired glucose homeostasis (Fig. 82).

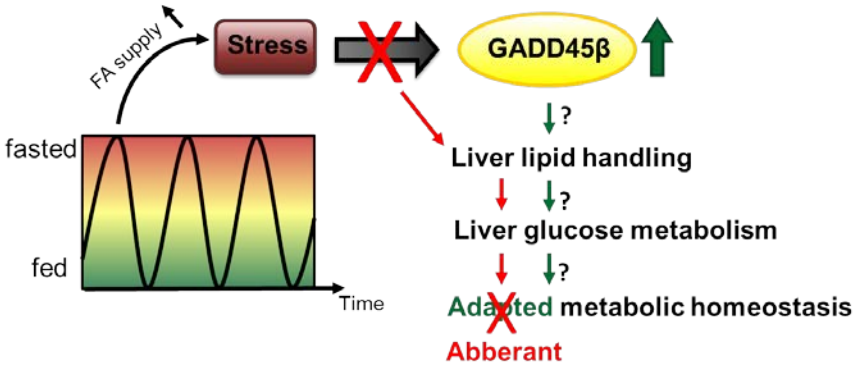

Figure 82: Effects of GADD45β induction on metabolic homeostasis. Gadd45β is induced in a fasting-feeding cycle dependent manner, when fasting leads to nutrient stress situations. Gadd45β supports the organism to adapt to changing lipid supply, which also affects glucose homeostasis and leads to an overall correct metabolic function (green arrows). If Gadd45β is absent (indicated by the red cross), this adaptation response is impaired (red arrows), resulting in aberrant metabolic homeostasis characterised by dysregulated lipid and glucose metabolism. How Gadd45β mediated its effect on lipid and glucose homeostasis is not known.

In summary, the results at hand demonstrate the possibility of a novel connection between lipid accumulation and insulin resistance via the stress-induced gene GADD45β. This is thereby the first report of a GADD45 protein to be involved in system and liver adaptation to the stress of nutrient deprivation and overload. Further investigation should be done to elucidate the specific site of GADD45β action. This might help to find novel targets and sites for pharmacological intervention in the aim for a treatment of metabolic disorders.

4.5 Outlook

Since most experiments utilised whole-body knockout mice, it cannot be excluded that the effects on lipid and glucose homeostasis are influenced by alterations in other organs than the liver. While we could show, that (1) the fasting-induced upregulation of *Gadd45b* was liver-specific and intrinsic to hepatocytes, and that (2) we could partially rescue the observed effects with liver-specific GADD45β overexpression, experiments with hepatocyte-specific knockdown of GADD45β should be repeated. We have already produced the tools for a loss of function study (an AAV bearing a miRNA against GADD45β) and tested them in pilot studies for their functionality. We aim to use them in the context of a HFD, where a significant worsening of insulin sensitivity with GADD45β KO was observed. Since this study was terminated in the fed state, the 24 hours fasting (GADD45β KO), *db/db* and rescue studies however the fasted state, mice should be sacrificed after 24 hours food withdrawal to examine if this dietary challenge reveals a difference in serum and liver metabolites between the treated groups.

Even though depletion of GADD45β was not accompanied by a compensatory induction of the other family members GADD45α and GADD45γ, it cannot be ruled out that the presence of either of them influences the response of the animals towards changes in nutrient supply and during the stage of disease and aging. Indeed, GADD45γ was the initial gene to be found inflexibly dysregulated in *db/db* mice, and we could also show this induction pattern in aged mice.

Furthermore, GADD45γ has been already described to exert a role in metabolic adaptation [230]. Moreover, GADD45 proteins can form homo- and hetero-dimers [150,151]. Hence, the exclusive involvement of GADD45β in the observed effects on lipid and glucose homeostasis can only be confirmed by using a GADD45β(-/-)/GADD45γ(-/-) double KO strategy. To avoid only getting female DKO mice (GADD45γ KO male mice cannot form gonads [257]), one can either use adeno-associated virus (AAV) to knockdown GADD45γ in GADD45β KO males, or one might generate liver-specific DKO using the Cre-lox technology [369-371]. Thereby two loxP sites (specific 34-base pair sequences consisting of an 8-bp core sequence, where recombination takes place) flanking one or two exons of GADD45β/γ are inserted into the genome, and the mouse carrying the floxed allele (GADD45β/$\gamma^{fl/fl}$) is subsequently crossed with a albumin-Cre mouse to generate a hepatocyte-specific knockout *(*GADD45β/$\gamma^{fl/fl}$ albumin-CRE^{+}) since the Cre recombinase under the control of the albumin promotor mediates a deletion of the floxed segment.

Since transcriptional regulation does not seem to be affected, GADD45β might exert its function by interacting with proteins, thereby either stimulating or inhibiting their activity as it has been shown for MEKK4 [165] and MKK7 [199]. Thus, one might identify binding partners of GADD45β. This can be done in several approaches [372]. One common assay is the yeast-2-hybrid screen (Y2H). Yeast cells are transfected with two plasmids, one encoding the bait, which is the protein of interest fused with the DNA-binding domain of a yeast transcription factor like Gal4, and one encoding the prey, which is a library of cDNA fragments linked to the activation domain of the transcription factor. Transcription of reporter genes only occurs when bait and prey interact with each other and form a functional transcription factor [373]. A modification of the Y2H screen is the mammalian-2-hybrid screen, which is based on the same principle but can be performed in cell lines and hence may better mimic actual *in vivo* interactions [374,375]. Positive interaction partners can be confirmed by protein complex-immunoprecipitation with concomitant detection via immunoblotting. Thereby, the endogenous (not overexpressed and not tagged) protein of interest is isolated with a specific antibody from cell or tissue lysates and interaction partners which stick to this protein are subsequently identified by Western Blotting. For screening approaches, affinity purification of the tagged protein of interest coupled to its interacting protein followed by mass spectrometry can be performed [376,377]. It would be interesting to see whether GADD45β indeed is involved in the uptake and esterification of FA by binding some of the key enzymes responsible for these processes (e.g. CD36, FABP4, FATP and ACS, or 1-glycerol-3-phosphate acyltransferase (GPAT), diglyceride acyltransferase (DGAT) and acyl-glycerol-3-phosphate acyltransferase (AGPAT)), which have been implicated in the development of steatosis and insulin resistance [378,379], or whether GADD45β has an influence on proteins of the insulin signalling pathway, or both. In this context, one might also perform metabolomic profiling in order to find intermediates that accumulate upon KO depletion [380-383].

To close the circle it is not only interesting to find the downstream effector of GADD45β, but also which upstream regulator(s) might mediate GADD45β induction. We question a hormonal control,

such as insulin, but think that a senor for nutrient depletion or overload might signal via GADD45β. A prominent candidate in this regard is AMP-activated protein kinase (AMPK), which is a crucial cellular energy gauge and activated upon nutrient deficiency. It indeed mildly induced *Gadd45b* mRNA expression. It is known that AMPK induces p53 activation and promotes survival [384]. On the other hand GADD45α has a p53-binding element in the third intron [168] and p53 can contribute to the positive regulation of the promoter [385]. Since GADD45 proteins are structurally similar, GADD45β might be induced via AMPK→p53. Alternatively, also a transcription factor might be triggering the effects via GADD45β. One might perform a large-scale RNA interference (RNAi) screen in AML12 cells. In this method micro RNA (miRNA) or small interfering RNA (siRNA) are used for post-transcriptional gene silencing typically by causing the destruction of the messenger RNA (mRNA). By introduction selective miRNA or siRNA into the cell one can suppression the expression of specific genes and find out, for example, which transcription factor is responsible for the induction of GADD45β during nutrient deprivation [386,387].

4.6 Summary and Conclusion

In summary, we could demonstrate that GADD45β is a stress-induced gene in mouse and human which is differentially expressed in disease and ageing. We could show for the first time that GADD45β exerts a protective effect on the adaptive metabolism during the stress of nutrient deprivation and nutrient oversupply. Even though the exact underlying mechanisms are still to be unravelled, the absence of GADD45β led to an accumulation of triglycerides in the liver upon food deprivation and to an increased insulin resistance in times of nutrient overload. Gain-of-function experiments could reverse the dysregulated fasting lipid handling in GADD45β KO mice and improve insulin sensitivity in obese-diabetic *db/db* mice. Hence, we conclude that GADD45β may be a missing link between lipid and glucose homeostasis under conditions of nutrient stress which protects from ageing-related metabolic dysfunction.

5. METHODS

5.1 Molecular Biology and Biochemistry

5.1.1 Bacterial Work

5.1.1.1 Transformation of Eschericha Coli

Sure 2 supercompetent cells were used for the cloning of DNA fragments for the production of AAV, for all other cloning procedures DH5α or TOP10™ *E. coli* cells were used. All cells were transformed by chemical transformation. Therefore, 50 µl cells were thawed on ice and incubated with either 0.1-1 µg plasmid DNA or 1-5 µl of ligation reaction for 20-30 min on ice. Following a short heat shock for 45 seconds at 42°C in a water bath and a cool down on ice for 2 minutes, 250 µl of either LB medium (for DH5α or TOP10™) or SOC medium (for Sure 2) was added. The mix was then incubated at 37°C and slight shaking for another hour. Afterwards, 200 µl of cell suspension was spread on agar plates containing the required antibiotics. Plates were incubated at 37°C overnight for bacterial growth and stored at 4°C.

5.1.1.2 Bacterial liquid cultures

Single colonies were picked with a sterile pipette tip and transferred to 5 ml of LB medium with the appropriate antibiotics. These small scale cultures were incubated over night at 37°C with shaking (~160 rpm). For large scale liquid cultures, either small scale liquid cultures, which have been pre-incubated for only 5-8 hours, or an inoculation loop full of cells from a glycerol stock were directly given to 200-2000 ml of LB medium, depending on the required DNA yield. Subsequently, the cultures were incubated over night at 37°C with shaking (~160 rpm).

5.1.1.3 Preparation of bacterial glycerol stocks

For long term storage small scale cultures were mixed 1:1 with 50% glycerol and kept at -80°C.

5.1.1.4 Preparation of plasmid DNA from Eschericha Coli

Small scale plasmid preparation (Mini Prep)

4 ml of small scale bacterial liquid cultures was used for the plasmid preparation using the Qiaprep Plasmid Miniprep Kit provided by Qiagen following the manufacturer's instruction. The DNA was eluted with 50 µl H_2O and stored at -20°C.

Large scale plasmid preparation (Maxi or Mega Prep)

Plasmid preparation from large scale bacterial liquid cultures was performed using the Qiaprep Plasmid Maxi- or Megaprep Kit provided by Qiagen following the manufacturer's instruction. The DNA was eluted with 200 µl or 800 µl 1x TE buffer, respectively, and stored at -20°C.

5.1.2 DNA work

5.1.2.1 Preparation of genomic DNA

DNA for genotyping

200 ml of NID buffer + 2 µl Proteinase K was added to a piece of mouse tip and incubated over night at 56°C with slight shaking. The next day, the digestion was stopped by cooking the samples for 10 min at 95°C. After cooling down on ice, 2 µl of the digest was used for PCR.

DNA from liver tissue

20 mg of pulverised liver tissue was digested in 500 µl lysis buffer + 0.5 mg/ml proteinase K for 3 hrs at 60°C and subsequently overnight at 56°C with shaking. Genomic DNA was extracted by adding 500 µl phenol/chlorophorm/isoamylalcohol (25:24:1), vortexing and centrifugation for 10 minutes at 13.000 rpm, 4°C. The upper phase was transferred to a new tube and the extraction step was repeated. The upper phase was transferred to a new tube with 500 µl chloroform. After spinning again for 10 minutes at 13.000 rpm, 4°C, the upper phase was given to 500 µl isopropanol. After vortexing the DNA was pelleted during an incubation at -80°C for 30 minutes, followed by spinning for 45 minutes at 13000 rpm, 4°C. The pellet was washed with 75% ethanol, dried, and resuspended in 100 µl TE buffer. For complete resuspension the DNA was incubated at 60°C for 2 hours and afterwards stored at 4°C until use. For qPCR, 50 ng/ml was used.

5.1.2.2 Determination of DNA concentration

DNA concentration and the degree of contamination with salts or proteins were determined with the NanoDrop ND-1000 spectrophotometer. 1 µl of DNA solution was used for each measurement, with the according solvent as blank. The DNA concentration was measured at 260 nm, potential contaminations between 220 and 300 nm.

5.1.2.3 DNA sequencing

DNA was diluted to 800 ng in 10 µl H_2O and sent to the company LGC genomics (Berlin) for sequencing. Primers at 5 pmol/µl were added either directly or by the company. Primers used for sequencing are listed in the material part 6.8.

5.1.2.4 PCR

DNA from plasmids or genomic DNA was amplified by polymerase chain reactions using a thermocycler (T3000, Biometra) and Phusion polymerase (Finnzymes). The primers used are listed in the material part 6.8.

A typical PCR reaction is shown below:

DNA from plasmid

	Amount	**Final concentration**
5x Phusion GC buffer	10 µl	1x
10 mM dNTP	1 µl	0,2 mM
10 µM Primer for	2,5 µl	0,5 µM
10 µM Primer rev	2,5 µl	0,5 µM

DMSO	1,5 µl	
Phusion (2000 U/ml)	0,5 µl	20 U/ml
DNA	2 µl	100 ng
Double distilled water	30 µl	
total	50 µl	

Gadd45b genotyping

	Amount	**Final concentration**
5x Phusion GC buffer	4 µl	1x
10 mM dNTP	0,5 µl	0,25 mM
10 µM Primer Gadd45b_for	0,5 µl	0,25 µM
10 µM Primer Gadd45b_rev	0,5 µl	0,25 µM
10 µM Primer Gadd45b_neo	0,5 µl	0,25 µM
Phusion (2000 U/ml)	0,2 µl	20 U/ml
DNA	2 µl	
Double distilled water	11,8 µl	
total	20 µl	

Gadd45g genotyping

	Amount	**Final concentration**
5x Phusion GC buffer	4 µl	1x
2 mM dNTP	4 µl	0,4 mM
100 µM Primer Gadd45g_for	0,1 µl	0,5 µM
100 µM Primer Gadd45g_rev	0,1 µl	0,5 µM
100 µM Primer Gadd45g_pgk	0,1 µl	0,5 µM
Phusion (2000 U/ml)	0,2 µl	20 U/ml
DNA	2 µl	
Double distilled water	9,5 µl	
total	20 µl	

A typical PCR reaction was programmed as followed:

Step	**Temperature**	**Time**
1. Denaturation	98°C	30 sec
2. Denaturation	98°C	5 sec
3. Primer annealing	55 – 65°C	20 sec
4. Extension	72°C	20 sec
5. Go to 2		25x
6. Extension	72°C	5-10 min
7. Hold	4°C	∞

The annealing temperature was adjusted depending on the length and G/C content of the primers. The extension time was adjusted depending on the size of the desired PCR product.

For genotyping the program was as followed:

Step	Temperature	Time
8. Denaturation	98°C	30 sec
9. Denaturation	98°C	15 sec
10. Primer annealing	57°C	15 sec
11. Extension	72°C	45 sec
12. Go to 2		40x
13. Extension	72°C	3 min
14. Hold	4°C	∞

5.1.2.5 Purification of PCR fragments

DNA from PCR reactions was purified using the QIAquick PCR purification kit provided by Qiagen following the manufacturer's instructions. DNA was eluted in 30 µl H_2O.
Alternatively, fragments were purified by gel extraction as described below. The amplified DNA product for genotyping was not purified.

5.1.2.6 Agarose gel electrophoresis

Agarose gel electrophoresis was used to separate DNA fragments. The percentage of the gel depends on the DNA fragments to be separated. Usually a 1-2% agarose gel was made. Since the DNA fragments for genotyping are rather small (~130 – 268 bp), a 3% agarose gel was used therefore. The agarose was dissolved in 1x TAE, and 1 µg/ml ethidium bromide was added to the still liquid but not too hot agarose solution. 20 µl of DNA sample were mixed with 4 µl of 6x Orange G loading dye and separated at 80-130 V. Gel pictures were taken under UV light (254 nm) with the Gel imager (Intas).

The genotyping results were as followed:

Gadd45b:	WT	130 base pairs
	KO	190 base pairs
	Heterozygous	both band
Gadd45g:	WT	268 base pairs
	KO	217 base pairs
	Heterozygous	both bands

5.1.2.7 Gel extraction of DNA

DNA fragments were isolated from agarose gels under a UV lamp using a scalpel and purified using the QIAquick Gel Extraction Kit, according to the manufacturer's instructions.

5.1.2.8 DNA restriction

DNA restriction was performed by using restriction enzymes from New England Biolabs. The enzymes were used at a concentration of 10-20 U per µg DNA with the corresponding buffers provided. Reactions were incubated at the required temperatures for 1-12 h.

5.1.2.9 DNA ligation

Ligation of insert and vector DNA was performed using a T4 DNA ligase (Invitrogen). The molar ratio of insert to vector was adjusted to 3:1 applying the following formula:

$$\left(\frac{100 \text{ vector [ng]} \times \text{insert [bp]}}{\text{vector [bp]}}\right) \times 3 = \text{insert [ng]}$$

2 U enzyme was used in 1x ligase buffer for the ligation reactions which were performed in 20 µl total volume and incubated for 1 hour at room temperature. After the ligation reaction, the enzyme was heat inactivated for 10 minutes at 65°C.

5.1.3 RNA work

5.1.3.1 RNA isolation

RNA isolation from cell culture samples

After aspirating the medium from each well, the cells were washed once with PBS. Afterwards 1 ml Qiazol™ Lysis reagent was added per well. The cells were lysed and scratched from the plate using a pipette and transferred into DNase/RNase-free reaction tubes. The obtained cell lysates were stored at -80°C or immediately used for RNA isolation, as described for liver samples.

RNA isolation from liver samples

Liver was first homogenised using the TissueLyser™ (Qiagen). Through mechanical force the tissue was pulverized in grinding jars. Therefore, all instruments were cooled in liquid nitrogen to avoid a thawing of the frozen tissue. To extract total RNA from pulverized liver, approximately 50 mg of liver were transferred into a 2 ml RNase/DNase-free reaction tube containing a stainless steel bead. 1 ml of Qiazol™ Lysis (Qiagen) reagent was added directly. The samples were lysed using the TissueLyser™ for 2 times 30 seconds at a frequency of 30 Hz. The homogenate was transferred into a fresh 1.5 ml RNase/ DNase-free safe-lock tube containing 200 µl of chloroform. Mixtures were vigorously inverted 15 times and incubated on ice until the phases started to separate. Then the lysates were centrifuged for 30 minutes at 13,000 rpm. The upper aqueous solution containing the RNA, was carefully transferred into a fresh RNA-free reaction tube containing 500 µl of iso-propanol and incubated at room temperature for 10 minutes, followed by a 10 minutes centrifugation step at 12,000 rpm. The supernatant was discarded and the pellet was washed once with 1 ml of 75% ethanol. The ethanol was carefully removed using a pipette. The pellet was briefly air-dried (max. 2 minutes) at 55°C and re-solubilised in 100 µl water. To

increase solubilisation, the RNA was incubated at 55°C for 10 min. The samples were stored at -80°C or directly used for cDNA synthesis.
For RNAseq expression profiling, RNA isolated using Qiazol™ Lysis reagent was purified using the RNeasy Mini purification kit provided by Qiagen. RNA was transferred to into a fresh reaction tube containing 525 µl of 100 % ethanol. RNA was then purified following the manufacturer's instruction. The optional DNA digestion step was included. RNA was eluted in 60 µl H_2O.

5.1.3.2 Determination of RNA concentration

As for DNA, the RNA concentration and the degree of contamination with proteins or ethanol were determined with the NanoDrop ND-1000 spectrophotometer. 1 µl of RNA solution was used for each measurement. The RNA concentration was measured at 260 nm, potential contaminations was assessed with the ratio 260 nm/280 nm.

5.1.3.3 Assessment of RNA quality

Agarose gel electrophoresis was used to assess RNA quality. Therefore, 1% agarose gels were made with RNase free agarose in 1x TBE buffer made with DEPC-water. The chamber and tools for the electrophoresis were washed in DEPC-water and 10 µM NaOH for 30 minutes before use. 500 ng RNA sample were added to 10 µl RNA denaturing buffer and incubated for 10 minutes at 65°C and 2 min on ice. Since this buffer contains already ethidium bromide, no additional ethidium bromide was added to the gel. The quality of the RNA was determined visually by estimating the ratio between 28S to 18S ribosomal RNA, which is 2:1 for intact RNA.

5.1.3.4 cDNA Synthesis

cDNA synthesis was performed using the cDNA synthesis kit (Fermentas). 2 µg of RNA was used for the reaction. Specifically, the reaction volume was first adjusted to 10 µl per sample using RNase/DNase-free water and 1 µl of oligo$(dT)_{18}$ primers were added. To allow for oligo annealing to the mRNA poly-A tails, reactions were incubated at 65°C for 10 min. Afterwards, 4 µl 5 x reaction buffer, 2 µl 10 mM dNTP mix, 1 µl Ribolock™ Ribonuclease inhibitor and 2 µl M-MutLV reverse transcriptase were added to each reaction. As a negative control for contamination one sample without reverse transcriptase was included. With this mix the following program was run on a thermocycler (T3000, Biometra):

Temperature	**Time**
37°C	1 h
70°C	10 min
4°C	**∞**

After completion, cDNA samples were diluted 10 fold in RNase-free water and stored at -20°C or used directly for quantitative real-time PCR.

5.1.3.5 Quantitative PCR

In general, 5 µl of the diluted cDNA samples were used for quantitative PCR and technical duplicates of all samples were performed. Water was used as a negative control and samples containing no reverse transcriptase served as controls for genomic DNA contamination. 15 µl PCR master mix per well was transferred into a MicroAmp Optical 96 well reaction plate and then the sample was added. Quantitative PCR was performed using the StepOnePlus Real Time PCR System (Applied Biosystems). RNA expression data were quantified according to the method as described elsewhere [388,389] and normalized to RNA levels of TATA-box binding protein (TBP) if not indicated otherwise.

Taqman

The TaqMan probes were obtained either from Applied Biosystems or MWG and are listed in the material section. Depending on the used TaqMan probes two different master mixes were prepared.

Probe/company	**Master Mix per reaction**
Life Technologies™	10 µl TaqMan® Gene Expression Master Mix
	0,5 µl TaqMan® Primer/Probe Set
	4,5 µl dH_2O
Eurofins MWG Operon	10 µl TaqMan® Gene Expression Master Mix
	1,0 µl Forward Primer (10 µM)
	1,0 µl Reverse Primer (10 µM)
	0,5 µl Probe (5 µM)
	2,5 µl dH_2O

The qPCR program was as followed:

Temperature	**Time**	
50°C	2 min	
95°C	10 min	
95°C	15 sec	40x
60°C	1 min	

SYBR

The SYBR probes used were obtained from Qiagen and are listed in the material section. A master mix was prepared containing 10 µl 2x QuantiTect SYBR Mix, 2 µl 10x QuantiTect Primer Assay and 3 µl dH_2O.

The qPCR program was as followed:

Temperature	Time	
95°C	15 min	
94°C	15 sec	40x
55°C	30 sec	
42°C	30 sec	

5.1.3.6 Gene expression profiling with RNAseq

For expression profiling of liver transcripts, RNA was isolated from liver samples of 6 GADD45β KO and 6 GADD45β WT male mice which were starved for 24 hours as described in 5.2.3. The RNA isolation procedure was performed as described in 5.1.3.1. An equal amount (1 µg) of RNA from two non-littermate WT or two non-littermate KO mice were pooled for sequencing, but KO and WT were from the same litter. The sequencing was performed at the Genomics and Proteomics Core Facility of the dkfz. Specifically, they performed a single read, 50 bp multiplexed run on 3 HiSeq lanes without reading direction with subsequent poly-A purification. The analysis of differentially expressed transcripts was performed by Dr. Emil Karaulanov from the Institute of Molecular Biology, Mainz. He checked the sample consistency and data quality with FastQC (Bioinformatics Group at the Babraham Institute, UK, http://www.bioinformatics.bbsrc.ac.uk/projects/fastqc/) and QualiMap (http://qualimap.bioinfo.cipf.es/) [390]. His analysis focused on differential expression, visualisation and pathway/network analysis with special interests in transcription factors and receptors. His strategy was to perform several parallel workflows with different popular and established software tools and then compare the results in order to filter the robust (consensus) hits. More precisely, he used TopHat and Genomatix GMS for read mapping and CuffDiff (v1.0.3, Galaxy) and DESeq (v1.10.1, Genomatix) for differential expression analysis. Afterwards, he filtered consensus DE hits, performed annotation, visualised and further analysed them. A false positive rate of a=0.01 with FDR correction was applied to determine significance. Pathway and gene function analysis was performed with the Kyoto Encyclopedia of Genes and Genomes (KEGG, http://www.genome.jp/kegg/) and DAVID Bioinformatics Resources 6.7 (National institute of allergy and infectious diseases, NIH, http://david.abcc.ncifcrf.gov).

5.1.4 Protein work

5.1.4.1 Preparation of protein extracts

Protein extracts from cells

Embryonic Kidney (HEK) cells were washed once with PBS and lysed by the addition of an appropriate volume of 2 x SDS sample buffer. Samples were boiled for 10 min at 95°C and stored at -20°C until further use.

Protein extracts from tissue samples

50 mg of liver powder was transferred to a 2 ml safe-lock tube containing a stainless bead and lysed after the addition of 700 µl ice cold RIPA buffer containing phosphatase and proteinase inhibitors for 2x 30 seconds at 30 Hz with the TissueLyser^{TM}. The protein concentration was determined using the BCA kit (Pierce, see 5.1.4.2) and subsequently adjusted to 2 mg/ml for SDS-PAGE with water and 5x SDS sample buffer. Afterwards the samples were boiled for 10 min at 95°C.

5.1.4.2 Determination of Protein Concentration

Protein concentrations were determined using the BCA kit (Pierce) following the manufacturer's protocol. Specifically, protein lysates were diluted 1:20 to fall into the linear range of the assay, and the BCA reagents were mixed 1:50 (B:A). In addition to the samples, 10 µl of different BSA concentrations ranging from 0 to 2 µg/ml were loaded to obtain a standard curve. 200 µl of the reagent was added to 10 µl of sample and standard. The plate was incubated at 37°C for 30 minutes and measured in the Mithras LB-940 plate reader at 562 nm. Blank values were subtracted and the standard curve was subsequently used to determine the protein concentrations of the samples.

5.1.4.3 SDS Polyacrylamide Gel Electrophoresis (SDS-PAGE) and Immunoblotting

30 µg of protein was loaded onto a 6-15% SDS-polyacrylamide gel depending on the size of the protein to be identified and quantified. Following table gives an overview of the SDS-gel composition:

Compound	**Stacking gel**	**Separation gel**		
	5%	**6%**	**12%**	**15%**
H_2O	1,4 ml	2,6 ml	1,6 ml	1,1 ml
30% Bisacrylamide	0,33 ml	1,0 ml	2,0 ml	2,5 ml
1 M Tris (pH 6,8)	0,25 ml	-	-	-
1,5 M Tris (pH 8,8)	-	1,3 ml	1,3 ml	1,3 ml
10% SDS	0,02 ml	0,05 ml	0,05 ml	0,05 ml
10% APS	0,02 ml	0,05 ml	0,05 ml	0,05 ml
TEMED	0,002 ml	0,004 ml	0,002 ml	0,002 ml

After running for 1 hour at 120 V, proteins were blotted onto a PVDF membrane (small proteins) or a nitrocellulose membrane (medium sized and large proteins) in a wet blotting procedure for 1,5 h at 80 V in transfer buffer. PVDF membranes were activated with methanol prior to use. Membranes were subsequently blocked by incubation in 5% milk or 5% BSA dissolved in TBS-T for 1 hour. Specific primary antibodies diluted in 5% milk or BSA, according to the manufacturer's recommendations, were incubated with the membranes overnight at 4°C. The membranes were washed with TBS-T the next day and incubated with the secondary antibody conjugated to horse radish peroxidase (HRP) at a dilution of 1:5000 for 1 hour. To detect specific bands the enhanced chemiluminescence system (ECL) Western Blotting Detection Reagent was applied. The

chemiluminescent signal produced by the blots was detected with the ChemiDoc detector (BioRad). Exposure times differed based on the quality of specific antibodies and protein concentrations. Densitometric analysis of protein expression levels was done with Image Lab™ Software (BioRad) and normalized to levels of valosin-containing protein (VCP).

5.1.5 Liver work

5.1.5.1 Isolation of Hepatic Lipids from Liver Tissue Samples

Extraction of lipids from pulverised liver tissue was performed by using a 1:2 mixture of methanol/chloroform (v:v) with subsequent equilibration with a saline solution, when the mixture partitions into two layers, of which the lower is composed of chloroform-methanol-water and contains all of the lipids [391]. Therefore, 50 mg of pulverized liver sample (weight was noted) was added into a 2 ml safe-lock tube containing 1.5 ml chloroform/methanol and a stainless steel bead. The tissue was homogenized using the TissueLyser system two times for 30 seconds at 30 Hz. Thereafter, the samples were briefly spun down and mixed at 1400 rpm for 20 minutes on a heat block (Thermomixer) at room temperature. Afterwards, the samples were centrifuged at 13000 rpm for 30 minutes. 1 ml of the supernatant was transferred to a new 1,5 ml tube containing 200 µl 150 mM (0.9%) sodium chloride solution. The mix was spun down at 2000 rpm for 5 minutes at room temperature. 200 µl of the lower organic phase were transferred to a fresh tube containing 40 µl of a Triton-X 100/chloroform (1:1 v/v) mixture. The chloroform was evaporated overnight in a SpeedVac and the remaining triton-lipid solution was resuspended in 200 µl water on a rotation wheel for 1 hour at room temperature. These extracts were used to determine non-esterified fatty acids, cholesterol and triglyceride levels in the liver as described in 5.1.6. For longer storage, extracts were kept at -80°C.

5.1.5.2 Isolation of Hepatic Glycogen from Liver Tissue Samples

Liver glycogen was extracted from snap frozen and pulverized liver tissue. About 45-55 mg of tissue (exact values were noted down) were added to a 2 ml safe-lock tube containing a stainless steel bead and 500 µl 30% Potassium Hydroxide. The tissue was homogenized with the TissueLyser 2x 30 seconds at a frequency of 30 Hz. The obtained homogenates were transferred to fresh safe-lock tubes and incubated at 95°C for one hour. Glycogen was precipitated by adding 1,4 ml of 95% ethanol and storing the tubes at -20°C for 30 minutes. Afterwards the samples were spun down for 20 minutes at 3000xg. The resulting pellets were first washed in 95% ethanol and then dissolved in 250 µl H_2O for 30 minutes at 37°C with mild shaking (350 rpm).

For measuring liver glycogen content the dissolved glycogen had to be digested with amyloglucosidase. Therefore, 50 µl of the glycogen solution were mixed with 250 µl amyloglycosidase solution (10-20 Units/ml Amyloglycosidase from *Aspergillus niger* (Sigma-Aldrich) dissolved in 0,2 M NaAc pH 4,8). The digestion was performed overnight at 37°C with shaking. The samples were neutralized by adding 6 µl of 30% KOH.

The resulting glucose was measured using the Glucose (HK) Assay Kit (Sigma-Aldrich). Hereby, glucose is phosphorylated by ATP into glucose-6-phosphate in a reaction catalyzed by

hexokinase and subsequently further processed into 6-phosphogluconate by NAD+, which is catalyzed by glucose-6-phosphatase dehydrogenase. The consequent increase in absorbance at 340 nm is directly proportional to the original glucose concentration in the sample. The assay was performed with 20 µl of glycogen digest according to the manufacturer's instructions. For fed mice digests were diluted 1:4 prior to assaying. The glucose liver sample concentration was determined using a glucose standard curve.

5.1.6 Metabolit assays

5.1.6.1 Determination of Free Fatty Acid Levels

Non-esterified (or free) fatty acids were determined in serum and liver lipid extraction samples using a 2-step colorimetric assay with 2 reads at 540 nm from WAKO (NEFA kit) following the manufacturer's instructions. Hereby, NEFA are first converted by acyl-CoA synthetase (ACS) into acetyl-CoA, which is subsequently metabolised in several steps involving H_2O_2 into a quinoneimine dye, which can be quantified. 2 µl of serum sample and 4 µl of liver lipid extract were measured in duplicates alongside a water control and the NEFA standard (oleic acid 1 mmol/l). For serum samples the free fatty acid concentration was determined according to the formula:

$$\frac{\text{sample OD} - \text{blank OD}}{\text{standard OD} - \text{blank OD}} \text{ x standard conc. [mM]} = \text{sample conc. [mM]}$$

For liver lipid extracts also the dilution factors (1,125 and 1280 (organic phase out of 1600 µl tissue homogenate)) from the lipid extraction procedure and the weight of the liver used for the assay were included into the calculation.

5.1.6.2 Determination of Triglyceride and Glycerol Levels

Triacylglycerides (TG or triglycerides) in serum and liver lipid samples were quantified using a 2-reaction assay with 2 reads at 540 nm from Sigma (TG determination kit) according to manufacturer's instructions. This colorimetric assay is based on the separation of TG into its basic components: one glycerol and three fatty acids molecules by a lipase and measuring the glycerol after being metabolised into a quinoneimine dye involving H_2O_2. 2 µl of serum sample or lipid extract were pipetted in quadruplicates alongside a water control and the TG standard (2,5 mg/ml TG including 0,26 mg/ml free glycerol) into a transparent 96-well plate. 100 µl free glycerol reagent were added to two of the replicates (blank value), while to the remaining two replicates 100 µl of TG reagent were added. This mixture contains the enzyme lipase, which catalyses the release of fatty acids from TGs. In order to determine the TG levels (TG-bound glycerol), free glycerol values were subtracted from the total glycerol measurement. For serum samples the TG concentration was determined according to the formula:

$$\frac{\text{sample OD} - \text{blank OD}}{\text{standard OD} - \text{blank OD}} \text{ x standard conc. [mM]} = \text{sample conc. [mM]}$$

For liver lipid extracts also the dilution factors (1,125 and 1280 (organic phase out of 1600 µl tissue homogenate)) from the lipid extraction procedure and the weight of the liver used for the assay were included into the calculation.

5.1.6.3 Determination of Cholesterol Levels

Liver or serum cholesterol concentrations were determined using a colorimetric assay with 1 read at 492 nm from Randox (cholesterol determination kit) following the manufacturer's instructions. Hereby, cholesterol esters are separated into fatty acids and free cholesterol, which is further metabolised into a quinoneimine dye in two subsequent reactions involving H_2O_2. 3 µl of serum sample or 4 µl of lipid extract were measured in duplicates alongside a water control and the cholesterol standard (5,1 mmol/l). For serum samples the cholesterol concentration was determined according to the formula:

$$\frac{\text{sample OD} - \text{blank OD}}{\text{standard OD} - \text{blank OD}} \text{ x standard conc. [mM]} = \text{sample conc. [mM]}$$

For liver lipid extracts also the dilution factors (1,125 and 1280 (organic phase out of 1600 µl tissue homogenate)) from the lipid extraction procedure and the weight of the liver used for the assay were included into the calculation.

5.1.6.4 Determination of Ketone Bodies Levels

The concentration of ketone bodies in the serum was determined using a kinetic assay with 2 reads at 405 nm from WAKO (Autokit Total Ketone Bodies) following the manufacturer's instructions. The principle of the assay is an enzymatic reaction where the rate of Thio-NADH production depends on the concentration of total ketone bodies in the sample and can be determined using a photometer. A standard curve was prepared by serially diluting the calibrator provided in the kit. 2 µl of serum sample was used for measuring absorbance at 405 nm and the concentration determined according to the formula:

$$\frac{\text{sample OD} - \text{blank OD}}{\text{standard OD} - \text{blank OD}} \text{ x standard conc. [mM]} = \text{sample conc. [mM]}$$

5.1.6.5 Determination of Serum Insulin Levels

Serum insulin levels were determined using an ELISA kit (ALPCO) following the manufacturer's instructions. 5 µl of each sample or standard (provided in the kit) were used for the measurement of absorbance at 450 nm. Insulin concentrations were calculated using the standard curve resulting from the standards provided with the kit. Some of the used samples needed to be diluted, especially from mice fed a high fat diet for 4 months or *db/db* mice, in order to fit the concentrations within the standard curve of the assay.

5.1.6.6 Determination of Serum ALT Levels

Serum levels of Alanine Aminotransferase (ALT) were determined by a kinetic calorimetric assay in order to estimate liver damage. Serum ALT levels were assessed using the Infinity ALT Liquid Stable Reagent (Thermo Electron, Melbourne) following the manufacturer's instructions, measuring absorbance after 1 minute and after another 9 minutes incubation time at 355 nm (instead of 340 as stated in the instructions). This caloric assay is based on ALT's ability to catalyse the conversion of L-alanine and 2-oxoglutarate into pyruvate and L-glutamate. Pyruvate is then reduced to lactate by lactate dehydrogenase (LDH) present in the kit with the simultaneous oxidation of NADH to NAD+, and the reaction is monitored by measuring the decrease in absorbance due to the oxidation of NADH. The activity was then calculated as change in absorbance per min multiplied by a factor (total reaction volume (105 µl) x 1000 divided by absorption coefficient of NADH at 355 nm (4,76) x sample volume (5 µl) x reading path length (0,4 cm) which equals 11029,4). Hence, ALT activity is calculated with the following formula:

$$\frac{\Delta \text{ absorbance x } 11029{,}4}{9 \text{ min}} = \text{activity } \left[\frac{U}{L}\right]$$

5.1.6.7 Determination of Liver and Serum Amino Acid and Acyl Carnitine Levels

In general, liver and serum levels of amino acids and acyl carnitines were determined by our collaborator Dr. Jürgen Okun and his technician Kathrin Schmidt at the University Children's Hospital in Heidelberg. They developed an electrospray-ionisation mass spectrometry (ESI-MS/MS) technique for acyl carnitine and amino acid determination in plasma according to a modified protocol used for these derivatives in dried blood spot. The ESI-MS/MS technique is not able to separate isobaric compounds e.g. leucine / isoleucine but gives for all the other amino acids reliable results within 2,5 minutes. Sample preparation contains an extraction and a derivatization step which was also performed by our collaborators.

Serum samples were directly sent to them for a duplicate measurement. 5 µl of serum was used for one experimental run which contained measurement of amino acids and acyl carnitines. Liver homogenates were achieved by lysing 50 mg of pulverized liver sample mechanically using the TissueLyser in 10 volumes of PBS containing protease inhibitors (i.e. 500 µl to 50 mg). Afterwards, these extracts were centrifuged at 4°C at 17000 x g and the supernatant used for analysis.

For analysis of the obtained data, acyl carnitine and amino acid concentrations were normalized to total acyl carnitines and total amino acids, respectively, due to a high scatter between the different groups.

For the starvation experiment with GADD45β WT and KO mice, serum alanine and branched chain amino acids were measured using a colorimetric assay from BioVision (L-alanine Assay Kit and Branched Chain Amino acid Assay Kit). Serum samples were deproteinised with PCA using the Deproteinizing Sample Preparation Kit (Biovision) according to the manufacturer's instructions prior of measuring the amino acids. Assay reagents preparation and procedure were

performed according to the manufacturer's instructions. The concentrations were determined with the use of a standard curve with the standard being provided with the kit.

5.1.6.8 Determination of Blood Glucose Levels

Blood glucose levels were determined using a drop of blood obtained from the tail vein and an automatic glucose monitor (One Touch, Lifescan).

5.2 Cell Biology

5.2.1 Cell culture conditions

All experiments with eukaryotic cells were performed under sterile conditions. Cells were cultivated at 37°C, 5% CO_2 and 95% humidity. All media and additives were warmed to 37°C prior to use. Cells were cultivated in 6-well or 12-well plates or 15 cm cell culture dishes. A list of the media used for cell culture experiments is shown below:

Cell line	Medium	FCS	Antibiotics	Further additives
HEK293	DMEM	10%	1% P/S	
HEK293A	DMEM	10%	1% P/S	1% NAA
HEK293A AD titration	DMEM	2%	1% P/S	1% NAA
HEK293T	DMEM	10%	1% P/S	1% NAA
Hepa1c1	DMEM	10%	1% P/S	1% NAA
Hepa1c1 starvation	HBSS	1%	1%	
AML12	DMEM/F-12	10%	1% P/S	ITS, Dexamethasone

5.2.2 Thawing of cells

Eukaryotic cells were stored in liquid nitrogen tanks in 1 ml aliquots containing about $1*10^6$ cells in freeze medium (DMEM, 20% FCS, 10% DMSO). Following thawing at 37°C, cells were carefully mixed with 10ml pre-warmed culture medium and centrifuged for 3 minutes at 2000 rpm to remove DMSO. The pellet was resuspended in 10 ml medium. Those 10 ml were distributed to two 15 cm tissue culture plates (3 ml and 7 ml) containing 20 ml culture medium.

5.2.3 Determination of cell number

The cell counting system Countess® (Life Technologies) was used to determine cell number and viability. For this, 10 µl of Trypan Blue (Life Technologies) were mixed with 10 µl of cell suspension. 10 µl of this mixture were transferred onto a Countess® slide and loaded into the counter for measurement.

5.2.4 Cultivation of Human Embryonic Kidney (HEK), HEK293A and HEK293T cells

HEK293 cells were cultivated on 15 cm cell culture plates in 25 ml culture medium (DMEM 4,5 mg/l glucose and additives). They were passaged twice a week with a split factor of 1:10 – 1:20.

For passaging, the cells were washed from the cell culture plate using 10 ml of the culture medium they were growing in and were pelleted by centrifugation at 2000 rpm for 3 minutes. Subsequently, the pellet was resuspended in 10 ml fresh culture medium and 500 µl of the cell suspension was plated onto a 15 cm cell culture plate containing 24,5 ml culture medium.

5.2.5 Cultivation of Hepa1c1 cells

Hepa1c1 cells were maintained and propagated in 15 cm dishes containing 25 ml culture medium (DMEM plus additives). For passaging, the cells were first washed in 1x PBS and trypsinized, then the detached cells were resuspended in 10 ml of fresh medium. Cells were pelleted by centrifugation at 2000 rpm for 3 minutes and subsequently resuspended in 10 ml fresh medium. Cells were split twice a week by the factor 1:10.

5.2.6 Cultivation of AML12 cells

AML12 cells were cultivated in 15 cm culture plates containing 25 ml of culture medium (DMEM/F-12 supplemented with 0,005 mg/ml insulin, 5 ng/ml transferrin, 5 ng/ml selenium (ITS, Roche) and 40 ng/ml dexamethasone). Cells never exceeded a confluency of 80 - 90% and were never cultured longer than passage 20. They were split 1:10 twice a week by first washing them in 1x PBS and trypsinizing them, then the detached cells were resuspended in 10 ml of fresh medium.

5.2.7 Transient transfection of HEK cells

HEK293 cells were transfected with DNA for the production of Adenovirus and Adeno-associated virus (see 5.3.1. and 5.3.5, respectively) either using Lipofectamine 2000 transfection reagent (Invitrogen) or the PEI method, respectively.

For the production of adenovirus 1 µg of plasmid and 3 µl Lipofectamine were used for transfection. Lipofectamine was added to 250 µl of serum free Opti-MEM medium. The mixture was combined with DNA which was diluted in the same medium, and the mixture was incubated at room temperature for 20 minutes to allow complex formation. The DNA/Lipofectamine complexes were added dropwise to the cells in antibiotic-free medium. Medium change to the normal culture medium was performed the following day.

For the production of AAV 1 µg of DNA and 8 µl of PEI were used for transfection. In one tube the plasmid DNA was topped up with water to 20 ml and mixed with 20 ml 300 mM NaCl. In another tube 18 ml PEI, 2 ml water and 20 ml 300 mM NaCl were mixed. Both mixtures were combined and incubated at room temperature for 10 minutes to allow complex formation. In the meantime, medium of the cells was changed. Afterwards, the mixture was added drop wise to the cells. Cells were harvested 48 hours post-transfection.

5.2.8 Transient transfection of Hepa1c1 cells

Hepa1c1 cells were used for the *in vitro* induction of *Gadd45b* and subsequent functionality test of the generated miRNA against *Gadd45b*. Therefore, the plasmid containing the *Gadd45b* miRNA sequence (pcDNA6.2GW/EmGFP-miR mGadd45b) or the empty vector (pcDNA6.2/GWEmGFPmiR-NC) or a positive control (vector encoding eGFP to verify that transfection worked) were transfected into the cells. For higher transfection efficiency Lipofectamine 2000 transfection reagent was used. One day prior of transfection, cells were seeded onto 12-well plates at $1x10^5$ cells per well in normal growth medium without antibiotics. The next day, 2µl Lipofectamine was added to 100 µl of serum free Opti-MEM medium. The mixture was combined with 800 ng DNA which was diluted in the same medium, and the mixture was incubated at room temperature for 20 minutes to allow complex formation. 200 µl of the DNA/Lipofectamine complexes were added drop wise to the cells in antibiotic-free medium. 12 hours later the medium was changed either to normal culture medium (DMEM with additives) or to starvation medium (HBSS with additives). Cells were harvested 8 hours later in 2x sample buffer containing urea to stabilize the proteins.

5.2.9 Nutrient withdrawal of AML12 cells

To determine which nutrient is causing the potent upregulation of *Gadd45b*, AML12 cells were used [248]. In a series of experiments cells were incubated with specified culture media which were depleted of different nutrients and *Gadd45b* mRNA expression was measured. For that purpose, a culture medium on the basis of the composition of DMEM/F-12 was made which contained all the basic components crucial for the survival of the cell. It is called “PBS full” in this work and described in the following table:

Component	Stock conc.	Volume	End conc.
DPBS	10x	25 ml	1x
Glutamine	100x	2,5 ml	1x
Essential Amino Acids	50x	5 ml	1x
NEAA	100x	2,5 ml	1x
Vitamins	100x	2,5 ml	1x
Glucose	2 M	2,2 ml	17,5 mM
HEPES	1 M	3,75 ml	15 mM
Sodium Pyruvate	100x	2,5 ml	1x
Purine/Pyrimidine	1000x	0,25 ml	1x
Lipid Mixture 1	10 mg/L each linoleic, linolenic, oleic, palmic and stearic acid	1,25 mg/L each	0,05 mg/L
P/S	100x	2,5 ml	1%
FCS	10x	25 ml	10%
Dexamethasone	250 µM	0,102 ml	$1,02 \times 10^4$ mM
I T S	1000x	0,25 ml	1x

Sodium Bicarbonate	7,5%= 890 mM	4 ml	14,3 mM
Water		170,70 ml	
Total		250 ml	

In a first experiment an induction of *Gadd45b* by the addition of "PBS full" had to be excluded. Therefore, AML12 cells were seeded onto 6-well plates and the next day, when they were ~75% confluent, the medium was changed to either DMEM/F-12 or "PBS-full". Cells were harvested after 8 or 24 hours with Qiazol Lysis Reagent (after washing 1x with PBS) followed by RNA extraction, cDNA synthesis and RT-qPCR for the *Gadd45b* expression.

In a follow-up experiment the combination of all those components whose concentration in the body changes depending on the nutritional status and which could cause an induction of Gadd45β was reduced in the culture medium. Therefore, a medium containing all components essential for growth (so-called "Base medium") and a medium containing all variable components (so-called "Supplement medium") were made. The composition is listed below:

2x base medium	**Stock conc.**	**Volume**	**2x conc.**	**End conc.**
DPBS	10x	50 ml	2x	1x
Vitamins	100x	5 ml	2x	1x
HEPES	1000 mM	7,5 ml	30 mM	15 mM
P/S	100	5 ml	2%	1%
Dialysed FCS	10	50 ml	20%	10%
Dexamethasone	250000 nM	0,204 ml	204 nM	102 nM
I T S	1000x	0,5 ml	2x	1x
Sodium Bicarbonate	890 mM	8 ml	28,6 mM	14,3 mM
Water		123,76 ml		
Total		250 ml		

2x suppl. medium	**Stock conc.**	**Volume**	**2x conc**	**End conc.**
Glutamine	100x	5 ml	2x	1x
Essential Amino Acids	50x	10 ml	2x	1x
NEAA	100x	5 ml	2x	1x
Glucose	2 M	4,4 ml	35 mM	17,5 mM
Sodium Pyruvate	100x	5 ml	2x	1x
Purine/Pyrimidine	1000x	0,5 ml	2x	1x
Lipid Mixture 1	10 mg/L each linoleic, linolenic, oleic, palmitic and stearic acid	2,5 mg/L each	0,1 mg/L	0,05 mg/L
Water		217,63 ml		
Total		250 ml		

Dialysed FCS was used to significantly reduce the concentrations of small molecules such as amino acids, hormones and cytokines. The two media were mixed 1:1, 1:2, 1:10, 1:20 or 1:100 in order to get a final concentration of the variable nutrients of 100%, 50%, 10%, 5% or 1%, respectively. Cells were seeded as mentioned before and incubated with the different media for 8 hours before harvest.

In a third experiment the cells were incubated in culture media depleted in one specific nutrient and *Gadd45b* mRNA levels were measured. The "Base media" was prepared as before. The "Supplement media" was lacking one component which was added to a final concentration of 1% after both media were mixed in a 1:1 ratio. Therefore, 7 different "Supplement media" had to be made, each missing another component. A "Supplement medium" containing all nutrients was included in the experimental setup. The cells were incubated with the culture media for 8 hours before harvest.

In a last experiment, cells were incubated in media missing two components. Therefore "Supplement media" were made lacking two nutrients. The "Base medium" was the same as before. Both media were mixed 1:1 and given to the cells for 8 hours before harvest.

5.2.10 Infection of cells with adenovirus

To test whether adenovirus administration leads to an overexpression of GADD45β 3x 10^5 HEK293 cells were seeded on 6-well plates and infected with different amounts of adenovirus (AD- GADD45β OE and AD-NC as control) 12 hours after plating. MOIs of 0.1, 1 and 10 were used (MOI = cells in well/virus ifu per µl). The desired amounts of virus were diluted in DMEM culture medium and added to the cells. Cells were incubated 24 hours until harvest.

5.3 Virus biology

5.3.1 Cloning of adenoviruses

Adenoviruses were used for the overexpression of GADD45β in the murine liver. The BLOCKiT™ Adenoviral RNAi Expression System was used to generate adenoviruses either overexpressing murine GADD45β or harbouring a non-specific sequence as control. Forward and reverse oligonucleotides against the target gene sequence (mGadd45b_for and mGadd45b_rev, see Material section) were annealed on the pCMV-SPORT6-mGadd45b vector and the *Gadd45b* sequence isolated via Phusion PCR. The DNA was then cloned into the pENTR-Flag vector harbouring the CMV promoter according to the manufacturer's instructions. The correct resulting constructs were first confirmed by restriction digestion and sequencing (primer CMV-for and TkpA-rev, see Material section), and then recombined with the pAd/BLOCK-iT™ DEST vector, which contains the adenovirus serotype 5 DNA, but lacks the E1 and E3 genes that are required for viral replication. The viral vector containing the *Gadd45b* sequence was confirmed via sequencing (primer CMV-for). The vector was linearized by restriction digest using the enzyme PacI and transfected into HEK 239A cells using Lipofectamine reagent according to the

manufacturer's instructions. 1 µg of *Pac* I-digested pAd/BLOCK-iT™-DEST expression plasmid and 3 µl Lipofectamine were used for transfection (for further details, see section 5.2.7). HEK293A cells express the viral E1 and E3 genes necessary for viral outbreak, allowing the virus to expand in this cell line. Viral plaques appeared 6 to 10 days after transfection and cells started to detach from the cell culture dish. Once about 70% of cells were floating, they were harvested.

5.3.2 Adenovirus harvest

HEK293A cells were harvested, when 70-90% were rounded up and had detached from the plate. Remaining adherent cells were washed of the plate by squirting them off the plate with a 10 ml tissue culture pipette in the medium they were cultivated in. The medium was collected from twenty 15 cm cell culture plates per virus and centrifuged for 10 minutes at 2000 rpm. The supernatant was discarded and the cell pellet was resuspended in 3 ml PBS-TOSH buffer per virus and shock frozen in liquid nitrogen. Three subsequent freeze and thaw cycles led to a lease of the virus from the cells. For that, the cell suspension was thawed at 37°C with vigorous vortexing and then shock frozen in liquid nitrogen. After cell lysis the mixture was centrifuged at 3000 rpm for 5 minutes, to remove cell debris. The crude supernatant was stored at -80°C or directly used for purification using a caesium chloride gradient.

5.3.3 Adenovirus purification

Caesium chloride (CsCl) gradient centrifugation is a type of density gradient centrifugation for the purification of viral particles. Virus lysates from twenty 15 cm culture dishes were thawed on ice. PBS-TOSH was added to a final volume of 20 ml. Gradients were prepared in ultracentrifuge tubes (Beckmann Polyallomer 25mm x 89 mm) and were balanced after addition of each solution. All solutions were adjusted to pH 7.2. The first gradient was layered with 9 ml 4.4 M CsCl, 9 ml 2.2 M CsCl and 20 ml virus in PBS-TOSH. After ultracentrifugation (2 hours, 4 °C, 24000 rpm, Beckmann XL-70, SW28 rotor) a clear virus band was visible between the 4,4 M and 2,2 M caesium chloride layers. The virus band was removed by piercing the tube with a 5 ml syringe. The obtained virus (about 3 – 3,5 ml) was mixed with an equal volume of saturated caesium chloride solution and transferred into a 12 mL centrifuge tube (Beckmann Polyallomer 14mm x 89 mm). The second gradient was layered with 6-7 ml virus in CsCl, 2 ml 4,4 M CsCl und 2 ml 2,2 M CsCl. Following the second ultracentrifugation (3 hours, 4 °C, 35000 rpm, SW40Ti rotor) the virus band could be seen between the 4 M and 2,2 M CsCl layers. The band was removed with a 1 ml syringe in the smallest possible volume (~700 µl). To remove CsCl from the viral solution, viruses were transferred to a dialysis membrane and dialyzed against 1 litre PBS containing 10 % glycerol (v/v) 2 times (1 and 24 hours) at 4°C. After dialysis, aliquots of 20–100 µl were prepared and stored at -80°C until further use.

5.3.4 Virus Titration

The Tissue Culture Infectious Dose 50 ($TCID_{50}$) assay was used to titrate adenovirus. For that purpose, 10^4 HEK293A cells were seeded in 100 µl virus titration medium (DMEM medium containing 2% FCS (v/v), 1% penicillin/streptomycin and 1% non–essential amino acids) in each well of a 96 well plate and infected with decreasing amounts of virus after 4 hours of adhesion. Serial dilutions of the virus from 10^{-7} to 10^{-14} were prepared in titration medium and 100 µl of each dilution added to the cells. Double measurements were performed for each virus and 100 µl of medium without virus were added to negative control wells. 10-12 days after infection and incubation at 37°C the plaques were counted using a microscope. Every well in which at least one plaque could be detected was considered a positive well. The titre was calculated by the following formula:

T_a= viruses per 100 µl = $10^{1+(s-0.5)}$
s = sum of positive wells starting from the 10^{-1} dilution; 10 positive wells per dilution = 1
T= viruses per 1 ml = 10 x T_a

5.3.5 Cloning of AAV

Adeno-associated viruses encoding *Gadd45b* -specific or non-specific control miRNAs were used for long-term hepatocyte-specific inactivation of GADD45β. The BLOCKiT™ Pol II miR RNAi Expression System was used to generate the adeno-associated viruses. Oligonucleotide sequences were chosen using Invitrogen's RNAi Designer tool. Forward and reverse oligonucleotides against the target gene sequence (miR-Gadd45b_for and miR-Gadd45b_rev, see Material section) were annealed and cloned into the pcDNA6.2-GW/EmGFP-miR vector according to the manufacturer's instructions. Subsequently, they were transferred into the previously described double stranded pdsAAV-LP1-EGFPmut AAV vector [240,242] using the restriction enzymes BglII and SalI. The correct identity of the resulting construct was verified by a restriction digestion panel and by sending the DNA to sequencing (primer EGFP-C1-F, see Material section). The plasmids encoding the miRNA constructs were contransfected into HEK293T cells with the pDGΔVP helper plasmid [277] and a mutated p5E18-VD2/8 expression vector [278] encoding AAV2 rep and a mutated AAV8 cap protein (aa 589-592: QNTA to GNRQ). The transfection procedure is described in section 5.2.7.

5.3.6 AAV production

For virus production, HEK293T cells from five 80-90% confluent 15 cm plates were suspended in 1100 ml medium (DMEM containing 5% FCS (v/v) and 1% penicillin/streptomycin). 1000 ml of the cell suspension was transferred to a 10x cell-stack chamber and 100 ml were transferred to a 1x-cell stack chamber (control chamber for analysis under the microscope). 24 hours after plating, the cells were approximately 70-80% confluent and were transfected with the plasmids encoding the viral genes using the PEI method in the amounts stated below.

Plasmid	Amount (per virus)
AAV-miRNA expression vector	395 µg
p5E18 VD2/8 helper plasmid	994 µg
pDGΔVP helper plasmid	2706 µg

Once the cell monolayer was approximately 90% confluent, cells were washed with PBS, before they were released from the plate using 10 ml (1x cell stack) or 100 ml (10x cell stack) trypsin-EDTA for 2 minutes at 37°C. Fresh medium was added (40 ml or 350 ml respectively) and the cells were transferred to a 500 ml conical tube. The chambers were washed with PBS and used for a second round of transfection. Cells were centrifuged at 2000 rpm for 10 minutes. The supernatant was removed and the pellets were resuspended in 8 ml lysis-buffer containing 150 mM NaCl and 50 mM Tris-HCl, pH 8,5. The lysates were transferred into 15 ml falcons, vortexed, snap-frozen in liquid nitrogen and stored at -80°C.

5.3.7 AAV purification

After two subsequent rounds of transfection and harvest, AAV lysates underwent two freeze thaw cycles as described before and were then centrifuged at 3500 g for 10 minutes at 4°C. The supernatant was collected and the pellets were resuspended in 5 ml lysis buffer and snap-frozen. The freeze-thaw cycle was repeated three times followed by a centrifugation at 3500 g for 10 minutes at 4°C. The supernatants were collected again and the pellets were resuspended in 5 ml lysis buffer and snap-frozen as before. Afterwards, the lysates were solubilised using a sonicator in a water bath at 48 W for 1 minute. The suspensions were then mixed with 5 mM $MgCl_2$ and digested with benzonase (50 U/ml) for 30 minutes at 37°C. This solution was then centrifuged at 4°C and 3500 g for 10 minutes. The final supernatant was pooled with the two other supernatants and the virus was stored at -80°C until purification using an iodixanol gradient.

Purifying virus by iodixanol gradient leads to a separation of packed and unpacked AAV capsids, as they migrate differentially upon ultracentrifugation. The gradient, ranging from 15% iodixanol to 60% iodixanol, was prepared on top of the viral solution in a Beckman Quickseal tube using a Pasteur pipette, as described below.

Layer (from top to bottom)	Component
15 %-iodixanol dilution (7 ml)	1,75 ml OptiPrep
	5,25 ml PBS-MK-NaCl
25 %- iodixanol dilution (5 ml)	2,08 ml OptiPrep
	2,29 ml PBS-MK
	12,5 µl phenol red (0,5 %)
40 %- iodixanol dilution (4 ml)	2,67 ml OptiPrep
	1,33 ml PBS-MK
60 %- iodixanol dilution (4 ml)	4 ml OptiPrep
	10 µl phenol red (0,5 %)

Virus	Crude AAV lysate

About 1 ml of space was left above the gradient. Tubes were sealed and centrifuged in a 50.2 Ti rotor at 50000 g and 10°C for 2 hours. Two gradients were run for each virus (two rounds of transfection). After centrifugation, the 40% iodixanol layer (~3.5 ml) was carefully collected by inserting a 5 ml syringe with a 20G needle from underneath. Aliquots of 15 µl were taken for the determination of the virus concentration by qPCR as described in the next section. The rest of the virus was kept at -80°C until use.

5.3.8 AAV titration

Viral DNA was isolated by mixing 5 µl of virus suspension with 5 µl H_2O and 10 µl 2 M NaOH. The mixture was incubated at 56°C for 30 minutes and the reaction was then neutralized by adding 10 µl 2 M HCl. After adding 970 µl H_2O, the titre was determined by qPCR using an EGFP standard curve. This standard curve was created three independent times by serial dilutions of pdsAAV-LP1-EGFPmut-miRNC. The qPCR was performed using these standard dilutions and duplicates of the samples. The primers used were from Eurofins MWG Operon and are listed in the material section. The qPCR was performed as described in 5.1.3.5.

5.4 Animal experiments

5.4.1 General procedures and housing

The animals were housed according to international standard conditions with a 12 hours dark, 12 hours light cycle and regular unrestricted diet with free access to water if not stated otherwise. Animal handling and experimentation was performed in accordance with NIH guidelines and approved by local authorities (Regierungspräsidium Karlsruhe). Blood was taken after cervical dislocation. Organs including liver, fat pads, and gastrocnemius muscles were collected, weighed, snap-frozen in liquid nitrogen and used for further analysis.

5.4.2 Mouse models

5.4.2.1 24h fasting

For a starvation challenge, 11-13 weeks old male GADD45β+/+ and Gadd45β-/- littermates (in this work called GADD45β WT and KO, respectively) were used. They were generated as described elsewhere [155]. They are inbred with the dkfz facility for many generations and are on a pure C57Bl6/J background. They were kept on control diet for a week before food withdrawal. A blood sample of 50 µl was taken before the removal of food. The mice were sacrificed 24 hours later. The grouping was as follows:

Genotype	Animals
GADD45β WT	5
GADD45β KO	8

In another starvation study, male 16 weeks old Gadd45β WT and KO mice were single housed and kept on control diet for a week as described. Afterwards, the animals were transferred to the PhenoMaster system (TSE). The TSE PhenoMaster is a high-throughput phenotyping platform for fully automated metabolic, behavioural, and physiological monitoring. Measured parameters included body weight, food and water intake, indirect gas calorimetry and activity. The mice were acclimated to that system for 4 days before food withdrawal. 24 hours later food was given back and the mice were monitored for another period of 3 days before sacrifice. The grouping was as follows:

Genotype	Animals
GADD45β WT	4
GADD45β KO	6

To study the effect of the other GADD45β family member GADD45γ, 13-20 week old GADD45γ WT and KO littermates were also examined under the stress of nutrition deprivation. The experimental setting was the same as for the first 24 hour fasting study with GADD45β WT and KO mice. Since GADD45γ KO male mice cannot form gonads during embryogenesis and are hence not to be called “male” [257], the study was conducted only with female (XX) mice. The grouping was as follows:

Genotype	Animals
GADD45γ WT	5
GADD45γ KO	5

5.4.2.2 Methionine/choline deficiency studies

For a methionine/choline deficiency (MCD) study, mice at an average age of 12 weeks were first acclimated for a week on control diet (Con) before switching to either MCD diet or control diet for 3 weeks. Mice were single housed to determine food intake and feed efficiency and not sacrificed in the fasted state. At the beginning and at the end of the study, body composition was measured (see 5.4.3.1). The grouping was as follows:

Genotype	Diet	Animals
GADD45β WT	Con	2
GADD45β WT	MCD	2
GADD45β KO	Con	6
GADD45β KO	MCD	6

5.4.2.3 Fasting and Refeeding

For an extensive fasting and refeeding study, male C57Bl6/J mice at the age of 13 weeks were used. Different groups of mice were fasted for 8 hours, 24 hours and 48 hours, respectively, and subsequently refed for 1 hour, 6 hours or 24 hours before the sacrifice. The study was performed by Drs. Mauricio Berriel Diaz and Julia Jäger who kindly offered liver samples for *Gadd45b* mRNA expression analysis.

5.4.2.4 Aging model

To study the effect of GADD45β in the more natural condition of altered metabolism during aging, male C57Bl6/J mice of different ages were faced a feeding and fasting challenge. More specifically, the mice were either 22 months old or 12 weeks young and were either fasted for 16 hours or refed for 6 hours. Dr. Katharina Niopek who has run this study kindly provided cDNA from liver samples to study the *Gadd45b* mRNA expression levels. The grouping was as follows:

Age	Nutritional status	Animals
22 months	16 hours fasted	5
22 months	6 hours refed	5
12 weeks	16 hours fasted	5
12 weeks	6 hours refed	5

5.4.2.5 Streptozotocin treatment

Streptozotocin (STZ) is a diabetogenic agent that leads to the destruction of the insulin secreting β-cells of the islets of Langerhans in the pancreas by generating ROS [250,392]. Without β-cells insulin secretion is shut down and the individual becomes type 1 diabetic. STZ is commonly used to induce diabetes in rodent disease models [251]. Male rodents are more susceptible to STZ-induced hyperglycaemia compared to females [251]. The study was performed by Dr. Anja Krones-Herzig and Tjeerd Petrus Sijmonsma and liver samples were kindly offered to measure *Gadd45b* mRNA expression levels. STZ was obtained from Axxora (LKT) and a 6 mg/ml solution in sodium citrate (0,05M, pH 4,5, sterile filtered) was freshly prepared. Male 8 weeks old C57Bl6/J mice were weighed and 60 mg/kg STZ were injected intraperitoneally on 6 subsequent days. Control animals were injected with vehicle (sodium citrate). Diabetes was verified 20 days later by measuring blood glucose. To avoid access mortality, Caninsulin® was administered intraperitoneally twice a week to stabilize the blood glucose levels around 350 mg/dl. Mice were sacrificed 6 months after STZ administration was started. The grouping was as follows:

Group	Animals
Vehicle	10
STZ	13

5.4.2.6 Obesity models

db/db mice

12 week old male BKS.Cg-m+/+ Lepr DB/J (in this work called *db/db*) or C57Bl6/J control mice were acclimated for a week on regular unrestricted diet. After a week food was removed from half of the mice in both groups and those animals were fasted for 24 hours before sacrifice. This study was performed by my colleague Dr. Roldan de Guia who measured the serum metabolites by himself and kindly offered liver, fat and gastrocnemius muscle powder for the analysis of liver metabolites and *Gadd45b* mRNA levels in the different tissues. The grouping was as follows:

Genotype	Nutritional status	Animals
WT	Random fed	4
WT	24h fast	4
db/db	Random fed	4
db/db	24h fast	4

ob/ob mice

A similar experiment to the *db/db* study was performed with B6.Cg-*Lep*^{ob}/J mice (in this work called ob/ob). 7 weeks old ob/ob mice or C57Bl6/J control mice were acclimated for two weeks before food was removed from half of the mice in both groups. The mice were sacrificed 24 hours later. This study was conducted by Dr. Mauricio Berriel Diaz who kindly provided cDNA from liver samples to study the mRNA expression of *Gadd45b*. The grouping was as follows:

Genotype	Nutritional status	Animals
WT	Random fed	4
WT	24h fast	4
ob/ob	Random fed	4
ob/ob	24h fast	4

NZO/NZB mice

To test whether the *Gadd45b* mRNA levels were also affected in a third mouse model of obesity, New-Zealand-obese (NZO) mice and matching control animals (New-Zealand black, NZB) were ordered from Charles Rivers at the age of 12 weeks and maintained on normal chow diet acclimation. For a starvation experiment, animals were allowed free access to food or were food deprived for 24 hours before sacrifice. This study was also performed by Dr. Mauricio Berriel Diaz who kindly provided cDNA from liver samples to study the mRNA expression of *Gadd45b*. The grouping was as follows:

Genotype	Nutritional status	Animals
NZB	Random fed	4
NZB	24h fast	4
NZO	Random fed	4
NZO	24h fast	4

High-fat diet induced obesity

In high-fat diet experiments, 12 week old male GADD45β WT and KO littermates were acclimated on low-fat control diet for a week before fed a high-fat diet (HFD) or low-fat control diet (NFD) for a period of 16 weeks. After 4 weeks on diet a glucose tolerance test and after 15 weeks on diet an insulin tolerance test was conducted. For details see sections 5.4.3.2 and 5.4.3.3. Furthermore at the beginning and at the end of the study, body composition was measured (see 5.4.3.1). The grouping was as follows:

Genotype	Diet	Animals
GADD45β WT	NFD	6
GADD45β WT	HFD	6
GADD45β KO	NFD	8
GADD45β KO	HFD	9

5.4.2.7 Adenovirus injections for GADD45β overexpression

Pilot studies

To test for the liver-specific overexpression of GADD45β, 1 x10^9 infectious units per recombinant virus were administered via tail vein injection into GADD45β WT and KO mice one week after acclimation on control diet. The virus was diluted in PBS/10% glycerol, pH 7,2, and 100 µl was injected into each mouse. Two pilot studies were conducted. For the first study, only 14 weeks old GADD45β WT received the AD-GADD45β OE. After another week, fasting was conducted 24 hours before sacrifice for half of the animals. For the second pilot study, AD-NC and AD-GADD45β OE particles were administered to 6 months old GADD45β KO mice which were sacrificed in the random fed state. For both studies genomic DNA and RNA was extracted to measure the hepatic viral load via RT-qPCR (primer pADBlockit-Any provided with the BLOCKiT™ Adenoviral RNAi Expression System, Invitrogen) and *Gadd45b* mRNA levels, respectively. The grouping was as follows:

Genotype	Nutritional status/virus	Animals
GADD45β WT	Random fed	2
GADD45β WT	24h fasted	3
GADD45β KO	AD-NC	3
GADD45β KO	AD-Gadd45b OE	3

Rescue experiments

For studies with overexpression of GADD45β in the murine liver, 1 x10^9 infectious units per recombinant virus were administered via tail vein injection into either male *db/db* and C57Bl6/J control mice or GADD45β WT and KO littermates one week after acclimation on control diet, all at the age of 12 weeks. Another week later, mice were fasted for 24 hours before sacrifice. A blood sample (50 µl) was always taken before food withdrawal. Additionally, a blood sample was also taken from the *db/db* and control animals before virus injection. The grouping of both studies was as follows:

Genotype	Virus	Animals
WT	AD-NC	5
WT	AD-GADD45β OE	4
db/db	AD-NC	6
db/db	AD-GADD45β OE	5
GADD45β WT	AD-NC	7

GADD45β WT	AD-Gadd45b OE	7
GADD45β KO	AD-NC	7
GADD45β KO	AD-Gadd45b OE	8

5.4.2.8 AAV injection for GADD45β knockdown

Pilot study

To test for the miRNA-mediated hepatocyte-specific knockdown of GADD45β, 2 $x10^{11}$ virus particles per recombinant AAV were administered via tail vein injection into 6 months old male C57Bl6/J mice. The virus with less volume (but same number of viral genomes) was filled up with 40% iodixanol to 50 µl so that all animals got the same volume of iodixanol. This virus dilution was mixed with 50 µl PBS before injection. After three weeks on control diet, fasting was conducted for 24 hours before sacrifice. *Gadd45b* mRNA levels were determined in the liver via RT-qPCR. The grouping was as follows:

Virus	**Animals**
AAV-NC	3
AAV-GADD45β KD	5

HFD-induced obesity

In another study, hepatocyte-specific GADD45β knockdown was accompanied with HFD treatment. After one week of acclimation on control diet, at the age of 9 weeks, 2 $x10^{11}$ virus particles per recombinant AAV were administered via tail vein injection into male C57Bl6/J mice. One week later half of the animals switched to HFD. The grouping was as follows:

Virus	**Diet**	**Animals**
AAV-NC	LFD	8
AAV-GADD45β KD	HFD	8
AAV-NC	LFD	8
AAV-GADD45β KD	HFD	8

The study was ongoing at the time of preparation of this work. Planned was an insulin tolerance test after 15 weeks on HFD and the sacrifice after 16 weeks, after 24 hours of fasting.

5.4.2.9 Mice for isolation of primary hepatocytes and cell fractionation

Primary mouse hepatocytes were isolated and cultured as described [393] from 6 male 11 weeks old GADD45β WT mice. Half of the animals were deprived of food 24 hours prior to the isolation of hepatocytes while the other half had free access to food. The mice were anesthetized by intraperitoneal injection of 5 mg 10% ketamine hydrochloride / 100 mg body weight and 1 mg 2% xylazine hydrochloride / 100 mg body weight. After opening the abdominal cavity, the liver was perfused with HANKS I buffer via the portal vein for 5 minutes at 37°C and subsequently with HANKS II buffer for 5-7 minutes until disintegration of the liver structure could be observed. The liver capsule was removed and the cell suspension was filtered through a 70 µm cell stainer into a

50 ml collection tube. Cells were centrifuged at 30 x g for 3 minutes. The pellet was kept for RNA isolation (called hepatocytes) while the supernatant was spun down again at 30 x g for 3 minutes. The second pellet was discarded while the supernatant of this second round was centrifuged again at 300 x g for 3 minutes. The pellet (called non-parenchymal cells) was kept for RNA isolation, cDNA synthesis and RT-qPCR.

5.4.3 Treatment

5.4.3.1 Body composition analysis

Total lean mass and body fat content was determined using an Echo MRI™ body composition analyser (Echo Medical Systems, Houston).

5.4.3.2 Glucose Tolerance Test

In a glucose tolerance test (GTT), glucose is injected into the peritoneum of fasted mice and blood samples are taken to determine how quickly the sugar can be cleared from the blood. Improved insulin signalling results in lower glucose levels as the sugar load induces a better clearance from the blood stream. The animals were transferred to fresh cages with no food and fasted for 6 hours prior to the GTT. Before food withdrawal, a blood sample (50 µl) was taken and the initial blood glucose levels were determined by cutting the tail tip with a razor blade. Blood glucose was measured using a glucometer strip. 5 µl/g body weight of a 20% glucose solution (in 0,9% NaCl) were then injected (to give a dose of 1g/kg body weight) and the blood glucose was monitored after 20, 60 and 120 minutes.

5.4.3.3 Insulin Tolerance Test

An insulin tolerance test (ITT) is a procedure in which insulin is injected into the peritoneum of fasted mice to assess if it can still induce its full function. If mice are insulin resistant, blood glucose levels are elevated over time. The animals were transferred to fresh cages with no food and fasted for 6 hours prior to the ITT. Before food withdrawal, the body weight of all animals was determined, a blood sample (50 µl) was taken and the initial blood glucose levels were determined by cutting the tail tip with a razor blade. Blood glucose was measured using a glucometer strip. For the insulin tolerance test a stock solution of 200 mU insulin/ml was prepared using 0,9% NaCl. 5 µl per gram body weight of the stock solution, which makes 1 U insulin/kg body weight, was injected intraperitoneally. The blood glucose levels were monitored after 10, 20, 30, 60 and 120 minutes. If the blood glucose levels dropped under 20 mg/dl mice had to be rescued by injecting 100 µl of a 20% glucose solution (in 0,9% NaCl) and consequently were excluded from the analysis.

5.4.4 Preparation of Blood serum

Blood serum was obtained by storing of blood samples at 4°C for 30-60 minutes and subsequent centrifugation for 1 hour at 3000 rpm, 4°C. The serum (upper phase) was transferred to a new tube and stored at -80°C.

5.5 Human subjects

Liver tissue samples were obtained from 37 Caucasian lean and obese men, 14 with and 23 without T2D, who underwent open abdominal surgery for Roux-en-Y bypass, sleeve gastrectomy or elective cholecystectomy by Prof. Dr. Matthias Blüher and colleagues from the University Hospital Leipzig, Germany. Liver biopsy was taken during the surgery, immediately frozen in liquid nitrogen and stored at -80°C until further use. The phenotypic characterization of the cohort has been performed as described previously [394]. Serum samples were taken between 8 am and 10 am after an overnight fast. The study was approved by the local ethics committee of the University of Leipzig, Germany (363-10-13122010 and 017-12-230112). All patients gave preoperative written informed consent for the use of their samples. The grouping was as follows:

Glucose Tolerance	Body composition	Men
Type 2 diabetes	Lean	3
	Subcutaneous fat	3
	Visceral fat	8
Normal glucose tolerant	Lean	8
	Subcutaneous fat	13
	Visceral fat	2

5.6 Nomenclature of genes and proteins

In general, mRNA and cDNA transcripts of genes are addressed using italicised characters, whereas proteins are addressed using upright characters. Human gene symbols are italicized, with all letters in uppercase (e.g. *GADD45B*); protein designations are the same as the gene symbol, but are not italicized, with all letters in uppercase (GADD45β). Mouse gene symbols generally are italicized, with only the first letter in uppercase and the remaining letters in lowercase (*Gadd45b*); protein designations are the same as the gene symbol, but are not italicized and all are upper case (GADD45β).

5.7 Statistical Analysis

Data plotted in figures are mean ± standard error of the mean (SEM). Statistical analyses were performed using either a 2-way analysis of variance (ANOVA) with Holm-Sidak-adjusted post-tests in two-factorial designs, a 2-way repeated measurement ANOVA with Holm-Sidak-adjusted post-tests tests in two-factorial designs when factors of the same subject were determined repeatedly at different time points, or t-test in one-factorial designs. Correlation was determined using Shearman's correlation coefficient. $p < 0.05$ was considered statistically significant. *$p < 0.05$, **$p < 0.01$, ***$p < 0.001$.

6. MATERIAL

6.1 Buffers and Solutions

All buffers are 1x and diluted in H_2O, unless indicated otherwise.

Name	Component
2x SDS sample buffer	120 mM Tris /HCl pH 6.8
	4% SDS
	20% glycerol
	200 mM DTT
	0.01% bromophenol blue
5x SDS sample buffer	250 mM Tris/HCl pH 6.8
	10 % SDS
	50 % glycerol
	0.5 M DTT
	0.01% bromophenol blue
HANKS I buffer	8 g NaCl
	0.4 g KCl
	3.57 g Hepes
	0.06 g KH_2PO_4
	0.06 g Na_2HPO_4 x 2 H_2O
	add 1L distilled H_2O
	2.5 mM EGTA
	0.1% Glucose
	pH 7.4
HANKS II buffer	8 g NaCl
	0.4 g KCl
	3.57 g Hepes
	0.06 g KH_2PO_4
	0.06 g Na_2HPO_4 x 2 H_2O
	add 1L distilled H_2O
	3 mg/ml Collagenase CLSII 5 mM $CaCl_2$
	0.1% Glucose
	pH 7.4
LB medium	10 g/l Trypton
	5 g/l Yeast extract
	10 g/l NaCl
	pH 7.0
Lysis buffer (AAV)	150 mM NaCl
	50 mM Tris HCl

	pH 8.5
Lysis Buffer (DNA extraction)	100 mM NaCl 10 mM Tris 15 mM EDTA 0,5 % SDS pH 8,0
NID buffer	50 mM KCl 10 mM Tris HCl, pH 8,3 2 mM $MgCl_2$ 0,1 mg/ml gelatin 0,45 % NP-40 0,45 % Tween-20
Orange G loading dye (6x)	10 mM EDTA 70% Glycerol A pinch Orange G
PBS (10x)	1.4 M NaCl 27 mM KCl 100 mM Na_2HPO_4 8 mM KH_2PO_4 pH 6.8
PBS-MK	1x PBS 1 mM $MgCl_2$ 2,5 mM KCl
PBS-MK-NaCl	1x PBS 1 mM $MgCl_2$ 2,5 mM KCl 1 M NaCl
PBS-TOSH	30.8 mM NaCl 120.7 mM KCl 8.1 mM Na_2HPO_4 1.46 mM KH_2PO_4 10 mM $MgCl_2$ pH 7.2, sterile filtrated
RIPA Buffer	50 mM Tris HCl pH 8,0 150 mM NaCl 1 mM EDTA pH 8,0 1% NP-40 0,1% SDS 0,5% Sodium deoxycholate
RNA denaturing buffer (100 µl)	0,5 µl 10 mg/ml ethidium bromide

	5 µl 10x MOPS 50 µl Formamide 17,5 µl 37% Formaldehyde 16,7 µl 6x Orange G 10,3 µl RNase-free water
SDS running buffer (10x)	0.25 M Tris 1.92 M Glycine 1% SDS
TAE buffer (10x)	400 mM Tris 1 mM EDTA 20 mM acetic acid pH 8.0
TBE buffer (10x)	20 mM Tris 137 mM NaCl pH 7,6
TE buffer (10x)	1 mM EDTA 10 mM Tris HCl pH 8.0
Transfer buffer	25 mM Tris 192 mM Glycine 20% Methanol 0.01% SDS
TBS	20 mM Tris 137 mM NaCl pH 7,6
TBS-T	1x TBS 0.1% Tween 20

6.2 Chemicals and Reagents

Chemical/Reagent	**Distributor**
Acetic acid (99%)	Sigma, Munich
Acetone	Sigma, Munich
Acrylamide-bisacrylamide Solution (37.5 : 1)	Carl Roth GmbH, Karlsruhe
Agarose	Sigma, Munich
Ammonium persulfate (APS)	Carl Roth GmbH, Karlsruhe
Antibiotics	Sigma, Munich
Bovine serum albumin (BSA)	Sigma, Munich
Bromophenol blue	Sigma, Munich
Cesium chloride	Carl Roth GmbH, Karlsruhe

Chloroform	DKFZ
Desoxynucleotides (dATP, dCTP, dGTP, dTTP)	Roche, Mannheim
Dexamethasone	Sigma, Munich
Dimethyl sulfoxide (DMSO)	Sigma, Munich
DTT (Dithiothreitol)	Sigma, Munich
Dulbecco's modified Eagle's medium (DMEM)	Invitrogen, Karlsruhe
Dulbecco's modified Eagle's medium (DMEM)/F-12	Invitrogen, Karlsruhe
Dulbecco's Phosphate Buffered Saline (D-PBS) (10X)	Invitrogen, Karlsruhe
Ethanol (99%)	DKFZ
Ethidium bromide	Carl Roth GmbH, Karlsruhe
Ethylenediaminetetraacetic acid (EDTA)	Sigma, Munich
Ethylenglycoltetraacetic acid (EGTA)	Sigma, Munich
Fetal calf serum (FCS)	Invitrogen, Karlsruhe
Gelatin from bovine skin, Type B	Sigma, Munich
Glucose	Sigma, Munich
Glycerol	Baker, Deventer, NL
Glycine	Sigma, Munich
Hank's balanced salt solution (HBSS)	Invitrogen, Karlsruhe
Hepes	Roth, Karlsruhe
High Range DNA ladder	Fermentas, St. Leon Rot
Hydrochloric acid (HCl) 37%	Acros Organics, New Jersey, USA
Igepal (Nonidet NP40)	Sigma, Munich
Isopropanol	Sigma, Munich
Insulin (human, 100 units/ml)	Lilly Germany, Gießen
Insulin-transferrin-selenium supplement	Roche, Penzberg
LB-Agar	Carl Roth GmbH, Karlsruhe
LB-Medium	Carl Roth GmbH, Karlsruhe
L-Glutamine	Invitrogen, Karlsruhe
Lipid Mixture 1	Sigma, Munich
Lipofectamine2000 Reagent	Invitrogen, Karlsruhe
Loading dye solution (6x)	Fermentas, St. Leon Rot
Low Range DNA ladder	Fermentas, St. Leon Rot
Magnesium chloride (MgCl2)	Merck, Darmstadt
MEM Amino Acids Solution (50X)	Invitrogen, Karlsruhe
MEM Vitamin Solution (100X)	Invitrogen, Karlsruhe
Methanol (100%)	Sigma, Munich
Milk powder	Sigma, Munich
Non-essential amino acids (100x)	Invitrogen, Karlsruhe
Oligo(dT)18 Primer	Fermentas, St. Leon Rot
OptiMEM	Invitrogen, Karlsruhe

OptiPrep(R) Density Gradient Medium	Sigma, Munich
Orange G	Sigma, Munich
Page Ruler^{TM} Prestained Protein Ladder	Fermentas, St. Leon Rot
Penicillin / Streptomycin (P/S)	Invitrogen, Karlsruhe
Phosphatase Inhibitor Cocktail	Roche, Penzberg
Polyamine Supplement (1000×)	Sigma, Munich
Polyethylenimine	Polysciences Inc., Warrington, US
Ponceau-S Solution	Sigma, Munich
Potassium chloride (KCl)	Sigma, Munich
Potassium dihydrogen phosphate >99% (KH_2PO_4)	Carl Roth GmbH, Karlsruhe
Proteinase inhibitor cocktail	Roche, Penzberg
Qiazol Lysis Reagent	Qiagen, Hilden
RiboLock Ribonuclease Inhibitor	Fermentas, St. Leon Rot
Sodium bicarbonate solution 7,5%	Invitrogen, Karlsruhe
Sodium chloride (NaCl)	Invitrogen, Karlsruhe
Sodium deoxycholate 97%	Sigma, Munich
Sodium dodecyl sulfate (SDS)	Gerbu Biotechnik GmbH, Gaiberg
Sodium fluoride (NaF)	Sigma, Munich
Sodium hydrogen phosphate dibasic dihydrate (Na_2HPO_4)	Sigma, Munich
Sodium hydroxide (NaOH)	Sigma, Munich
Sodium orthovanadate	Sigma, Munich
Sodium pyruvate	Invitrogen, Karlsruhe
N,N,N',N'-Tetramethylenediamine (TEMED)	Carl Roth GmbH, Karlsruhe
Tris base	Sigma, Munich
Triton X-100	Sigma, Munich
Trypsin-EDTA solution	Invitrogen, Karlsruhe
Tween-20	Sigma, Munich
Urea	Sigma, Munich
β-Mercaptoethanol (98%)	Sigma, Munich
Williams Medium E	Sigma, Munich

6.3 Consumabales

Consumable	**Distributor**
1-stack cell culture dishes	Sigma, Munich
10-stack cell culture dishes	Sigma, Munich
6 well tissue culture dishes	Falcon, Gräfeling-Lochham
96 well MicroAmp plates	Applied Biosystems
96-well *Microtiter*® luminescense plates	Nunc, Wiesbaden

Cell strainer (70 µm)	Falcon, Gräfeling-Lochham
Centrifuge tubes (500 ml)	Corning, Wiesbaden
Combitips advanced® (0.5, 5, 10 ml), sterile	Eppendorf, Hamburg
Countess™ cell counting chamber slides	Invitrogen, Darmstadt
Cryo tubes (2 ml)	Cryo tubes (2 ml)
Dialysis tubing	Carl Roth GmbH, Karlsruhe
Disposable scalpels	Feather, Cuome, JP
DNase / RNase free water	Invitrogen, Karlsruhe
Filters (0.22 µm)	Millipore, Eschborn
Filters (0.45 µm)	Millipore, Eschborn
Filters (0.8 µm)	Millipore, Eschborn
Filters (5 µm)	Millipore, Eschborn
Gel staining boxes (Mini)	Carl Roth GmbH, Karlsruhe
Gloves (*Blossom*®)	Mexpo International, Hayward
Gloves (*Safe Skin Purple Nitrile*)	Kimberly Clark, BE
Glucose test stripes, OneTouch® Ultra	LifeScan, Neckargemünd
Insulin Syringes *(Micro-Fine™+ Demi)*	BD Medical, Heidelberg
Millex-GV filter unit PVDF, 0.22 µm	Merck KGaA, Darmstadt
Mouth protection	Meditrade, Kiefersfelden
NeedleSterican®, 20G	B. Braun, Melsungen
NeedleSterican®, 27G	B. Braun, Melsungen
Nitrocellulose membrane	Schleicher and Schüll, Dassel
Parafilm	Pechinery Inc., Wisconsin, USA
Pasteur pipettes	Brand, Wertheim
PCR tubes	Kisker Biotech, Steinfurt
Petri dishes	Greiner, Kremsmünster, AU
Pipette tips (0.1 – 1000 µl)	Starlab, Helsinki, FI
Pipette tips (0.1 – 1000 µl) (Tip One Filter Tips)	Starlab, Helsinki, FI
Pipette tips (Electrophoresis / Protein)	Biorad, Munich
Pipette tips for Liquidator™ (200 µl)	Steinbrenner, Wiesenbach
Polyallomer tubes (14mm x 89 mm)	Beckmann, Munich
Polyallomer tubes (25 mm x 89 mm)	Beckmann, Munich
Round bottom tubes (14 ml)	Falcon, Gräfeling-Lochham
Safelock micro test tubes (1.5 ml and 2 ml)	Eppendorf, Hamburg
Serological pipettes (5 ml, 10 ml, 25 ml, 50 ml)	BD Biosciences, San Jose, USA
SpeedVac	Eppendorf, Hamburg
Stainless Steel Beads (5 mm)	Qiagen, Hilden
Syringes (5 ml)	Terumo, Leuven
Syringes (10 ml Luer Lock)	Terumo, Leuven
Syringes (50 ml)	Terumo, Leuven

Test tubes (15 ml and 50 ml)	Falcon, Gräfeling-Lochham
Tissue culture dishes (10 cm and 15 cm)	Falcon, Gräfeling-Lochham
Whatman™ paper	GE Healthcare, Solingen

6.4 Kits

Kit	Distributor
Alanine Assay Kit	BioVison, Mountain View, US
BLOCK-iT™ U6 RNAi Entry Vector Kit	Invitrogen, Karlsruhe
Branched Chain Amino Acid Assay Kit	BioVison, Mountain View, US
Cholesterol determination Kit	Randox, Crumlin, UK
Dnase Set, Rnase-free	Qiagen, Hilden
Enhanced Chemiluminescence (ECL) Kit	Amersham Biosciences, Freiburg
First Strand cDNA Synthesis Kit	Fermentas, St. Leon-Rot
Glucose (HK) Assay Kit	Sigma-Aldrich, München
Infinity ALT Kit	Thermo Electron, Melbourne
Insulin ELISA Kit (mouse)	Alpco
NEFA – C Determination Kit	Wako, Neuss
Pierce® BCA Protein Assay Kit	Thermo Fisher Scientific, Schwerte
Phusion Polymerase Kit	Finnzymes, Vantaa
QiaPrep Plasmid Miniprep Kit	Qiagen, Hilden
QiaQuick Gel Extraction Kit	Qiagen, Hilden
QIAGEN Plasmid Mega Kit	Qiagen, Hilden
QiaQuick PCR Purification Kit	Qiagen, Hilden
QuantiTect SYBR Green PCR Kit	Qiagen, Hilden
RNeasy® RNA Extraction Kit	Qiagen, Hilden
TaqMan® Gene Expression Master Mix	Life Technologies, Damstadt
Triglycerides Determination Kit	Sigma, Munich

6.5 Antibodies

All phospho antibodies were diluted in 5% BSA/TBS-T. All other antibodies were diluted in 2% skim milk/TBS-T.

Primary Antibody	Dilution	Isotope	Distributor
Actin	1:1000	Mouse	Sigma, A5441
Akt	1:1000	Rabbit	Cell Signaling, #9272
Phospho Akt (Ser473)	1:1000	Rabbit	Cell Signaling, #9271
Phospho Akt (Thr308)	1:1000	Rabbit	Cell Signaling, #13038
Flag M2	1:1000	Mouse	Sigma, #A8592
FoxO1	1:1000	Rabbit	Cell Signaling,# 9454

Phospho FoxO1 (Ser256)	1:1000	Rabbit	Cell Signaling,# 9461
GADD45β	1:250	Goat	Santa Cruz, sc-8776
GSK3β	1:1000	Rabbit	Cell Signaling, #9315
Phospho GSK3β (Ser9)	1:1000	Rabbit	Cell Signaling, #9336
IRS-1	1:1000	Rabbit	Cell Signaling, #3407
Phospho IRS-1 (Ser1101)	1:1000	Rabbit	Cell Signaling, #2385
JNK	1:1000	Rabbit	Cell Signaling, #9252
Phospho JNK (Thr183/Tyr185)	1:1000	Rabbit	Cell Signaling, #9255
Phospho p38 (Thr180/Tyr182)	1:1000	Rabbit	Cell Signaling, #9211
p85 (PI3K)	1:1000	Rabbit	Cell Signaling, #4292
S6K1	1:1000	Rabbit	Cell Signaling, #2708
Phospho S6K1 (Thr389)	1:1000	Rabbit	Cell Signaling, #9234
VCP	1:10000	Mouse	Abcam, #ab11433

Secondary Antibody	**Dilution**	**Isotope**	**Distributor**
Anti-goat, Fc Fragment Specific, IgG-HRP	1:5000	Rabbit	Thermo Scientific, #31433
Anti-mouse IgG-HRP	1:5000	Goat	Biorad, #170-6516
Anti-rabbit, IgG-HRP	1:5000	Goat	Biorad, #172-1019

6.6 Enzymes

Enzyme	**Distributor**
Amyloglucosidase	Sigma, Munich
Benzonase	Sigma, Munich
Collagenase Type ll	Sigma, Munich
DNase I	Qiagen, Hilden
Proteinase K	Thermo Scientific, Schwerte
T4 Ligase	Invitrogen, Karlsruhe

6.7 Plasmids

Plamid	**Distributor**
pCMV-SPORT6 mGadd45b	imaGenes, Berlin
pENTR-Flag	Invitrogen, Karlsruhe
pAd-BlockIT-DEST	Invitrogen, Karlsruhe
pcDNA6.2-GW/EmGFP-miR	Invitrogen, Karlsruhe
pdsAAV-LP1-GFPmut-miR-NC	unknown
pDGΔVP	D. Grimm *et al.*, 1998
p5E18-VD2/8	G.P. Gao *et al.*, 2002

6.8 Oligonucleotides

All oligonucleotides possessed a G/C content between 40% and 60% and were approximately 20-30bp in length.

Restriction sites for specific enzymes were added to the cloning primers in 5'→3' orientation, allowing directed insertion into a specific target vector. Six thymidine residues were added to the 5' ends of the restriction sites in order to facilitate cleavage. The primers were designed to hybridize at temperatures of approximately 60°C.

Oligonucleotide	**Purpose**	**Sequence (5' → 3')**
miR-Gadd45b_for	AAV production	TGCTGACATTCATCAGTTTGGCCGCCGTTTTGGCCACTGACTGACGGCGGCCACTGATGAATGT
miR-Gadd45b_rev	AAV production	CCTGACATTCATCAGTGGCCGCCGTCAGTCAGTGGCCAAAACGGCGGCCAAACTGATGAATGTC
mGadd45b_for	AD production	TTTTTGCGGCCGCCACCCTGGAAGAGCTGGTGGCG
mGadd45b_rev	AD production	TTTTTCTCGAGTCAGCGTTCCTCTAGAGAGATATAG
Gadd45b_for	Genotyping	GGGACAGTGAACTGTGCATAAG
Gadd45b_rev	Genotyping	CAAGCGATCTGTCTTGCTCA
Gadd45b_neo	Genotyping	GCATGCTCCAGACTGCCTT
Gadd45g_for	Genotyping	GCTGTGCTTTCCGGAACTGTA
Gadd45g_rev	Genotyping	GTGGGCTCTATGGCTTCTGA
Gadd45g_pgk	Genotyping	CCTGCCGCCTCATTTGCA
EGFP-C1-F	Sequencing	GAAGCGCGATCACATGGTC
CMV-for	Sequencing	CGCAAATGGGCGGTAGGCGTG
TkpA-rev	Sequencing	GTGGGGTATCGACAGAGTGC

6.9 Taqman and SYBR probes

6.9.1 Taqman probes from Life Technologies

Gene	Assay ID
Abca1	mm00442646_m1
Acly	Mm00652520_m1
Atp6v0d2	Mm01222963_m1
Cd31	mm01242584_m1
Cd36	Mm00432403_m1
Ces4a	mm00600647_m1
Cidec	Mm00617672_m1
Cyp2b9	Mm00657910_m1

Cyp2b10	Mm00456591_m1
Desmin	mm00802455_m1
Emr1	mm00802529_m1
Fabp5	mm00445880_m1
Gadd45a	Mm00432802_m1
Gadd45b	Mm00435121_g1
Gadd45g	Mm01352550_g1
GAPDH	Mm99999915_g1
G6Pase	Mm00839363_m1
GCK	Mm00439129_m1
HNF4a	mm00433964_m1
Pck1	mm00440636_m1
Serpina4-ps1	Mm00657552_m1
Slco1a1	Mm00649796_m1
Tsc22d1	mm00493633_m1

6.9.2 Taqman probes from Eurofin MWG

Gene	Sequence
TBP forward	TTGACCTAAAGACCATTGCACTTC
TBP reverse	TTCTCATGATGACTGCAGAAA
TBP probe	5'FAM-TGCAAGAAATGCTGAATATAATCCCAAGCG-3'TAMRA
EGFP-ANY_for	GAGCGCACCATCTTCTTCAAG
EGFP-ANY_rev	TGTCGCCCTCGAACTTCAC
EGFP-ANY_probe	FAM-ACGACGGCAACTACA-TAMRA

6.9.3 SYBR probes from Qiagen

Gene	Assay ID
Derl3	QT00159880
Klf12	QT00109487
Lcn2	QT00113407
Lcor	QT01073541
Lnpep	QT01764812
N4bp2	QT00306404
Nudt7	QT00110740
Onecut1	QT00297815
Saa2	QT00144151
Vps13b	QT01073247

Zbed6	QT02330083
Zfp369	QT00142401

6.10 Cell lines

Cell line	Distributor
HEK 293 (human embryonic kidney) cell line	ATTC, Wesel
HEK 293-T (human embryonic kidney) cell line	ATTC, Wesel
HEK 293-A (human embryonic kidney) cell line	ATTC, Wesel
Hepa1c1 mouse hepatoma cell line	ATTC, Wesel
AML12 (alpha mouse liver 12) cell line	ATTC, Wesel
E. coli SURE2® Chemically Competent Cells	Qiagen, Hilden
E. coli TOP 10 Chemically Competent Cells	Invitrogen, Karlsruhe

6.11 Animals and Diets

Mouse	Distributor
BKS.Cg-m+/+ Lepr DB/J (db/db)	Charles River, Brussels, Belgium
B6.Cg-*Lep*^{ob}/J (ob/ob)	Charles River, Brussels, Belgium
New Zealand obese (NZO)	Charles River, Brussels, Belgium
New Zealand black (NZB)	Charles River, Brussels, Belgium
C57Bl6/J	Charles River, Brussels, Belgium
B6.CgGADD45β^{tm1Daa}	DKFZ in house breeding
B6.CgGADD45γ^{tm1Daa}	Prof. C. Niehrs, IMB Mainz, Germany

Diet	Composition (kcal %)	Distributor
Low fat diet (LFD)/Control diet, γ-irradiated	Protein: 20 Carbohydrates: 70 Fat:10	Research Diets Inc., New Brunswick, US
High fat diet (HFD), γ-irradiated	Protein: 20 Carbohydrates: 20 Fat: 60	Research Diets Inc., New Brunswick, US
Methionine-Choline-Deficient (MCD) diet, γ-irradiated	Protein: 16 Carbohydrates: 63 Fat: 21	Research Diets Inc., New Brunswick, US
Control diet for MCD, γ-irradiated	Protein: 16 Carbohydrates: 63 Fat: 21	Research Diets Inc., New Brunswick, US

6.12 Software

Software	Distributor
Endnote	Thomson, Carlsbad, USA
Geneious	Auckland, New Zealand
Image Lab	Bio-Rad Laboratories
Microsoft Office	Microsoft, Unterschleißheim
Photoshop	Adobe, San Jose, USA
Pubmed	http://www.pubmedcentral.nih.gov
StepOne Plus	Applied Biosystems, Darmstadt System Software

6.13 Intruments and Equipment

Equipment	Distributor
Accu-Chek® Performa MIC	Roche Diagnostics, Mannheim
Analytical scales	Satorius, Göttingen
Bacterial shaker	Infors AG, Böttmingen, CH
Bunsen Burner	Campingaz, Hattersheim
Centrifuge (2K15)	Sigma, Munich
Centrifuge (*Biofuge fresco*)	Heraeus, Hanau
Centrifuge (*Biofuge pico*)	Heraeus, Hanau
Centrifuge (*Function Line*)	Heraeus, Hanau
Centrifuge (*Micro 22R*)	Hettich GmbH & Co, Tuttlingen
Centrifuge (*Super T21*)	Heraeus Sorvall, Langenselbold
ChemiDoc	BioRad, Munich
CO2-incubator	Sanyo, Munich
CO2-incubator (*Forma Scientific*)	Labotect, Göttingen
Countess Cell counter	Invitrogen, Karlsruhe
Echo MRI™ Analyser	Echo Medical Systems, Houston
Electrophoresis chamber	Steinbrenner, Wiesenbach
Electrophoresis power supply (*Power Pack Basic*)	BioRad, Munich
Electrophoresis power supply (*Power Pack HC*)	BioRad, Munich
Freezer, -20°C	Liebherr, Biberach
Freezer, -80°C (*Hera Freeze*)	Heraeus, Heilbronn
Fridge, 4°C	Liebherr, Biberach
Gel imager	Intas, Göttingen
Heat block (Thermomixer comfort)	Eppendorf, Hamburg
Horizontal shaker (*Duomax 1030*)	Heidolph, Kehlheim
Hotplate / stirrer	VWR, Darmstadt

Incubator (*Function Line*)	Heraeus, Hanau
Liquidator™ 96	Mettler Toledo, Gießen
Microplate Reader (*Spectro Star Omega)*	BMG Labtech, Ortenberg
Microplate Reader *(Mithras LB 940)*	Berthold Technologies, Bad Wildbad
Microscope (*Axiovert 40 CFL*)	Carl Zeiss, Jena
Microwave	Bosch, Stuttgart
Multistep pipette	Eppendorf, Hamburg
Nitrogen tank	Thermo Electron corp., Erlangen
pH-meter	VWR, Darmstadt
Photometer (*NanoDrop ND-1000*)	Peqlab Biotechnology, Erlangen
Pipetteboy	Integra, Fernwald
Pipettes (2 µl, 10 µl, 20 µl, 100 µl, 200 µl, 1000 µl)	Starlab, Helsinki, FI
Multi-Channel pipette 0,5 – 10 µl	Eppendorf, Hamburg
Multi-Channel pipette 10 – 100 µl	Eppendorf, Hamburg
Real time PCR System StepOne Plus	Applied Biosystems, Darmstadt
Rotating wheel	Neolab, Heidelberg
Scale	Kern und Sohn GmbH, Balingen
Scale (*BL 1500 S*)	Satorius, Göttingen
Scanner	Epson, Meerbusch
SDS electrophoresis chambers	BioRad, Munich
Sonicator Bioruptor™	Diagenode, Liège, Belgium
Stand	Carl Roth GmbH, Karlsruhe
Sterile benches (Class II type A/B3)	Sterilgard, Sanford, USA
Tabletop centrifuges (*Mini Spin Plus*)	Eppendorf, Hamburg
Thermocycler *(T3000)*	Biometra, Göttingen
Tissue Lyser	Qiagen, Hilden
Titer Plate Shaker	Thermo Scientific, Osterode
Ultracentrifuge (*Sorvall WX Ultra 80*)	Thermo Scientific, Osterode
Vacuum pump	Neolab, Heidelberg
Vortex mixer (*REAX 2000*)	Heidolph, Kehlheim
Water bath	Neolab, Heidelberg
Water bath (*WBS*)	Fried Electric, Haifa, IL
Western Blot Chamber	BioRad, Munich

7. FIGURES AND TABLES

7.1 Figure legends

7.2 Table legends

8. REFERENCES

8.1 Literature

1. Storlien L, Oakes ND, Kelley DE (2004) Metabolic flexibility. Proc Nutr Soc 63: 363-368.
2. Galgani JE, Moro C, Ravussin E (2008) Metabolic flexibility and insulin resistance. Am J Physiol Endocrinol Metab 295: E1009-1017.
3. Kelley DE, Mandarino LJ (2000) Fuel selection in human skeletal muscle in insulin resistance: a reexamination. Diabetes 49: 677-683.
4. Ferrannini E (1988) The theoretical bases of indirect calorimetry: a review. Metabolism 37: 287-301.
5. Kelley DE, Goodpaster B, Wing RR, Simoneau JA (1999) Skeletal muscle fatty acid metabolism in association with insulin resistance, obesity, and weight loss. Am J Physiol 277: E1130-1141.
6. Flatt JP (1995) Body composition, respiratory quotient, and weight maintenance. Am J Clin Nutr 62: 1107S-1117S.
7. Kopelman PG (2000) Obesity as a medical problem. Nature 404: 635-643.
8. Ridaura VK, Faith JJ, Rey FE, Cheng J, Duncan AE, et al. (2013) Gut microbiota from twins discordant for obesity modulate metabolism in mice. Science 341: 1241214.
9. Tilg H, Kaser A (2011) Gut microbiome, obesity, and metabolic dysfunction. J Clin Invest 121: 2126-2132.
10. De Pergola G, Silvestris F (2013) Obesity as a major risk factor for cancer. J Obes 2013: 291546.
11. Lavie CJ, Milani RV, Ventura HO (2009) Obesity and cardiovascular disease: risk factor, paradox, and impact of weight loss. J Am Coll Cardiol 53: 1925-1932.
12. Reaven GM (1988) Banting lecture 1988. Role of insulin resistance in human disease. Diabetes 37: 1595-1607.
13. Grundy SM, Brewer HB, Jr., Cleeman JI, Smith SC, Jr., Lenfant C, et al. (2004) Definition of metabolic syndrome: report of the National Heart, Lung, and Blood Institute/American Heart Association conference on scientific issues related to definition. Arterioscler Thromb Vasc Biol 24: e13-18.
14. Alberti KG, Eckel RH, Grundy SM, Zimmet PZ, Cleeman JI, et al. (2009) Harmonizing the metabolic syndrome: a joint interim statement of the International Diabetes Federation Task Force on Epidemiology and Prevention; National Heart, Lung, and Blood Institute; American Heart Association; World Heart Federation; International Atherosclerosis Society; and International Association for the Study of Obesity. Circulation 120: 1640-1645.
15. Alberti KG, Zimmet P, Shaw J (2006) Metabolic syndrome--a new world-wide definition. A Consensus Statement from the International Diabetes Federation. Diabet Med 23: 469-480.

16. Pollex RL, Hegele RA (2006) Genetic determinants of the metabolic syndrome. Nat Clin Pract Cardiovasc Med 3: 482-489.
17. Xi B, He D, Zhang M, Xue J, Zhou D (2014) Short sleep duration predicts risk of metabolic syndrome: a systematic review and meta-analysis. Sleep Med Rev 18: 293-297.
18. Edwardson CL, Gorely T, Davies MJ, Gray LJ, Khunti K, et al. (2012) Association of sedentary behaviour with metabolic syndrome: a meta-analysis. PLoS One 7: e34916.
19. Cornier MA, Dabelea D, Hernandez TL, Lindstrom RC, Steig AJ, et al. (2008) The metabolic syndrome. Endocr Rev 29: 777-822.
20. Bays H, Blonde L, Rosenson R (2006) Adiposopathy: how do diet, exercise and weight loss drug therapies improve metabolic disease in overweight patients? Expert Rev Cardiovasc Ther 4: 871-895.
21. Fulop T, Tessier D, Carpentier A (2006) The metabolic syndrome. Pathol Biol (Paris) 54: 375-386.
22. Bechmann LP, Hannivoort RA, Gerken G, Hotamisligil GS, Trauner M, et al. (2012) The interaction of hepatic lipid and glucose metabolism in liver diseases. J Hepatol 56: 952-964.
23. Fabbrini E, Sullivan S, Klein S (2010) Obesity and nonalcoholic fatty liver disease: biochemical, metabolic, and clinical implications. Hepatology 51: 679-689.
24. Hoyumpa AM, Jr., Greene HL, Dunn GD, Schenker S (1975) Fatty liver: biochemical and clinical considerations. Am J Dig Dis 20: 1142-1170.
25. Kleiner DE, Brunt EM, Van Natta M, Behling C, Contos MJ, et al. (2005) Design and validation of a histological scoring system for nonalcoholic fatty liver disease. Hepatology 41: 1313-1321.
26. Cohen JC, Horton JD, Hobbs HH (2011) Human fatty liver disease: old questions and new insights. Science 332: 1519-1523.
27. Boden G, Shulman GI (2002) Free fatty acids in obesity and type 2 diabetes: defining their role in the development of insulin resistance and beta-cell dysfunction. Eur J Clin Invest 32 Suppl 3: 14-23.
28. Bugianesi E, Gastaldelli A, Vanni E, Gambino R, Cassader M, et al. (2005) Insulin resistance in non-diabetic patients with non-alcoholic fatty liver disease: sites and mechanisms. Diabetologia 48: 634-642.
29. Seppala-Lindroos A, Vehkavaara S, Hakkinen AM, Goto T, Westerbacka J, et al. (2002) Fat accumulation in the liver is associated with defects in insulin suppression of glucose production and serum free fatty acids independent of obesity in normal men. J Clin Endocrinol Metab 87: 3023-3028.
30. Sun Z, Lazar MA (2013) Dissociating fatty liver and diabetes. Trends Endocrinol Metab 24: 4-12.
31. Monetti M, Levin MC, Watt MJ, Sajan MP, Marmor S, et al. (2007) Dissociation of hepatic steatosis and insulin resistance in mice overexpressing DGAT in the liver. Cell Metab 6: 69-78.

32. Minehira K, Young SG, Villanueva CJ, Yetukuri L, Oresic M, et al. (2008) Blocking VLDL secretion causes hepatic steatosis but does not affect peripheral lipid stores or insulin sensitivity in mice. J Lipid Res 49: 2038-2044.
33. Watt MJ (2009) Storing up trouble: does accumulation of intramyocellular triglyceride protect skeletal muscle from insulin resistance? Clin Exp Pharmacol Physiol 36: 5-11.
34. Yamaguchi K, Yang L, McCall S, Huang J, Yu XX, et al. (2007) Inhibiting triglyceride synthesis improves hepatic steatosis but exacerbates liver damage and fibrosis in obese mice with nonalcoholic steatohepatitis. Hepatology 45: 1366-1374.
35. Samuel VT, Shulman GI (2012) Mechanisms for insulin resistance: common threads and missing links. Cell 148: 852-871.
36. Schroder M, Kaufman RJ (2005) The mammalian unfolded protein response. Annu Rev Biochem 74: 739-789.
37. Ozcan U, Cao Q, Yilmaz E, Lee AH, Iwakoshi NN, et al. (2004) Endoplasmic reticulum stress links obesity, insulin action, and type 2 diabetes. Science 306: 457-461.
38. Gregor MF, Yang L, Fabbrini E, Mohammed BS, Eagon JC, et al. (2009) Endoplasmic reticulum stress is reduced in tissues of obese subjects after weight loss. Diabetes 58: 693-700.
39. Puri P, Mirshahi F, Cheung O, Natarajan R, Maher JW, et al. (2008) Activation and dysregulation of the unfolded protein response in nonalcoholic fatty liver disease. Gastroenterology 134: 568-576.
40. Shoelson SE, Herrero L, Naaz A (2007) Obesity, inflammation, and insulin resistance. Gastroenterology 132: 2169-2180.
41. Solomon SS, Odunusi O, Carrigan D, Majumdar G, Kakoola D, et al. (2010) TNF-alpha inhibits insulin action in liver and adipose tissue: A model of metabolic syndrome. Horm Metab Res 42: 115-121.
42. Weisberg SP, McCann D, Desai M, Rosenbaum M, Leibel RL, et al. (2003) Obesity is associated with macrophage accumulation in adipose tissue. J Clin Invest 112: 1796-1808.
43. Kolak M, Westerbacka J, Velagapudi VR, Wagsater D, Yetukuri L, et al. (2007) Adipose tissue inflammation and increased ceramide content characterize subjects with high liver fat content independent of obesity. Diabetes 56: 1960-1968.
44. Guilherme A, Virbasius JV, Puri V, Czech MP (2008) Adipocyte dysfunctions linking obesity to insulin resistance and type 2 diabetes. Nat Rev Mol Cell Biol 9: 367-377.
45. Kawakami M, Murase T, Ogawa H, Ishibashi S, Mori N, et al. (1987) Human recombinant TNF suppresses lipoprotein lipase activity and stimulates lipolysis in 3T3-L1 cells. J Biochem 101: 331-338.
46. van Hall G, Steensberg A, Sacchetti M, Fischer C, Keller C, et al. (2003) Interleukin-6 stimulates lipolysis and fat oxidation in humans. J Clin Endocrinol Metab 88: 3005-3010.
47. Rasouli N, Kern PA (2008) Adipocytokines and the metabolic complications of obesity. J Clin Endocrinol Metab 93: S64-73.

48. Senn JJ, Klover PJ, Nowak IA, Mooney RA (2002) Interleukin-6 induces cellular insulin resistance in hepatocytes. Diabetes 51: 3391-3399.

49. Klover PJ, Zimmers TA, Koniaris LG, Mooney RA (2003) Chronic exposure to interleukin-6 causes hepatic insulin resistance in mice. Diabetes 52: 2784-2789.

50. Zimmet P, Alberti KG, Shaw J (2001) Global and societal implications of the diabetes epidemic. Nature 414: 782-787.

51. Smyth S, Heron A (2006) Diabetes and obesity: the twin epidemics. Nat Med 12: 75-80.

52. Fowler MJ (2008) Microvascular and macrovascular complications of diabetes. Clinical diabetes 26: 77-82.

53. Mouse Genome Sequencing C, Waterston RH, Lindblad-Toh K, Birney E, Rogers J, et al. (2002) Initial sequencing and comparative analysis of the mouse genome. Nature 420: 520-562.

54. Rosenthal N, Brown S (2007) The mouse ascending: perspectives for human-disease models. Nat Cell Biol 9: 993-999.

55. Kennedy AJ, Ellacott KL, King VL, Hasty AH (2010) Mouse models of the metabolic syndrome. Dis Model Mech 3: 156-166.

56. Kanuri G, Bergheim I (2013) In Vitro and in Vivo Models of Non-Alcoholic Fatty Liver Disease (NAFLD). Int J Mol Sci 14: 11963-11980.

57. Osborn O, Sanchez-Alavez M, Brownell SE, Ross B, Klaus J, et al. (2010) Metabolic characterization of a mouse deficient in all known leptin receptor isoforms. Cell Mol Neurobiol 30: 23-33.

58. Hummel KP, Dickie MM, Coleman DL (1966) Diabetes, a new mutation in the mouse. Science 153: 1127-1128.

59. Ingalls AM, Dickie MM, Snell GD (1950) Obese, a new mutation in the house mouse. J Hered 41: 317-318.

60. Kluge R, Scherneck S, Schurmann A, Joost HG (2012) Pathophysiology and genetics of obesity and diabetes in the New Zealand obese mouse: a model of the human metabolic syndrome. Methods Mol Biol 933: 59-73.

61. Kurtz TW, Morris RC, Pershadsingh HA (1989) The Zucker fatty rat as a genetic model of obesity and hypertension. Hypertension 13: 896-901.

62. Peterson RG, Shaw WN, Neel M-A, Little LA, Eichberg J (1990) Zucker Diabetic Fatty Rat as a Model for Non-insulin-dependent Diabetes Mellitus. ILAR Journal 32: 16-19.

63. Balthasar N, Dalgaard LT, Lee CE, Yu J, Funahashi H, et al. (2005) Divergence of melanocortin pathways in the control of food intake and energy expenditure. Cell 123: 493-505.

64. Huszar D, Lynch CA, Fairchild-Huntress V, Dunmore JH, Fang Q, et al. (1997) Targeted disruption of the melanocortin-4 receptor results in obesity in mice. Cell 88: 131-141.

65. Winzell MS, Ahren B (2004) The high-fat diet-fed mouse: a model for studying mechanisms and treatment of impaired glucose tolerance and type 2 diabetes. Diabetes 53 Suppl 3: S215-219.

66. Buettner R, Scholmerich J, Bollheimer LC (2007) High-fat diets: modeling the metabolic disorders of human obesity in rodents. Obesity (Silver Spring) 15: 798-808.

67. Montgomery MK, Hallahan NL, Brown SH, Liu M, Mitchell TW, et al. (2013) Mouse strain-dependent variation in obesity and glucose homeostasis in response to high-fat feeding. Diabetologia 56: 1129-1139.

68. Surwit RS, Kuhn CM, Cochrane C, McCubbin JA, Feinglos MN (1988) Diet-induced type II diabetes in C57BL/6J mice. Diabetes 37: 1163-1167.

69. Rinella ME, Green RM (2004) The methionine-choline deficient dietary model of steatohepatitis does not exhibit insulin resistance. J Hepatol 40: 47-51.

70. Rinella ME, Elias MS, Smolak RR, Fu T, Borensztajn J, et al. (2008) Mechanisms of hepatic steatosis in mice fed a lipogenic methionine choline-deficient diet. J Lipid Res 49: 1068-1076.

71. Spruss A, Bergheim I (2009) Dietary fructose and intestinal barrier: potential risk factor in the pathogenesis of nonalcoholic fatty liver disease. J Nutr Biochem 20: 657-662.

72. Tappy L, Le KA, Tran C, Paquot N (2010) Fructose and metabolic diseases: new findings, new questions. Nutrition 26: 1044-1049.

73. Charlton M, Krishnan A, Viker K, Sanderson S, Cazanave S, et al. (2011) Fast food diet mouse: novel small animal model of NASH with ballooning, progressive fibrosis, and high physiological fidelity to the human condition. Am J Physiol Gastrointest Liver Physiol 301: G825-834.

74. Tsuchiya H, Ebata Y, Sakabe T, Hama S, Kogure K, et al. (2013) High-fat, high-fructose diet induces hepatic iron overload via a hepcidin-independent mechanism prior to the onset of liver steatosis and insulin resistance in mice. Metabolism 62: 62-69.

75. Ford ES, Giles WH, Dietz WH (2002) Prevalence of the metabolic syndrome among US adults: findings from the third National Health and Nutrition Examination Survey. JAMA 287: 356-359.

76. Vishram JK, Borglykke A, Andreasen AH, Jeppesen J, Ibsen H, et al. (2014) Impact of age and gender on the prevalence and prognostic importance of the metabolic syndrome and its components in Europeans. The MORGAM Prospective Cohort Project. PLoS One 9: e107294.

77. Bertolotti M, Lonardo A, Mussi C, Baldelli E, Pellegrini E, et al. (2014) Nonalcoholic fatty liver disease and aging: epidemiology to management. World J Gastroenterol 20: 14185-14204.

78. Baratta JL, Ngo A, Lopez B, Kasabwalla N, Longmuir KJ, et al. (2009) Cellular organization of normal mouse liver: a histological, quantitative immunocytochemical, and fine structural analysis. Histochem Cell Biol 131: 713-726.

79. Prager R, Wallace P, Olefsky JM (1987) Direct and indirect effects of insulin to inhibit hepatic glucose output in obese subjects. Diabetes 36: 607-611.

80. Lewis GF, Zinman B, Groenewoud Y, Vranic M, Giacca A (1996) Hepatic glucose production is regulated both by direct hepatic and extrahepatic effects of insulin in humans. Diabetes 45: 454-462.

81. Ito K, Maruyama H, Hirose H, Kido K, Koyama K, et al. (1995) Exogenous insulin dose-dependently suppresses glucopenia-induced glucagon secretion from perfused rat pancreas. Metabolism 44: 358-362.

82. Sindelar DK, Chu CA, Rohlie M, Neal DW, Swift LL, et al. (1997) The role of fatty acids in mediating the effects of peripheral insulin on hepatic glucose production in the conscious dog. Diabetes 46: 187-196.

83. Edgerton DS, Ramnanan CJ, Grueter CA, Johnson KM, Lautz M, et al. (2009) Effects of insulin on the metabolic control of hepatic gluconeogenesis in vivo. Diabetes 58: 2766-2775.

84. Davis SN, Colburn C, Dobbins R, Nadeau S, Neal D, et al. (1995) Evidence that the brain of the conscious dog is insulin sensitive. J Clin Invest 95: 593-602.

85. la Fleur SE, Kalsbeek A, Wortel J, Buijs RM (2000) Polysynaptic neural pathways between the hypothalamus, including the suprachiasmatic nucleus, and the liver. Brain Res 871: 50-56.

86. Sindelar DK, Chu CA, Venson P, Donahue EP, Neal DW, et al. (1998) Basal hepatic glucose production is regulated by the portal vein insulin concentration. Diabetes 47: 523-529.

87. Edgerton DS, Lautz M, Scott M, Everett CA, Stettler KM, et al. (2006) Insulin's direct effects on the liver dominate the control of hepatic glucose production. J Clin Invest 116: 521-527.

88. Buettner C, Patel R, Muse ED, Bhanot S, Monia BP, et al. (2005) Severe impairment in liver insulin signaling fails to alter hepatic insulin action in conscious mice. J Clin Invest 115: 1306-1313.

89. Okamoto H, Obici S, Accili D, Rossetti L (2005) Restoration of liver insulin signaling in Insr knockout mice fails to normalize hepatic insulin action. J Clin Invest 115: 1314-1322.

90. Rose AJ, Herzig S (2013) Metabolic control through glucocorticoid hormones: an update. Mol Cell Endocrinol 380: 65-78.

91. Lin HV, Accili D (2011) Hormonal regulation of hepatic glucose production in health and disease. Cell Metab 14: 9-19.

92. Nguyen P, Leray V, Diez M, Serisier S, Le Bloc'h J, et al. (2008) Liver lipid metabolism. J Anim Physiol Anim Nutr (Berl) 92: 272-283.

93. Ginsberg HN, Zhang YL, Hernandez-Ono A (2005) Regulation of plasma triglycerides in insulin resistance and diabetes. Arch Med Res 36: 232-240.

94. Mead JR, Irvine SA, Ramji DP (2002) Lipoprotein lipase: structure, function, regulation, and role in disease. J Mol Med (Berl) 80: 753-769.

95. Narvekar P, Berriel Diaz M, Krones-Herzig A, Hardeland U, Strzoda D, et al. (2009) Liver-specific loss of lipolysis-stimulated lipoprotein receptor triggers systemic hyperlipidemia in mice. Diabetes 58: 1040-1049.

96. Lusis AJ, Pajukanta P (2008) A treasure trove for lipoprotein biology. Nat Genet 40: 129-130.
97. Daniels TF, Killinger KM, Michal JJ, Wright RW, Jr., Jiang Z (2009) Lipoproteins, cholesterol homeostasis and cardiac health. Int J Biol Sci 5: 474-488.
98. Fisher EA, Ginsberg HN (2002) Complexity in the secretory pathway: the assembly and secretion of apolipoprotein B-containing lipoproteins. J Biol Chem 277: 17377-17380.
99. Loh KC, Tan MH (1996) Reverse cholesterol transport: its contribution to cholesterol catabolism in normal and disease states. Can J Cardiol 12: 944-950.
100. van der Velde AE (2010) Reverse cholesterol transport: from classical view to new insights. World J Gastroenterol 16: 5908-5915.
101. Mahley RW, Huang Y, Weisgraber KH (2006) Putting cholesterol in its place: apoE and reverse cholesterol transport. J Clin Invest 116: 1226-1229.
102. Cooney MT, Dudina A, De Bacquer D, Wilhelmsen L, Sans S, et al. (2009) HDL cholesterol protects against cardiovascular disease in both genders, at all ages and at all levels of risk. Atherosclerosis 206: 611-616.
103. Ginsberg HN (1996) Diabetic dyslipidemia: basic mechanisms underlying the common hypertriglyceridemia and low HDL cholesterol levels. Diabetes 45 Suppl 3: S27-30.
104. Chahil TJ, Ginsberg HN (2006) Diabetic dyslipidemia. Endocrinol Metab Clin North Am 35: 491-510, vii-viii.
105. Klop B, Elte JW, Cabezas MC (2013) Dyslipidemia in obesity: mechanisms and potential targets. Nutrients 5: 1218-1240.
106. Mooradian AD (2009) Dyslipidemia in type 2 diabetes mellitus. Nat Clin Pract Endocrinol Metab 5: 150-159.
107. Bays HE, Toth PP, Kris-Etherton PM, Abate N, Aronne LJ, et al. (2013) Obesity, adiposity, and dyslipidemia: a consensus statement from the National Lipid Association. J Clin Lipidol 7: 304-383.
108. Russo MW, Hoofnagle JH, Gu J, Fontana RJ, Barnhart H, et al. (2014) Spectrum of statin hepatotoxicity: experience of the drug-induced liver injury network. Hepatology 60: 679-686.
109. Fuhrmeister J, Tews M, Kromer A, Moosmann B (2012) Prooxidative toxicity and selenoprotein suppression by cerivastatin in muscle cells. Toxicol Lett 215: 219-227.
110. Rader DJ, Daugherty A (2008) Translating molecular discoveries into new therapies for atherosclerosis. Nature 451: 904-913.
111. Kosmas CE, Frishman WH (2014) New and Emerging LDL Cholesterol-Lowering Drugs. Am J Ther.
112. Korenblat KM, Fabbrini E, Mohammed BS, Klein S (2008) Liver, muscle, and adipose tissue insulin action is directly related to intrahepatic triglyceride content in obese subjects. Gastroenterology 134: 1369-1375.
113. Kim JK, Fillmore JJ, Chen Y, Yu C, Moore IK, et al. (2001) Tissue-specific overexpression of lipoprotein lipase causes tissue-specific insulin resistance. Proc Natl Acad Sci U S A 98: 7522-7527.

114. Hajri T, Han XX, Bonen A, Abumrad NA (2002) Defective fatty acid uptake modulates insulin responsiveness and metabolic responses to diet in CD36-null mice. J Clin Invest 109: 1381-1389.

115. Stefan N, Kantartzis K, Machann J, Schick F, Thamer C, et al. (2008) Identification and characterization of metabolically benign obesity in humans. Arch Intern Med 168: 1609-1616.

116. Fabbrini E, Magkos F, Mohammed BS, Pietka T, Abumrad NA, et al. (2009) Intrahepatic fat, not visceral fat, is linked with metabolic complications of obesity. Proc Natl Acad Sci U S A 106: 15430-15435.

117. Stefan N, Haring HU (2013) The role of hepatokines in metabolism. Nat Rev Endocrinol 9: 144-152.

118. Abdul-Wahed A, Gautier-Stein A, Casteras S, Soty M, Roussel D, et al. (2014) A link between hepatic glucose production and peripheral energy metabolism via hepatokines. Mol Metab 3: 531-543.

119. Szendroedi J, Phielix E, Roden M (2012) The role of mitochondria in insulin resistance and type 2 diabetes mellitus. Nat Rev Endocrinol 8: 92-103.

120. Martin SD, Morrison S, Konstantopoulos N, McGee SL (2014) Mitochondrial dysfunction has divergent, cell type-dependent effects on insulin action. Mol Metab 3: 408-418.

121. Koliaki C, Roden M (2014) Do mitochondria care about insulin resistance? Mol Metab 3: 351-353.

122. Schenk S, Saberi M, Olefsky JM (2008) Insulin sensitivity: modulation by nutrients and inflammation. J Clin Invest 118: 2992-3002.

123. Nagle CA, Klett EL, Coleman RA (2009) Hepatic triacylglycerol accumulation and insulin resistance. J Lipid Res 50 Suppl: S74-79.

124. Perry RJ, Samuel VT, Petersen KF, Shulman GI (2014) The role of hepatic lipids in hepatic insulin resistance and type 2 diabetes. Nature 510: 84-91.

125. Ng Y, Ramm G, James DE (2010) Dissecting the mechanism of insulin resistance using a novel heterodimerization strategy to activate Akt. J Biol Chem 285: 5232-5239.

126. Dong XC, Copps KD, Guo S, Li Y, Kollipara R, et al. (2008) Inactivation of hepatic Foxo1 by insulin signaling is required for adaptive nutrient homeostasis and endocrine growth regulation. Cell Metab 8: 65-76.

127. Lu M, Wan M, Leavens KF, Chu Q, Monks BR, et al. (2012) Insulin regulates liver metabolism in vivo in the absence of hepatic Akt and Foxo1. Nat Med 18: 388-395.

128. Cheng Z, White MF (2012) The AKTion in non-canonical insulin signaling. Nat Med 18: 351-353.

129. Rebrin K, Steil GM, Getty L, Bergman RN (1995) Free fatty acid as a link in the regulation of hepatic glucose output by peripheral insulin. Diabetes 44: 1038-1045.

130. Bergman RN, Ader M (2000) Free fatty acids and pathogenesis of type 2 diabetes mellitus. Trends Endocrinol Metab 11: 351-356.

131. Mittelman SD, Fu YY, Rebrin K, Steil G, Bergman RN (1997) Indirect effect of insulin to suppress endogenous glucose production is dominant, even with hyperglucagonemia. J Clin Invest 100: 3121-3130.

132. Ferreira DM, Castro RE, Machado MV, Evangelista T, Silvestre A, et al. (2011) Apoptosis and insulin resistance in liver and peripheral tissues of morbidly obese patients is associated with different stages of non-alcoholic fatty liver disease. Diabetologia 54: 1788-1798.

133. Garcia-Monzon C, Lo Iacono O, Mayoral R, Gonzalez-Rodriguez A, Miquilena-Colina ME, et al. (2011) Hepatic insulin resistance is associated with increased apoptosis and fibrogenesis in nonalcoholic steatohepatitis and chronic hepatitis C. J Hepatol 54: 142-152.

134. Alkhouri N, Gornicka A, Berk MP, Thapaliya S, Dixon LJ, et al. (2010) Adipocyte apoptosis, a link between obesity, insulin resistance, and hepatic steatosis. J Biol Chem 285: 3428-3438.

135. Krijnen PA, Simsek S, Niessen HW (2009) Apoptosis in diabetes. Apoptosis 14: 1387-1388.

136. Unger RH, Orci L (2002) Lipoapoptosis: its mechanism and its diseases. Biochim Biophys Acta 1585: 202-212.

137. Elledge SJ (1996) Cell cycle checkpoints: preventing an identity crisis. Science 274: 1664-1672.

138. Canman CE, Lim DS (1998) The role of ATM in DNA damage responses and cancer. Oncogene 17: 3301-3308.

139. Lakin ND, Jackson SP (1999) Regulation of p53 in response to DNA damage. Oncogene 18: 7644-7655.

140. Dhanasekaran DN, Reddy EP (2008) JNK signaling in apoptosis. Oncogene 27: 6245-6251.

141. Chen YR, Wang X, Templeton D, Davis RJ, Tan TH (1996) The role of c-Jun N-terminal kinase (JNK) in apoptosis induced by ultraviolet C and gamma radiation. Duration of JNK activation may determine cell death and proliferation. J Biol Chem 271: 31929-31936.

142. Wada T, Penninger JM (2004) Mitogen-activated protein kinases in apoptosis regulation. Oncogene 23: 2838-2849.

143. Abdollahi A, Lord KA, Hoffman-Liebermann B, Liebermann DA (1991) Sequence and expression of a cDNA encoding MyD118: a novel myeloid differentiation primary response gene induced by multiple cytokines. Oncogene 6: 165-167.

144. Zhang W, Bae I, Krishnaraju K, Azam N, Fan W, et al. (1999) CR6: A third member in the MyD118 and Gadd45 gene family which functions in negative growth control. Oncogene 18: 4899-4907.

145. Fornace AJ, Jr., Alamo I, Jr., Hollander MC (1988) DNA damage-inducible transcripts in mammalian cells. Proc Natl Acad Sci U S A 85: 8800-8804.

146. Fornace AJ, Jr., Nebert DW, Hollander MC, Luethy JD, Papathanasiou M, et al. (1989) Mammalian genes coordinately regulated by growth arrest signals and DNA-damaging agents. Mol Cell Biol 9: 4196-4203.

147. Flicek P, Amode MR, Barrell D, Beal K, Brent S, et al. (2011) Ensembl 2011. Nucleic Acids Res 39: D800-806.

148. Vairapandi M, Balliet AG, Fornace AJ, Jr., Hoffman B, Liebermann DA (1996) The differentiation primary response gene MyD118, related to GADD45, encodes for a nuclear protein which interacts with PCNA and p21WAF1/CIP1. Oncogene 12: 2579-2594.

149. Kearsey JM, Coates PJ, Prescott AR, Warbrick E, Hall PA (1995) Gadd45 is a nuclear cell cycle regulated protein which interacts with p21Cip1. Oncogene 11: 1675-1683.

150. Kovalsky O, Lung FD, Roller PP, Fornace AJ, Jr. (2001) Oligomerization of human Gadd45a protein. J Biol Chem 276: 39330-39339.

151. Schrag JD, Jiralerspong S, Banville M, Jaramillo ML, O'Connor-McCourt MD (2008) The crystal structure and dimerization interface of GADD45gamma. Proc Natl Acad Sci U S A 105: 6566-6571.

152. Tornatore L, Marasco D, Dathan N, Vitale RM, Benedetti E, et al. (2008) Gadd45 beta forms a homodimeric complex that binds tightly to MKK7. J Mol Biol 378: 97-111.

153. Liebermann DA, Tront JS, Sha X, Mukherjee K, Mohamed-Hadley A, et al. (2011) Gadd45 stress sensors in malignancy and leukemia. Crit Rev Oncog 16: 129-140.

154. Wang XW, Zhan Q, Coursen JD, Khan MA, Kontny HU, et al. (1999) GADD45 induction of a G2/M cell cycle checkpoint. Proc Natl Acad Sci U S A 96: 3706-3711.

155. Gupta M, Gupta SK, Balliet AG, Hollander MC, Fornace AJ, et al. (2005) Hematopoietic cells from Gadd45a- and Gadd45b-deficient mice are sensitized to genotoxic-stress-induced apoptosis. Oncogene 24: 7170-7179.

156. De Smaele E, Zazzeroni F, Papa S, Nguyen DU, Jin R, et al. (2001) Induction of gadd45beta by NF-kappaB downregulates pro-apoptotic JNK signalling. Nature 414: 308-313.

157. Zhan Q, Lord KA, Alamo I, Jr., Hollander MC, Carrier F, et al. (1994) The gadd and MyD genes define a novel set of mammalian genes encoding acidic proteins that synergistically suppress cell growth. Mol Cell Biol 14: 2361-2371.

158. Fan W, Richter G, Cereseto A, Beadling C, Smith KA (1999) Cytokine response gene 6 induces p21 and regulates both cell growth and arrest. Oncogene 18: 6573-6582.

159. Vairapandi M, Balliet AG, Hoffman B, Liebermann DA (2002) GADD45b and GADD45g are cdc2/cyclinB1 kinase inhibitors with a role in S and G2/M cell cycle checkpoints induced by genotoxic stress. J Cell Physiol 192: 327-338.

160. Smith ML, Chen IT, Zhan Q, Bae I, Chen CY, et al. (1994) Interaction of the p53-regulated protein Gadd45 with proliferating cell nuclear antigen. Science 266: 1376-1380.

161. Hall PA, Kearsey JM, Coates PJ, Norman DG, Warbrick E, et al. (1995) Characterisation of the interaction between PCNA and Gadd45. Oncogene 10: 2427-2433.

162. Azam N, Vairapandi M, Zhang W, Hoffman B, Liebermann DA (2001) Interaction of CR6 (GADD45gamma) with proliferating cell nuclear antigen impedes negative growth control. J Biol Chem 276: 2766-2774.

163. Zhan Q, Antinore MJ, Wang XW, Carrier F, Smith ML, et al. (1999) Association with Cdc2 and inhibition of Cdc2/Cyclin B1 kinase activity by the p53-regulated protein Gadd45. Oncogene 18: 2892-2900.

164. Jin S, Antinore MJ, Lung FD, Dong X, Zhao H, et al. (2000) The GADD45 inhibition of Cdc2 kinase correlates with GADD45-mediated growth suppression. J Biol Chem 275: 16602-16608.

165. Takekawa M, Saito H (1998) A family of stress-inducible GADD45-like proteins mediate activation of the stress-responsive MTK1/MEKK4 MAPKKK. Cell 95: 521-530.

166. Kastan MB, Zhan Q, el-Deiry WS, Carrier F, Jacks T, et al. (1992) A mammalian cell cycle checkpoint pathway utilizing p53 and GADD45 is defective in ataxia-telangiectasia. Cell 71: 587-597.

167. Zhan Q, Bae I, Kastan MB, Fornace AJ, Jr. (1994) The p53-dependent gamma-ray response of GADD45. Cancer Res 54: 2755-2760.

168. Hollander MC, Alamo I, Jackman J, Wang MG, McBride OW, et al. (1993) Analysis of the mammalian gadd45 gene and its response to DNA damage. J Biol Chem 268: 24385-24393.

169. Yoo J, Ghiassi M, Jirmanova L, Balliet AG, Hoffman B, et al. (2003) Transforming growth factor-beta-induced apoptosis is mediated by Smad-dependent expression of GADD45b through p38 activation. J Biol Chem 278: 43001-43007.

170. Selvakumaran M, Lin HK, Sjin RT, Reed JC, Liebermann DA, et al. (1994) The novel primary response gene MyD118 and the proto-oncogenes myb, myc, and bcl-2 modulate transforming growth factor beta 1-induced apoptosis of myeloid leukemia cells. Mol Cell Biol 14: 2352-2360.

171. Papa S, Zazzeroni F, Pham CG, Bubici C, Franzoso G (2004) Linking JNK signaling to NF-kappaB: a key to survival. J Cell Sci 117: 5197-5208.

172. Karin M (2014) Whipping NF-kappaB to Submission via GADD45 and MKK7. Cancer Cell 26: 447-449.

173. Rai K, Huggins IJ, James SR, Karpf AR, Jones DA, et al. (2008) DNA demethylation in zebrafish involves the coupling of a deaminase, a glycosylase, and gadd45. Cell 135: 1201-1212.

174. Barreto G, Schafer A, Marhold J, Stach D, Swaminathan SK, et al. (2007) Gadd45a promotes epigenetic gene activation by repair-mediated DNA demethylation. Nature 445: 671-675.

175. Niehrs C, Schafer A (2012) Active DNA demethylation by Gadd45 and DNA repair. Trends Cell Biol 22: 220-227.

176. Ma DK, Guo JU, Ming GL, Song H (2009) DNA excision repair proteins and Gadd45 as molecular players for active DNA demethylation. Cell Cycle 8: 1526-1531.

177. Carrier F, Georgel PT, Pourquier P, Blake M, Kontny HU, et al. (1999) Gadd45, a p53-responsive stress protein, modifies DNA accessibility on damaged chromatin. Mol Cell Biol 19: 1673-1685.

178. Sytnikova YA, Kubarenko AV, Schafer A, Weber AN, Niehrs C (2011) Gadd45a is an RNA binding protein and is localized in nuclear speckles. PLoS One 6: e14500.

179. Kaufmann LT, Gierl MS, Niehrs C (2011) Gadd45a, Gadd45b and Gadd45g expression during mouse embryonic development. Gene Expr Patterns 11: 465-470.

180. Liebermann DA, Hoffman B (2008) Gadd45 in stress signaling. J Mol Signal 3: 15.

181. Huang HS, Kubish GM, Redmond TM, Turner DL, Thompson RC, et al. (2010) Direct transcriptional induction of Gadd45gamma by Ascl1 during neuronal differentiation. Mol Cell Neurosci 44: 282-296.

182. de la Calle-Mustienes E, Glavic A, Modolell J, Gomez-Skarmeta JL (2002) Xiro homeoproteins coordinate cell cycle exit and primary neuron formation by upregulating neuronal-fate repressors and downregulating the cell-cycle inhibitor XGadd45-gamma. Mech Dev 119: 69-80.

183. Johnen H, Gonzalez-Silva L, Carramolino L, Flores JM, Torres M, et al. (2013) Gadd45g is essential for primary sex determination, male fertility and testis development. PLoS One 8: e58751.

184. Kawahara A, Che YS, Hanaoka R, Takeda H, Dawid IB (2005) Zebrafish GADD45beta genes are involved in somite segmentation. Proc Natl Acad Sci U S A 102: 361-366.

185. Ijiri K, Zerbini LF, Peng H, Correa RG, Lu B, et al. (2005) A novel role for GADD45beta as a mediator of MMP-13 gene expression during chondrocyte terminal differentiation. J Biol Chem 280: 38544-38555.

186. Ma DK, Jang MH, Guo JU, Kitabatake Y, Chang ML, et al. (2009) Neuronal activity-induced Gadd45b promotes epigenetic DNA demethylation and adult neurogenesis. Science 323: 1074-1077.

187. Thalheimer FB, Wingert S, De Giacomo P, Haetscher N, Rehage M, et al. (2014) Cytokine-regulated GADD45G induces differentiation and lineage selection in hematopoietic stem cells. Stem Cell Reports 3: 34-43.

188. Hoffman B, Liebermann DA (2007) Role of gadd45 in myeloid cells in response to hematopoietic stress. Blood Cells Mol Dis 39: 344-347.

189. Yang J, Zhu H, Murphy TL, Ouyang W, Murphy KM (2001) IL-18-stimulated GADD45 beta required in cytokine-induced, but not TCR-induced, IFN-gamma production. Nat Immunol 2: 157-164.

190. Lu B, Yu H, Chow C, Li B, Zheng W, et al. (2001) GADD45gamma mediates the activation of the p38 and JNK MAP kinase pathways and cytokine production in effector TH1 cells. Immunity 14: 583-590.

191. Ju S, Zhu Y, Liu L, Dai S, Li C, et al. (2009) Gadd45b and Gadd45g are important for anti-tumor immune responses. Eur J Immunol 39: 3010-3018.

192. Liu L, Tran E, Zhao Y, Huang Y, Flavell R, et al. (2005) Gadd45 beta and Gadd45 gamma are critical for regulating autoimmunity. J Exp Med 202: 1341-1347.

193. Matsunaga E, Nambu S, Oka M, Iriki A (2015) Comparative analysis of developmentally regulated expressions of Gadd45a, Gadd45b, and Gadd45g in the mouse and marmoset cerebral cortex. Neuroscience 284: 566-580.

194. Sultan FA, Sweatt JD (2013) The role of the Gadd45 family in the nervous system: a focus on neurodevelopment, neuronal injury, and cognitive neuroepigenetics. Adv Exp Med Biol 793: 81-119.

195. Liu B, Li LL, Tan XD, Zhang YH, Jiang Y, et al. (2014) Gadd45b Mediates Axonal Plasticity and Subsequent Functional Recovery After Experimental Stroke in Rats. Mol Neurobiol.

196. Leach PT, Poplawski SG, Kenney JW, Hoffman B, Liebermann DA, et al. (2012) Gadd45b knockout mice exhibit selective deficits in hippocampus-dependent long-term memory. Learn Mem 19: 319-324.

197. Harkin DP, Bean JM, Miklos D, Song YH, Truong VB, et al. (1999) Induction of GADD45 and JNK/SAPK-dependent apoptosis following inducible expression of BRCA1. Cell 97: 575-586.

198. Hildesheim J, Bulavin DV, Anver MR, Alvord WG, Hollander MC, et al. (2002) Gadd45a protects against UV irradiation-induced skin tumors, and promotes apoptosis and stress signaling via MAPK and p53. Cancer Res 62: 7305-7315.

199. Papa S, Zazzeroni F, Bubici C, Jayawardena S, Alvarez K, et al. (2004) Gadd45 beta mediates the NF-kappa B suppression of JNK signalling by targeting MKK7/JNKK2. Nat Cell Biol 6: 146-153.

200. Nagai H, Noguchi T, Takeda K, Ichijo H (2007) Pathophysiological roles of ASK1-MAP kinase signaling pathways. J Biochem Mol Biol 40: 1-6.

201. Oh-Hashi K, Maruyama W, Isobe K (2001) Peroxynitrite induces GADD34, 45, and 153 VIA p38 MAPK in human neuroblastoma SH-SY5Y cells. Free Radic Biol Med 30: 213-221.

202. Yamamoto Y, Moore R, Flavell RA, Lu B, Negishi M (2010) Nuclear receptor CAR represses TNFalpha-induced cell death by interacting with the anti-apoptotic GADD45B. PLoS One 5: e10121.

203. Tian J, Huang H, Hoffman B, Liebermann DA, Ledda-Columbano GM, et al. (2011) Gadd45beta is an inducible coactivator of transcription that facilitates rapid liver growth in mice. J Clin Invest 121: 4491-4502.

204. Columbano A, Ledda-Columbano GM, Pibiri M, Cossu C, Menegazzi M, et al. (2005) Gadd45beta is induced through a CAR-dependent, TNF-independent pathway in murine liver hyperplasia. Hepatology 42: 1118-1126.

205. Yi YW, Kim D, Jung N, Hong SS, Lee HS, et al. (2000) Gadd45 family proteins are coactivators of nuclear hormone receptors. Biochem Biophys Res Commun 272: 193-198.

206. Jazwinski SM (1998) Genetics of longevity. Exp Gerontol 33: 773-783.

207. Saunders LR, Verdin E (2009) Cell biology. Stress response and aging. Science 323: 1021-1022.

208. Moskalev AA, Smit-McBride Z, Shaposhnikov MV, Plyusnina EN, Zhavoronkov A, et al. (2012) Gadd45 proteins: relevance to aging, longevity and age-related pathologies. Ageing Res Rev 11: 51-66.

209. Plyusnina EN, Shaposhnikov MV, Moskalev AA (2011) Increase of Drosophila melanogaster lifespan due to D-GADD45 overexpression in the nervous system. Biogerontology 12: 211-226.

210. Moskalev A, Plyusnina E, Shaposhnikov M, Shilova L, Kazachenok A, et al. (2012) The role of D-GADD45 in oxidative, thermal and genotoxic stress resistance. Cell Cycle 11: 4222-4241.

211. Bgatova N, Dubatolova T, Omelyanchuk L, Plyusnina E, Shaposhnikov M, et al. (2014) Gadd45 expression correlates with age dependent neurodegeneration in Drosophila melanogaster. Biogerontology.

212. Zhang W, Hoffman B, Liebermann DA (2001) Ectopic expression of MyD118/Gadd45/CR6 (Gadd45beta/alpha/gamma) sensitizes neoplastic cells to genotoxic stress-induced apoptosis. Int J Oncol 18: 749-757.

213. Sun L, Gong R, Wan B, Huang X, Wu C, et al. (2003) GADD45gamma, down-regulated in 65% hepatocellular carcinoma (HCC) from 23 chinese patients, inhibits cell growth and induces cell cycle G2/M arrest for hepatoma Hep-G2 cell lines. Mol Biol Rep 30: 249-253.

214. Jiang F, Wang Z (2004) Gadd45gamma is androgen-responsive and growth-inhibitory in prostate cancer cells. Mol Cell Endocrinol 213: 121-129.

215. Ying J, Srivastava G, Hsieh WS, Gao Z, Murray P, et al. (2005) The stress-responsive gene GADD45G is a functional tumor suppressor, with its response to environmental stresses frequently disrupted epigenetically in multiple tumors. Clin Cancer Res 11: 6442-6449.

216. Hollander MC, Sheikh MS, Bulavin DV, Lundgren K, Augeri-Henmueller L, et al. (1999) Genomic instability in Gadd45a-deficient mice. Nat Genet 23: 176-184.

217. Hollander MC, Kovalsky O, Salvador JM, Kim KE, Patterson AD, et al. (2001) Dimethylbenzanthracene carcinogenesis in Gadd45a-null mice is associated with decreased DNA repair and increased mutation frequency. Cancer Res 61: 2487-2491.

218. Tront JS, Hoffman B, Liebermann DA (2006) Gadd45a suppresses Ras-driven mammary tumorigenesis by activation of c-Jun NH2-terminal kinase and p38 stress signaling resulting in apoptosis and senescence. Cancer Res 66: 8448-8454.

219. Zhang W, Li T, Shao Y, Zhang C, Wu Q, et al. (2010) Semi-quantitative detection of GADD45-gamma methylation levels in gastric, colorectal and pancreatic cancers using methylation-sensitive high-resolution melting analysis. J Cancer Res Clin Oncol 136: 1267-1273.

220. Munoz-Najar U, Sedivy JM (2011) Epigenetic control of aging. Antioxid Redox Signal 14: 241-259.

221. Tront JS, Huang Y, Fornace AJ, Jr., Hoffman B, Liebermann DA (2010) Gadd45a functions as a promoter or suppressor of breast cancer dependent on the oncogenic stress. Cancer Res 70: 9671-9681.

222. Torp R, Su JH, Deng G, Cotman CW (1998) GADD45 is induced in Alzheimer's disease, and protects against apoptosis in vitro. Neurobiol Dis 5: 245-252.

223. Santiard-Baron D, Gosset P, Nicole A, Sinet PM, Christen Y, et al. (1999) Identification of beta-amyloid-responsive genes by RNA differential display: early induction of a DNA damage-inducible gene, gadd45. Exp Neurol 158: 206-213.

224. Stokes AH, Freeman WM, Mitchell SG, Burnette TA, Hellmann GM, et al. (2002) Induction of GADD45 and GADD153 in neuroblastoma cells by dopamine-induced toxicity. Neurotoxicology 23: 675-684.

225. Thum T, Borlak J (2008) LOX-1 receptor blockade abrogates oxLDL-induced oxidative DNA damage and prevents activation of the transcriptional repressor Oct-1 in human coronary arterial endothelium. J Biol Chem 283: 19456-19464.

226. Papa S, Zazzeroni F, Fu YX, Bubici C, Alvarez K, et al. (2008) Gadd45beta promotes hepatocyte survival during liver regeneration in mice by modulating JNK signaling. J Clin Invest 118: 1911-1923.

227. Fausto N, Campbell JS, Riehle KJ (2006) Liver regeneration. Hepatology 43: S45-53.

228. Hocker R, Walker A, Schmitz I (2013) Inhibition of autophagy through MAPK14-mediated phosphorylation of ATG5. Autophagy 9: 426-428.

229. Keil E, Hocker R, Schuster M, Essmann F, Ueffing N, et al. (2013) Phosphorylation of Atg5 by the Gadd45beta-MEKK4-p38 pathway inhibits autophagy. Cell Death Differ 20: 321-332.

230. Gantner ML, Hazen BC, Conkright J, Kralli A (2014) GADD45gamma regulates the thermogenic capacity of brown adipose tissue. Proc Natl Acad Sci U S A 111: 11870-11875.

231. Ebert SM, Dyle MC, Kunkel SD, Bullard SA, Bongers KS, et al. (2012) Stress-induced skeletal muscle Gadd45a expression reprograms myonuclei and causes muscle atrophy. J Biol Chem 287: 27290-27301.

232. Bongers KS, Fox DK, Ebert SM, Kunkel SD, Dyle MC, et al. (2013) Skeletal muscle denervation causes skeletal muscle atrophy through a pathway that involves both Gadd45a and HDAC4. Am J Physiol Endocrinol Metab 305: E907-915.

233. Bruemmer D, Yin F, Liu J, Berger JP, Sakai T, et al. (2003) Regulation of the growth arrest and DNA damage-inducible gene 45 (GADD45) by peroxisome proliferator-activated receptor gamma in vascular smooth muscle cells. Circ Res 93: e38-47.

234. Yin F, Bruemmer D, Blaschke F, Hsueh WA, Law RE, et al. (2004) Signaling pathways involved in induction of GADD45 gene expression and apoptosis by troglitazone in human MCF-7 breast carcinoma cells. Oncogene 23: 4614-4623.

235. Bortoff KD, Keeton AB, Franklin JL, Messina JL (2010) Anti-Inflammatory Action of Insulin via Induction of Gadd45-beta Transcription by the mTOR Signaling Pathway. Hepat Med 2001: 79-85.

236. Li H, Yu X (2013) Emerging role of JNK in insulin resistance. Curr Diabetes Rev 9: 422-428.

237. Hirosumi J, Tuncman G, Chang L, Gorgun CZ, Uysal KT, et al. (2002) A central role for JNK in obesity and insulin resistance. Nature 420: 333-336.

238. Berriel Diaz M, Krones-Herzig A, Metzger D, Ziegler A, Vegiopoulos A, et al. (2008) Nuclear receptor cofactor receptor interacting protein 140 controls hepatic triglyceride metabolism during wasting in mice. Hepatology 48: 782-791.

239. Herzig S, Long F, Jhala US, Hedrick S, Quinn R, et al. (2001) CREB regulates hepatic gluconeogenesis through the coactivator PGC-1. Nature 413: 179-183.

240. Kulozik P, Jones A, Mattijssen F, Rose AJ, Reimann A, et al. (2011) Hepatic deficiency in transcriptional cofactor TBL1 promotes liver steatosis and hypertriglyceridemia. Cell Metab 13: 389-400.

241. Lemke U, Krones-Herzig A, Berriel Diaz M, Narvekar P, Ziegler A, et al. (2008) The glucocorticoid receptor controls hepatic dyslipidemia through Hes1. Cell Metab 8: 212-223.

242. Rose AJ, Berriel Diaz M, Reimann A, Klement J, Walcher T, et al. (2011) Molecular control of systemic bile acid homeostasis by the liver glucocorticoid receptor. Cell Metab 14: 123-130.

243. Zumbrun SD, Hoffman B, Liebermann DA (2009) Distinct mechanisms are utilized to induce stress sensor gadd45b by different stress stimuli. J Cell Biochem 108: 1220-1231.

244. Salvador JM, Brown-Clay JD, Fornace AJ, Jr. (2013) Gadd45 in stress signaling, cell cycle control, and apoptosis. Adv Exp Med Biol 793: 1-19.

245. Papathanasiou MA, Kerr NC, Robbins JH, McBride OW, Alamo I, Jr., et al. (1991) Induction by ionizing radiation of the gadd45 gene in cultured human cells: lack of mediation by protein kinase C. Mol Cell Biol 11: 1009-1016.

246. Wang X, Hu Z, Hu J, Du J, Mitch WE (2006) Insulin resistance accelerates muscle protein degradation: Activation of the ubiquitin-proteasome pathway by defects in muscle cell signaling. Endocrinology 147: 4160-4168.

247. Caro JF, Amatruda JM (1982) The regulation of lipid synthesis in freshly isolated and primary cultures of hepatocytes from fasted rats: the primary role of insulin. Metabolism 31: 14-18.

248. Wu JC, Merlino G, Fausto N (1994) Establishment and characterization of differentiated, nontransformed hepatocyte cell lines derived from mice transgenic for transforming growth factor alpha. Proc Natl Acad Sci U S A 91: 674-678.

249. Hardie DG, Ross FA, Hawley SA (2012) AMPK: a nutrient and energy sensor that maintains energy homeostasis. Nat Rev Mol Cell Biol 13: 251-262.

250. Szkudelski T (2001) The mechanism of alloxan and streptozotocin action in B cells of the rat pancreas. Physiol Res 50: 537-546.

251. Leiter EH (1982) Multiple low-dose streptozotocin-induced hyperglycemia and insulitis in C57BL mice: influence of inbred background, sex, and thymus. Proc Natl Acad Sci U S A 79: 630-634.

252. Houtkooper RH, Argmann C, Houten SM, Canto C, Jeninga EH, et al. (2011) The metabolic footprint of aging in mice. Sci Rep 1: 134.

253. Yue F, Cheng Y, Breschi A, Vierstra J, Wu W, et al. (2014) A comparative encyclopedia of DNA elements in the mouse genome. Nature 515: 355-364.

254. Felig P (1973) The glucose-alanine cycle. Metabolism 22: 179-207.

255. Adibi SA (1976) Metabolism of branched-chain amino acids in altered nutrition. Metabolism 25: 1287-1302.

256. Sewell AC, Bohles HJ (1995) Acylcarnitines in intermediary metabolism. Eur J Pediatr 154: 871-877.

257. Gierl MS, Gruhn WH, von Seggern A, Maltry N, Niehrs C (2012) GADD45G functions in male sex determination by promoting p38 signaling and Sry expression. Dev Cell 23: 1032-1042.

258. Matthews DR, Hosker JP, Rudenski AS, Naylor BA, Treacher DF, et al. (1985) Homeostasis model assessment: insulin resistance and beta-cell function from fasting plasma glucose and insulin concentrations in man. Diabetologia 28: 412-419.

259. Moore David D (2012) Nuclear Receptors Reverse McGarry's Vicious Cycle to Insulin Resistance. Cell Metabolism 15: 615-622.

260. Newgard CB, An J, Bain JR, Muehlbauer MJ, Stevens RD, et al. (2009) A branched-chain amino acid-related metabolic signature that differentiates obese and lean humans and contributes to insulin resistance. Cell Metab 9: 311-326.

261. Newgard CB (2012) Interplay between lipids and branched-chain amino acids in development of insulin resistance. Cell Metab 15: 606-614.

262. Lu J, Xie G, Jia W, Jia W (2013) Insulin resistance and the metabolism of branched-chain amino acids. Front Med 7: 53-59.

263. Mai M, Tonjes A, Kovacs P, Stumvoll M, Fiedler GM, et al. (2013) Serum levels of acylcarnitines are altered in prediabetic conditions. PLoS One 8: e82459.

264. Zhang X, Zhang C, Chen L, Han X, Ji L (2014) Human serum acylcarnitine profiles in different glucose tolerance states. Diabetes Res Clin Pract 104: 376-382.

265. Schooneman MG, Vaz FM, Houten SM, Soeters MR (2013) Acylcarnitines: reflecting or inflicting insulin resistance? Diabetes 62: 1-8.

266. Mihalik SJ, Goodpaster BH, Kelley DE, Chace DH, Vockley J, et al. (2010) Increased levels of plasma acylcarnitines in obesity and type 2 diabetes and identification of a marker of glucolipotoxicity. Obesity (Silver Spring) 18: 1695-1700.

267. Koves TR, Ussher JR, Noland RC, Slentz D, Mosedale M, et al. (2008) Mitochondrial overload and incomplete fatty acid oxidation contribute to skeletal muscle insulin resistance. Cell Metab 7: 45-56.

268. Connelly S, Mech C (2004) Delivery of adenoviral DNA to mouse liver. Methods Mol Biol 246: 37-52.

269. Shayakhmetov DM, Li ZY, Ni S, Lieber A (2004) Analysis of adenovirus sequestration in the liver, transduction of hepatic cells, and innate toxicity after injection of fiber-modified vectors. J Virol 78: 5368-5381.

270. Nakatani Y, Kaneto H, Kawamori D, Hatazaki M, Miyatsuka T, et al. (2004) Modulation of the JNK pathway in liver affects insulin resistance status. J Biol Chem 279: 45803-45809.

271. Liu Z, Cao W (2009) p38 mitogen-activated protein kinase: a critical node linking insulin resistance and cardiovascular diseases in type 2 diabetes mellitus. Endocr Metab Immune Disord Drug Targets 9: 38-46.

272. Vallerie SN, Hotamisligil GS (2010) The role of JNK proteins in metabolism. Sci Transl Med 2: 60rv65.

273. Um SH, D'Alessio D, Thomas G (2006) Nutrient overload, insulin resistance, and ribosomal protein S6 kinase 1, S6K1. Cell Metabolism 3: 393-402.

274. Um SH, Frigerio F, Watanabe M, Picard F, Joaquin M, et al. (2004) Absence of S6K1 protects against age- and diet-induced obesity while enhancing insulin sensitivity. Nature 431: 200-205.

275. Bae EJ, Xu J, Oh DY, Bandyopadhyay G, Lagakos WS, et al. (2012) Liver-specific p70 S6 Kinase Depletion Protects against Hepatic Steatosis and Systemic Insulin Resistance. Journal of Biological Chemistry 287: 18769-18780.

276. Chirmule N, Propert K, Magosin S, Qian Y, Qian R, et al. (1999) Immune responses to adenovirus and adeno-associated virus in humans. Gene Ther 6: 1574-1583.

277. Grimm D, Kern A, Rittner K, Kleinschmidt JA (1998) Novel tools for production and purification of recombinant adenoassociated virus vectors. Hum Gene Ther 9: 2745-2760.

278. Gao GP, Alvira MR, Wang L, Calcedo R, Johnston J, et al. (2002) Novel adeno-associated viruses from rhesus monkeys as vectors for human gene therapy. Proc Natl Acad Sci U S A 99: 11854-11859.

279. Graham T, McIntosh J, Work LM, Nathwani A, Baker AH (2008) Performance of AAV8 vectors expressing human factor IX from a hepatic-selective promoter following intravenous injection into rats. Genet Vaccines Ther 6: 9.

280. Hakvoort TB, Moerland PD, Frijters R, Sokolovic A, Labruyere WT, et al. (2011) Interorgan coordination of the murine adaptive response to fasting. J Biol Chem 286: 16332-16343.

281. Zhang F, Xu X, Zhou B, He Z, Zhai Q (2011) Gene expression profile change and associated physiological and pathological effects in mouse liver induced by fasting and refeeding. PLoS One 6: e27553.

282. Bauer M, Hamm AC, Bonaus M, Jacob A, Jaekel J, et al. (2004) Starvation response in mouse liver shows strong correlation with life-span-prolonging processes. Physiol Genomics 17: 230-244.

283. Shan J, Lopez MC, Baker HV, Kilberg MS (2010) Expression profiling after activation of amino acid deprivation response in HepG2 human hepatoma cells. Physiol Genomics 41: 315-327.

284. Kersten S, Seydoux J, Peters JM, Gonzalez FJ, Desvergne B, et al. (1999) Peroxisome proliferator-activated receptor alpha mediates the adaptive response to fasting. J Clin Invest 103: 1489-1498.

285. Cariou B, van Harmelen K, Duran-Sandoval D, van Dijk T, Grefhorst A, et al. (2005) Transient impairment of the adaptive response to fasting in FXR-deficient mice. FEBS Lett 579: 4076-4080.

286. Ding X, Lichti K, Kim I, Gonzalez FJ, Staudinger JL (2006) Regulation of constitutive androstane receptor and its target genes by fasting, cAMP, hepatocyte nuclear factor alpha, and the coactivator peroxisome proliferator-activated receptor gamma coactivator-1alpha. J Biol Chem 281: 26540-26551.

287. Yoon JC, Puigserver P, Chen G, Donovan J, Wu Z, et al. (2001) Control of hepatic gluconeogenesis through the transcriptional coactivator PGC-1. Nature 413: 131-138.

288. Zhang YK, Wu KC, Klaassen CD (2013) Genetic activation of Nrf2 protects against fasting-induced oxidative stress in livers of mice. PLoS One 8: e59122.

289. Shoelson SE, Lee J, Goldfine AB (2006) Inflammation and insulin resistance. J Clin Invest 116: 1793-1801.

290. Schrauwen P, Hesselink MK (2004) Oxidative capacity, lipotoxicity, and mitochondrial damage in type 2 diabetes. Diabetes 53: 1412-1417.

291. Montgomery MK, Turner N (2015) Mitochondrial dysfunction and insulin resistance: an update. Endocr Connect 4: R1-R15.

292. Rains JL, Jain SK (2011) Oxidative stress, insulin signaling, and diabetes. Free Radic Biol Med 50: 567-575.

293. Miquilena-Colina ME, Lima-Cabello E, Sanchez-Campos S, Garcia-Mediavilla MV, Fernandez-Bermejo M, et al. (2011) Hepatic fatty acid translocase CD36 upregulation is associated with insulin resistance, hyperinsulinaemia and increased steatosis in non-alcoholic steatohepatitis and chronic hepatitis C. Gut 60: 1394-1402.

294. Koonen DP, Jacobs RL, Febbraio M, Young ME, Soltys CL, et al. (2007) Increased hepatic CD36 expression contributes to dyslipidemia associated with diet-induced obesity. Diabetes 56: 2863-2871.

295. McGarry JD, Foster DW (1973) Acute reversal of experimental diabetic ketoacidosis in the rat with (+)-decanoylcarnitine. J Clin Invest 52: 877-884.

296. Hashimoto T, Cook WS, Qi C, Yeldandi AV, Reddy JK, et al. (2000) Defect in peroxisome proliferator-activated receptor alpha-inducible fatty acid oxidation determines the severity of hepatic steatosis in response to fasting. J Biol Chem 275: 28918-28928.

297. Xu HE, Stanley TB, Montana VG, Lambert MH, Shearer BG, et al. (2002) Structural basis for antagonist-mediated recruitment of nuclear co-repressors by PPARalpha. Nature 415: 813-817.

298. Kehrer JP, Biswal SS, La E, Thuillier P, Datta K, et al. (2001) Inhibition of peroxisome-proliferator-activated receptor (PPAR)alpha by MK886. Biochem J 356: 899-906.

299. Anderson CM, Stahl A (2013) SLC27 fatty acid transport proteins. Mol Aspects Med 34: 516-528.

300. Greco D, Kotronen A, Westerbacka J, Puig O, Arkkila P, et al. (2008) Gene expression in human NAFLD. Am J Physiol Gastrointest Liver Physiol 294: G1281-1287.

301. Memon RA, Fuller J, Moser AH, Smith PJ, Grunfeld C, et al. (1999) Regulation of putative fatty acid transporters and Acyl-CoA synthetase in liver and adipose tissue in ob/ob mice. Diabetes 48: 121-127.

302. de Guia RM, Rose AJ, Sommerfeld A, Seibert O, Strzoda D, et al. (2014) microRNA-379 couples glucocorticoid hormones to dysfunctional lipid homeostasis. EMBO J.

303. Bartelt A, Bruns OT, Reimer R, Hohenberg H, Ittrich H, et al. (2011) Brown adipose tissue activity controls triglyceride clearance. Nat Med 17: 200-205.

304. Olofsson SO, Bostrom P, Andersson L, Rutberg M, Perman J, et al. (2009) Lipid droplets as dynamic organelles connecting storage and efflux of lipids. Biochim Biophys Acta 1791: 448-458.

305. Okumura T (2011) Role of lipid droplet proteins in liver steatosis. J Physiol Biochem 67: 629-636.

306. Bell M, Wang H, Chen H, McLenithan JC, Gong DW, et al. (2008) Consequences of lipid droplet coat protein downregulation in liver cells: abnormal lipid droplet metabolism and induction of insulin resistance. Diabetes 57: 2037-2045.

307. Li H, Song Y, Zhang LJ, Gu Y, Li FF, et al. (2012) LSDP5 enhances triglyceride storage in hepatocytes by influencing lipolysis and fatty acid beta-oxidation of lipid droplets. PLoS One 7: e36712.

308. Chen C, Dudenhausen EE, Pan YX, Zhong C, Kilberg MS (2004) Human CCAAT/enhancer-binding protein beta gene expression is activated by endoplasmic reticulum stress through an unfolded protein response element downstream of the protein coding sequence. J Biol Chem 279: 27948-27956.

309. Fang DL, Wan Y, Shen W, Cao J, Sun ZX, et al. (2013) Endoplasmic reticulum stress leads to lipid accumulation through upregulation of SREBP-1c in normal hepatic and hepatoma cells. Mol Cell Biochem 381: 127-137.

310. Werstuck GH, Lentz SR, Dayal S, Hossain GS, Sood SK, et al. (2001) Homocysteine-induced endoplasmic reticulum stress causes dysregulation of the cholesterol and triglyceride biosynthetic pathways. J Clin Invest 107: 1263-1273.

311. Zhang K, Wang S, Malhotra J, Hassler JR, Back SH, et al. (2011) The unfolded protein response transducer IRE1alpha prevents ER stress-induced hepatic steatosis. EMBO J 30: 1357-1375.

312. Mandard S, Zandbergen F, van Straten E, Wahli W, Kuipers F, et al. (2006) The fasting-induced adipose factor/angiopoietin-like protein 4 is physically associated with lipoproteins and governs plasma lipid levels and adiposity. J Biol Chem 281: 934-944.

313. Kuipers F, Jong MC, Lin Y, Eck M, Havinga R, et al. (1997) Impaired secretion of very low density lipoprotein-triglycerides by apolipoprotein E- deficient mouse hepatocytes. J Clin Invest 100: 2915-2922.

314. Misiewicz M, Dery MA, Foveau B, Jodoin J, Ruths D, et al. (2013) Identification of a novel endoplasmic reticulum stress response element regulated by XBP1. J Biol Chem 288: 20378-20391.

315. Morris JA, Dorner AJ, Edwards CA, Hendershot LM, Kaufman RJ (1997) Immunoglobulin binding protein (BiP) function is required to protect cells from endoplasmic reticulum stress but is not required for the secretion of selective proteins. J Biol Chem 272: 4327-4334.

316. Singh R, Kaushik S, Wang Y, Xiang Y, Novak I, et al. (2009) Autophagy regulates lipid metabolism. Nature 458: 1131-1135.

317. Liu K, Czaja MJ (2013) Regulation of lipid stores and metabolism by lipophagy. Cell Death Differ 20: 3-11.

318. Wang Y, Singh R, Xiang Y, Czaja MJ (2010) Macroautophagy and chaperone-mediated autophagy are required for hepatocyte resistance to oxidant stress. Hepatology 52: 266-277.

319. Wang Y, Singh R, Massey AC, Kane SS, Kaushik S, et al. (2008) Loss of macroautophagy promotes or prevents fibroblast apoptosis depending on the death stimulus. J Biol Chem 283: 4766-4777.

320. Shen S, Kepp O, Michaud M, Martins I, Minoux H, et al. (2011) Association and dissociation of autophagy, apoptosis and necrosis by systematic chemical study. Oncogene 30: 4544-4556.

321. Schaffer JE (2003) Lipotoxicity: when tissues overeat. Curr Opin Lipidol 14: 281-287.

322. Das SK, Mondal AK, Elbein SC (2010) Distinct gene expression profiles characterize cellular responses to palmitate and oleate. J Lipid Res 51: 2121-2131.

323. Kyrylkova K, Kyryachenko S, Leid M, Kioussi C (2012) Detection of apoptosis by TUNEL assay. Methods Mol Biol 887: 41-47.

324. Kwon YW, Ueda S, Ueno M, Yodoi J, Masutani H (2002) Mechanism of p53-dependent apoptosis induced by 3-methylcholanthrene: involvement of p53 phosphorylation and p38 MAPK. J Biol Chem 277: 1837-1844.

325. Bulavin DV, Saito S, Hollander MC, Sakaguchi K, Anderson CW, et al. (1999) Phosphorylation of human p53 by p38 kinase coordinates N-terminal phosphorylation and apoptosis in response to UV radiation. EMBO J 18: 6845-6854.

326. Fuchs SY, Adler V, Pincus MR, Ronai Z (1998) MEKK1/JNK signaling stabilizes and activates p53. Proc Natl Acad Sci U S A 95: 10541-10546.

327. Vousden KH, Ryan KM (2009) p53 and metabolism. Nat Rev Cancer 9: 691-700.

328. Berkers CR, Maddocks OD, Cheung EC, Mor I, Vousden KH (2013) Metabolic regulation by p53 family members. Cell Metab 18: 617-633.

329. Liu Y, He Y, Jin A, Tikunov AP, Zhou L, et al. (2014) Ribosomal protein-Mdm2-p53 pathway coordinates nutrient stress with lipid metabolism by regulating MCD and promoting fatty acid oxidation. Proc Natl Acad Sci U S A 111: E2414-2422.

330. Tao W, Levine AJ (1999) Nucleocytoplasmic shuttling of oncoprotein Hdm2 is required for Hdm2-mediated degradation of p53. Proc Natl Acad Sci U S A 96: 3077-3080.

331. Derdak Z, Villegas KA, Harb R, Wu AM, Sousa A, et al. (2013) Inhibition of p53 attenuates steatosis and liver injury in a mouse model of non-alcoholic fatty liver disease. J Hepatol 58: 785-791.

332. Saha AK, Laybutt DR, Dean D, Vavvas D, Sebokova E, et al. (1999) Cytosolic citrate and malonyl-CoA regulation in rat muscle in vivo. Am J Physiol 276: E1030-1037.

333. Rahimi Y, Camporez JP, Petersen MC, Pesta D, Perry RJ, et al. (2014) Genetic activation of pyruvate dehydrogenase alters oxidative substrate selection to induce skeletal muscle insulin resistance. Proc Natl Acad Sci U S A 111: 16508-16513.

334. Haemmerle G, Lass A, Zimmermann R, Gorkiewicz G, Meyer C, et al. (2006) Defective lipolysis and altered energy metabolism in mice lacking adipose triglyceride lipase. Science 312: 734-737.

335. Wu JW, Wang SP, Casavant S, Moreau A, Yang GS, et al. (2012) Fasting energy homeostasis in mice with adipose deficiency of desnutrin/adipose triglyceride lipase. Endocrinology 153: 2198-2207.

336. Schweiger M, Schreiber R, Haemmerle G, Lass A, Fledelius C, et al. (2006) Adipose triglyceride lipase and hormone-sensitive lipase are the major enzymes in adipose tissue triacylglycerol catabolism. J Biol Chem 281: 40236-40241.

337. Defronzo RA (2009) Banting Lecture. From the triumvirate to the ominous octet: a new paradigm for the treatment of type 2 diabetes mellitus. Diabetes 58: 773-795.

338. Gerich JE (2010) Role of the kidney in normal glucose homeostasis and in the hyperglycaemia of diabetes mellitus: therapeutic implications. Diabet Med 27: 136-142.

339. Mithieux G, Rajas F, Gautier-Stein A (2004) A novel role for glucose 6-phosphatase in the small intestine in the control of glucose homeostasis. J Biol Chem 279: 44231-44234.

340. She P, Burgess SC, Shiota M, Flakoll P, Donahue EP, et al. (2003) Mechanisms by which liver-specific PEPCK knockout mice preserve euglycemia during starvation. Diabetes 52: 1649-1654.

341. Puigserver P, Spiegelman BM (2003) Peroxisome proliferator-activated receptor-gamma coactivator 1 alpha (PGC-1 alpha): transcriptional coactivator and metabolic regulator. Endocr Rev 24: 78-90.

342. Puigserver P, Rhee J, Donovan J, Walkey CJ, Yoon JC, et al. (2003) Insulin-regulated hepatic gluconeogenesis through FOXO1-PGC-1alpha interaction. Nature 423: 550-555.

343. Tuncman G, Hirosumi J, Solinas G, Chang L, Karin M, et al. (2006) Functional in vivo interactions between JNK1 and JNK2 isoforms in obesity and insulin resistance. Proc Natl Acad Sci U S A 103: 10741-10746.

344. Aguirre V, Uchida T, Yenush L, Davis R, White MF (2000) The c-Jun NH(2)-terminal kinase promotes insulin resistance during association with insulin receptor substrate-1 and phosphorylation of Ser(307). J Biol Chem 275: 9047-9054.

345. Nguyen MT, Satoh H, Favelyukis S, Babendure JL, Imamura T, et al. (2005) JNK and tumor necrosis factor-alpha mediate free fatty acid-induced insulin resistance in 3T3-L1 adipocytes. J Biol Chem 280: 35361-35371.

346. Schwabe RF, Brenner DA (2006) Mechanisms of Liver Injury. I. TNF-alpha-induced liver injury: role of IKK, JNK, and ROS pathways. Am J Physiol Gastrointest Liver Physiol 290: G583-589.

347. Urano F, Wang X, Bertolotti A, Zhang Y, Chung P, et al. (2000) Coupling of stress in the ER to activation of JNK protein kinases by transmembrane protein kinase IRE1. Science 287: 664-666.

348. Gupta M, Gupta SK, Hoffman B, Liebermann DA (2006) Gadd45a and Gadd45b protect hematopoietic cells from UV-induced apoptosis via distinct signaling pathways, including p38 activation and JNK inhibition. J Biol Chem 281: 17552-17558.

349. Tremblay F, Brule S, Hee Um S, Li Y, Masuda K, et al. (2007) Identification of IRS-1 Ser-1101 as a target of S6K1 in nutrient- and obesity-induced insulin resistance. Proc Natl Acad Sci U S A 104: 14056-14061.

350. Zhang J, Gao Z, Yin J, Quon MJ, Ye J (2008) S6K directly phosphorylates IRS-1 on Ser-270 to promote insulin resistance in response to TNF-(alpha) signaling through IKK2. J Biol Chem 283: 35375-35382.

351. Rajan MR, Fagerholm S, Jonsson C, Kjolhede P, Turkina MV, et al. (2013) Phosphorylation of IRS1 at serine 307 in response to insulin in human adipocytes is not likely to be catalyzed by p70 ribosomal S6 kinase. PLoS One 8: e59725.

352. Herrema H, Lee J, Zhou Y, Copps KD, White MF, et al. (2014) IRS1Ser(3)(0)(7) phosphorylation does not mediate mTORC1-induced insulin resistance. Biochem Biophys Res Commun 443: 689-693.

353. Krebs M (2005) Amino acid-dependent modulation of glucose metabolism in humans. Eur J Clin Invest 35: 351-354.

354. Linn T, Santosa B, Gronemeyer D, Aygen S, Scholz N, et al. (2000) Effect of long-term dietary protein intake on glucose metabolism in humans. Diabetologia 43: 1257-1265.

355. Schulze MB, Manson JE, Willett WC, Hu FB (2003) Processed meat intake and incidence of Type 2 diabetes in younger and middle-aged women. Diabetologia 46: 1465-1473.

356. Krebs M, Krssak M, Bernroider E, Anderwald C, Brehm A, et al. (2002) Mechanism of amino acid-induced skeletal muscle insulin resistance in humans. Diabetes 51: 599-605.

357. Shah OJ, Wang Z, Hunter T (2004) Inappropriate activation of the TSC/Rheb/mTOR/S6K cassette induces IRS1/2 depletion, insulin resistance, and cell survival deficiencies. Curr Biol 14: 1650-1656.

358. Harrington LS, Findlay GM, Gray A, Tolkacheva T, Wigfield S, et al. (2004) The TSC1-2 tumor suppressor controls insulin-PI3K signaling via regulation of IRS proteins. J Cell Biol 166: 213-223.

359. Messner DJ, Rhieu BH, Kowdley KV (2013) Iron overload causes oxidative stress and impaired insulin signaling in AML-12 hepatocytes. Dig Dis Sci 58: 1899-1908.

360. Kohli R, Pan X, Malladi P, Wainwright MS, Whitington PF (2007) Mitochondrial reactive oxygen species signal hepatocyte steatosis by regulating the phosphatidylinositol 3-kinase cell survival pathway. J Biol Chem 282: 21327-21336.

361. Softic S, Kirby M, Berger NG, Shroyer NF, Woods SC, et al. (2012) Insulin concentration modulates hepatic lipid accumulation in mice in part via transcriptional regulation of fatty acid transport proteins. PLoS One 7: e38952.

362. Ozcan U, Yilmaz E, Ozcan L, Furuhashi M, Vaillancourt E, et al. (2006) Chemical chaperones reduce ER stress and restore glucose homeostasis in a mouse model of type 2 diabetes. Science 313: 1137-1140.

363. Hummasti S, Hotamisligil GS (2010) Endoplasmic reticulum stress and inflammation in obesity and diabetes. Circ Res 107: 579-591.

364. Fu S, Watkins SM, Hotamisligil GS (2012) The role of endoplasmic reticulum in hepatic lipid homeostasis and stress signaling. Cell Metab 15: 623-634.

365. Kolb H, Eizirik DL (2012) Resistance to type 2 diabetes mellitus: a matter of hormesis? Nat Rev Endocrinol 8: 183-192.

366. Kammoun HL, Chabanon H, Hainault I, Luquet S, Magnan C, et al. (2009) GRP78 expression inhibits insulin and ER stress-induced SREBP-1c activation and reduces hepatic steatosis in mice. J Clin Invest 119: 1201-1215.

367. Ye R, Jung DY, Jun JY, Li J, Luo S, et al. (2010) Grp78 heterozygosity promotes adaptive unfolded protein response and attenuates diet-induced obesity and insulin resistance. Diabetes 59: 6-16.

368. Salminen A, Kaarniranta K (2010) ER stress and hormetic regulation of the aging process. Ageing Res Rev 9: 211-217.

369. Sauer B, Henderson N (1988) Site-specific DNA recombination in mammalian cells by the Cre recombinase of bacteriophage P1. Proc Natl Acad Sci U S A 85: 5166-5170.

370. Sternberg N, Hamilton D, Hoess R (1981) Bacteriophage P1 site-specific recombination. II. Recombination between loxP and the bacterial chromosome. J Mol Biol 150: 487-507.

371. Utomo AR, Nikitin AY, Lee WH (1999) Temporal, spatial, and cell type-specific control of Cre-mediated DNA recombination in transgenic mice. Nat Biotechnol 17: 1091-1096.

372. Phizicky EM, Fields S (1995) Protein-protein interactions: methods for detection and analysis. Microbiol Rev 59: 94-123.

373. Fields S, Song O (1989) A novel genetic system to detect protein-protein interactions. Nature 340: 245-246.

374. Luo Y, Batalao A, Zhou H, Zhu L (1997) Mammalian two-hybrid system: a complementary approach to the yeast two-hybrid system. Biotechniques 22: 350-352.

375. He R, Li X (2008) Mammalian two-hybrid assay for detecting protein-protein interactions in vivo. Methods Mol Biol 439: 327-337.

376. Puig O, Caspary F, Rigaut G, Rutz B, Bouveret E, et al. (2001) The tandem affinity purification (TAP) method: a general procedure of protein complex purification. Methods 24: 218-229.

377. Gunzl A, Schimanski B (2009) Tandem affinity purification of proteins. Curr Protoc Protein Sci Chapter 19: Unit 19 19.

378. Jornayvaz FR, Birkenfeld AL, Jurczak MJ, Kanda S, Guigni BA, et al. (2011) Hepatic insulin resistance in mice with hepatic overexpression of diacylglycerol acyltransferase 2. Proc Natl Acad Sci U S A 108: 5748-5752.

379. Villanueva CJ, Monetti M, Shih M, Zhou P, Watkins SM, et al. (2009) Specific role for acyl CoA:Diacylglycerol acyltransferase 1 (Dgat1) in hepatic steatosis due to exogenous fatty acids. Hepatology 50: 434-442.

380. Gibbons H, O'Gorman A, Brennan L (2015) Metabolomics as a tool in nutritional research. Curr Opin Lipidol 26: 30-34.

381. Menni C, Fauman E, Erte I, Perry JR, Kastenmuller G, et al. (2013) Biomarkers for type 2 diabetes and impaired fasting glucose using a nontargeted metabolomics approach. Diabetes 62: 4270-4276.

382. Shearer J, Duggan G, Weljie A, Hittel DS, Wasserman DH, et al. (2008) Metabolomic profiling of dietary-induced insulin resistance in the high fat-fed C57BL/6J mouse. Diabetes Obes Metab 10: 950-958.

383. Wang-Sattler R, Yu Z, Herder C, Messias AC, Floegel A, et al. (2012) Novel biomarkers for pre-diabetes identified by metabolomics. Mol Syst Biol 8: 615.

384. Jones RG, Plas DR, Kubek S, Buzzai M, Mu J, et al. (2005) AMP-activated protein kinase induces a p53-dependent metabolic checkpoint. Mol Cell 18: 283-293.

385. Zhan Q, Chen IT, Antinore MJ, Fornace AJ, Jr. (1998) Tumor suppressor p53 can participate in transcriptional induction of the GADD45 promoter in the absence of direct DNA binding. Mol Cell Biol 18: 2768-2778.

386. Berns K, Hijmans EM, Mullenders J, Brummelkamp TR, Velds A, et al. (2004) A large-scale RNAi screen in human cells identifies new components of the p53 pathway. Nature 428: 431-437.

387. Paddison PJ, Silva JM, Conklin DS, Schlabach M, Li M, et al. (2004) A resource for large-scale RNA-interference-based screens in mammals. Nature 428: 427-431.

388. Heid CA, Stevens J, Livak KJ, Williams PM (1996) Real time quantitative PCR. Genome Res 6: 986-994.

389. Slack JL, Bi W, Livak KJ, Beaubier N, Yu M, et al. (2001) Pre-clinical validation of a novel, highly sensitive assay to detect PML-RARalpha mRNA using real-time reverse-transcription polymerase chain reaction. J Mol Diagn 3: 141-149.

390. Garcia-Alcalde F, Okonechnikov K, Carbonell J, Cruz LM, Gotz S, et al. (2012) Qualimap: evaluating next-generation sequencing alignment data. Bioinformatics 28: 2678-2679.

391. Folch J, Lees M, Sloane Stanley GH (1957) A simple method for the isolation and purification of total lipides from animal tissues. J Biol Chem 226: 497-509.

392. Takasu N, Komiya I, Asawa T, Nagasawa Y, Yamada T (1991) Streptozocin- and alloxan-induced H2O2 generation and DNA fragmentation in pancreatic islets. H2O2 as mediator for DNA fragmentation. Diabetes 40: 1141-1145.

393. Klingmuller U, Bauer A, Bohl S, Nickel PJ, Breitkopf K, et al. (2006) Primary mouse hepatocytes for systems biology approaches: a standardized in vitro system for modelling of signal transduction pathways. Syst Biol (Stevenage) 153: 433-447.

394. Kloting N, Fasshauer M, Dietrich A, Kovacs P, Schon MR, et al. (2010) Insulin-sensitive obesity. Am J Physiol Endocrinol Metab 299: E506-515.

8.2 Other references

R. d Guia, PhD Thesis (2014) Hepatic MicroRNA-379 links Glucocorticoid Signalling to Dysfunctional Phenotypes of the Metabolic Syndrome, submitted to combined faculties for the Natural Sciences and for Mathematics of the Ruperto-Carola University of Heidelberg, Germany.

K. Niopek, PhD thesis (2014) Linking Inflammation to Perturbations in Liver Metabolic Homeostasis via the Transcription Factor GAbp, submitted to combined faculties for the Natural Sciences and for Mathematics of the Ruperto-Carola University of Heidelberg, Germany.

P. Narvekar, PhD thesis (2009) Role of the Lipolysis Stimulated Lipoprotein Receptor (LSR) in Metabolic Dyslipidemia, submitted to combined faculties for the Natural Sciences and for Mathematics of the Ruperto-Carola University of Heidelberg, Germany.

A. Wendler, internship (2014) GAbp in Aging, performed at AG Herzig, German Cancer Research Center Heidelberg, Germany.

WHO fact sheet No 311, 2013

9. APPENDIX

9.1 Glossary

AA	Amino Acid
AAV	Adeno-associated virus
AC	Acylcarnitine
ACLY	ATP citrate lyase
AD	Adenovirus
AICAR	Aminoimidazole carboxamide ribonucleotide
AKT	Protein kinase B (PKB)
ALT	Alanine aminotransferase
AML12	Alpha mouse liver 12
AMP	Adenosine monophosphate
AMPK	AMP-activated kinase
ANOVA	Analysis of Variance
ATF	Activating transcription factor
ATP	Adenosine triphosphate
AU	Arbitrary units
AUC	Area Under the Curve
aWAT	Abdominal white adipose tissue
BAT	Brown adipose tissue
BCAA	Branched-chain amino acid
BF	Body fat
BMI	Body mass index
Bp	Base pairs
BW	Body weight
C	Celsius
CAR	Constitutive androstane receptor
CD	Cluster of Differentiation
cDNA	Complementary DNA
CE	Cholester-ester
CETP	Cholesterylester transfer protein
CMV	Cytomegalovirus
CVD	Cardiovascular Disease
DAG	Diacylglycerol
db/db	BKS.Cg-Dock7m +/+ Leprdb/J
DGAT	Diglyceride acyltransferase

DMEM	Dulbeccos's modified eagle medium
DNA	Deoxyribonucleic acid
DNL	*De novo* lipogenesis
dNTP	deoxyribonucleotide triphosphates
ECL	Enhanced chemiluminescence
EDTA	Ethylenediaminetetraacetic acid
EGFP	Enhanced green fluorescent protein
ELISA	Enzyme-linked immunosorbent assay
ER	Endoplasmic Reticulum
ETC	Electron transport chain
FA	Fatty acids
FABP	Fatty acid binding protein
FASN	Fatty acid synthase
FATP	Fatty acid transport protein
FCS	Fetal calf serum
FFA	Free fatty acid
Fig	Figure
FoxO1	Forkhead box protein O1
FPG	Fasting plasma glucose
G6Pase	Glucose-6-phosphatase
GADD45α	Growth arrest and DNA damage-inducible α
GADD45β	Growth arrest and DNA damage-inducible β
GADD45γ	Growth arrest and DNA damage-inducible γ
GCM	Gastrocnemius muscle
GS	Glycogen synthase
GSK3β	Glycogen synthase kinase 3β
GTT	Glucose tolerance test
h	Hour
HbA1c	Glycated hemoglobin
HBSS	Hank's buffered saline solution
HDL	High density lipoprotein
HEK	Human embryonic kidney cells
HFD	High fat diet
HGP	Hepatic glucose production
HL	Hepatic lipase
HOMA	Homeostasis model assessment
HPRT1	Hypoxanthine-guanine phosphoribosyltransferase

HRP	Horseradish peroxidase
Hz	Hertz
IDL	Intermediate density lipoprotein
INFγ	Interferone γ
ip	Intra-peritoneal
IRE1α	Inositol requiring enzyme-1 α
IRS1	Insulin receptor substrate 1
ITT	Insulin tolerance test
JNK	c-Jun N-Terminal kinase
KB	Ketone Bodies
KD	Knockdown
KO	knockout
LB	Ludmilla Broth
LDL	Low density lipoprotein
LDLR	LDL receptor
LM	Lean mass
LPA	Lysophosphatidic acid
LPL	Lipoprotein lipase
LRP	LDL receptor related protein
LSR	Lipolysis stimulated lipoprotein receptor
MC4R	Melanocortin 4 receptor
MCD	Methionine choline deficient diet
MEKK4	MAP kinase kinase kinase 4 (MTK1)
Min	Minute
miRNA	microRNA
MKK4	MAP kinase kinase 4
MMS	Methyl methanesulfonate
MOI	Multiplicity of infection
MRI	Magnetic resonance imaging
mRNA	Messenger RNA
mTOR	Mammalian target of rapamycin
MTP	Microsomal TG transport protein
NADPH	Nicotinamide adenine dinucleotide phosphate
NAFLD	Non-alcoholic fatty liver disease
NASH	Non-alcoholic steatohepatitis
NC	Negative control
NEAA	Non-essential amino acids

NEFA	Non-esterified fatty acids
NFD	Normal fat diet
NF-κB	Nuclear factor kappa-light-chain enhancer of activated B cells
NGT	Normal glucose tolerance
NP	Non-parenchymal
NZB	New Zealand Black
NZO	New Zealand Obese
ob/ob	B6.Cg- Leprob/J
OE	Overexpression
P/S	Penicillin/Streptomycin
PA	Phosphatidic acid
PBS	Phosphate buffered saline
PCA	Principle component analysis
PCK1	Phosphoenolpyruvate carboxykinase 1 (PEPCK)
PDK	Pyruvate dehydrogenase kinase
PEI	Polyethylenimine
PIP_2	Phosphatidylinositol 4,5-bisphosphate
PIP_3	Phosphatidylinositol (3,4,5)-trisphosphate
PGC1	PPARgamma co-activator 1
PI3K	Phosphatidylinositol-3-kinase
PKC	Protein kinase C
PPAR	peroxisome proliferator-activated receptors
RT-qPCR	Real time quantitative polymerase chain reaction
RCT	Reverse cholesterol transport
RER	Respiratory exchange ratio
RNA	Ribonucleic acid
ROS	Reactive oxygen species
RQ	Respiratory quotient
SDS	Sodium dodecyl sulfate
sec	Second
S6K1	Ribosomal protein S6 kinase 1
SEM	Standard error of the mean
SRB1	Scavenger receptor 1
SREBP1	Sterol Regulatory Element-Binding Protein 1
STZ	Streptozotocin
T1D	Type 1 Diabetes

T2D	Type 2 Diabetes
TCID	Tissue culture infection dose
TG	Triglyceride
TGFβ	Transforming growth factor beta
TNFα	Tumor necrosis factor alpha
TSC1/2	Tuberous sclerosis 1/2
UCP1	Uncoupling protein 1
UPR	Unfolded protein response
UV	Ultra Violet
VCP	Valosin-containing protein
VLDL	Very low density lipoprotein
WB	Western Blot
WHO	World health organisation
WT	Wild type

Abbreviations for acylcarnitines and amino acids can be found in suppl. table 4 and 5, respectively.

9.2 Plasmid Maps

9.2.1 pCMV-SPORT6

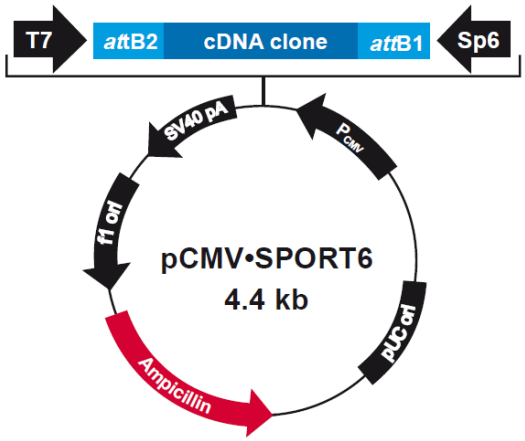

Comments for pCMV•SPORT6 (no insert)
4396 nucleotides

T7 promoter/priming site: bases 16-35
*att*B2: bases 36-60
*att*B1: bases 153-177
Sp6 promoter/priming site (c): bases 177-196
CMV promoter (c): bases 266-859
pUC origin: bases 1236-1908
Ampicillin (*bla*) resistance gene (c): bases 2112-2977
bla promoter (c): bases 2972-3029
f1 origin (c): bases 3260-3720
SV40 early polyadenylation signal (c): bases 3847-4113
(c) = complementary strand

9.2.2 pENTR-Flag

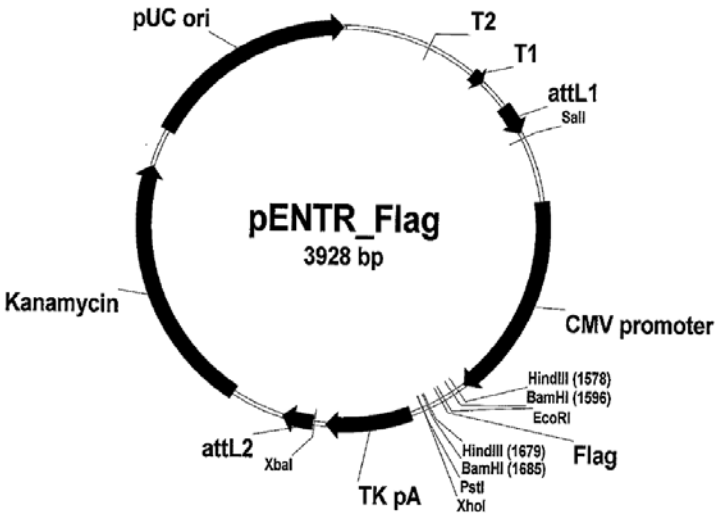

9.2.3 pAd-Block-iT™-DEST

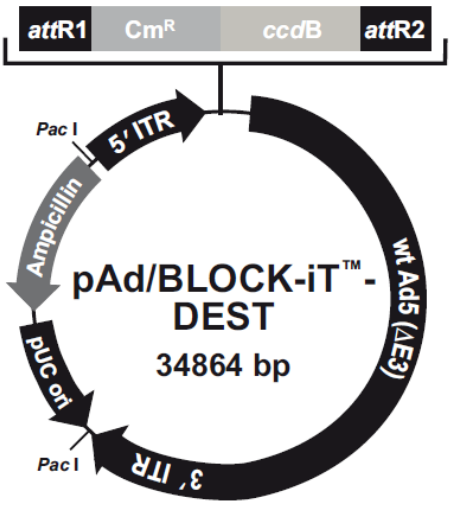

Comments for pAd/BLOCK-iT™-DEST
34864 nucleotides

Human Ad5 sequences (wt 1-458; includes 5′ L-ITR and packaging signal): 1-458
pAd forward priming site: bases 361-384
*att*R1 site: bases 512-636
Chloramphenicol resistance gene (Cm^R): bases 745-1404
*ccd*B gene: bases 1746-2051
*att*R2 site: bases 2092-2216
Human Ad5 sequences (wt 3513-35935; E3 region deleted, includes 3′ R-ITR): bases 2234-32782
pAd reverse priming site: bases 2237-2260
pUC origin: bases 32959-33620 (C)
Ampicillin (*bla*) resistance gene: bases 33746-34606 (C)
bla promoter: bases 34607-34705 (C)
Pac I restriction sites: bases 32788 and 34862
(C) = complementary strand

9.2.4 pcDNA6.2-GW/EmGFP-miR

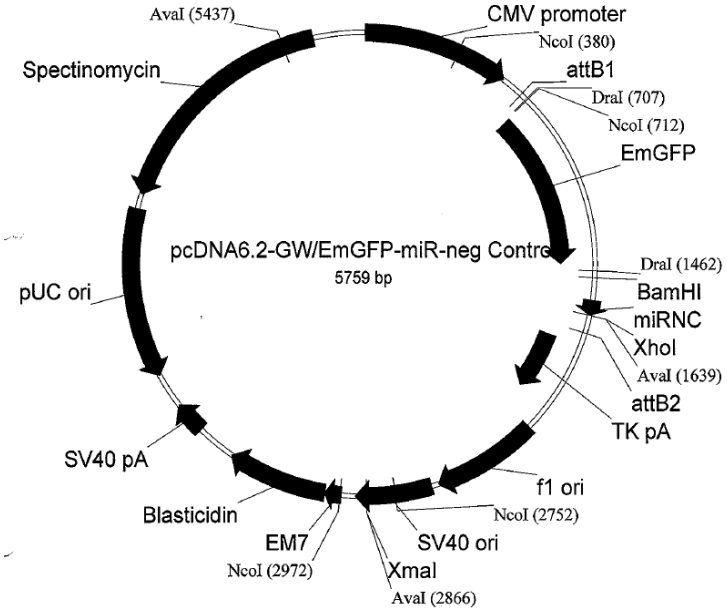

9.2.5 pdsAAV2-LP1-GFPmut-miR-NC

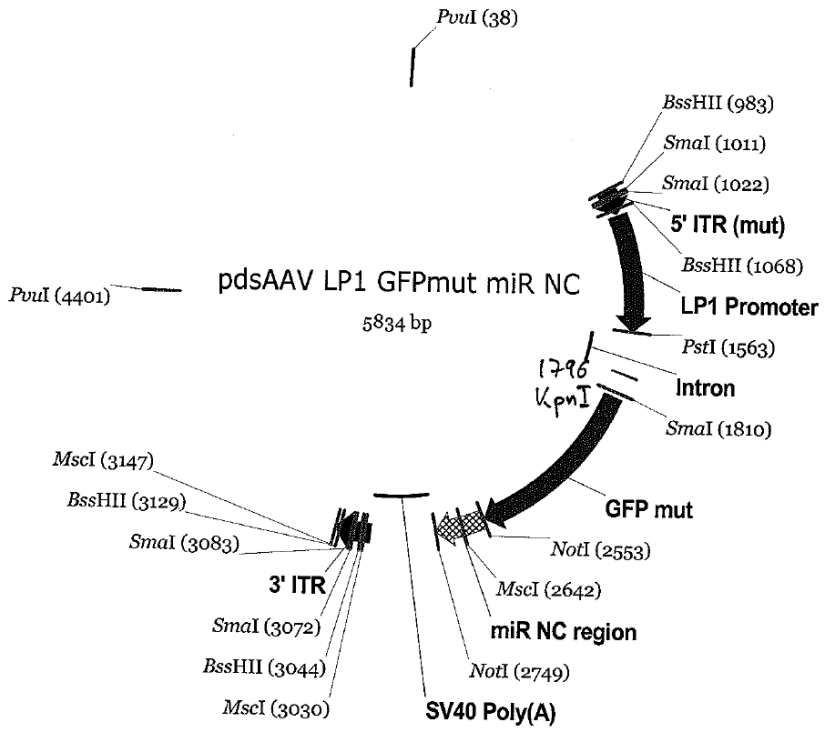

9.3 Supplementary Figures

Suppl. figure 1: DAVID enrichment analysis of >2fold down regulated genes in the liver of GADD45β KO mice. Male GADD45β KO and WT littermates were sacrificed after being fasted for 24h hours. Functional annotation analysis on RNAseq hits from Suppl. table 2 was performed with DAVID Bioinformatics Resources 6.7 (National institute of allergy and infectious diseases, NIH, http://david.abcc.ncifcrf.gov). n=3 per group

Category	Term	RT	Genes	Count	%	P-Value	Fold Enrichment	Bonferroni	Benjamini
INTERPRO	Serine/threonine protein kinase-related	RT		3	10,7	4,4E-2	8,4	9,6E-1	8,0E-1
GOTERM_MF_FAT	transcription factor activity	RT		4	14,3	3,7E-2	4,9	9,1E-1	9,1E-1
SP_PIR_KEYWORDS	phosphoprotein	RT		12	42,9	3,7E-2	1,7	9,2E-1	9,2E-1
INTERPRO	Serine/threonine protein kinase, active site	RT		3	10,7	4,1E-2	8,7	9,5E-1	9,5E-1
GOTERM_BP_FAT	phosphate metabolic process	RT		5	17,9	1,6E-2	4,6	9,8E-1	9,8E-1
GOTERM_BP_FAT	phosphorus metabolic process	RT		5	17,9	1,6E-2	4,6	9,8E-1	9,8E-1
GOTERM_BP_FAT	cell cycle	RT		4	14,3	3,3E-2	5,2	1,0E0	9,8E-1
GOTERM_BP_FAT	phosphorylation	RT		4	14,3	4,9E-2	4,5	1,0E0	9,8E-1
UP_SEQ_FEATURE	short sequence motif:Nuclear localization signal	RT		3	10,7	4,5E-2	8,3	9,8E-1	9,8E-1

Suppl. figure 2: Simplified scheme of the insulin signalling pathway. For appreviations see section 9.1.

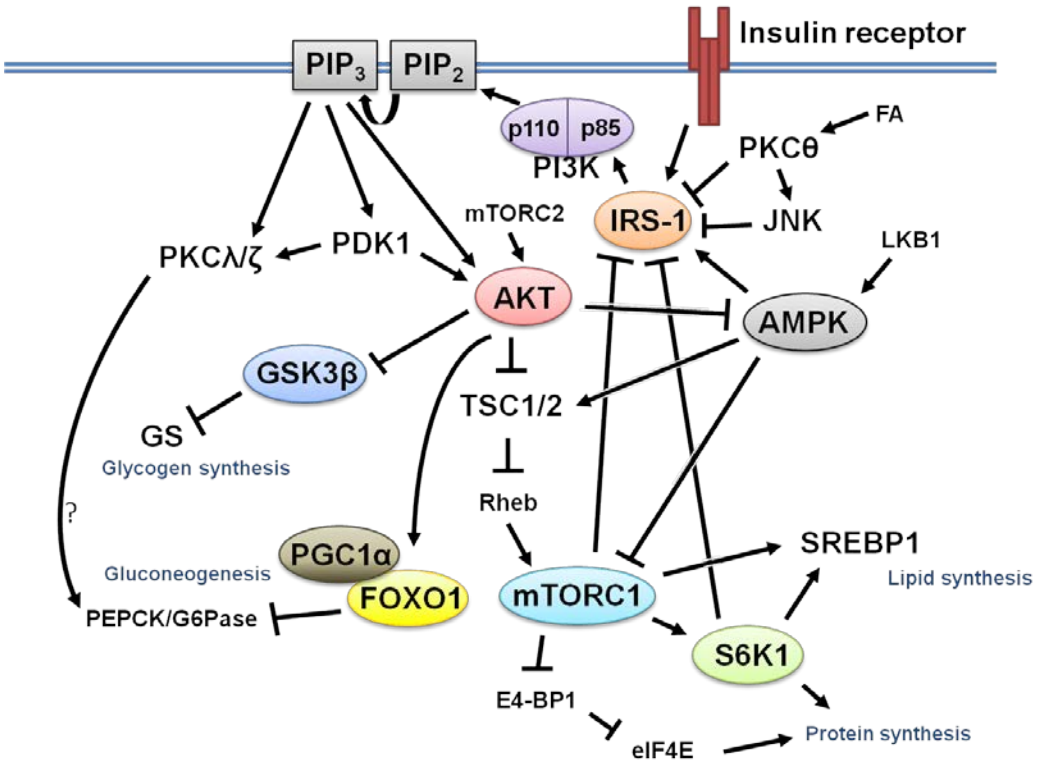

9.4 Supplementary Tables

Suppl. table 1: Induction of GADD45 proteins by various stressors. Adapted and modified from [208].

Stress	GADD45 member	Reference
UV-radiation	GADD45α, GADD45β, GADD45γ	PMID: 10327059; 3194391; 8208528; 11078829; 11251170; 12164919; 15616591; 15616591
X-rays	GADD45α	PMID: 1990262, 11747551

α-radiation	GADD45α, GADD45β, GADD45γ	PMID: 10327059; 11251170; 11382918; 11873496
Low-frequency electromagnetic fields	GADD45α	PMID: 16116041
Hypoxia	GADD45α	PMID: 1617653; 18087215
Peroxynitrite free radicals	GADD45α	PMID: 11163539
Hyperosmotic stress	GADD45α, GADD45β, GADD45γ	PMID: 9593703; 12372778; 19834918
Oncogenic stress	GADD45α	PMID: 12748288
Low pH	GADD45α	PMID: 16113055
Arsenic As(III)	GADD45α	PMID: 10910055; 11429707; 16814109; 11353140; 12883267; 15493360
Sodium arsenite	GADD45β	PMID: 15797874
Chromium Cr(VI)	GADD45α	PMID: 14971655
Cisplatin	GADD45α	PMID: 10327059; 8996528
Methyl methanesulfonate (MMS)	GADD45α, GADD45β, GADD45γ	PMID: 1990262; 11251170
Ethanol	GADD45α	PMID: 16131858
Cigarette smoke condensate	GADD45α	PMID: 15208684; 15170813
Mitomycin C	GADD45α	PMID: 10327059
Bacterial lipopolysaccharides	GADD45β, GADD45γ	PMID: 15797874, 16116230
Pro-inflammatory cytokines (IL-6, IL-12, IL-18)	GADD45β	PMID: 18501677; 11175814;
IL-2, IL-6	GADD45γ	PMID: 10490824
Pro-apoptotic cytokines (TGFβ, TNFα)	GADD45β	PMID: 8139540; 12456654; 12933797; 18501677; 15797874

Suppl. table 2: >2fold down regulated genes in the liver of GADD45β KO mice. Male GADD45β KO and WT littermates were sacrificed after being fasted for 24h hours. Expression profiling of liver transcripts was subsequently performed by RNAseq analysis. Shown are the Fragments Per Kilobase Of Exon Per Million Fragments Mapped (fpkm). A false positive rate (FDR) of a=0.01 was applied. n=3 per group.

Symbol	Name	Feature Type	Entrez Gene ID	WT fpkm	KO fpkm	KO/WT fold change	q value (FDR)	~ expression level
4930565N06Rik	RIKEN cDNA 4930565N06 gene	unclassified non-coding RNA gene	68306	0,256	0,021	0,082	0,000271	low
Atp6v0d2	ATPase, H+ transporting, lysosomal V0 subunit D2	protein coding gene	242341	1,130	0,364	0,322	1,36E-07	moderate
BC005561	cDNA sequence BC005561	protein coding gene	100042165	1,384	0,500	0,361	1,15E-11	moderate
Bmpr2	Bone morphogenetic protein receptor, type II (serine/threonine kinase)	protein coding gene	12168	2,381	0,800	0,336	2,38E-14	moderate
Cbl	Casitas B-lineage lymphoma	protein coding gene	12402	0,926	0,399	0,431	2,10E-06	low
Cdk6	Cyclin-dependent kinase 6	protein coding gene	12571	2,553	1,170	0,458	9,35E-07	moderate
F830016B08Rik	RIKEN cDNA F830016B08 gene	protein coding gene	240328	4,940	1,154	0,234	0	moderate
G530011O06Rik	RIKEN cDNA G530011O06 gene	lincRNA gene	654820	0,349	0,100	0,285	0,000946	low
Gadd45b	*Growth arrest and DNA-damage-inducible 45 beta*	*protein coding gene*	*17873*	*3,034*	*0,000*	*0,000*	*5,09E-22*	*moderate*
Gprin3	GPRIN family member 3	protein coding gene	243385	1,406	0,561	0,399	2,11E-07	moderate

Klf12	Kruppel-like factor 12	protein coding gene	16597	6,002	2,973	0,495	2,66E-12	moderate
Klhl11	Kelch-like 11	protein coding gene	217194	1,627	0,693	0,426	5,02E-06	moderate
Lcn2	Lipocalin 2	protein coding gene	16819	30,585	11,018	0,360	0	high
Lcor	Ligand dependent nuclear receptor corepressor	protein coding gene	212391	0,689	0,158	0,229	4,47E-12	low
Lmbrd2	LMBR1 domain containing 2	protein coding gene	320506	8,871	2,987	0,337	0	moderate
Lnpep	Leucyl/cystinyl aminopeptidase	protein coding gene	240028	1,273	0,417	0,328	9,68E-13	moderate
Mib1	Mindbomb homolog 1 (Drosophila)	protein coding gene	225164	7,297	3,555	0,487	2,91E-12	moderate
N4bp2	NEDD4 binding protein 2	protein coding gene	333789	4,208	1,923	0,457	1,60E-13	moderate
Ptar1	Protein prenyltransferase alpha subunit repeat containing 1	protein coding gene	72351	0,668	0,262	0,393	0,001653	low
Ptpn4	Protein tyrosine phosphatase, non-receptor type 4	protein coding gene	19258	0,777	0,383	0,493	0,000509	low
Rel	Reticuloendotheliosis oncogene	protein coding gene	19696	1,198	0,567	0,473	0,000478	moderate
Sesn3	Sestrin 3	protein coding gene	75747	3,001	1,368	0,456	4,92E-07	moderate
Themis	Thymocyte selection associated	protein coding gene	210757	0,256	0,101	0,396	0,009662	low
Uhmk1	U2AF homology motif (UHM) kinase 1	protein coding gene	16589	6,640	3,111	0,469	1,00E-09	moderate
Xpo4	Exportin 4	protein coding gene	57258	1,631	0,805	0,493	2,99E-05	moderate
Xrn1	5'-3' exoribonuclease 1	protein coding gene	24127	1,605	0,670	0,417	3,81E-10	moderate
Zbed6	Zinc finger, BED domain containing 6	protein coding gene	667118	4,443	0,416	0,094	0	moderate
Zfp369	Zinc finger protein 369	protein coding gene	170936	1,452	0,431	0,297	2,35E-11	moderate
Zfp433	RIKEN cDNA 1700123A16 gene	protein coding gene	73610	3,310	1,530	0,462	5,09E-10	moderate

Suppl. table 3: >2fold up regulated genes in the liver of GADD45β KO mice. Male GADD45β KO and WT littermates were sacrificed after being fasted for 24h hours. Expression profiling of liver transcripts was subsequently performed by RNAseq analysis. Shown are the Fragments Per Kilobase Of Exon Per Million Fragments Mapped (fpkm). A false positive rate (FDR) of a=0.01 was applied. n=3 per group.

Symbol	Name	Feature Type	Entrez Gene ID	WT fpkm	KO fpkm	KO/WT fold change	q value (FDR)	~ expression level
Ces4a	carboxylesterase 4A	protein coding gene	234677	0,413	1,844	4,461	2,41E-14	moderate
Cgref1	cell growth regulator with EF hand domain 1	protein coding gene	68567	0,824	2,710	3,289	8,82E-12	moderate
Cidec	cell death-inducing DFFA-like effector c	protein coding gene	14311	7,506	18,243	2,430	0	high
Cntnap1	contactin associated protein-like 1	protein coding gene	53321	0,625	1,767	2,827	2,03E-13	moderate
Derl3	Der1-like domain family, member 3	protein coding gene	70377	2,600	8,672	3,336	0	moderate
Lad1	ladinin	protein coding gene	16763	1,600	3,434	2,145	1,22E-08	moderate

Nudt7	nudix (nucleoside diphosphate linked moiety X)-type motif 7	protein coding gene	67528	79,821	169,659	2,125	0	high
Onecut1	one cut domain, family member 1	protein coding gene	15379	5,009	11,485	2,293	1,82E-13	high
Peg10	paternally expressed 10	protein coding gene	170676	0,124	0,280	2,265	0,003468	low
Pfkfb3	6-phosphofructo-2-kinase/fructose-2,6-biphosphatase 3	protein coding gene	170768	1,360	2,767	2,034	0	moderate
Pitx3	paired-like homeodomain transcription factor 3	protein coding gene	18742	2,540	5,657	2,227	1,50E-07	moderate
Serpina12	serine (or cysteine) peptidase inhibitor, clade A (alpha-1 antiproteinase, antitrypsin), member 12	protein coding gene	68054	1,915	4,000	2,089	3,19E-09	moderate
Serpina4-ps1	serine (or cysteine) peptidase inhibitor, clade A, member 4, pseudogene 1	pseudogene	321018	7,210	36,964	5,127	0	high
Slc35f1	solute carrier family 35, member F1	protein coding gene	215085	0,030	0,197	6,524	4,88E-05	low

Suppl. table 4: Correlation analysis of liver *GADD45B* levels and parameters to assess the diabetic status of lean and obese men with and without Type 2 Diabetes. Diabetic and healthy patients were pooled for the analysis and only separated by their body composition into lean men or men with subcutaneous (SC) or visceral (VIS) fat. Correlation was determined using Shearman's correlation coefficient.

Correlation *GADD45B*

Parameter	Group	r^2	p
	Lean	-0,464	0,141
FPG [mmol/L]	SC	-0,489	0,053
	VIC	-0,103	0,759
	Lean	-0,609	0,0427
Serum NEFA [mmol/L]	SC	-0,193	0,463
	VIC	0,171	0,607
	Lean	-0,564	0,065
Serum TG [mmol/L]	SC	-0,374	0,149
	VIC	-0,370	0,275
	Lean	-0,355	0,27
HOMA-IR	SC	-0,174	0,512
	VIC	0,297	0,384
	Lean	-0,355	0,27
FPI [pmol/L]	SC	-0,097	0,713
	VIC	0,382	0,258
	Lean	-0,284	0,384
Hb1Ac [%]	SC	-0,258	0,325
	VIC	-0,231	0,49
	Lean	-0,041	0,881
Cholesterol [mmol/L]	SC	-0,156	0,556
	VIC	-0,212	0,535

Suppl. table 5: Acylcarnitines and their full names.

Abbreviation	Name
C0	free Carnitine
C2	Acetylcarnitine
C3	Propionylcarnitine
C4	Butyrylcarnitine
C5	Isovalerylcarnitine
C6	Hexanoylcarnitine
HMB	2-OH-3- Methyl-butyrylcarnitine
C5OH	3-OH-Isovalerylcarnitine
C8:1	Octenoylcarnitine
C8	Octanoylcarnitine
C10:1	Decenoylcarnitine
C10	Decanoylcarnitine
MMA (C4DC)	Methylmalonylcarnitine
Glut (C5DC)	Glutarylcarnitine
C12	Dodecanoylcarnitine
MeGlut	3-Methylglutarylcarnitine
3HMG	3-Hydroxy-3-methylglutarylcarnitine
C14:1	Myristoleylcarnitine
C14	Myristoylcarnitine
C14OH	3-OH-Myristoylcarnitine
C16:1	Palmitoleylcarnitine
C16	Palmitoylcarnitine
C16OH	3-OH-Palmitoylcarnitine
C16:1OH	Hydroxyhexadecenoylcarnitine
C18:2	Linoleylcarnitine
C18:1	Octadecenoylcarnitine
C18	Stearoylcarnitine
C18:1OH	3-OH-Octadecenoylcarnitine
C18OH	3-OH-Stearoylcarnitine

Suppl. table 6: Amino acids and their full names.

Abbreviation	Name
Ala	Alanine
Arg	Arginine

Asa	Asparagine
Asp	Aspartic Acid
Cit	Citrulline
Glu	Glutamic Acid
Gly	Glycine
Hci	Homocysteine
His	Histidine
Leu/Ile	Leucin/Isoleucin
Met	Methionine
Orn	Ornithine
Phe	Phenylalanine
Pro	Proline
Pyg	Pyridylglycine
Thr	Threonine
Trp	Tryptophan
Tyr	Tyrosine
Val	Valine